UNIVERSITAT DE BARCELONA

Targeting *Plasmodium falciparum* protein aggregation as a new antimalarial design strategy

Inés Bouzón Arnáiz

UNIVERSITAT DE BARCELONA

FACULTAT DE FARMÀCIA I CIÈNCIES DE L'ALIMENTACIÓ

DOCTORAT EN BIOTECNOLOGIA

Targeting *Plasmodium falciparum* protein aggregation as a new antimalarial design strategy.

Inés Bouzón Arnáiz

2022

Universitat de Barcelona.

Facultat de Farmacia i Ciències de l'alimentació.

Programa de doctorat en Biotecnologia.

Targeting *Plasmodium falciparum* protein aggregation as a new antimalarial design strategy.

Inés Bouzón Arnáiz

Institut de Bioengenyeria de Catalunya (IBEC) - Institut de Salut Global de Barcelona (ISGlobal)

Memòria presentada per Inés Bouzón Arnáiz per optar al títol de doctora per la universitat de Barcelona.

Director: Xavier Fernàndez Busquets

Tutora: Josefa Badía Palacín

Abstract

Malaria caused 241 million cases and 627,000 deaths worldwide in 2020, representing one of the biggest threats for global health nowadays. The currently available arsenal of antimalarial drugs is insufficient to progress towards eradication of the disease, a scenario that is worsened by the rampant evolution of resistance by *Plasmodium*, the causative agent of malaria.

Protein aggregation in malaria parasites is prominent during their whole life cycle. Aggregative proteins are distributed throughout the parasite's cytosol, especially in the endoplasmic reticulum adjacent areas, where protein translation and folding take place. In this thesis, we intended to target the aggregative features of the *Plasmodium falciparum* proteome with the final objective of developing an effective antimalarial strategy.

Firstly, based on *in silico* and *in vivo* data, we selected a group of aggregative peptides present in parasite proteins. Those peptides formed aggregates in vitro; however, attempts to further increase the high aggregation propensity of the *P. falciparum* proteome by delivering them to *in vitro* cultures did not significantly decrease the viability of the pathogen. To confirm the lack of activity of the peptides on *P. falciparum* viability, their entrance inside the parasite was improved combining two different methods: their tagging with cell-penetrating peptides and their encapsulation inside ghost red blood cells. Despite the significantly enhanced entrance of the peptides inside parasites using these two approaches, *P. falciparum* growth was not affected.

To test the alternative hypothesis, i.e. if inhibiting protein aggregation in the parasite might impair its development, we treated *in vitro* cultures with amyloid pan-inhibitors, which are molecules able to prevent amyloid fibril formation. All of these compounds showed some extent of antiplasmodial activity. Particularly one of them, the double pyridinium salt YAT2150, exhibited potent antimalarial activity with an *in vitro* IC_{50} of 90 nM. This drug was also effective on the sexual forms of *P. falciparum* and on the hepatic stages of *P. berghei*. In relation with its mode of action, YAT2150 is a powerful inhibitor of the aggregation of the amyloid β peptide fragment 40 *in vitro* and it reduced in *P. falciparum* cultures the amyloid content and the quantity of ubiquitinated proteins, as well as the amount in aggregative proteins detected with thioflavin T. Thus, YAT2150 antimalarial mode of action is the inhibition of protein aggregation in the parasite. Moreover, we observed that YAT2150 resistance emergence is not easily developed by *P. falciparum* cultures and that already acquired resistances to other antimalarial compounds do not affect YAT2150 activity.

In this thesis we show that targeting *P. falciparum* protein aggregation is a valid antimalarial strategy and that YAT2150, belonging to a chemical family with no other

antimalarials described, acting through a new antiparasitic mechanism not shared by other currently used drugs, and targeting many gene products, is a good candidate to significantly contribute to malaria eradication.

Resumen

Se estima que en el año 2020 se produjeron en todo el mundo 241 millones de casos de malaria. Esta enfermedad, causada por parásitos del género *Plasmodium*, sigue siendo una gran amenaza para la salud global. Sin embargo, los antipalúdicos usados actualmente son insuficientes para combatir la malaria, especialmente porque se han detectado parásitos resistentes a la gran mayoría de ellos. Por otro lado, sabemos que la agregación de proteínas en *Plasmodium* es prominente, de hecho aquí mostramos que se detecta en todas las fases del desarrollo del parásito. Esta tesis se centra, precisamente, en el uso de las proteínas agregativas de *P. falciparum* como dianas terapéuticas para el desarrollo de nuevas estrategias antipalúdicas. Exploramos dos hipótesis complementarias: el aumento de los niveles basales de agregación proteica en el parásito mediante la administración de péptidos agregativos presentes en el proteoma de *P. falciparum*, y la inhibición de la agregación de las proteínas agregativas del parásito mediante el tratamiento con compuestos inhibidores de la formación de amiloides. Mientras la primera estrategia no reduce de manera efectiva la viabilidad del parásito, la segunda sí lo hace. Especialmente, uno de los compuestos testados, YAT2150, tiene un efecto nocivo tanto para las formas asexuales como sexuales de *P. falciparum* y para las hepáticas de *P. berghei*. Además, este compuesto inhibe la agregación proteica en *P. falciparum in vivo* (reduce el contenido de proteínas amiloides, de proteínas ubiquitinadas y de proteínas detectadas por tioflavina-T) y no permite el desarrollo de resistencias en cultivos *in vitro* del parásito.

Index

Abbreviations

A	Adenine
ACTs	Artemisinin combination therapies
ALIX	Apoptosis-linked gene 2–interacting protein X
ARTs	Artemisinin derivatives
Aβ	β-amyloid peptide
BiP	Immunoglobulin heavy chain binding protein
CLEM	Correlative light-electron microscopy
CPP	Cell penetrating peptide
DV	Digestive vacuole
eEF	Eukaryote elongation factor
eIF	Eukaryote initiation factor
ER	Endoplasmid reticulum
eRF	Eukaryote release factor
ESCRT	Endosomal sorting complex required for transport
EVs	Extracellular vesicles
hpi	hours post invasion
hPrP	Human prionic protein
HSF1	Heat shock factor 1
Hsps	Heat shock proteins
ILVs	Intraluminal vesicles
LCR	Low complexity region
MSP2	Merozoite surface protein 2
MSPs	Merozoite surface proteins
MVBs	Multivesicular bodies
N	Asparagine
NGD	No-go decay
NMD	Non-sense mediated decay
NSD	Non-stop decay
PCR	Polymerase chain reaction
PIP3	Phosphatidylinositol 3-phosphate
PKG	c-GMP-dependent protein kinase
PLP1	Perforin-like protein 1
pRBCs	Parasitized RBCs
PV	Parasitophorous vacuole
RBC	Red blood cell
RDTs	Rapid diagnostic tests
Rpn6	Proteasome lid subunit 6
SNARE	Soluble NSF attachment protein receptor
SOD1	Superoxide dismutase 1
T	Thymine
TEM	Transmission electron microscopy
Th-T	Thioflavin-T
UPR	Unfolded protein response

UPS	Ubiquitin-proteasome system
WHO	World Health Organization

Introduction

1. Malaria: a global issue.

Malaria is a vector-borne infectious disease caused by parasites belonging to the genus *Plasmodium* and transmitted to humans by female *Anopheles* mosquitos.

Historically, the cradle of malaria seems to be Ethiopia (Bruce-Chwatt, 1965). After spreading through the African continent, probably following the Nile valley, malaria reached the Mediterranean shores, Mesopotamia and finally India and China (Bruce-Chwatt, 1965). From these regions, malaria started the invasion of a wider part of the old world, mainly thanks to the exploring nature of humans who traveled and migrated taking with them their malarial baggage (Schlagenhauf, 2004). On the contrary, the arrival of malaria to America is a bit more controversial, but the most accepted theory is that early travelers brought malaria to areas in Central and South America before Columbus landing (Schlagenhauf, 2004).

The first written reference of what was almost certainly malaria was found in a Chinese document dated back from 2700 BC. This is not the only ancient mention to malaria; Mesopotamian clay tablets from 2000 BC, Egyptian papyri from 1570 BC and the treatise “On Airs, Waters and Places” written by Hippocrates in around 400 BC also recorded cases of malaria. (Cox, 2010; Hempelmann & Krafts, 2013)

Even though humans have been affected by malaria for thousands of years, the disease is still a current and global issue. In 2020, 241 million cases of malaria and 627,000 deaths were registered worldwide (WHO, 2021c). According to the World Health Organization (WHO) most of these cases (95%) affected African regions, followed by far by South-East Asia (2%) (Figure 1A). Optimistically, the incidence rate of malaria was estimated to have fallen by 18% globally from 2010 to 2016. However, this decline was reduced to less than 2% from 2015 to 2019 (WHO, 2020) and it increased in 2020 almost an 11% compared to the previous year (WHO, 2021c), indicating a worrying slowing — or even a reversion — of the decline of the incidence rate of the disease in the world (Figure 1B).

The population group at the highest risk of malaria is children under five years of age (77% of all malaria deaths occur in this group) (WHO, 2021c). Special attention should also be paid to pregnant women, as malaria infection during pregnancy increases the risk of mother death before and after childbirth and can lead to stillbirth as well as to poor fetal development, thus impairing the normal growth of the newborn (WHO, 2017). In 2020, in the African region, 34% of pregnant women were exposed to malaria infection (WHO, 2021c).

The dramatic impact of malaria worldwide makes imperative not only the development of novel and effective treatments, preventive therapies and diagnostic tools, but also the ambitious achievement of totally eradicating the disease. By 2030

WHO aims to reduce malaria mortality rates and incidence at least 90% compared to 2015 and completely eliminate malaria from at least 35 countries (WHO, 2016). From 1955 to 2021, 40 countries in which malaria was an endemic disease had been certified as malaria free areas by WHO, being China and El Salvador the last ones included in this list (WHO, 2021a). Despite these good news, 85 countries in the world reported malaria cases in 2020 (WHO, 2021c).

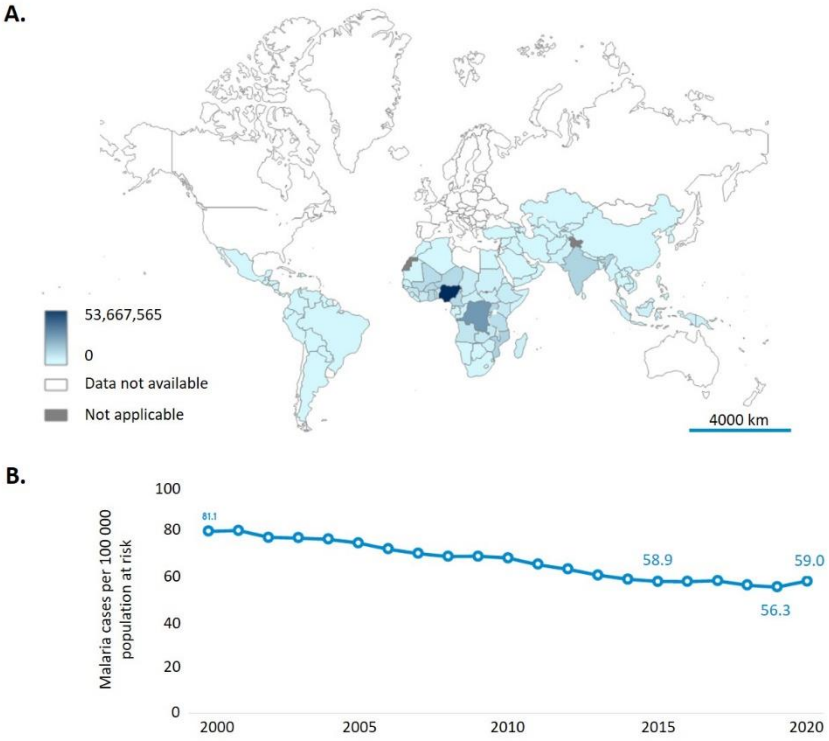

***Figure 1**. A) World map of the global distribution of malaria cases in 2019. Adapted from (WHO, 2020). B) Malaria deaths per 100,000 population at risk from 2000 to 2020. Adapted from (WHO, 2021c) .*

1.1. *Plasmodium*: the cause of malaria.

The causative agent of malaria remained unclear for several centuries. One of the first theories that tried to explain malaria etiology was the "bad air" or miasma hypothesis, which suggested that bad smells, especially those emanating from marshy areas, were responsible for the onset of malaria (Guillemin, 2001) (Figure 2A). In fact, the word malaria itself comes from the Italian *mal'aria*, which literally means bad air. This idea of "bad air" prevailed until the end of the 19th century (Hempelmann & Krafts, 2013), when, in 1880, Charles Louis Alphonse Laveran, a French military physician, discovered the malaria parasite analyzing a blood sample of a soldier in Algeria. Laveran called this parasite *Oscillaria malariae* (Cox, 2010; Guillemin, 2001) (Figure 2B). It was not until 1922 when the main *Plasmodium* species infecting humans were identified with certainty (Keeling & Rayner, 2015).

Plasmodium species, like others included in the phylum Apicomplexa, are obligate intracellular parasites. Five of these species are known to cause malaria in humans: *Plasmodium falciparum, Plasmodium vivax, Plasmodium malariae, Plasmodium knowlesi* and *Plasmodium ovale.* The most severe form of malaria and the one presenting the highest mortality rates is caused by *P. falciparum* (Warrell et al., 2010).

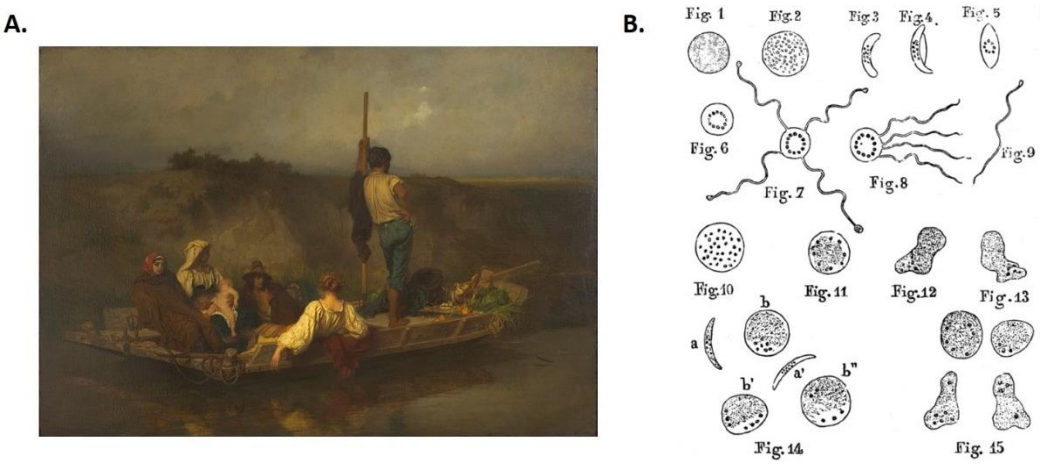

***Figure 2**. A) "La Mal'aria" painting by Ernest Hébert after his personal experience in Italy. The painting depicts a family escaping from a malaria epidemic (Hébert, 1848-1849). B)* Oscillaria malariae *stages drawn by Charles Louis Alphonse Laveran (Laveran, 1880).*

- → In 2020, 241 million cases of malaria and 627,000 deaths were registered worldwide.
- → A slowing trend in the decline of the incidence rate of the disease in the world is being observed since 2015.
- → The most severe form of malaria and the one presenting the highest mortality rates is caused by *P. falciparum.*

Plasmodium parasites divide their life cycle in two parts: one within the vertebrate host and the other one within the insect vector, a mosquito of the *Anopheles* genus. Inside the human host two stages of the parasite can be distinguished: (i) the liver or exoerythrocytic stage and (ii) the erythrocytic or intraerythrocytic stage.

The cycle starts (Figure 3A) when a female mosquito inoculates the motile forms of the parasite, the sporozoites, in the human host. Sporozoites travel through the bloodstream and access the liver by a process known as traversal, which consists on (i) crossing the sinusoidal barrier of the liver and (ii) migrating through various hepatocytes before definitively infecting one (Mota et al., 2001; Tavares et al., 2013; Yang et al., 2017). The crossing of these physical barriers is done without the lysis of

hepatocytes, in whose surface pores are formed so sporozoites are able to enter and exit them (Kumar & Tolia, 2019). Even though the reason for cell traversal to occur is still under discussion, it is clear that it is mandatory for the final hepatocyte infection, in fact, the targeted disruption of one of the proteins involved in this process, perforin-like protein 1 (PLP1) reduces infectivity of sporozoites in the liver (Yang et al., 2017).

During the liver stage, each sporozoite undergoes several rounds of asexual replication to form up to 40,000 merozoites (Cowman et al., 2016), which are released into the bloodstream where they infect erythrocytes. This is the beginning of the erythrocytic stage of the *Plasmodium* life cycle.

Merozoites invade erythrocytes in a very fast way, and in only 2 minutes they complete the invasion process (Cowman et al., 2016). Merozoite surface proteins (MSPs) are crucial for invasion, and complexes formed by MSP1 together with other MSPs are responsible for the first interaction of the parasite with the erythrocyte to invade (Lin et al., 2016; Paul et al., 2018). MSP1 is the largest and the most abundant MSP member and, together with MSP2, coat approximately two-thirds of the merozoite membrane surface (Gilson et al., 2006). Blocking MSP1 with heparin-like molecules (Boyle et al., 2010) or deleting one of the genes encoding for MSP1, *msp7* (Kadekoppala et al., 2008), badly impairs red blood cell (RBC) invasion. On the other hand, it has been shown that parasites lacking MSP1, even though with a lower efficacy, are still able to invade erythrocytes (Cowman et al., 2017), suggesting the existence of other invasion pathways that do not depend on a first interaction via MSP1.

The next step in erythrocytes invasion is a reorientation of the merozoite to put in contact its apical part with the RBC (Tham et al., 2012). Afterwards, junctions between the merozoite and the RBC membrane are formed through adhesins, which trigger the weakening and detachment of cytoskeletal proteins from the RBC membrane in the merozoite entry site (Aniweh et al., 2017). After destabilizing the RBC membrane, merozoites are propelled into erythrocytes at the same time that they begin the formation of the parasitophorous vacuole (PV) thanks to the formation of the parasitophorous membrane due to the secretion of lipids stored in a specific organelle of the merozoite, the rhoptry (Bannister et al., 1986).

Once the parasite has entered a RBC and is enclosed inside the PV, it displays a 48-hour replicative cycle (Figure 3B) during which it progresses through the ring (0-24 hours post invasion [hpi]), trophozoite (24-36 hpi) and schizont (36-48 hpi) developmental stages (Rudlaff et al., 2019).

Thus, the first intraerythrocytic stage after invasion is the ring form, which has been typically described as a thin, discoidal, flat shape. At the end of this stage, the parasite reduces its diameter and moves to a fixed position in the periphery of the

RBC. During this process, the digestive vacuole (DV) of the parasite (an acidic compartment also known as food vacuole where hemoglobin digestion takes place) gets bigger and it is clearly visible in the next stage of the cycle, the trophozoite stage. It is in the last phase of the trophozoite stage when the parasite starts the preparation for chromosome replication and initiates DNA synthesis and nuclear division (Arnot et al., 2011). The following developmental stage, the schizont, starts when two daughter nuclear bodies (the future merozoites) have been already formed; however, more mitotic replication cycles will be performed until the parasite accumulates tens of daughter merozoites, approximately from 16 to 32, (Kumar & Tolia, 2019), which end up occupying most of the volume of the host cell.

Once the replication cycles have finished, merozoites are ready for exiting the RBC. Merozoites egress is a tightly coordinated process in which the protein PKG (c-GMP-dependent protein kinase) plays a central role as it initiates a protease cascade that triggers the swelling of the PV and its subsequent fragmentation (Thomas et al., 2018). The next step of the process is the destabilization of the RBC cytoskeleton and the final rupture of the RBC membrane allowing the merozoites to leave the erythrocyte. Osmotic pressure after RBC membrane rupture triggers the egress of a small proportion of merozoites, while the rest of them exit the host cell a few seconds later due to the curling and buckling of the membrane of the RBC (Abkarian et al., 2011).

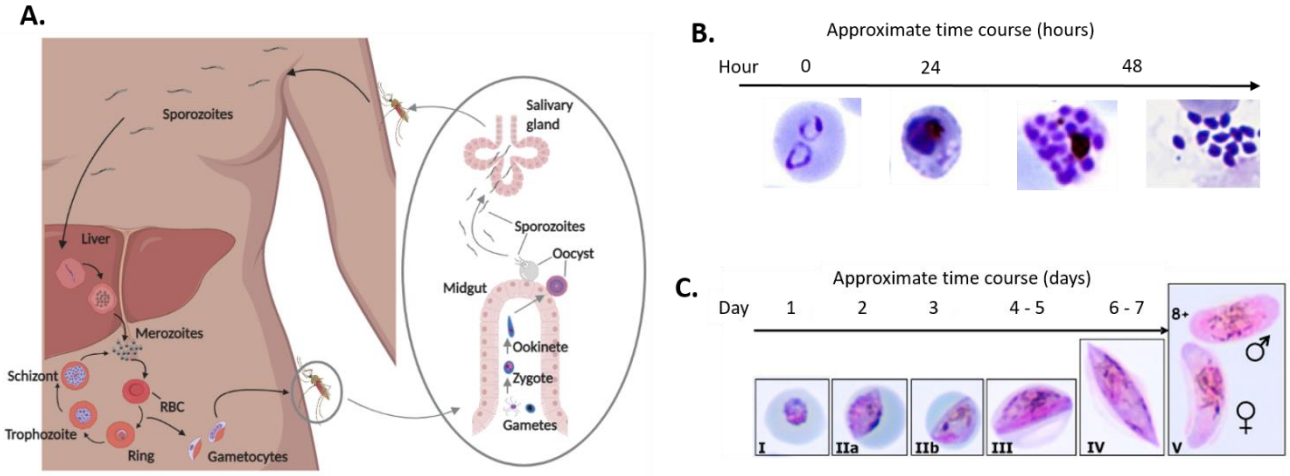

Figure 3. *A)* Plasmodium falciparum *life cycle in both human and mosquito hosts. Created with BioRender.com B) Asexual* Plasmodium falciparum *intraerythrocytic stages: rings, trophozoites, schizonts and merozoites. C)* Plasmodium falciparum *gametocytes stages: I, IIa, IIb, III, IV and V (male and female). Adapted from (Sutherland, 2009).*

After exiting the RBC, merozoites recognize, attach and invade new host cells (as previously described), thus perpetuating the intraerythrocytic parasite stage. Repeated cycles of erythrocytic invasion, growth and asexual replication quickly expand the parasite population among the RBCs of the human host.

Eventually, a variable, yet small number of blood-stage parasites differentiates into sexual forms, the gametocytes. It was proposed that this differentiation occurs during or before schizogony, as first observations showed that all merozoites inside a schizont will either continue with the asexual cycle or develop into gametocytes (Josling & Llinas, 2015). However, it was later observed that conditional activation of the main regulator of gametocytogenesis, the transcription factor AP2-G, can make individual asexual schizonts to produce a mixed progeny of both rings that express sexual markers and rings that do not express them (Bancells et al., 2019).

The trigger of gametocytogenesis by the parasite both in *in vitro* and *in vivo* conditions has been largely debated and associated to different kinds of environmental stresses, such as (i) high rate of asexual forms (Bruce et al., 1990); (ii) treatment with antimalarial drugs that target asexual forms of the parasite (Peatey et al., 2009); (iii) anemia (Sowunmi et al., 2008); (iv) host immune response activation (Bousema et al., 2006); (v) high proportion of young RBCs (Trager & Gill, 1992); (vi) oxidative stress affecting the endoplasmic reticulum of the parasite and its proteostasis (Chaubey et al., 2014); or (vii) conditioned culture medium (Brancucci et al., 2015).

Apart from the study of the factors triggering sexual conversion in *P. falciparum*, the molecular mechanisms underlying this process have also been explored during decades and, probably, the major finding in this regard was the discovery of the role of the transcription factor AP2-G as the master regulator of gametocytogenesis (Kafsack et al., 2014; Sinha et al., 2014). In asexual parasites, the *ap2-g* locus is epigenetically silenced (Brancucci et al., 2014; Coleman et al., 2014), but when the moment of gametocytogenesis arrives, the repression of the *ap2-g* locus is reverted allowing its transcription (Filarsky et al., 2018). Once transcribed, AP2-G is able to bind to its own promoter and to some others that regulate early gametocyte genes, and in this way *ap2-g* activation creates a positive regulation loop that boosts parasites' sexual conversion (Josling et al., 2020).

Once sexual conversion is started, *P. falciparum* gametocytes complete their maturation through five different phases (stages I-V) (Figure 3C) mediated by different transcriptional changes in each stage (van Biljon et al., 2019; Young et al., 2005). Stage I gametocytes are not morphologically distinguishable from asexual trophozoites but their transcriptional profile has already changed. From stage II to stage V, gametocytes remodel the host RBC and take different shapes. Male-specific genetic markers can be detected earlier (stage I-II) than female-specific ones (stage II-III) (van Biljon et al., 2019). However, the molecular mechanisms that regulate the differentiation in either male or female forms and how this process is triggered are still unclear.

After completing the whole maturation process, female and male gametocytes (stage V) can be ingested by a female *Anopheles* mosquito when it bites an infected human. Inside the mosquito, mature gametocytes are stimulated to form male and

female gametes that, after fertilization, give rise to a zygote, which in turn develops into a motile ookinete (Vinetz, 2005). The ookinete moves through the mosquito midgut wall and forms an oocyst. The oocyst undergoes various series of asexual replication and produces sporozoites, which, after the rupture of the oocyst, migrate to the salivary glands of the mosquito (Wang et al., 2005). During the next blood meal, the sporozoites accumulated in the salivary glands are injected into the human host, thus restarting the whole infection cycle.

→ *P. falciparum* life cycle starts when a parasitized female mosquito bites a human host and inoculates the sporozoites, which invade the liver and replicate to form thousands of merozoites. Merozoites enter the bloodstream and infect RBCs, in which they start a 48-hour replicative cycle, progressing through ring, trophozoite and schizont developmental stages to finally produce new merozoites that will invade new RBCs. Part of the invading parasites are able to develop into gametocytes that are taken by a mosquito when it bites the infected human and the whole process

1.2. Malaria pathology.

The best-known symptom of malaria is fever, which is also the first clinical sign of the disease when the incubation period is finished. This period lasts about twelve days in the case of *P. falciparum* malaria (Warrell, 2002) and it extends from the moment in which the patient is inoculated with the parasite by a mosquito to the outbreak of the first symptoms, produced when parasites have already reached RBCs after their maturation in the liver.

At first, in *falciparum* malaria, fever is usually irregular and appears with other symptoms such as fatigue, anorexia, epigastric discomfort and diarrhea (Bartoloni & Zammarchi, 2012) (Figure 4A). Later on, the progression of the disease produces in most of the cases the so-called “malaria paroxysms” (Figure 4B), which are composed by three phases (Crutcher & Hoffman, 1996): (i) a cold stage with shivers; (ii) a fever stage, reaching body temperatures as high as 41 °C from 2 to 6 hours, and (iii) a sweating stage in which the fever drops and the patient rapidly recovers its basal temperature. This febrile reaction is caused by the rupture in the bloodstream of mature schizonts at the end of the intraerythrocytic cycle. In *falciparum* malaria, the intraerythrocytic cycle is completed in 48 hours, so fever is supposed to occur every two days, although in many cases the periodicity of fever episodes is not as regular as expected (Crutcher & Hoffman, 1996).

Most times, these fever episodes together with mild symptoms are followed by the recovery of the patient. However, severe disease can be developed in some cases. Although complications of severe *falciparum* malaria have been traditionally divided

into three different clinical syndromes: (i) impaired consciousness or cerebral malaria, (ii) severe anemia, and (iii) respiratory distress (Marsh et al., 1995), we now know that other complications can appear as other organs can be affected by the infection. Roughly, parasitized RBCs (pRBCs) express different ligands on their surface that allow them to adhere to endothelial cells, leading to their sequestration in the vasculature of a target organ. This sequestration of pRBCs can trigger a fatal deregulated inflammatory response (Clark et al., 2004) damaging the brain (cerebral malaria), the spleen (severe anemia), lungs (respiratory distress), kidneys (acute kidney injury) (Moxon et al., 2020), and liver (Balaji et al., 2020), or producing a shock-like syndrome if the impaired inflammatory response is systemic (Schofield & Grau, 2005). Also, sequestration of parasites in the placenta was described more than twenty years ago (Fried & Duffy, 1996) and is responsible for placental malaria which mainly causes fetal growth restriction and pre-term birth (Brabin et al., 2004) but also higher morbidity of the disease during the first years of life (Schwarz et al., 2008) (Figure 4C).

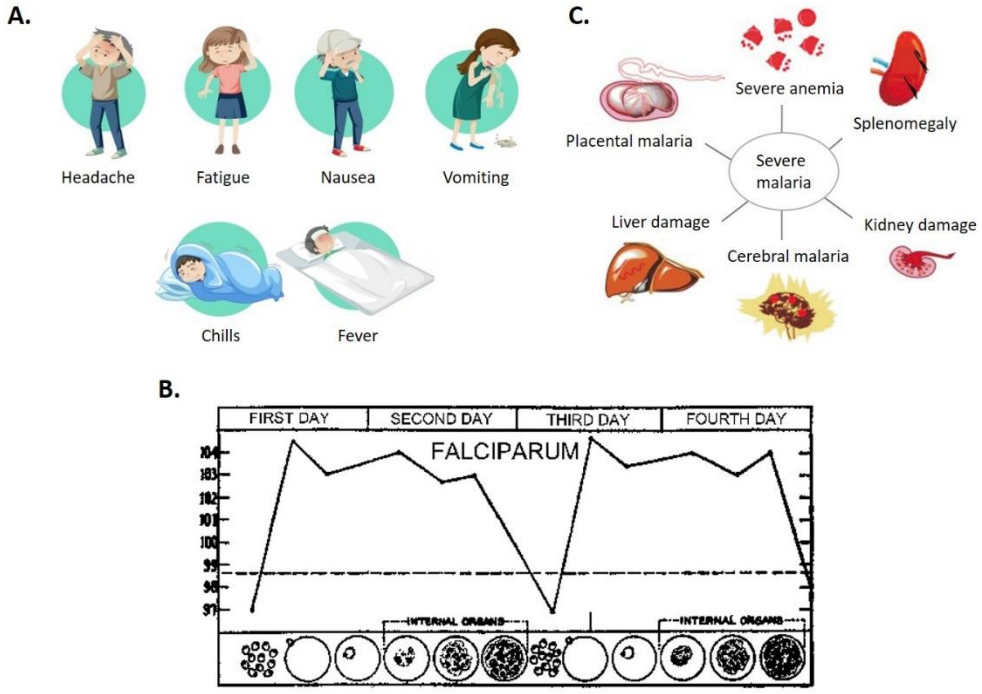

***Figure 4**. A) Malaria symptoms. Adapted from (brgfx) B) Malaria paroxysms graph. Adapted from (Neva & Brown, 1996) C) Affected organs in severe malaria. Adapted from (Balaji et al., 2020).*

1.3. Malaria prevention and diagnosis.

The fight against malaria starts with prevention. Preventive strategies encouraged by WHO are focused in either (i) using chemoprevention, specially to protect vulnerable groups, such as pregnant women and children or (ii) avoiding mosquitos' bite ((WHO), 2020). Vector control strategies are usually based on the use of long-lasting insecticides, which are used in bed nets and in indoor wall spraying. In

fact, the combination of those two strategies was estimated to have prevented 517 million cases of malaria from 2000 to 2015 in Africa (Bhatt et al., 2015). However, according to the WHO, the number of people protected worldwide against malaria with insecticide-based means dropped from 161 million in 2010 to 87 million in 2020 ((WHO), 2021c). Moreover, resistances to insecticides have already been detected, reducing the effectiveness of bed nets and indoor spraying (Hemingway et al., 2016). New ways of vector control have been explored, including the use of ivermectin, an endectocide with lethal effects on a wide variety of parasites and vectors (Omura & Crump, 2004), which has successfully been used in mass administration programs and has led to the almost eradication of onchocerciasis (Remme et al., 1990) and lymphatic filariasis (Ottesen et al., 2008). In the case of malaria, ivermectin possesses antiplasmodial activity (Panchal et al., 2014) and at the same time when it is orally administered to humans, it remains in the blood and is capable of killing the mosquito after its blood-meal (Chaccour et al., 2010).

Another prevention strategy that has largely been explored by the scientific community are vaccines. Until January 2022, 134 *falciparum* malaria vaccines clinical trials have been completed (NIH) without producing a definitive and full effective vaccine against the disease. Some attempts have been promising, like RTS,S/AS01, a pre-erythrocytic vaccine based on the repetition of a fragment of *P. falciparum* circumsporozoite protein together with three T-cell epitopes and the hepatitis B surface antigen (Laurens, 2020). RTS,S/AS01 was the first malaria vaccine tested in phase III clinical trials. However, the vaccine efficacy (proportionate reduction in disease among the vaccinated group) 20 months after administration was lower than 30% in infants from 6 to 12 weeks and lower than 45% in children from 5 to 17 months, with a quick waning of efficacy since 48 months after vaccination it dropped to less than 19% and 29% respectively (RTS, 2015).

As important as prevention is the rapid and accurate diagnosis of the infection. Microscopy observation of stained blood smears is still the preferred diagnostic method despite its numerous drawbacks, including the need of trained experts and the difficulty of detecting very low parasitemias (Fitri et al., 2022). An alternative to microscopy that has gained importance throughout the last decade are rapid diagnostic tests (RDTs), especially those based on the detection of histidine-rich protein 2 (Organization, 2018). These tests show the great advantage of being easy to use and providing results in a very short time. Nevertheless, RDTs only provide with qualitative data about the infection, i.e., they do not show the parasitemia of the sample, and false positives can be detected, especially when the parasite load in the blood is low (Samadoulougou et al., 2014). Parasite detection through polymerase chain reaction (PCR) is more a sensitive than microscopic observation and RDTs (Mfuh et al., 2019), which makes this technique more suitable for epidemiological studies and policy-driving surveys. However, its implementation in the clinical routine is difficult,

mainly because it is time-consuming and expensive. With the aim of reducing costs, pooling strategies consisting in mixing various samples in the same PCR reaction has been tested (Bharti et al., 2009). Efforts to design better diagnostic tools are continuously done with the objective of tackling the problems posed by the already in use techniques (Guasch-Girbau & Fernàndez-Busquets, 2021).

1.4. Malaria treatments and resistance development.

The number of antimalarial drugs that have had at some point clinical use together with those compounds described to show antimalarial potency is large, and thus I will focus here in those treatments currently recommended by the WHO. According to the last WHO report about malaria treatment (WHO, 2015), the recommended malaria treatments for uncomplicated malaria caused by *P. falciparum* are artemisinin-based combination therapies (ACTs). ACTs are a mixed treatment of an artemisinin derivative (usually artemether, artesunate or dihydroartemisinin) together with a drug from a different class with a longer half-life (e.g. lumefantrine, amodiaquine, mefloquine, piperaquine, sulfadoxine-pyrimethamine or pyronaridine) (WHO, 2021b). Many other compounds have been used to treat malaria in the past, but *Plasmodium* rapidly developed resistances to them (Figure 5A) (Haldar et al., 2018; Wicht et al., 2020), which is the leading reason for continuously searching new antimalarial agents.

1.4.1. Artemisinin derivatives (ARTs) and their resistances.

Artemisinin is a sesquiterpene lactone extracted from a plant called “sweet wormwood” (*Artemisia annua*). As early as in the 3rd century, *A. annua* beneficial effects against fever were described in a treatise of Chinese traditional medicine (Cui & Su, 2009). Much later, in 1967, the Chinese government launched “Project 523”, a national plan focused on finding new antimalarial drugs (Faurant, 2011). “Project 523” scientists identified 2000 plants with possible antimalarial effect in old Chinese medicine treatises including *A. annua*, which appeared to be the most effective one (F. Lu et al., 2019). Still, the concentration the active component of the plant (artemisinin) was highly increased by You-You Tu’s team in the early 70’s by extracting artemisinin with ether at low temperatures. This finding brought her a Nobel prize in 2015 (Foundation, 2019). After that, more stable and effective ARTs, such as artemether, artesunate and dihydroartemisinin (Tiwari & Chaudhary, 2020), were rapidly synthesized and chosen as the frontline treatment against *P. falciparum* uncomplicated malaria.

The mechanism of action of ARTs starts when they are activated inside the parasite’s cytoplasm and PV (Stocks et al., 2007) through the cleavage of their

endoperoxide bonds (Figure 5B). This cleavage is triggered by heme (J. Wang et al., 2015; S. Zhang et al., 2010), a molecule released during hemoglobin digestion, an essential metabolic pathway for the parasite. Once ARTs are activated they are able to alkylate heme itself (Meshnick et al., 1991), preventing its conversion into its non-toxic derivative, hemozoin. Instead, harmful free heme dimerizes and forms hematin, which causes lipid peroxidation in the parasite and the rupture of parasite's membranes together with a general oxidative stress affecting also to proteins and nucleic acids (Fitch et al., 1983; Gopalakrishnan & Kumar, 2015; Ismail et al., 2016). The alkylation process suffered by heme also affects *Plasmodium* proteins (Figure 5C); Ismail et al (Ismail et al., 2016) detected 79 alkylated proteins in *P. falciparum* after treatment with ARTs, and Wang et al. (J. Wang et al., 2015) detected 124 of them. These promiscuously alkylated proteins, which lose their function and structural stability, are related to many important processes for the parasite like protein biosynthesis, chaperone refolding of defective proteins or hemoglobin digestion (Ismail et al., 2016). Damaged proteins are usually targeted with ubiquitin and driven to the proteasome of the cell in order to be eliminated; in line with this, it has been shown that ARTs not only directly damage proteins leading to their unfolding but also inhibit the proteasome function (Bridgford et al., 2018) and a synergistic effect of ARTs with proteasome inhibitors has been described (Dogovski et al., 2015). This data points to an important deleterious effect of ARTs on parasites' proteostasis.

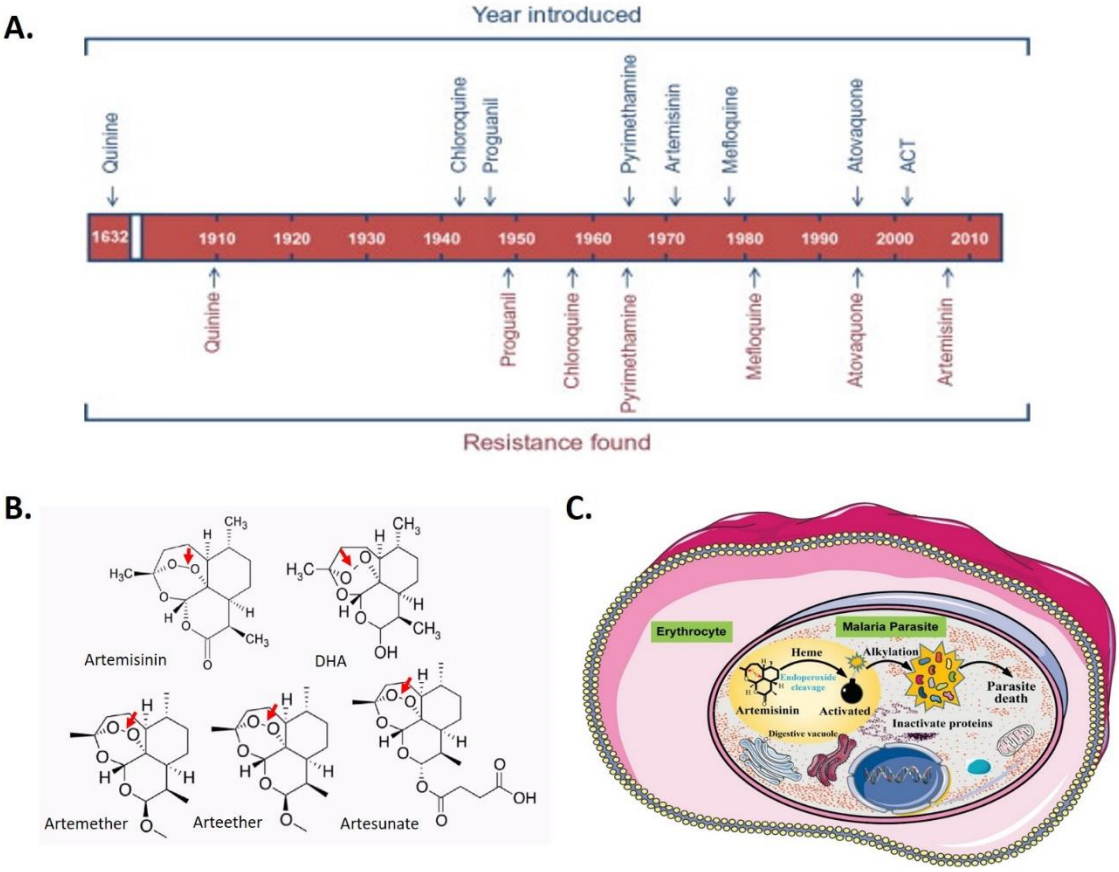

Figure 5. *A) Resistance evolution to antimalarial drugs. Taken from ("Progress in medicinal chemistry,"). B) Chemical structure of ARTs. Red arrows point endoperoxide bridges. Adapted from (B. W. Lu et al., 2019). C) ARTs mode of action. Taken from (Xie et al., 2020).*

ARTs resistance was firstly described in the early 2000s in *P. falciparum* isolates in Cambodia and other parts of Southeast Asia (Dondorp et al., 2009) (Figure 6A). This was considered one of the biggest threats in the whole history of malaria treatment. Resistant parasites were analyzed and various mutations in the gene *pfkelch13* (K13) impairing its function were proposed as responsible for ARTs resistance (Ménard et al., 2016). This was further corroborated by artificial manipulation of the gene in *in vitro* cultures (Straimer et al., 2015). K13 is involved in hemoglobin intake by the parasite and when it is defective, the parasite reduces its ability to endocyte hemoglobin, producing a reduction in heme availability; this prevents the activation of ARTs, conferring resistance to the parasite (Yang et al., 2019) (Figure 6B). However, further analysis of ARTs resistant parasites in different parts of the world showed that ARTs resistance is not only produced by mutations in *pfkelch13*, but more mutated genes were detected (Zhu et al., 2018) and ARTs resistance was associated with the up-regulation of genes involved in processes such as protein metabolism, unfolded protein binding, protein folding and protein export (Mok et al., 2015). In these cases, the mechanism leading to ARTs resistance would be explained as a better capacity of parasites to cope with the protein stress caused by activated ARTs (Mok et al., 2015) (Figure 6C).

Lastly, extracellular vesicles (EVs) have also been proposed as ARTs resistance mediators.As with the up-regulation of the unfolded protein response (UPR) in resistant parasites, vesiculation is enhanced (Bhattacharjee et al., 2018). Some voices speculate that those EVs could be loaded with misfolded proteins produced upon ARTs treatment that would be expelled from the parasite protecting it from their deleterious effects (Tandoh et al., 2021).

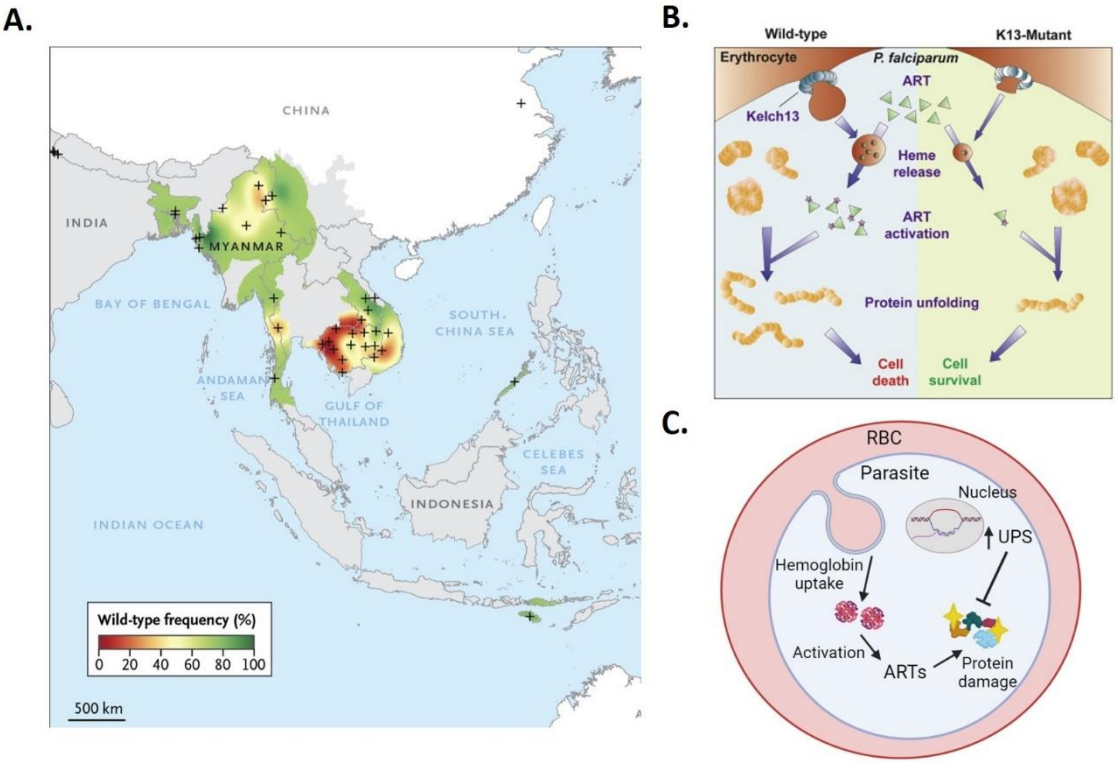

***Figure 6**. A) Distribution of ARTs resistance due to mutations in K13. Adapted from (Ménard et al., 2016). B) Mechanism of resistance to ARTs due to K13 mutations (Yang et al., 2019). C) Mechanism of resistance to ARTs explained by an up-regulation of the unfolded protein response (UPS). Created with BioRender®.*

1.4.2. Artemisinin partner drugs and their resistances.

1.4.2.1 Quinolines.

Quinolines included as part of ACTs by WHO are amodiaquine, mefloquine and piperaquine (Figure 7A). Amodiaquine and piperaquine are considered 4-aminoquinolines, whereas mefloquine is included in the group of quinoline methanols (Rawe & McDonnell, 2020a).

Quinine, extracted from the bark of the *Cinchona* tree, was the first effective antimalarial drug in Western medicine (Parhizgar & Tahghighi, 2017). Inspired by the chemical structure of quinine, chloroquine was firstly synthesized, together with other quinolines, in 1945 by a group of German scientists led by Hans Andersag (Figure 7B)

who, despite its good antimalarial activity, discarded chloroquine claiming that it was more toxic than quinacrine (Coatney, 1963; Krafts et al., 2012), the first-line antimalarial drug at that time. During World War II, the US captured some quinolines' formulations, re-discovered chloroquine and synthesized a bunch of analogues (Al-Bari, 2015). Since then, chloroquine was the most used antimalarial drug, both for malaria prophylaxis and treatment, for almost 40 years, when the first resistances to the drug started to appear (Hempelmann, 2007).

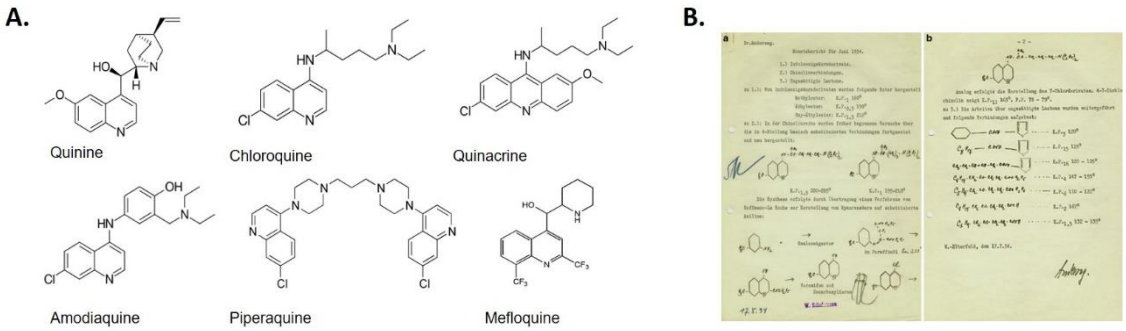

***Figure 7**. A) Schematic chemical structure of some aminoquinolines: quinine, chloroquine, quinacrine, amodiaquine, piperaquine and mefloquine. B) Hans Andersag's handwritten notes containing the synthesis process of chloroquine. Obtained from (Krafts et al., 2012).*

The target of 4-aminoquinolines inside the parasite is the hemoglobin digestion pathway (Figure 8A). 4-aminoquinolines are weak bases that accumulate inside the DV of the parasite due to the acidic pH of this compartment compared to the basic pH of the parasite's cytoplasm (Rawe & McDonnell, 2020a); there they are protonated, which renders them unable to exit the DV. In fact, analogues of effective 4-aminoquinolines that are not able to accumulate inside the DV lose their antimalarial potency (Hawley et al., 1998; Hawley et al., 1996). On the other hand, hemoglobin is physiologically digested in the DV so the parasite can obtain the amino acids required for its development inside the RBC (Rawe & McDonnell, 2020b). During hemoglobin digestion toxic heme groups are produced, which will bind together to form hematin, which will build hemozoin crystals (Francis et al., 1997), non-toxic structures for the parasite. 4-aminoquinolines have affinity to bind hematin and drug-hematin complexes are able to inhibit or slow down the formation of hemozoin crystals (Mungthin et al., 1998). In this way, the toxic subproducts of hemoglobin digestion cannot be detoxified and spread through different cellular structures of the parasite damaging them and leading to its death (Combrinck et al., 2013) (Figure 8B).

Quinoline methanols, like mefloquine, also inhibit hemozoin formation and heme detoxification by binding the hematin intermediate (Egan & Ncokazi, 2005). However they do not do it as potently as 4-aminoquinolines (Mullié et al., 2012),

mainly because quinoline methanols have one less protonable site than 4-aminoquinolines and they are not expected to be as effectively accumulated inside the DV (Olliaro, 2001). Some other proposed mechanisms of action of mefloquine are the tight interaction with phospholipids in *Plasmodium* membranes (Chevli & Fitch, 1982) and the inhibition of protein synthesis through direct interaction of mefloquine with *Plasmodium* 80S ribosome. The drug dramatically decreases its antimalarial effect when 80S ribosome amino acidic sequence is modified in the residues predicted to mediate the binding of the drug to the ribosome (Wong et al., 2017).

The first case of chloroquine resistance was reported in 1957 (Parhizgar & Tahghighi, 2017) in Southeast Asia (Figure 8C). In 2000, a genetic analysis of a *P. falciparum* chloroquine resistant strain showed that the mechanism underlying this resistance was a mutation in a transporter gene, *pfcrt*, which inhibited the accumulation of drug inside the DV (Fidock et al., 2000) by pumping the drug out from the vacuole (Martin et al., 2009). Later on, more mutations in *pfcrt* were found that explained not only chloroquine resistance but also amodiaquine and piperaquine resistances (Wicht et al., 2020). The other key protein in chloroquine resistance is PfMDR1, which is also a transport protein, but in this case PfMDR1 is predicted to interact with drugs in the cytosol and mediate their entrance inside the DV (Wicht et al., 2020). Mutations in *pfmdr1* cause resistance to chloroquine, amodiaquine and mefloquine (Atroosh et al., 2012; Price et al., 2004; Sanchez et al., 2008).

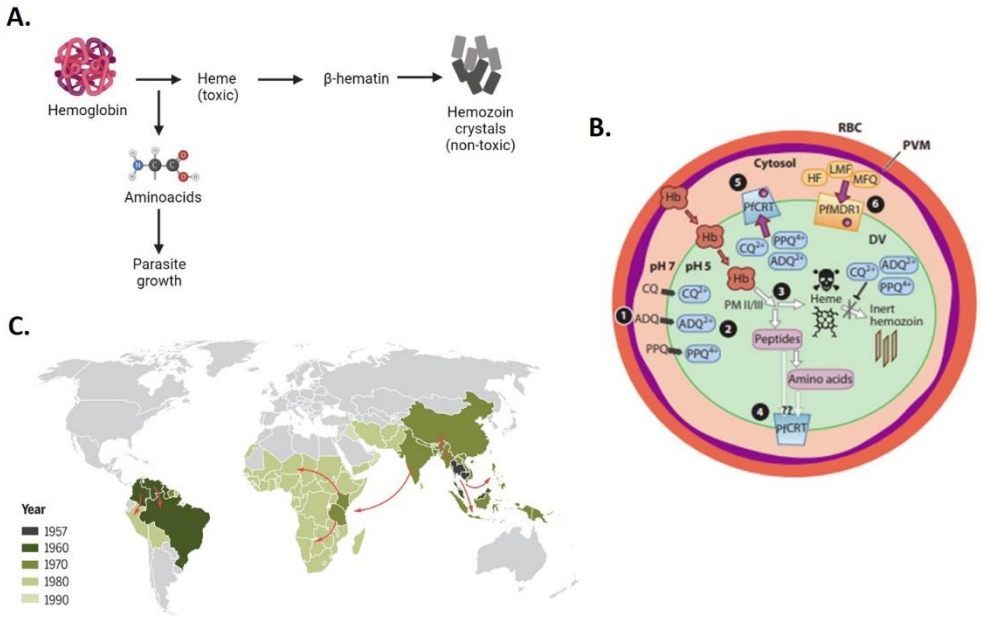

***Figure 8**. A) Hemoglobin metabolization pathway in* P. falciparum*. Created with BioRender®. B) Quinolines mechanism of action and resistances. CQ: chloroquine. ADQ:amodiaquine, PPQ:piperaquine, MFQ:mefloquine, LMF:lumefantrine, HF:halofantrine. (Wicht et al., 2020). C) Map of resistances to chloroquine (Roberts, 2016).*

1.4.2.2 Lumefantrine.

Lumefantrine is not a quinolone methanol but it is closely related to this family of compounds. It was discovered in 1976 thanks to the extension of the "Project 523", when a synergistic effect of lumefantrine and artemether was observed *in vitro* by scientists in the Chinese Academy of Military Medical Sciences (Cui & Su, 2009). They proposed the combination of lumefantrine and artemether as an effective antimalarial treatment in 1992 (Cui & Su, 2009), being in 2004 the first ACT accepted by the WHO (Premji, 2009). The most appealing characteristic of lumefantrine is its slow absorbance rate, which allows the drug to remain in the body for a longer time than its partner drug, artemether (Ezzet et al., 2000). Little is known about the mechanism of action of lumefantrine, but it has been shown that, similarly to quinolines, it inhibits hemozoin crystals formation and heme detoxification (Imbert Palafox et al., 2020; Stover et al., 2012).

Only one year after the WHO accepted lumefantrine-artemether as an antimalarial treatment, in 2005, a study conducted in Zanzibar showed the appearance of *P. falciparum* resistant parasites in malaria infected patients treated with the ACT (Sisowath et al., 2005). In this case, a quick clearance of parasitemia was achieved thanks to the effect of artemether, although in almost 25% of the patients a reemergence of the infection was observed from day 21 and a significant percentage of these resistant parasites carried the same mutation in the *pfmdr1* gene (Sisowath et al., 2005). Later on, mutations in *pfmdr1* and *pfcrt* genes producing artemether-lumefantrine resistance were found in other parts of the world (Humphreys et al., 2007; Somé et al., 2010). Genomic analysis of *in vitro P. falciparum* lumefantrine-resistant parasites generated by continuous exposure to the drug led to the identification of various genes differentially regulated in resistant parasites compared to the wild type strain, the majority of them involved in cellular transport processes and fatty acid synthesis (Mwai et al., 2012).

1.4.2.3 Sulfadoxine-pyrimethamine.

During their efforts to find a potent antimalarial drug during World War II, when chloroquine resistance was already a worrying event, the Americans produced some pyrimidine derivatives, like proguanil and pyrimethamine, which showed a good antimalarial activity but lost efficacy upon the rapid emergence of resistant parasites. Then, the idea of combining them with sulfonamides, like sulfadoxine (Venture) came up. Both sulfadoxine and pyrimethamine are folate antagonistic drugs. On one hand, sulfadoxine is a competitive inhibitor of the enzyme dihydropteroate synthase and on the other hand, pyrimethamine competitively inhibits the action of dihydrofolate reductase (Hyde, 2005). As they act at different points of the folate metabolism

pathway (Figure 9) their effects are synergistic (Sibley et al., 2001), producing a total blockade of the folate metabolism pathway, which, in physiological conditions, generates folate derivatives that are essential for the synthesis of purines, pyrimidines and methionine, which at the same time are needed for DNA and protein synthesis (Nzila et al., 2005).

An important characteristic of sulfadoxine and pyrimethamine is their long half-life, 116 hours and 81 hours respectively (Winstanley et al., 1997), which has been proposed as the main reason behind the quick resistance development to these drugs, as parasites are subjected to a constant pressure of the drug for a long time (Basco et al., 2000; Watkins & Mosobo, 1993). A paradigm of sulfadoxine-pyrimethamine resistance is Thailand, where resistance to the drugs appeared the same year, 1967, that they were introduced in the country (Wongsrichanalai et al., 2002).

Resistance to sulfadoxine-pyrimethamine is produced by various point mutations on the genes encoding the target enzymes of each drug: dihydropteroate synthase (*pfdhps*) and dihydrofolate reductase (*pfdhfr)* (Nzila et al., 2000; Wang et al., 1997).

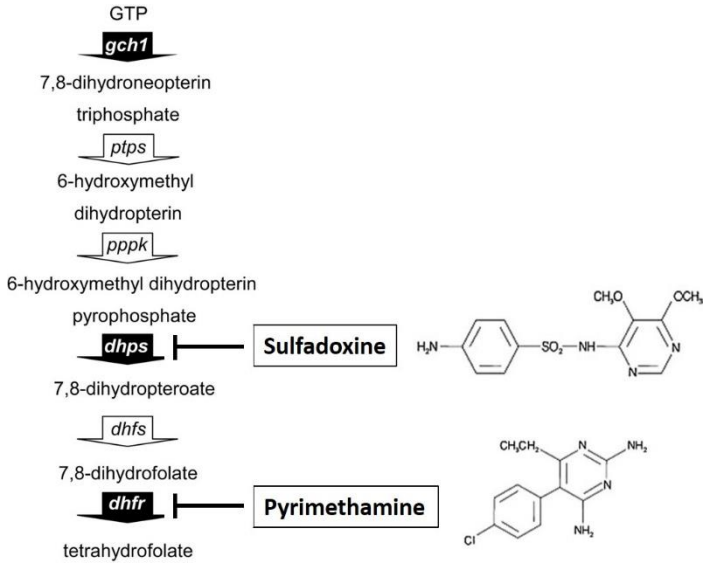

Figure 9*. Sulfadoxine and pyrimethamine chemical structures and folate metabolism pathway scheme showing the points where both drugs inhibit the process. Adapted from (Nair et al., 2008) and (Nnaemeka et al., 2015).*

1.4.2.4 Pyronaridine.

Pyronaridine was firstly synthesized by Chinese scientists in 1970 (Chang et al., 1992), when they were looking for new antimalarial drugs to overcome chloroquine resistance. They modified the quinacrine molecule by adding to it an aniline side-chain;

in this way they reduced the toxicity of the drug and engineered a new effective molecule against chloroquine-resistant parasites (Fu & Xiao, 1991). However, it was not until 2012 when the WHO included pyronaridine, in combination with artesunate, in the list of recommended antimalarial treatments (WHO, 2012).

Pyronaridine, as other similar compounds like aminoquinolines, is stored in the DV (Wu et al., 1988), where it has access to endocyted hemoglobin. Regarding its mode of action, pyronaridine forms complexes with β-hematin *in vitro* at the same ratio than chloroquine (Auparakkitanon et al., 2006). Pyronaridine binds to both ends of the forming hemozoin crystal inhibiting the addition of new β-hematin molecules and producing shorter crystals with conic ends in a process called "step bunching" (Sullivan, 2017).

Following the WHO recommendation in 2012, the use of pyronaridine-artesunate combination has shown promising results even in areas where artemisinin resistance has been massively detected, like the Greater Mekong region, where pyronaridine-artesunate has been successfully introduced in Vietnam (Quang Bui et al., 2020), Cambodia (Leang et al., 2016) and Myanmar (Han et al., 2020) among others. Furthermore, Pradines et al. (Pradines et al., 2010) used 23 *P. falciparum* strains obtained from different geographical sites that contained mutations in genes linked to quinolines resistance, like *pfcrt* and *pfmrp*, and none of the mutations present in these strains significantly affected the IC_{50} of pyronaridine. Even though no resistance to pyronaridine-artesunate has been reported yet in patients treated with the drugs, some voices claim that a resistance in the future could be developed as pyronaridine has been worldwide introduced very recently. In addition, when used against artemisinin-resistant parasites the parasitic clearance is slow, giving parasites more time to be exposed to pyronaridine and pushing the combined artesunate-pyronaridine treatment to strongly rely on pyronaridine alone (Quang et al., 2021). On the other hand, pyronaridine resistance has been found in *Plasmodium berghei*, a strain that infects mice, associated to alterations in the parasite's polyamine metabolism (Wu, 1988) or induced by the presence of an over-expressed protein of unknown function (Li et al., 1995). Having this in mind, a combination of artesunate and pyronaridine with a third antimalarial drug has been proposed in order to avoid the emergence of pyronaridine resistance in the future (White, 2019).

- → Malaria prevention strategies are useful but insufficient to fight the disease.
- → Until now, no vaccine has shown a clear protective effect against malaria infection.
- → Chemotherapies are the most useful tool nowadays against malaria, however rapid resistance development to most of them makes imperative a continuous effort towards the design of new treatments.
- → Artemisinin combination therapies (ACTs) are the recommended treatment for uncomplicated *falciparum* malaria by WHO.
- → ACTs target (i) parasite's hemoglobin metabolism; (ii) parasite's folate pathway; (iii) parasite's protein homeostasis by damaging proteins and inhibiting the proteasome.

2. Protein aggregation and *Plasmodium falciparum.*

2.1. Protein aggregation: an overview of a complex phenomenon.

The sequence of amino acids that form a protein is called primary structure. The secondary structure is the shape that an ensemble of amino acids adopts through the binding of its non-R groups. There are two main secondary structures: the β-sheet and the α-helix (Figure 10A). Both structures are formed when amino acids sequentially link their amino and carboxyl groups through a peptidic bond and are stabilized through hydrogen bonds. In the case of β-sheets, the polypeptide chains formed by peptidic bonds are aligned in such a way that one amino acid in a certain chain can bind through a hydrogen bond to the parallel amino acid (Bolognesi & Tartaglia, 2013). If one amino acid is bound to the two neighboring amino acids through peptide bonds, like in the β-sheet, but it is additionally bound to the third preceding and the third succeeding ones through hydrogen bonds, then the secondary structure will be a α-helix (Scholtz & Baldwin, 1992). The interactions among R groups of already structured amino acids give rise to the unique tertiary structure of the protein, which is formed by a combination of β-sheets, α-helices and unstructured regions. Finally, a protein can be formed by more than one subunit, which interact between them to form the quaternary structure of the protein (Floudas et al., 2006) (Figure 10B).

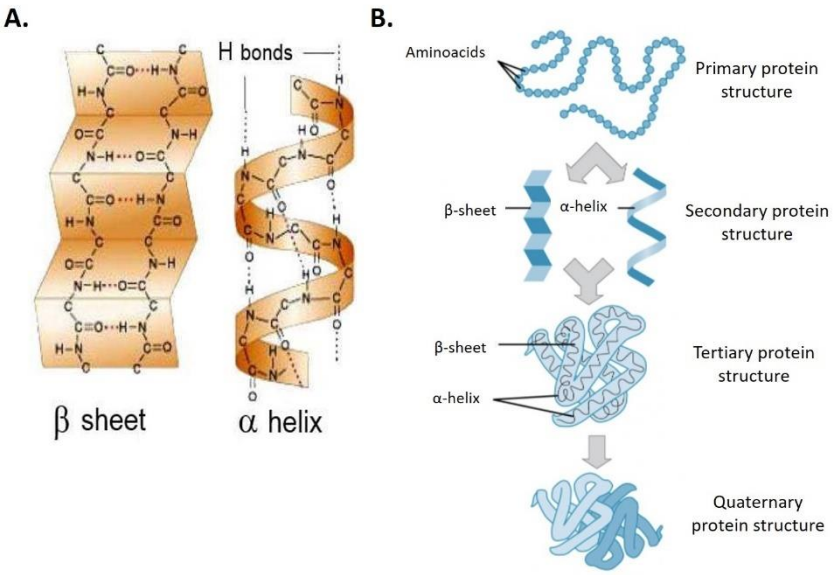

***Figure 10**. A) Schematic representation of β-sheet and α-helix structures. Hydrogen bonds (H bonds) are represented with dashed lines (di Marco, 2012). B) Primary, secondary, tertiary and quaternary structures of proteins. Adapted from (Molnar & Gair, 2015).*

The formation of the final native structure of a protein is accomplished through a folding process, which is a matter of energy. As previously mentioned, the final structure of the protein is obtained thanks to bonds among its amino acids. By means of these bonds, proteins fold and reach their lowest-energy conformation, which is the most stable and ordered one (Figure 11A). Folding consists in a trial-error process in which many random contacts between amino acids are tested and some intermediate structures appear until the native one is reached (Dobson, 2003). However, protein aggregates are extremely stable conformations in energetic and entropic terms, even more than natively folded proteins (Raskatov & Teplow, 2017) (Figure 11A).

In the cell, proteins are usually correctly folded, adopting an appropriate and functional tertiary and/or quaternary structure. However, the folding process can go wrong and proteins end up being misfolded. Misfolded proteins, as proteins with unstructured regions, expose their hydrophobic sites, which are otherwise buried and protected from the environment in the inside core of the protein. Hydrophobic areas present in the same or different proteins can easily interact with each other, promoting aggregation (Siddiqi et al., 2017) (Figure 11B). Nevertheless, this does not mean that only misfolded or unstructured proteins have the ability to form aggregates. Natively folded proteins can also end up aggregating, mainly due to disruptions of their native conformation that increase their free energy, making them unstable and promoting the transition to an aggregated precursor first and to a mature protein aggregate afterwards (Chiti & Dobson, 2009). There are many factors that trigger the transition of a protein from a native stable folded state to an aggregated one, e.g. protein and solvents concentration inside the cell, pH changes or temperature leaps (Li et al., 2010; Liu et al., 2017).

On the other hand, hydrophobic interactions are not the only ones responsible for protein aggregation, since other weak noncovalent bonds, like hydrogen bonds, Van der Waals and electrostatic forces, as well as covalent linkages, participate in the formation of protein aggregates (Andya et al., 2003; Karshikoff, 2021). But protein aggregates are not only diverse in terms of the interactions building them; Mahler et al. (Mahler et al., 2009) propose a classification of protein aggregates attending to four factors: type of bond, structure (fibrillar or amorphous as well as made of native folded proteins or misfolded ones), reversibility, and size (from small soluble oligomers to large insoluble structures).

One of the most studied aggregation forms are amyloids, since they have been associated to multiple pathological conditions, such as Alzheimer's disease (Selkoe, 1991), Parkinson's (Braak & Braak, 1990) or type II diabetes (Johnson et al., 1989). Amyloids are highly ordered aggregative fibers ranging from 10 nm to 10 μm (Alam et al., 2017) formed by β-sheets that run parallel along a straight axis and that are tightly packed against each other (Salvatella, 2013). Because the associations between β-sheet chains are mediated by hydrophobic interactions and hydrogen bonds, proteins

participating in the formation of the amyloid fiber expose unsatisfied hydrogen bonds and/or hydrophobic amino acids (Salvatella, 2013), and this is why misfolded and disordered proteins show a tendency to form amyloids.

The mechanism of amyloid formation (Figure 11C) is well established and involves two nucleation processes and an elongation step. Primary nucleation consists in the recruitment of the first protein monomers, which interact between them and form a nucleus that will further attract more monomers that elongate the fiber (Jarrett & Lansbury, 1993). Afterwards, a secondary nucleation can occur if (i) the fiber is fragmented, creating new aggregation nuclei, or (ii) new monomers are recruited on the sides of the already formed fiber creating a branched structure (Knowles et al., 2009).

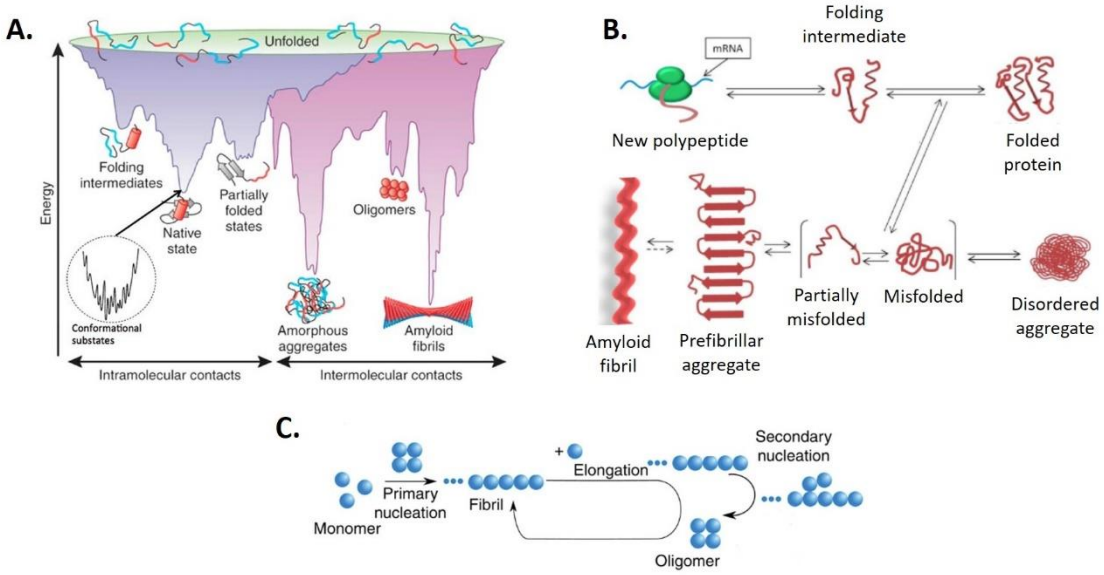

***Figure 11**. A) Energy during different steps of protein folding (Raskatov & Teplow, 2017). B) Process of protein folding, misfolding and aggregation in the cell (Alam et al., 2017). C) Formation of amyloid fibrils (Arosio et al., 2016).*

The prediction of amyloid formation and/or amorphous protein aggregation has attracted the interest of the scientific community for many years giving rise to a considerable number of predictive tools (Prabakaran et al., 2021; Saravanan et al., 2020) (Figure 12). The ten different tools shown in figure 12 are only a small selection of all the available algorithms and programs that have been designed and trained in order to predict the propensity of a certain peptidic sequence to aggregate. These predictors check either the aminoacidic composition of the input sequences (sequence-based) or their structure if it has been determined elsewhere (structure-based). Sequence-based predictors are the most common ones and can be classified according to the type of data in which they base their predictions (Santos et al., 2020):

(i) phenomenological algorithms use experimental data of amin oacid sequences aggregated *in vitro*; (ii) theoretical programs assess different features known to be related with protein aggregation and amyloid formation (e.g. β-sheet enrichment, hydrophobicity, or packing density); (iii) machine learning-based predictors use artificial intelligence systems to identify characteristics related to amyloids and protein aggregates formation; (iv) consensus programs compare and trim the data obtained from two or more predictors and transform it into a unique output.

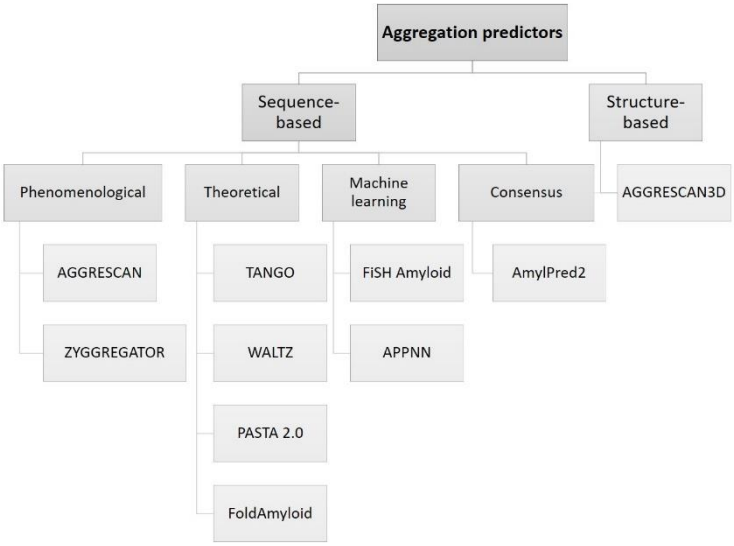

***Figure 12**. Selection and classification of protein aggregation predictive tools based on Santos et al., 2020 (Santos et al., 2020).*

→ Protein structure is formed by α-helices, β-sheets and unstructured regions.
→ Proteins need to be properly folded to perform their physiological functions, but sometimes they end-up being misfolded and aggregating.
→ Natively folded proteins can also form aggregates.
→ One of the most studied aggregation structures are amyloid fibrils, highly stable structures formed by packed β-sheets.
→ There are tens of aggregation predictors used to study the propensity of a certain amino acidic sequence to form amyloid fibrils and amorphous aggregates.

2.2. *Plasmodium falciparum* proteome and its aggregative features.

When the *P. falciparum* genome was fully sequenced in 2002 (Gardner et al., 2002), it was striking to see that it was extremely biased in adenine (A) and thymine (T) nucleotides, which make up an 81% of the whole genome, only comparable to the 77.4% of *Dictyostelium discoideum* (Eichinger et al., 2005) and the 71.4% of the

chromosome of *Borrelia burgdorferi* (Fraser et al., 1997). In accordance to this, a big number of *P. falciparum* genes contain poly-A tracks, this is repetitions of 12 or more As (Pavlovic Djuranovic et al., 2020). In *P. falciparum*, codons enriched in A nucleotides tend to be translated into a particular amino acid: asparagine (N), which comprises 11.3% of all amino acids in the parasite's proteome (Filisetti et al., 2013).

The abundance of asparagine in *P. falciparum* caused by the overrepresentation of A/Ts in its genome leads to an enrichment in the proteome of N repeats. These N repeats form low complexity regions (LCRs), which are defined as areas of the proteome with a poor diversity in its aminoacidic composition. LCRs can be formed by a limited set of amino acids consecutively repeated one after the other or by repetitions of only one amino acid (homorepeats). In *P. falciparum* 34% of genes encode one or more homorepeats and 73% of those are formed by N residues (Chaudhry et al., 2018) (Figure 13 A). Looking at LCRs in general terms, *P. falciparum* continues being an exception: whereas in most eukaryotes around 50% of proteins contain LCRs and they are rich in glutamine, in *P. falciparum* this percentage rises to almost 90% and asparagine is the most represented amino acid in them (DePristo et al., 2006) (Figure 13 B).

LCRs usually present a disordered tertiary structure, i.e. they do not fold themselves in the three dimensional plane and can adopt different conformations, depending on their interaction with other molecules and environmental conditions (Romero et al., 2001). In fact, in *P. falciparum* there is an almost 50% overlap between LCRs and intrinsically unstructured regions previously described in other organisms (DePristo et al., 2006). It is known that disordered polypeptidic regions, like LCRs, due to their conformational plasticity, play a crucial role in protein misfolding processes, which in turn can lead to protein aggregation and/or amyloid formation (Breydo & Uversky, 2011; Iadanza et al., 2018). Indeed, robustly structured globular proteins tend to hide their disordered regions keeping them in their part so they cannot be accessible to other proteins neither be affected by environmental factors that could lead to their aggregation (Linding et al., 2004).

On the other hand, there is strong evidence that N and glutamine (Q) stretches have a propensity to aggregate and end up forming amyloid fibrils and aggregated insoluble structures (Halfmann et al., 2011; Perutz et al., 2002). *In vivo*, in the yeast prion protein Sup35, the loss of N and Q residues in its prion domain leads to a defective and slow fibril formation (Derkatch et al., 2004; Liu et al., 2007). *In vitro,* the comparison between two polypeptides formed by 24 consecutive residues of either N or Q showed that, despite both of them were able to form amyloid fibrils, the N polypeptide aggregated much more rapidly and formed bigger structures than the Q polypeptide (Lu & Murphy, 2015) (Figure 13 C).

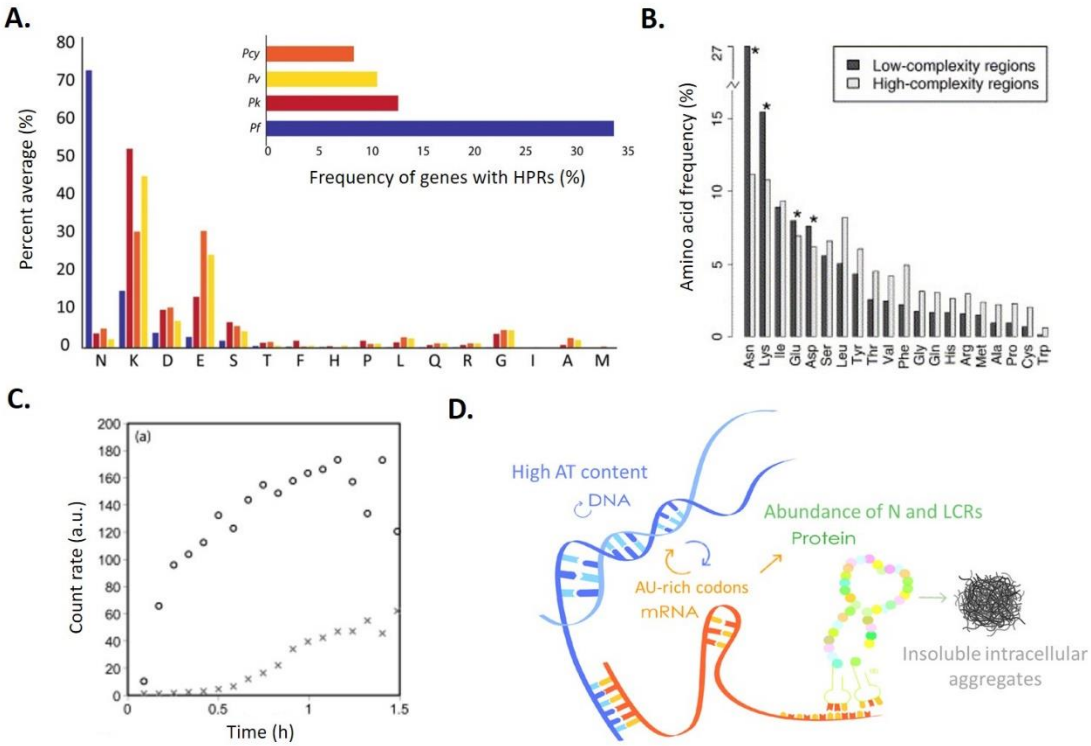

Figure 13*. A) On top, percentage of genes containing homorepeats (HPRs) in Pcy (*P. cynomolgi*), Pv (*P. vivax*), Pk (*P. knowlesi*) and Pf (*P. falciparum*). Bottom, percentage of amino acids forming homorepeats in different* Plasmodium *species. Adapted from (Chaudhry et al., 2018). B) Percentage of amino acids in* P. falciparum *low-complexity regions and high-complexity regions. Asterisk marks those amino acids more present in LCRs than HCRs (DePristo et al., 2006). C) Plot showing the aggregation rate of polypeptides formed by N repeats (white circle) and Q repeats (crosses) measured by light scattering. Adapted from (Lu & Murphy, 2015) D) Hypothesis of protein aggregation in* P. falciparum*. Adapted from (Zhang, 2017).*

Taken together, the high proportion of LCRs present in the *P. falciparum* proteome and its abundance in N amino acids, suggest a tendency of *P. falciparum* proteins to aggregate. Actually, a search of stretches of 80 or more Q/N residues in the *P. falciparum* proteome showed that approximately 24% of all proteins in the parasite contain this kind of aggregation-prone structures (Singh et al., 2004). A more stringent strategy, in which long stretches of Q/N residues were analyzed in order to select those with a clear similitude to *bona fide* prions and containing amyloidogenic sequences predicted to self-aggregate in physiological conditions, indicated that 10% of all *P. falciparum* proteins had a high intrinsic aggregation propensity (Pallarès et al., 2018).

It is clear now that, theoretically, the *P. falciparum* proteome has a tendency to aggregate due to its high proportion of LCRs, its abundance in N amino acids (Figure 13 D), and the presence in its proteome of predicted aggregation-prone proteins. Going further in the characterization of aggregative proteins present in *P. falciparum*, live

parasite cultures are positively stained with PROTEOSTAT®, a commercial dye that specifically binds protein aggregates (Pallarès et al., 2018).

→ *P. falciparum* genome is extremely biased in A/T nucleotides (81%).
→ In *P. falciparum*, codons enriched in A nucleotides tend to be translated into asparagines.
→ LCRs are abundant in *P. falciparum* proteome and they are mostly composed of asparagines.
→ N-rich regions as well as LCRs tend to form protein aggregates like amyloid fibrils.
→ Protein aggregation has been detected in *P. falciparum* both *in silico* and in live cultures.

2.2.1. Protein biosynthesis and protein homeostasis in the *Plasmodium falciparum* intraerythrocytic cycle.

Protein biosynthesis starts in the nucleus, where the genetic information encoded in the DNA is transcribed into mRNA, whose codons, triplets of nucleotides, will be further translated into amino acids in order to form the final protein product. In eukaryotes, translation has three phases: (i) initiation, mediated by eukaryote initiation factors (eIF), (ii) elongation, assisted by eukaryote elongation factors (eEF), and (iii) termination, mediated by eukaryote release factors (eRF). During initiation, mRNA molecules to be translated are embraced by ribosomes and the first amino acid of the future protein is transported by a specific tRNA to the translation complex. Afterwards, elongation consists in the scanning of the mRNA by ribosomes and the addition of new amino acids to the nascent polypeptide chain. Finally, termination occurs when ribosomes reach the STOP codon of the mRNA and the synthesized protein is released from the translation complex (Kozak, 1999, 2005) (Figure 14A).

Even though there are some similarities between the translation machinery of *P. falciparum* and other eukaryotes, the biased content in A/Us of the parasite transcriptome has led to some adaptations in many important translation participants, such as ribosomes. Long repeats of A nucleotides tend to slow down and even stall translation mainly because (i) amino acids required in this kind of regions interact with the ribosome exit channel clogging it (Arthur et al., 2015) and (ii) A/U repetitions tend to adopt a helical conformation that disrupt ribosome sliding from one codon to the next one (Tesina et al., 2020). Despite that, *P. falciparum* ribosomes are much more efficient and show higher fidelity rates when translating enriched A regions than those of other organisms, such as *Saccharomyces cerevisiae*, in which the expression of chimeric ribosomes containing *P. falciparum* rRNAs increased the translation accuracy and the growth rate of the yeast (Velichutina et al., 1998). In fact, *P. falciparum*

ribosomes are morphologically adapted to A/U repeats: they present a wider exit channel and a lower number of hydrophobic areas than other eukaryotes' ribosomes (Pavlovic Djuranovic et al., 2020).

No matter how efficient an organism's translation is, errors can happen, and this is why eukaryotes have developed three different systems to check their translation processes: **n**on-sense **m**ediated **d**ecay (NMD), **n**o-**g**o **d**ecay (NGD), and **n**on-**s**top **d**ecay (NSD). All these systems target the mRNA molecules where the translational machinery has stuck and promote the disassembling of the complex and the degradation of the mRNA (Erath et al., 2019). Even though some components of those systems have been predicted by homology in *P. falciparum*, key elements of these regulatory pathways are lacking in the parasite (Hughes et al., 2010), suggesting that the mRNA regulatory machinery in *P. falciparum* is far from being as complex and complete as its counterpart in other eukaryotes.

In other organisms, such as yeasts, the lack of functional mRNA translation surveillance systems leads to aggregation of the aberrant synthesized proteins causing proteotoxic stress (Choe et al., 2016; Jamar et al., 2018, 2021). Besides its poor translational regulatory machinery, protein homeostasis and aggregation in *P. falciparum* is also challenged by other aspects like (i) the constant need of newly synthesized proteins due to the parasite's complex life cycle and high replication rate, (ii) the temperature stress caused by the differences in the body temperatures of its two hosts (including fever periods in the human), and (iii) a large amount of proteins that need to pass through the endoplasmic reticulum (ER) in order to be exported to their final destination (Rathore et al., 2015). Interestingly, parasites are perfectly viable despite their weak translation surveillance systems, their aggregation-prone proteome and the numerous threats to their protein homeostasis.

There are three key elements in *P. falciparum* that play crucial roles in preserving its proteostasis: (i) the unfolded protein response (UPR), (ii) heat shock chaperone proteins, and (iii) the ubiquitin-proteasome system (UPS).

→ *P. falciparum* has adapted its translation machinery to its A/T rich genome.
→ *P. falciparum* lacks mRNA translation surveillance systems.
→ There are three systems that regulate proteostasis in *P. falciparum*: UPR, UPS and heat shock proteins.

2.2.1.1. *Plasmodium falciparum* unfolded protein response.

The ER is involved in many processes related to protein homeostasis, such as synthesis, modification, release and translocation of secreted and transmembrane proteins (Galluzzi et al., 2017). The physiological functions of the ER can be perturbed

by different kinds of stresses, e.g. oxidative stress, increase in protein translation rates, nutrient depletion or hypoxia (Chen & Cubillos-Ruiz, 2021) (Figure 14B). When this happens, misfolded and unfolded proteins accumulate in the ER triggering ER stress, which will activate the UPR in order to recover the normal functioning of the organelle.

In mammals, UPR is activated through three different pathways: IRE1, PERK and ATF6, and all of them are switched on by the same master regulator, the chaperone BiP (immunoglobulin heavy chain binding protein) (Galluzzi et al., 2017). In *P. falciparum*, a comparative evolutionary study (Gosline et al., 2011) showed that the parasite lacks IRE1 and ATF6 pathway components, whilst protein domains similar to PERK, eIF2α and BiP, the three main participants in the PERK pathway, were found. In fact, in *P. falciparum* three eIF2α kinases had been detected: IK1 (Fennell et al., 2009), IK2 (M. Zhang et al., 2010) and PK4 (Möhrle et al., 1997). The final outcome after eIF2α phosphorylation is the recovery of ER functions by means of a slowing down in protein translation as well as the activation of a specific transcription factor (ATF4) that promotes chaperones activation, protein degradation and antioxidants production (Gardner et al., 2013). However, in *P. falciparum* there's no ATF4, and thus, only the slowing down of protein translation can be assumed to happen (Figure 14C).

P. falciparum UPR has been proposed as a therapeutic target and, for instance, molecules that inhibit the parasite's BiP function show antimalarial activity in the same range as chloroquine (Chen et al., 2018). Furthermore, one of the known modes of actions of DHA is causing an excessive ER stress, provoking a prolonged activation of the parasites' PK4-eIF2α system (Bridgford et al., 2018)

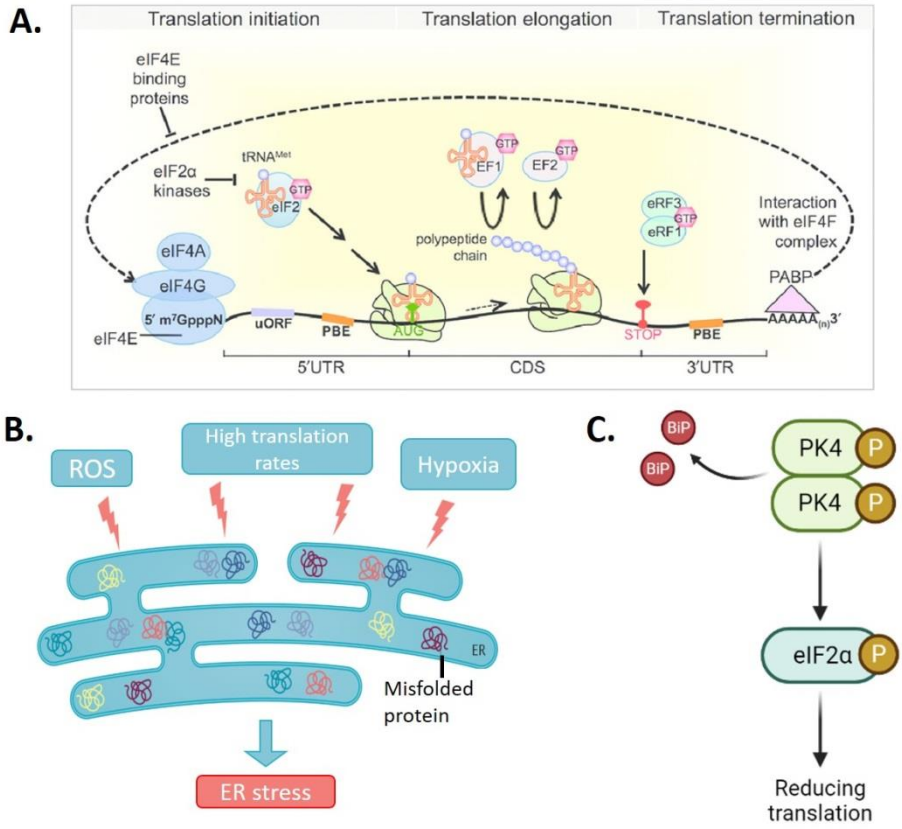

Figure 14*. A) Translation process in* P. falciparum *(Vembar et al., 2016). B) Schematic drawing of ER stress generators and misfolded protein accumulation. Adapted from (Chen & Cubillos-Ruiz, 2021) C) Scheme of the UPR mediated by PK4 and eIF2α in* P. falciparum*. Created with BioRender.*

2.2.1.2. *Plasmodium falciparum* heat shock proteins.

Heat shock proteins (Hsps) are the largest family of chaperones in nature and they are highly conserved among evolutionary distant organisms (Freilich et al., 2018). Chaperones directly interact with proteins in order to (i) promote their correct folding while they are being translated in the ribosomes, (ii) refold misfolded proteins, (iii) prevent protein aggregation, (iv) disaggregate already aggregated proteins, and (v) deliver aggregated or misfolded proteins to cellular degradation systems (Camberg et al., 2013) (Figure 15A). To avoid aberrant interactions during the folding process of proteins, chaperones protect the exposed hydrophobic sites of their client proteins by binding them in a reversible way (Balchin et al., 2020) through their middle domain's hydrophobic patch (Meyer et al., 2003). For more complex processes, involving the change in conformation of the proteins, Hsps need to co-operate with other chaperones or assistant proteins (chaperonins and cochaperonins) as well as to obtain energy provided by ATP hydrolysis, thus Hsps usually contain an ATPase domain and/or a site to interact with other chaperones (Blatch & Shonhai, 2014).

The *P. falciparum* genome encodes the non-depreciable number of 92 chaperones (Acharya et al., 2007) divided in the typical five different sub-classes according to their molecular weight: Hsp90, Hsp70 (containing the Hsp110 subgroup) (Figure 15B), Hsp60, Hsp40 and other small Hsps (Blatch & Shonhai, 2014). These Hsps are constitutively active and present in different cellular compartments; however, different stresses causing protein misfolding or affecting protein translation, like heat stress (Day et al., 2019; Lu et al., 2020), hyperoxia (Pallavi et al., 2010) or starvation (Torrentino-Madamet et al., 2011), provoke an upregulation of the Hsp network. Oxidative stress also enhances Hsps expression, in this case in a coordinated way with antioxidant enzymes (Akide-Ndunge et al., 2009).

In other eukaryotes, the rapid Hsps up-regulation upon heat shock and other stressors is mediated by heat shock factor 1 (HSF1) (Jolly et al., 1997), a transcription factor that is not present in *P. falciparum*. However, *P. falciparum* is perfectly able to stabilize its N-rich proteome and this is mainly thanks to its chaperones. For instance, PfHsp70-x shows more affinity to bind N-rich polypeptides than polypeptides containing other types of amino acids (Mabate et al., 2018). Also, ablating PfHsp70-z function in parasites leads to their death due to an accumulation of protein aggregates inside the parasite (Muralidharan et al., 2012). Moreover, *P. falciparum* Hsps maintain parasite's proteostasis in a more efficient way than other organisms' Hsps. As an example, PfHsp70-z was proved to avoid protein aggregation of *P. falciparum* N-rich proteins *in vivo* by 10-15 fold after heat shock, whereas human and yeast Hsp70-z orthologs only prevented it by 2-3 fold (Muralidharan et al., 2012). The question then is, how *P. falciparum* activates its Hsp network without HSF1? Tintó-Font et al. (Tintó-Font et al., 2021) analyzed heat-shock resistant and sensitive *P. falciparum* lines and discovered a mutation in an AP2 transcription factor that precluded a proper heat-shock response, making parasites more vulnerable to high temperature pulses. This transcription factor, PfAP2-HS, directly up-regulated the translation of *hsp70-1* and *hsp90*, setting up a rapid front-line response needed to keep the parasites alive (Figure 15C). Furthermore, parasites lacking a functional PfAP2-HS were more sensitive to the toxic effect of dihydroartemisinin and epoxomicin, two drugs that act through the disruption of the parasite's proteostasis by promoting protein aggregation and/or blocking the activity of the proteasome.

P. falciparum Hsps have been tested as therapeutic targets with promising results. Hsp90 has been targeted by geldanamycin and other novel compounds that interfere with the ATPase domain of the chaperone blocking its activity and inhibiting *P. falciparum* growth at low micromolar concentrations (Banumathy et al., 2003; Everson et al., 2021). Also, Hsp70 ATPase activity has been shown to be reduced when treating *P. falciparum* cultures with antimalarial compounds of the family of pyrimidinones (Chiang et al., 2009).

A.

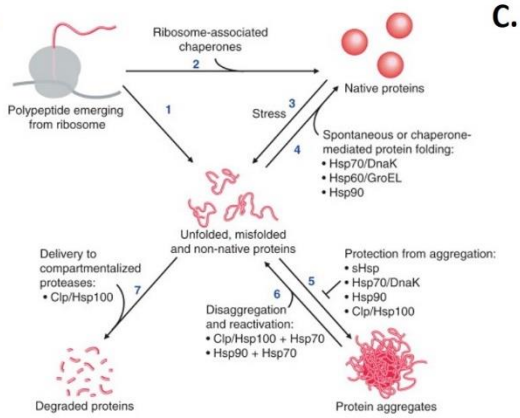

C.

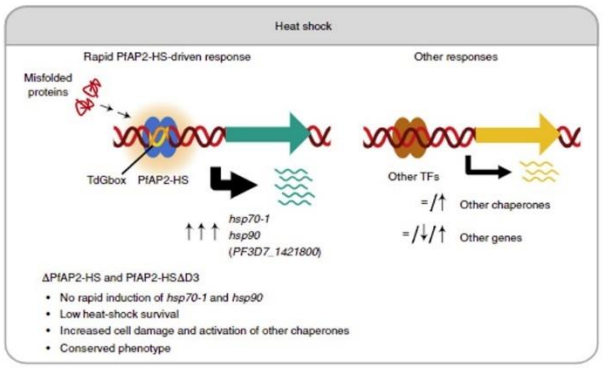

B.

Group	Subgroup	Name	Gene	Cellular Localization
Hsp90		PfHsp90_C	PF3D7_0708400	Cytoplasm, plasma membrane
		PfHsp90_ER	PF3D7_1222300	ER
		PfHsp90_A	PF3D7_1443900	Apicoplast, ER
		PfHsp90_M	PF3D7_1118200	Mitochondria
Hsp70		PfHsp70-1	PF3D7_0818900	Nucleus, cytoplasm
		PfHsp70-2	PF3D7_0917900	ER
		PfHsp70-3	PF3D7_1134000	Mitochondria, Maurer's clefts
		PfHsp70-x	PF3D7_0831700	Exported to host cell, Maurer's clefts, PV
	Hsp110	PfHsp70-y	PF3D7_1344200	ER
		PfHsp70-z	PF3D7_0708800	Cytoplasm

Figure 15. *A) Chaperones' cellular functions. Extracted from (Camberg et al., 2013). B) Members of Hsp90 and Hsp70 chaperones families in* P. falciparum*. C)* P. falciparum *heat shock response system induced by PfAP2-HS in wild type conditions or in parasite's strains without a functional PfAP2-HS (ΔPfAP2-HS and PfAP2-HSΔD3). Extracted from (Tintó-Font et al., 2021).*

2.2.1.3. *Plasmodium falciparum* ubiquitin-proteasome system.

The ubiquitin-proteasome system (UPS) is responsible for the degradation of misfolded or aberrant proteins as well as of proteins that are no longer needed by the cells (Bard et al., 2018). The typical eukaryotic proteasome (26S proteasome) is a large proteinase complex formed by the 20S core part and one or two 19S caps. The 20S proteolytic part is composed of two ring-shaped heptamers formed by 7 β subunits flanked by two other ring-shaped heptamers formed by 7 α subunits, altogether these four heptamers form a barrel-like structure (Figure 16A) that is covered in one or two of its sides by 19S regulatory particles (Tanaka, 2009). The 20S core part contains six proteolytic sites that degrade the client protein (Figure 16A), whereas the 19S regulatory part is responsible for recognizing, unfolding and inserting the protein to be degraded inside the 20S channel (Bard et al., 2018).

In *P. falciparum*, the 20S proteasome has been experimentally isolated in its free form, single or double-capped by 19S subunit(s) (Sessler et al., 2012; L. Wang et al., 2015) and forming complexes with a different regulatory cap, PA28 (Xie et al., 2019).

Proteins that need to be degraded in the proteasome are recognized by chaperones and tagged with at least four ubiquitin molecules. Ubiquitin is a small protein, well conserved across eukaryotes (Figure 16B), which covalently binds other proteins through seven lysine residues (L. Wang et al., 2015). The attachment of ubiquitin to target proteins is achieved thanks to the sequential action of three types of enzymes: E1, E2 and E3, and it finishes with the addition of the ubiquitin molecule to the protein (Callis, 2014). When ubiquitin lysine 48 is the amino acid forming the covalent bond with a protein, its final destination will be the proteasome (Williams et al., 2019) (Figure 16C). 8 E1, 14 E2 and 54 E3 proteins of the *P. falciparum* ubiquitin machinery have been described *in silico* by genomic and proteomic comparison analysis, but only a few of them have been characterized *in vivo* (Hamilton et al., 2014).

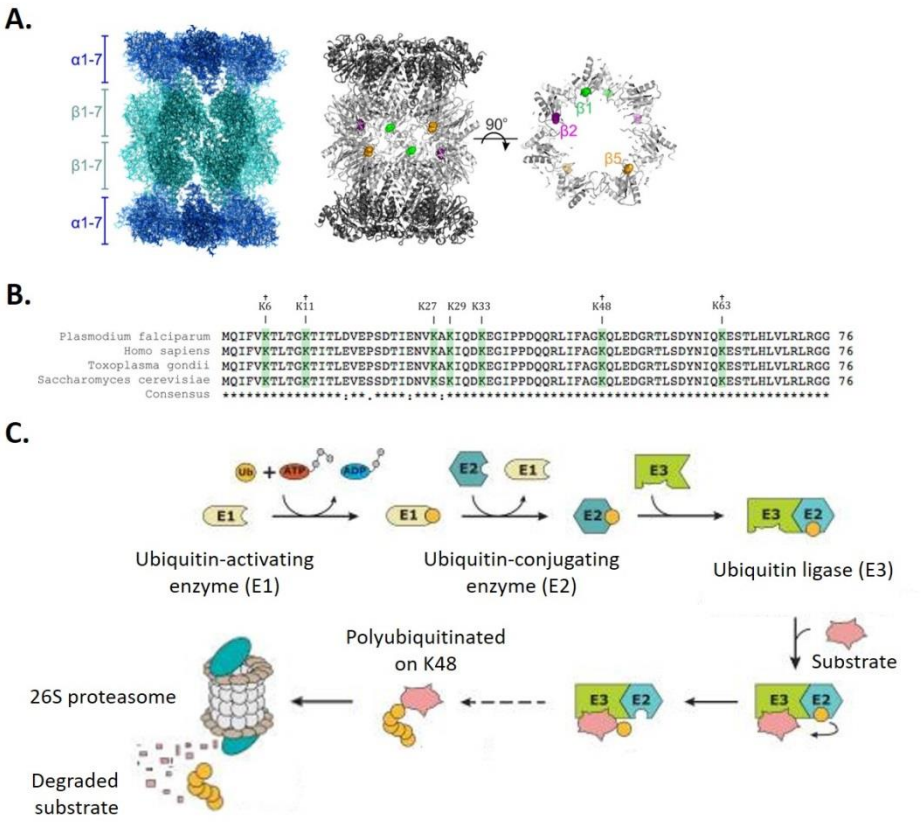

Figure 16. *A) Cryo-electron microscopy structure of* P. falciparum *20S proteasome. The six coloured dots represent the catalytic sites of the organelle. Extracted from (Li, Bogyo, et al., 2016). B) Comparison of the ubiquitin aminoacidic sequence of* Plasmodium falciparum*,* Homo sapiens*,* Toxoplasma gondii *and* Saccharomyces cervisiae*. Active lysine residues are highlighted in green. Extracted from (Hamilton et al., 2014). C) Ubiquitin proteasome system scheme. Adapted from (Hamilton et al., 2014).*

The UPS, especially the proteasome, has been extensively explored as a therapeutical target against malaria (Aminake et al., 2012). Molecules known to inhibit proteasome action, like artemisinin, epoxomicin, carmaphycin-B or MG132, produce an accumulation of misfolded and ubiquitinated proteins that cannot be degraded in the proteasome leading to the death of the parasite (Bridgford et al., 2018; Kreidenweiss et al., 2008; Lamonte et al., 2017; Prasad et al., 2013). Not only already known molecules have been assayed, but a bunch of novel proteasome inhibitors has been designed and tested against *P. falciparum* (Lamonte et al., 2017; Li, O'Donoghue, et al., 2016; Mata-Cantero et al., 2019). Inhibition of some components of the ubiquitination machinery has also been proved to be toxic for *P. falciparum*; as an example, the addition to parasite cultures of MLN7243, an inhibitor of an E1 enzyme (UBA1), stops the cycle progression in the schizont stage, preventing the bursting of the parasite (Green et al., 2020). The inhibition of E3 ubiquitin ligases also disrupts the regular development of the parasite at the schizont stage (Jain et al., 2017).

→ One UPR activation pathway has been described in *P. falciparum* (PERK).
→ The parasite has 92 chaperones that are up-regulated upon cellular stress and are more efficient than other eukaryotes' ones.
→ Inhibition of UPR, UPS and Hsps is toxic for *P. falciparum.*

2.3. Roles of aggregative proteins in *Plasmodium falciparum* and other organisms.

As explained in the previous sections, the *P. falciparum*'s load of proteins containing aggregative-prone sequences is higher than in any other organism in nature. This fact has not only been predicted *in silico* but has been proven *in vivo*, since protein aggregation has been detected in *Plasmodium* mosquito stages and in *in vitro* cultures of the parasite. On the other hand, the pathogen is perfectly able to cope with its aggregative proteome and presents an exceptionally efficient system of chaperones (HSPs), as well as a highly developed UPS and a functional UPR. The question now is; why does *P. falciparum* contain so many aggregative proteins? Do they have a functional role?

For years, aggregative proteins like amyloids or prions (a subclass of amyloid proteins that possess infectious capacity (Sabate et al., 2015)), have been negatively considered due to their association to numerous diseases. In type 2 diabetes, amylin, which in healthy conditions is secreted together with insulin by the pancreatic cells, forms amyloid fibrils that are deposited in the pancreatic islets damaging the organ (Jaikaran & Clark, 2001) (Figure 17A). In Alzheimer's disease, the aggregation of the β-amyloid peptide (Aβ) and the formation of fibrillary tangles by the tau protein are related to the pathology of the disease (Muralidar et al., 2020). Amyloid aggregation

also contributes to the impairment of the normal neuronal activity in other neurodegenerative diseases, like Parkinson's (Braak & Braak, 1990), Creutzfeldt-Jakob's (Debatin et al., 2008) or Huntington's (McGowan et al., 2000). Not only the nervous system and the pancreas can be affected by amyloid aggregation: toxic amyloid insoluble deposits have been detected in lungs, liver, kidneys, heart and the digestive system (Picken, 2020) (Figure 17B).

Nature, through evolution, clears out proteins that have a detrimental effect on cellular viability, like toxic aggregative proteins (Monsellier & Chiti, 2007). As an example of this, Navarro et al. (Navarro et al., 2014) expressed a fragment of the human Aβ protein (Aβ-42) in *Escherichia coli* cells. The Aβ-42 fragments contained different point mutations in their sequences, which affected the amyloid aggregation propensity of the polypeptide. By performing competitive selection experiments, they observed that bacteria expressing the most aggregative variant of Aβ-42 were rapidly purged out, whereas less aggregative variants were evolutionary favored. Going back to the initial question of this section, if aggregative proteins are harmful for organisms and evolution eliminates them, why *P. falciparum* has such an aggregative proteome?

A first step towards answering this question could be taking a look at the other side of the problem, i.e. certain protein aggregation phenomena can be beneficial for cells. Interestingly, in the last two decades an increasing body of evidence has proved the functionality of amyloid proteins in both prokaryotic and eukaryotic organisms, showing that some amyloid proteins are essential in certain physiological processes (Levkovich et al., 2021; Rubel et al., 2020). 29 families of amyloid proteins have been proved to take part in the biofilm formation or stabilization processes of different types of microorganisms, including pathogenic ones like *Staphylococcus aureus* or *Mycobacterium tuberculosis* (Levkovich et al., 2021). Many other biological processes in microorganisms are regulated by amyloid proteins (Figure 17C), for instance, something as crucial as cell cycle restart after stress is controlled by an amyloid protein in *S. cerevisiae*, the Cdc19 kinase. Cdc19 contains a LCR that promotes the formation of amyloid aggregates by the protein under stress conditions (Saad et al., 2017). When the stress disappears, Cdc19 is solubilized and rapidly recovers its function, allowing an immediate reactivation of the cell cycle (Saad et al., 2017).

In mammals, including humans, some amyloids have also important roles in certain cellular processes. Up to 30 human peptidic hormones, such as prolactin, growth hormone or adrenocorticotropic hormone, are stored in granules forming aggregative structures that are stained with classical amyloid dyes like thioflavin T and Congo Red (Maji et al., 2009). One of the most studied human functional amyloids is the protein PMEL17 (melanocyte protein PMEL), which acts as a scaffold to produce mature melanin molecules (Fowler et al., 2005). The loss of amyloid formation capacity by human PMEL17 impairs its physiological function (Hee et al., 2017) and, in other mammals, it has been observed that this lack of aggregative ability leads to

pigmentation disorders and eye problems (Watt et al., 2013). Other biological functions mediated by amyloid proteins in mammals are (i) long-term memory, (ii) RNA translation, (iii) protection of the oocyst once it is fertilized, (iv) inflammatory response, and (v) coagulation (Rubel et al., 2020).

It is clear then that protein aggregation is a complex phenomenon that goes beyond the traditional negative perspective provided by its participation in pathological processes. As explained above, functional amyloids exist and are crucial in many important biological pathways. In the specific case of *P. falciparum*, little is known about the roles of its abundant aggregative proteins. An assay conducted directly on a *P. falciparum* N-enriched protein (the proteasome lid subunit 6, Rpn6), which consisted in eliminating a sequence of 28 N residues in the protein, showed that Rpn6 is perfectly functional despite losing those 28 N residues (Muralidharan et al., 2011). On the contrary, Dalby proposed a positive selection of N-rich proteins in the *P. falciparum* proteome that did not occur in other *Plasmodium* species (Dalby, 2009), pointing at the possibility that those N-rich proteins could have a beneficial role for the parasite. This could be the case of merozoite surface protein 2 (MSP2), in which 25 amino acids of the N-terminal region of the protein form aggregates *in vitro* (Adda et al., 2009) (Figure 17D) and, at the same time, are essential in the interaction of the protein with membrane lipids, suggesting a role of this aggregative region in the invasion process of the parasite (C. Lu et al., 2019). However, these experiments were performed *in vitro* while in *in vivo* conditions, this aggregative region of the protein is known to be the signal peptide, which is not present in the mature form of the protein (Burdukiewicz et al., 2018). It has also been proposed that N-rich sequences in *P. falciparum* proteins can act as tRNA sponges that slow down the translation rate of the parasite's ribosomes minimizing in this way the risk of proteins to get misfolded (Filisetti et al., 2013; Frugier et al., 2010).

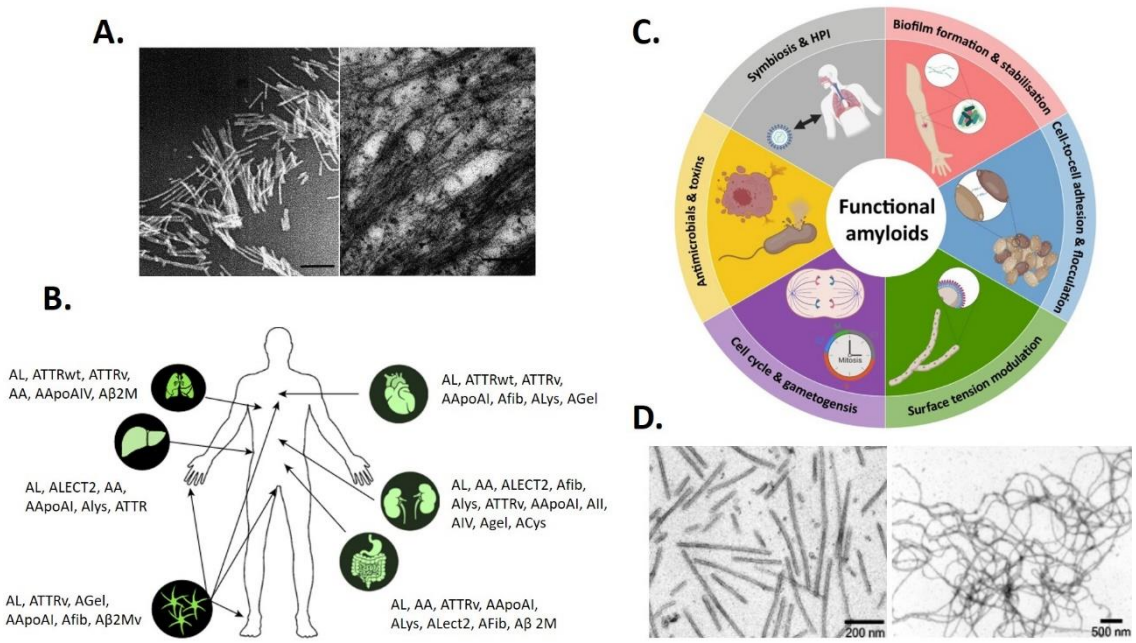

Figure 16. *A) Electron microscopy images of human pancreas extracts containing amyloid fibrils formed by amylin. Adapted from (Jaikaran & Clark, 2001). B) Pathological amyloid proteins present in different human organs. Adapted from (Picken, 2020). C) Functions of amyloid proteins in microorganisms. Extracted from (Levkovich et al., 2021). D) Electron microscopy images of amyloid fibrils formed by* P. falciparum *MSP2. Adapted from (Adda et al., 2009).*

2.4. Aggregative proteins as therapeutic targets.

Protein homeostasis has been successfully targeted in *P. falciparum* with therapeutic purposes. The UPR, UPS and chaperones network have been proved to be good candidates for novel antimalarial treatments and, in some particular cases, they are affected by already in use antiplasmodial compounds, like ARTs (see sections 2.2.1, 2.2.2 and 2.2.3). Protein aggregation itself has been targeted in bacteria by means of aggregative peptides, either naturally found in bacterial proteomes (Bednarska et al., 2016) or synthetically designed (Collins et al., 2018). In both cases, the antibiotic effect of the peptides was associated to high protein aggregation levels inside the cells that led to their death through the disruption of protein homeostasis (Bednarska et al., 2016; Collins et al., 2018).

Interestingly, some classical antimalarial drugs have the ability of promoting or inhibiting protein aggregation. For instance, artemisinin promotes the accumulation of misfolded and ubiquitinated proteins inside *P. falciparum* (Bridgford et al., 2018), but at the same time it inhibits amyloid fibrils formation of human amylin and Aβ proteins *in vitro* (Xu et al., 2019) (Figure 18A). Quinacrine directly interacts with the C-terminal region of the human prionic protein (hPrP) (Touil et al., 2006; Vogtherr et al., 2003) and it inhibits its accumulation in neuroblastoma cells *in vivo* (Doh-Ura et al., 2000). Also quinacrine (Figure 18B), as well as quinine and quinidine, inhibits hPrP

aggregation *in vitro* as assessed by circular dichroism and dynamic light scattering (Georgieva et al., 2006). Another quinoline, chloroquine, has been proved to prevent the degradation of Aβ fibrils in microglia cells, leading to the consequent toxic accumulation of the aggregated protein inside the cells (Chu et al., 1998). Methylene blue, for his side, inhibits the formation of amyloid fibrils by human superoxide dismutase 1 (SOD1) (Musteikyte et al., 2020) (Figure 18C) and lysozyme *in vitro* (How et al., 2018), but promotes the fibrillization of Aβ (Necula et al., 2007). Also curcumin, whose IC_{50} against *P. falciparum* is around 5 µM (Reddy et al., 2005), shows the ability of inhibiting protein aggregation of α-synuclein both *in vitro* and *in vivo* (Pandey et al., 2008).

Not only classical antimalarial drugs show anti-aggregative effect, a group of compounds, called amyloid pan-inhibitors, which potently inhibit amyloid aggregation of a wide variety of yeast, fungal, bacterial and mammal amyloid proteins, and that show structural similarities to amino-quinolines, have been shown to have antiplasmodial effects with IC_{50} values in some cases lower than 1 µM (Defaux et al., 2011; Espargaró et al., 2019; Sola et al., 2015).

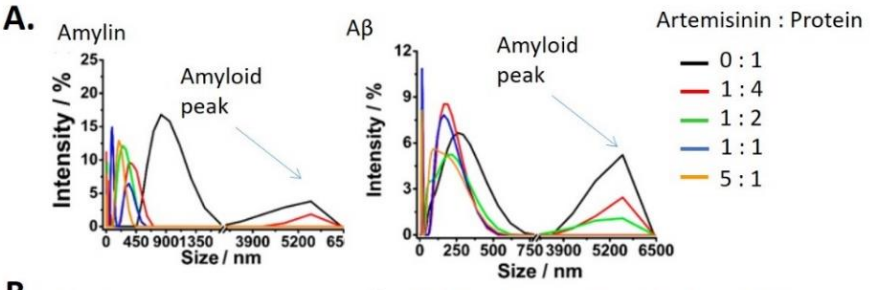

B.

Species	α-helical structure %	β-structure %	Turn %	Random structure %	Total structure %
Aggregated rhPrP (90–231) in the absence of anti-prions	23	22	21	31	97
Aggregated rhPrP (90–231) in the presence of quinacrine	51	0	27	21	99

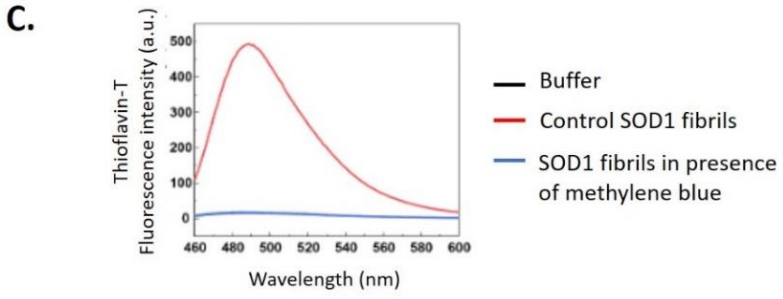

Figure 18. *A) Amylin and Aβ amyloid fibrils formation in presence of different amounts of artemisinin measured by dinamic light scattering. Adapted from (Xu et al., 2019). B) hPrP protein structure in the absence or presence of quinacrine measured by circular dichroism. Adapted from (Georgieva et al., 2006). C) Thioflavin-T signal of SOD1 amyloid fibrils in the presence or absence of methylene blue. Adapted from (Musteikyte et al., 2020).*

→ For years, aggregative proteins have been negatively considered due to its association to numerous diseases.
→ Recently, a great number of amyloid proteins with biological functions have been described.
→ In *P. falciparum*, little is known about the roles of its abundant aggregative proteins.
→ Protein aggregation has been successfully targeted in bacteria as therapeutical strategy.
→ Many molecules with antimalarial activity also show the ability of inhibiting or promoting protein aggregation.

Objectives

Objective 1

To characterize the aggregation-prone proteome of *P. falciparum* using *in silico* and *in vitro* methods with the aim of exploring protein aggregation as an antimalarial target.

Objective 2

To investigate the potential antimalarial effect of the promotion of protein aggregation in *P. falciparum* by the selection and treatment of *in vitro* cultures with aggregative peptides naturally present in the proteome of the parasite.

Objective 3

To explore the potential antimalarial effect of the inhibition of protein aggregation in *P. falciparum in vitro* cultures after their treatment with protein aggregation inhibitors.

Paper 1

AMERICAN SOCIETY FOR MICROBIOLOGY | Antimicrobial Agents and Chemotherapy®

PHARMACOLOGY

Detection of Protein Aggregation in Live *Plasmodium* Parasites

Arnau Biosca,[a,b,c] Inés Bouzón-Arnáiz,[a,b,c] Lefteris Spanos,[d] Inga Siden-Kiamos,[d] Valentín Iglesias,[e,f] Salvador Ventura,[e,f] Xavier Fernàndez-Busquets[a,b,c]

[a]Barcelona Institute for Global Health (ISGlobal), Hospital Clínic-Universitat de Barcelona, Barcelona, Spain
[b]Nanomalaria Group, Institute for Bioengineering of Catalonia (IBEC), The Barcelona Institute of Science and Technology, Barcelona, Spain
[c]Nanoscience and Nanotechnology Institute (IN2UB), University of Barcelona, Barcelona, Spain
[d]Institute of Molecular Biology and Biotechnology, FORTH, Heraklion, Greece
[e]Institut de Biotecnologia i de Biomedicina, Universitat Autònoma de Barcelona, Bellaterra, Spain
[f]Departament de Bioquímica i Biologia Molecular, Universitat Autònoma de Barcelona, Bellaterra, Spain

ABSTRACT The rapid evolution of resistance in the malaria parasite to every single drug developed against it calls for the urgent identification of new molecular targets. Using a stain specific for the detection of intracellular amyloid deposits in live cells, we have detected the presence of abundant protein aggregates in *Plasmodium falciparum* blood stages and female gametes cultured *in vitro*, in the blood stages of mice infected by *Plasmodium yoelii*, and in the mosquito stages of the murine malaria species *Plasmodium berghei*. Aggregated proteins could not be detected in early rings, the parasite form that starts the intraerythrocytic cycle. A proteomics approach was used to pinpoint actual aggregating polypeptides in functional *P. falciparum* blood stages, which resulted in the identification of 369 proteins, with roles particularly enriched in nuclear import-related processes. Five aggregation-prone short peptides selected from this protein pool exhibited different aggregation propensity according to Thioflavin-T fluorescence measurements, and were observed to form amorphous aggregates and amyloid fibrils in transmission electron microscope images. The results presented suggest that generalized protein aggregation might have a functional role in malaria parasites. Future antimalarial strategies based on the upsetting of the pathogen's proteostasis and therefore affecting multiple gene products could represent the entry to new therapeutic approaches.

KEYWORDS malaria, protein aggregation

According to the last World Malaria Report (1), around 228 million cases of malaria occurred worldwide in 2018 (up from 216 million in 2016), and the disease led to an estimated 405,000 deaths. Although the elimination of malaria is a priority for the global health system, the drugs currently used as front-line therapy are quickly becoming obsolete due to the evolution of resistance in the parasite causing the disease, *Plasmodium* spp. (2). The consequence of this loss in efficacy of available antimalarial compounds is that the former decline in mortality and incidence of malaria has stalled in the last few years, which leads to an urgent need for the identification of new therapeutic targets and alternative antimalarial strategies operating through novel mechanisms (3).

The life cycle of *Plasmodium* in the human host begins with the bite of a parasitized female mosquito of the genus *Anopheles*, when it inoculates sporozoites, the infectious form of the pathogen. Sporozoites quickly reach the liver, develop asexually inside hepatocytes, and produce merozoites (4), which eventually enter the bloodstream, where they initiate the intraerythrocytic phase (5). In the red blood cell (RBC), *Plasmodium* grows as it develops from ring to trophozoite stages until it finally undergoes multiple asexual divisions to form schizonts containing between 8 and 36 merozoites

Citation Biosca A, Bouzón-Arnáiz I, Spanos L, Siden-Kiamos I, Iglesias V, Ventura S, Fernàndez-Busquets X. 2020. Detection of protein aggregation in live *Plasmodium* parasites. Antimicrob Agents Chemother 64:e02135-19. https://doi.org/10.1128/AAC.02135-19.

Address correspondence to Xavier Fernàndez-Busquets, xfernandez_busquets@ub.edu.

Received 22 October 2019
Returned for modification 16 January 2020
Accepted 6 April 2020
Accepted manuscript posted online 13 April 2020
Published 21 May 2020

that egress from the RBC to invade new erythrocytes. Some parasites differentiate into gametocytes, the sole form of the pathogen that can be transmitted to *Anopheles* during its blood meal. In the midgut of the insect fertilization takes place, and the motile zygote, termed ookinete, traverses the intestine epithelium to lodge itself on the transluminal side to form an oocyst where sporozoites develop. Through the insect's hemolymph sporozoites migrate to the salivary glands, ready to start a new infectious cycle.

The most severe form of malaria and the majority of reported cases are caused by *Plasmodium falciparum*. The genome of this species (6) has some particularities, such as a clear bias in its DNA composition, which has an 80.6% AT content, comparable only to that found in *Dictyostelium discoideum* (7). Moreover, about one-third of the *P. falciparum* proteome exhibits low-complexity regions (LCRs) especially enriched in asparagine residues (8–11). Importantly, proteins with large LCR stretches having abundant glutamine/asparagine (Q/N) repeats show a strong tendency to form insoluble intracellular aggregates (12, 13). Out-of-control protein aggregation is potentially harmful for the organism and has been observed to be a characteristic feature of several pathological conditions, such as type II diabetes, systemic amyloidosis, and a number of neurodegenerative diseases (14). The aggregation of proteins can trigger aberrant molecular associations and permeate the plasma membrane, which often end up in cell death (15, 16). Evolution usually eliminates proteins that contain amino acid sequences with a high propensity to aggregate, except when these regions are required to maintain functionality (17, 18). Indeed, the aggregation of certain proteins has been found to have a functional role in several biological processes, e.g., innate immunity against certain viruses (19), the persistence of mammalian synaptic facilitation (20), and the inheritance in yeast of some particular phenotypes (21). In the course of a typical malaria infection, *Plasmodium* is exposed to fever episodes that can reach more than 40°C. Since protein misfolding and aggregation increase at higher temperatures, these heat shock periods could compromise parasite survival if only a fraction of its abundant asparagine repeat-containing proteins aggregated. Such havoc is avoided by the abundance in the proteome of the pathogen of chaperones which assist in protein folding (22–25).

In a previous work, an in-house-developed Python algorithm (26), which scans for consecutive 80-residue windows retrieving those containing $\geq$30 Q/N repeats, was applied to the *P. falciparum* 3D7 reference proteome containing 5,353 proteins. In good agreement with former studies (9), our algorithm identified 1,300 proteins with one or more Q/N-rich domains. These were further searched for intrinsically disordered regions with PAPA (27), obtaining 581 proteins. Finally, the pWALTZ script (28) was applied to scan within these disordered regions for the presence of soft amyloid cores, i.e., short stretches capable of facilitating the conversion of polypeptides into an amyloid-like conformation (26), resulting in a final data set of 503 proteins containing disordered regions potentially capable of nucleating aggregation events.

Encouraged by the prediction of that *in silico* analysis, we have evaluated here the presence of aggregative proteins in live *Plasmodium* cultures, using first an amyloid-specific staining for fluorescence microscopy and flow cytometry analysis. The observed existence of intracellular amyloid deposits in live parasite cells prompted the use of fractionation techniques and liquid chromatography with tandem mass spectrometry (LC-MS/MS) for the identification of individual proteins from the *P. falciparum* proteome.

RESULTS

Detection of protein aggregation in live *Plasmodium* stages. Previous preliminary data had shown the presence of aggregated proteins in *P. falciparum* early trophozoite stages (26), according to staining with the red fluorescent dye ProteoStat, which can detect the presence of intracellular amyloid-like deposits in live cells with high specificity (29). ProteoStat is a molecule whose fluorophore group, when excited in solution, releases energy by rotation; however, when the dye locks into the quater-

nary structure of protein aggregates and cannot rotate, it becomes highly fluorescent. This property has been used to detect protein aggregates in numerous studies. Amyloid aggregates in seminal plasma, where the intensity of background noise prevented the use of Congo red or Thioflavin-T (ThT) amyloid dyes, were satisfactorily detected by ProteoStat due to its higher noise-to-signal ratio (30). Other examples of the use of this reagent to detect protein aggregates are, to name just a few, following the formation of intracellular aggregates in HeLa cells upon induction of extracellular oxidative stress to demonstrate their colocalization with the aggregate p62 protein marker (31), staining of amyloid plaques in Alzheimer's brain sections (32), validating the binding of novel dyes to intracellular aggregates upon proteasome inhibition (33), and staining of intracellular aggregates of human α-crystallin truncated forms (34).

A detailed analysis performed in live *P. falciparum* cultures revealed that ProteoStat-stained protein aggregates were abundantly found in extraerythrocytic merozoites (Fig. 1A and B) and in all the blood forms except early rings, where their fluorescent signal was low or undetectable (Fig. 1C and D). ProteoStat fluorescence was detected throughout the parasite but not in the cytosol of the host RBC or in any noninfected erythrocytes. The only parasite stage capable of being transmitted from human to mosquito, the gametocyte, also showed an evident presence of aggregated proteins in all its stages (Fig. 1E to G). Female gametes, the first stage exclusive of the mosquito, have also been observed to be ProteoStat positive in *P. falciparum* (Fig. 1H to J). In the murine malaria parasite *Plasmodium berghei*, the rest of the mosquito stages were also ProteoStat positive, namely, male gametes, ookinetes, oocysts, and sporozoites (Fig. 2A to D), whereas no staining was observed in any *Anopheles* mosquito cells. *P. falciparum* sporozoites also had detectable aggregated protein deposits (see Fig. S1 in the supplemental material). *P. berghei* ring stages, which represent most of circulating parasitized RBCs (pRBCs) in this species (35), were negative for ProteoStat staining (Fig. S2). In another species also infecting mouse RBCs, *Plasmodium yoelii*, all blood stages could be observed in circulation and showed the presence of aggregated proteins (Fig. S2), with the possible exception of early rings. The existence of abundant amyloid structure in pRBCs, but not in uninfected erythrocytes, was confirmed with the use of an anti-amyloid fibril antibody (36) (Fig. S3).

Quantitative flow cytometry analysis of ProteoStat-stained *P. falciparum* cultures confirmed the fluorescence microscopy observations of blood stages. The intraerythrocytic parasite population with less DNA content, which included ring stages, showed the lowest aggregated protein amounts (Fig. 3). A significant fraction of these pRBCs harboring a single parasite cell and exhibiting positive ProteoStat signal likely corresponded to late ring/early trophozoite stages, as suggested by fluorescence microscopy data.

Functions of the aggregation-prone proteins identified in live *P. falciparum* late-form blood stages. In a first attempt to identify individual aggregation-prone proteins present in live *P. falciparum*, a late-stage pRBC culture homogenate was stained with ProteoStat and the positive aggregates were sorted by flow cytometry (Fig. 4). LC-MS/MS analysis provided 38 proteins present in the ProteoStat-stained aggregates (Table S1). Of these, only one was found among 342 proteins from the *P. falciparum* proteome that had been identified using the PLAAC algorithm to contain a prion-forming domain with strongly biased amino acid composition, most notably enriched in Q or N (Table S2). Since highly abundant and soluble proteins might be found in the protein aggregates sorted by flow cytometry, a second purification strategy was assayed with the objective of increasing the sensitivity of aggregated protein detection. This alternative approach consisted in collecting those aggregates from late-stage pRBC culture homogenates that resisted dissolution in the presence of 0.1% sodium dodecyl sulfate (SDS) (Fig. 5), which resulted in the identification of 369 parasite proteins (Table S3); of these, 85 were detected in the *in silico* analysis (Table 1) and 25 were captured by ProteoStat sorting (Fig. 6A).

Gene ontology analysis of the proteins found in 0.1% SDS-resistant aggregates revealed an enrichment in proteins involved in nuclear import (Fig. 6B); mitotic

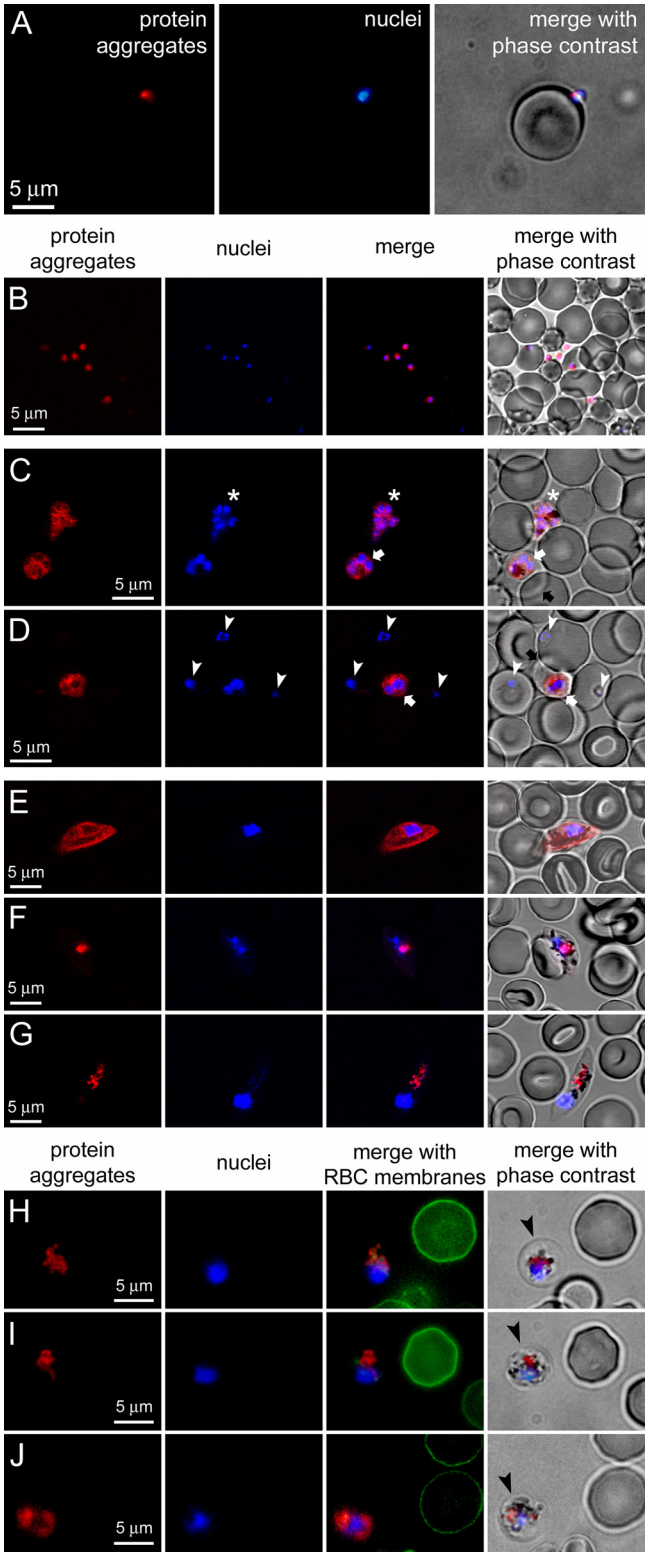

FIG 1 ProteoStat staining for the detection of intracellular protein aggregates in live *in vitro* cultures of *P. falciparum* blood stages and female gametes. (A) RBC-invading merozoite. (B) Egressed merozoites. (C and D) Intraerythrocytic blood stages: schizont (asterisk), trophozoites (arrows), and rings (arrowheads). The black arrows in phase contrast images indicate the boundary of two RBCs infected by trophozoite stages, to highlight the lack of fluorescence in the host RBC cytosol. (E to G) Gametocytes. (H to J) Egressed female gametes (arrowheads), which lack the RBC membrane otherwise stained by Oregon Green 488.

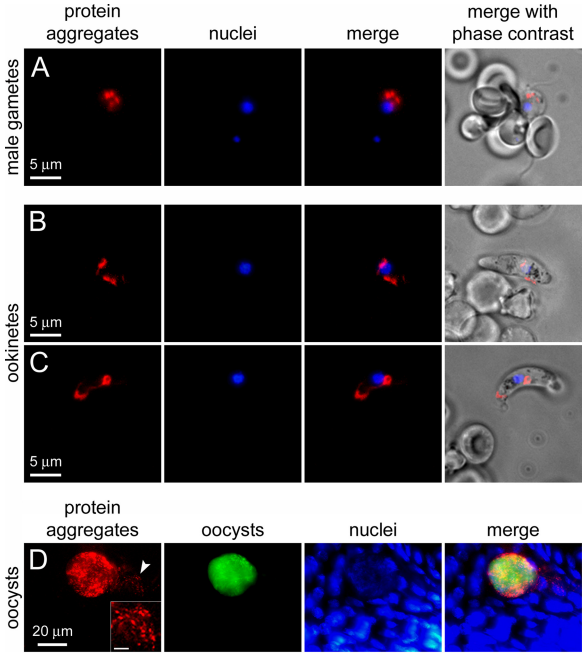

FIG 2 ProteoStat staining for the detection of intracellular protein aggregates in live *P. berghei* stages in *Anopheles gambiae* mosquitoes. (A) Male gametes. (B and C) Ookinetes. (D) Oocysts and sporozoites. The arrowhead indicates a stream of sporozoites leaving the oocyst; a blow-up of this region is shown in the inset of the protein aggregates panel (inset scale bar, 5 μm).

spindle and chromosome organization, Golgi body-to-endoplasmic reticulum transport, and drug response were other biological processes well represented in the selected protein pool. The main molecular functions in which SDS-insoluble *P. falciparum* proteins exhibited enrichment were binding to nuclear localization sequences, to specific protein domains, and to microtubules (Fig. 6C); structural proteins, protein transporters and transcription factors were also significantly abundant. The cellular components most enriched in the proteins from Table S3 were the nuclear pore and membrane, the coat protein complex I (COPI) vesicle coat, and the nucleosome (Fig. 6D), with a smaller but yet significant representation of cytosolic ribosomal subunits.

***In vitro* characterization of the aggregation of peptides selected from the live *P. falciparum* aggregation-prone protein pool.** The proteins identified in 0.1% SDS-resistant aggregates were individually analyzed for their content in aggregation-

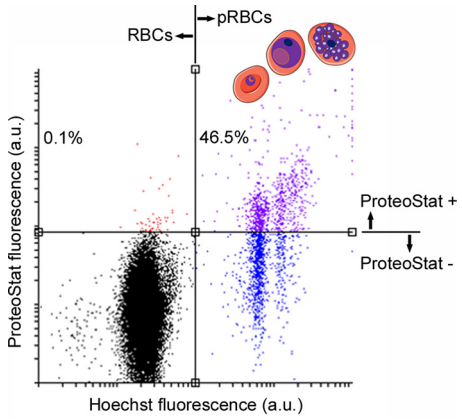

FIG 3 Flow cytometry analysis of ProteoStat-stained desynchronized *P. falciparum* cultures. The fraction of ProteoStat-positive RBCs and pRBCs is indicated (%), the latter consisting of late ring/early trophozoites and schizonts, the three stages represented in the cartoons.

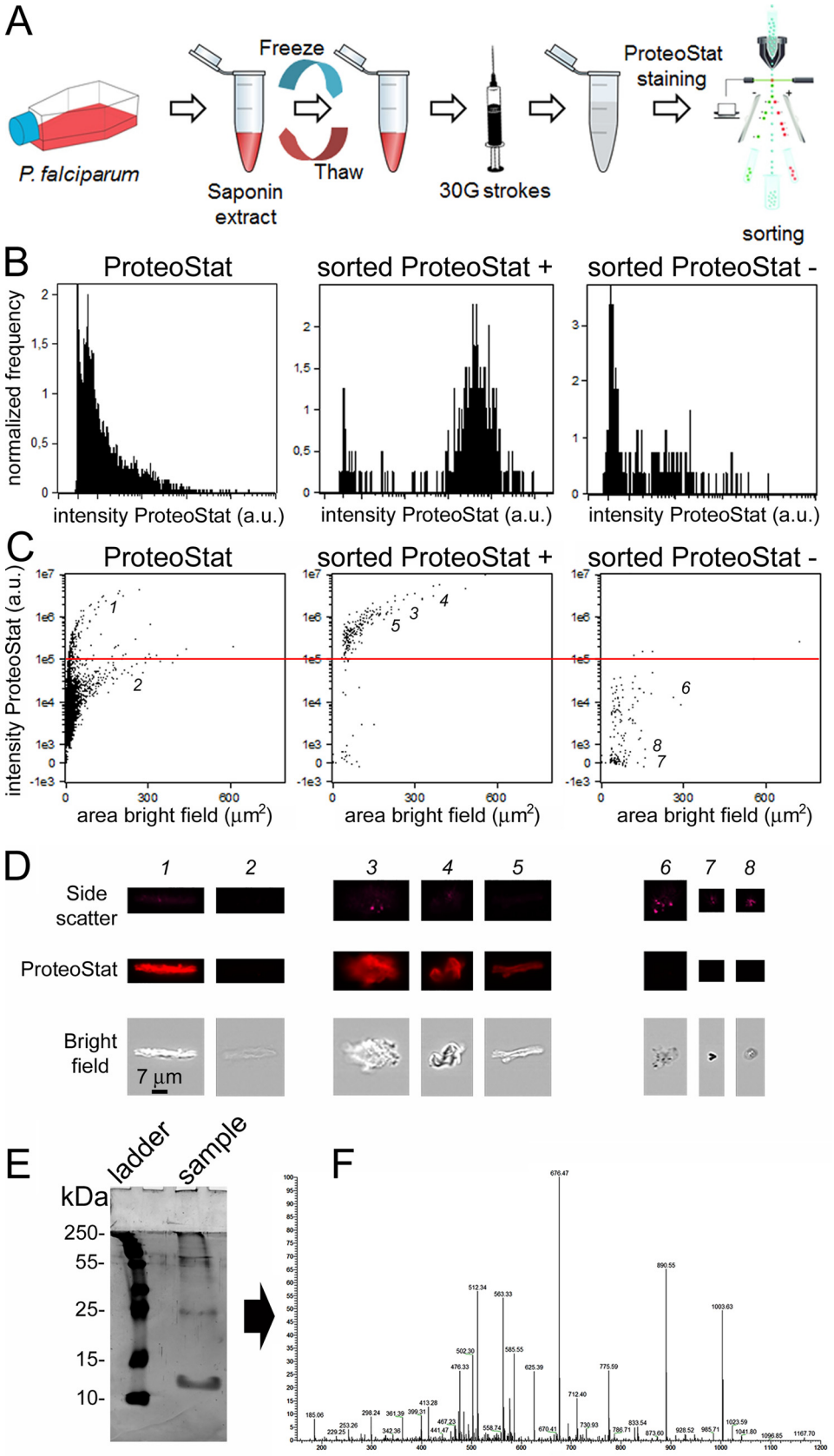

FIG 4 Flow cytometry sorting of ProteoStat-stained proteins in live *P. falciparum* blood stages. (A) Scheme of the process. (B) Histograms showing the intensity of ProteoStat signal versus the number of events, for the sample

(Continued on next page)

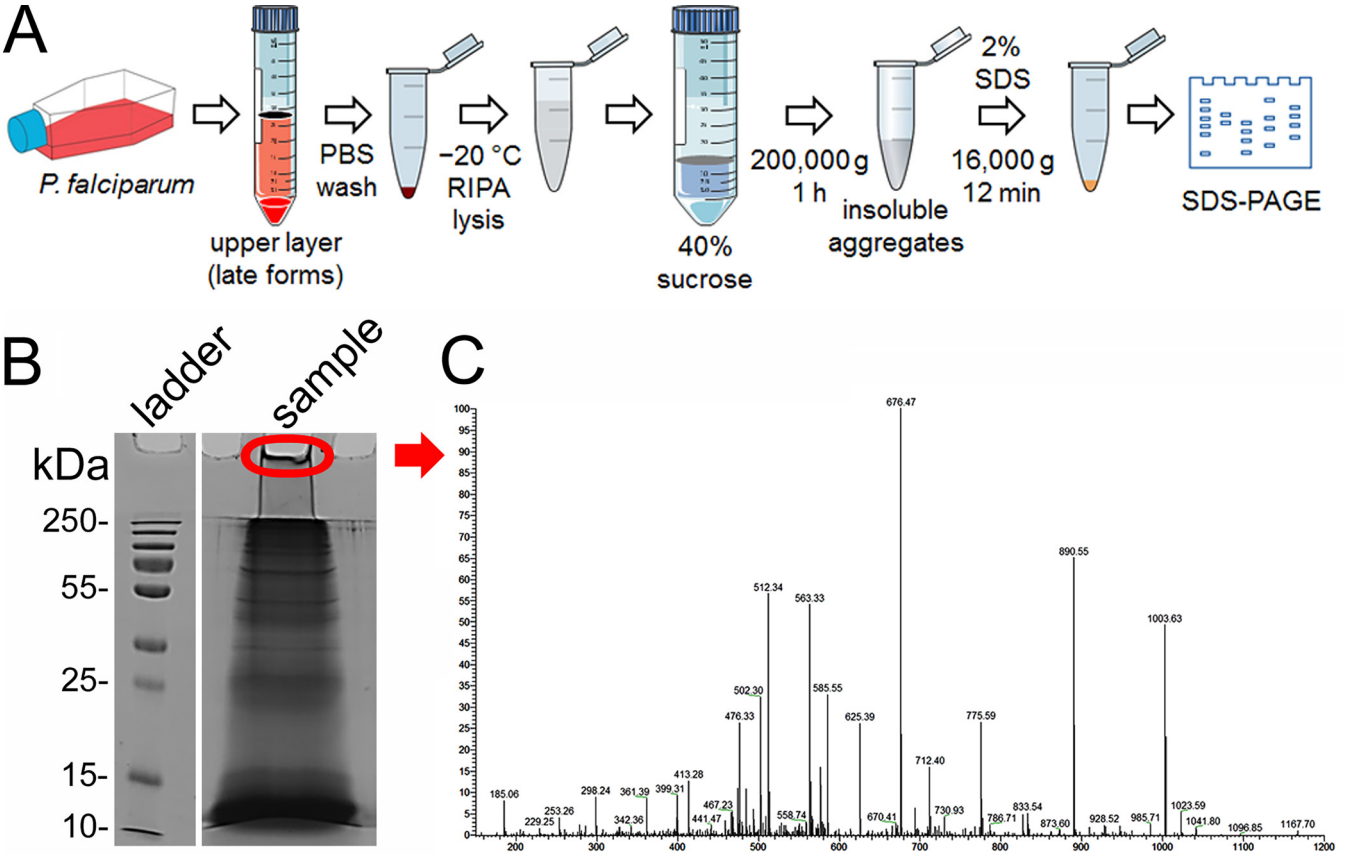

FIG 5 Isolation of *P. falciparum* aggregative proteins insoluble in 0.1% SDS. (A) Scheme of the process. (B) Silver-stained SDS-PAGE fractionation of the 0.1% SDS-resistant sample. (C) Schematic graph representing the LC-MS/MS analysis of Coomassie blue-stained material not entering the stacking gel, excised from a gel run in parallel to that of panel B. The results obtained are reported in Table S3.

prone amino acid sequences, and five peptides were selected to characterize their *in vitro* amyloid fibril forming capacity. A single copy of LQSNIG is present in a DNA-binding nucleoporin (accession number Q8I398), whose disruption might *a priori* be a good therapeutic target. NYN is part of the well-described self-assembling peptide NYNYNYN (37) and is found in ca. 85% of the proteome (4,533 *Plasmodium* proteins, in some of them more than once). The peptide NVNIYN, which is found in an uncharacterized protein (accession number C0H4L9) detected in the aggregates not solubilized by 0.1% SDS, was identified after a BLAST search to be also present as a single copy in four other proteins, among them an AP2 domain-containing transcription factor potentially implicated in heat shock responses (accession number C0H5G5). Two other single-copy peptides from this presumably essential protein which had been picked out in the *in silico* search, NFNNIYH and NNFYYNN, were also selected for further analysis. The abundance and aggregation propensity of the proteins containing these peptides are around the respective average values for these two parameters within the *P. falciparum* proteome (Fig. S4).

FIG 4 Legend (Continued)
before sorting (left panel) and the resulting ProteoStat$^+$ and ProteoStat$^-$ fractions. (C) Dot plot showing the intensity of the ProteoStat signal versus the size of each event, for the sample before sorting (left panel) and the resulting ProteoStat$^+$ and ProteoStat$^-$ fractions. (D) To monitor ProteoStat fluorescence, pictures at ×600 magnification were taken in the bright field and fluorescence channel BP596-660 upon excitation with a 488-nm laser. (E) Silver-stained SDS-PAGE fractionation of the ProteoStat$^+$ sample. (F) Schematic graph representing the LC-MS/MS analysis of Coomassie blue-stained bands excised from a gel run in parallel to that of panel E. The results obtained are reported in Table S1 in the supplemental material.

TABLE 1 Prion-like domain (PrLD)-containing proteins found in SDS-resistant aggregates

UniProt accession no.	Protein description	PrLD score
Q8IJP9	ADA2-like protein	289.599
O96124	Erythrocyte membrane protein 3	220.166
Q8I398	Nucleoporin NUP100/NSP100, putative	188.444
Q8IIS9	Polyadenylate-binding protein-interacting protein 1, putative	132.364
Q8I207	Uncharacterized protein	95.427
Q8ILR9	Protein PF14_0175	90.871
O96221	Protein transport protein SEC31	84.834
Q8IJG6	Chromodomain-helicase-DNA-binding protein 1 homolog, putative	82.683
Q8ID65	Uncharacterized protein	80.531
Q8I562	Clustered-asparagine-rich protein	67.567
Q8IJW6	Asparagine-rich antigen	65.462
Q8ID39	Uncharacterized protein MAL13P1.336	63.816
Q8ILC9	Uncharacterized protein	62.573
Q8I4U7	Uncharacterized protein	55.167
Q8IKH2	Transcription factor with AP2 domain(s)	54.992
O96201	Conserved *Plasmodium* protein	54.465
Q9U0K8	Uncharacterized protein	47.530
Q8I3X9	Uncharacterized protein	45.295
Q8I403	Uncharacterized protein	44.483
Q8IKB6	Histone deacetylase, putative	43.850
Q8I3V8	Pre-mRNA-splicing factor CWC2, putative	41.783
Q8IAU1	ATP-dependent RNA helicase DBP1, putative	41.607
O77328	Serine/threonine protein kinase, putative	40.696
Q8IAX8	DNA/RNA-binding protein Alba 1	38.471
C6KT67	Nuclear polyadenylated RNA-binding protein NAB2, putative	35.343
Q8IE71	Uncharacterized protein	35.082
Q8IJJ2	Conserved *Plasmodium* protein	34.839
Q8IB94	E3 ubiquitin-protein ligase, putative	34.785
Q8I1X5	Pre-mRNA-processing-splicing factor 8, putative	33.710
Q8ID63	Uncharacterized protein	31.733
Q8IL08	Uncharacterized protein	31.393
Q8IKJ2	Uncharacterized protein	31.334
Q8I0W8	Deoxyribodipyrimidine photolyase, putative	31.172
Q8IKY0	Transcription factor with AP2 domain(s), putative	30.505
Q8I3Z1	MATH and LRR domain-containing protein PFE0570w	30.497
Q8IHR4	Dynamin-like protein	30.270
Q8I259	Uncharacterized protein	30.050
C0H4L9	Uncharacterized protein	29.745
Q8IBU8	Uncharacterized protein	29.514
Q9TY99	Knob-associated histidine-rich protein	29.121
Q8ILS4	NOT family protein, putative	28.802
C6KTB7	Putative E3 ubiquitin-protein ligase protein PFF1365c	28.466
Q8IKZ0	Uncharacterized protein	28.376
Q8IM09	Uncharacterized protein	27.922
Q8ILZ2	WD repeat-containing protein, putative	27.869
Q8I517	Uncharacterized protein	27.552
Q8I5Y7	High-mobility-group protein B3, putative	26.923
C6KST7	Uncharacterized protein	26.876
Q8IIW4	CCR4-NOT transcription complex subunit 1, putative	26.381
Q8IHT5	Transcription factor with AP2 domain(s)	25.809
C0H4R8	Serine/threonine protein kinase, FIKK family	25.312
C6KSY0	Transcription factor with AP2 domain(s)	25.304
Q8IC35	Erythrocyte membrane-associated antigen	25.119
Q8IIS4	Transcription factor with AP2 domain(s)	24.751
Q9U0I0	Uncharacterized protein	24.746
Q8I3U0	Transcription factor with AP2 domain(s)	24.064
C0H4Y0	Ubiquitin conjugation factor E4 B, putative	23.863
Q8IKF6	Uncharacterized protein	23.691
C0H570	RNA-binding protein, putative	22.853
Q8IL84	Metacaspase-like protein	21.569
C6KSS4	Spindle assembly abnormal protein 6, putative	21.196
C0H530	Ran-binding protein, putative	21.141
Q8IIG8	Uncharacterized protein	20.697
Q8IE65	Uncharacterized protein	20.586
Q8IDI3	Inner membrane complex protein 1f, putative	19.991
Q8I3L2	Uncharacterized protein	19.764

(Continued on next page)

TABLE 1 (Continued)

UniProt accession no.	Protein description	PrLD score
C6KSN4	Uncharacterized protein	19.745
O96205	Conserved *Plasmodium* protein	19.732
Q8IES7	Uncharacterized protein	19.294
Q8II83	Uncharacterized protein	19.161
Q8I391	Uncharacterized protein	18.922
Q8ILQ6	Uncharacterized protein	18.334
Q9U0J0	Replication protein A1, large subunit	17.760
Q8I538	Uncharacterized protein	17.742
C6KSR4	Uncharacterized protein	17.304
Q8IJL2	Eukaryotic translation initiation factor subunit eIF2A, putative	17.131
C6KSN9	Transcription factor with AP2 domain(s)	15.297
O97239	Protein dopey homolog PFC0245c	14.519
Q8IBL5	Uncharacterized protein	13.571
Q8IM32	Uncharacterized protein	13.558
O97298	Uncharacterized protein	12.842
Q8I4T6	THO complex subunit 2, putative	12.479
Q8ILJ1	Uncharacterized protein	12.467
Q8I1N6	AP2/ERF domain-containing protein PFD0985w	12.226
Q8ID46	Uncharacterized protein	12.200

In vitro characterization of the five selected peptides revealed the existence of different aggregation behaviors. According to ThT staining (Fig. 7A), NFNNIYH fibrillated immediately upon dissolution in PBS. NNFYYNN had slower fibril-forming dynamics, but after 1 week it was the peptide with a stronger ThT fluorescence signal. NVNIYN and LQSNIG formed fibrils at a significantly slower quantitative ratio that the former two peptides, whereas the NYN spectrum did not differ from that of the ThT control in the absence of peptide. According to transmission electron microscopy analysis, the first four peptides were observed to form typical amyloid fibrils (Fig. 7B), whereas NYN samples lacked fibrils and contained only unstructured aggregates. The viability of the parasite in *in vitro P. falciparum* cultures was not significantly affected by any of the peptides up to a concentration of 100 μM (data not shown).

DISCUSSION

The amino acid sequence of the *P. falciparum* merozoite surface protein 2 (MSP2) has tandem repeats typical of intrinsically unstructured proteins (38, 39), in agreement with the observations that some MSP2 variants form *in vitro* amyloid-like fibrils (38, 40) and that merozoites bind Congo red, an amyloid-specific dye (41). The formation of MSP2 oligomers on merozoites was observed in immunofluorescence assays using a monoclonal antibody raised against the polymeric form of the protein (38). Given the evidences of amyloids interacting with RBCs (42, 43), it is reasonable to hypothesize that merozoite surface-bound MSP2 might have a role in the initial steps of erythrocyte invasion.

The presence of a clearly detectable aggregated protein content according to ProteoStat staining in egressed and invading merozoites and its absence in early intraerythrocytic ring stages suggest that the parasite's amyloid load is lost during the RBC invasion process. This would be in agreement with the observation that MSP2 is carried into the host erythrocyte on the surface of the invading merozoite and then rapidly degraded (44) and suggests that an amyloid coat might be part of the *Plasmodium* invasion machinery. However, MSP2 peptides were not detected in the 0.1% SDS-insoluble fraction prepared from late-blood-stage trophozoites and schizonts, a result which might indicate that if insoluble amyloid fibrils are formed by MSP2 on the merozoite surface, this phenomenon is triggered immediately before merozoite egress from the pRBC. In agreement with this hypothesis, previous reports indicated that it was the interaction of the N-terminal 25 residues of MSP2 with membranes what induced the peptide to form β-structure and to aggregate (45).

The results presented above support the notion that most of the aggregative

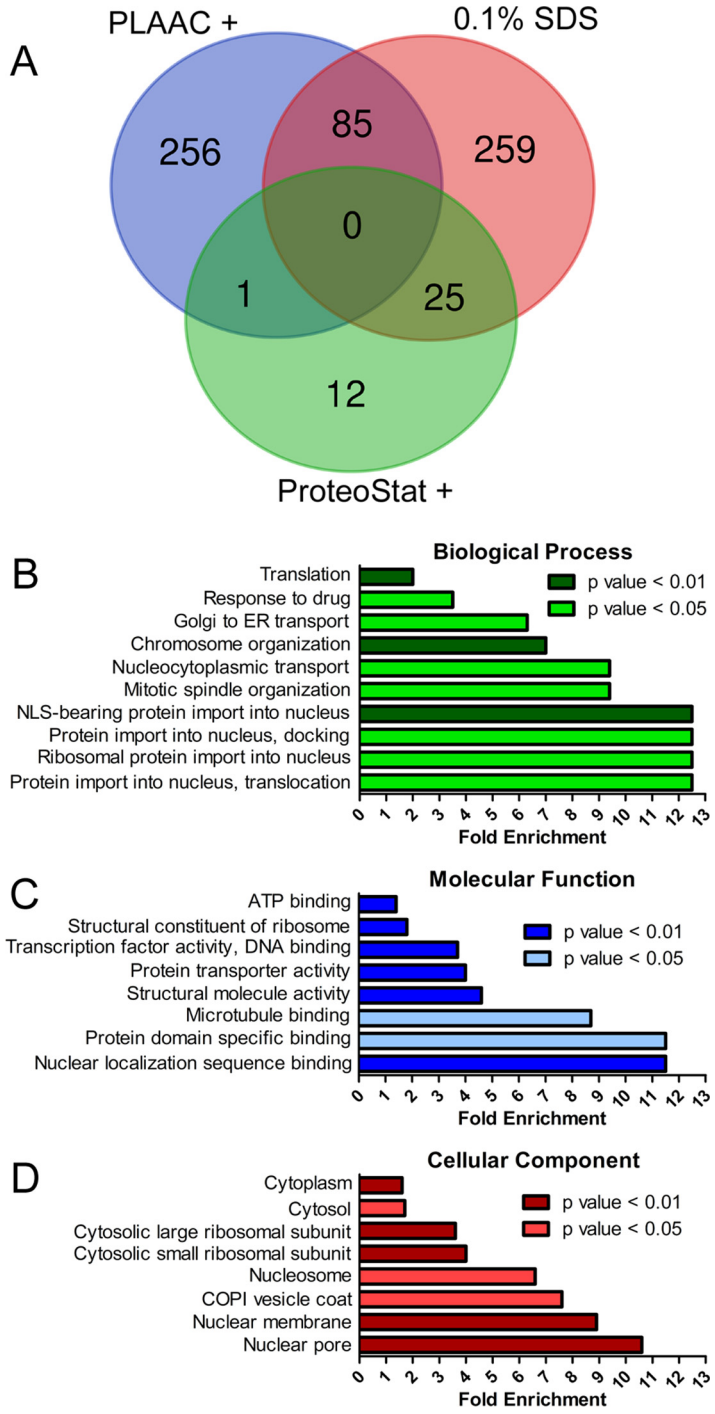

FIG 6 Analysis of *P. falciparum* aggregative proteins insoluble in 0.1% SDS. (A) Venn diagram (http://bioinformatics.psb.ugent.be/webtools/Venn/) showing the intersection between the proteins from the *P. falciparum* proteome containing a prion-forming domain identified by the PLAAC algorithm and the proteins identified in 0.1% SDS-resistant aggregates and in ProteoStat-stained aggregates sorted by flow cytometry. (B to D) Gene ontology analysis of the *P. falciparum* proteins identified in 0.1% SDS-resistant aggregates classified according to: biological process (B), molecular function (C), and cellular component (D).

proteins in live *Plasmodium* parasites are in the cytosol and in some organelles, such as the nuclear membrane. Until future research unveils the potential physiological role of amyloids in *Plasmodium*, perhaps this characteristic of the parasite could be exploited for the development of new therapeutic strategies. From a generic point of view,

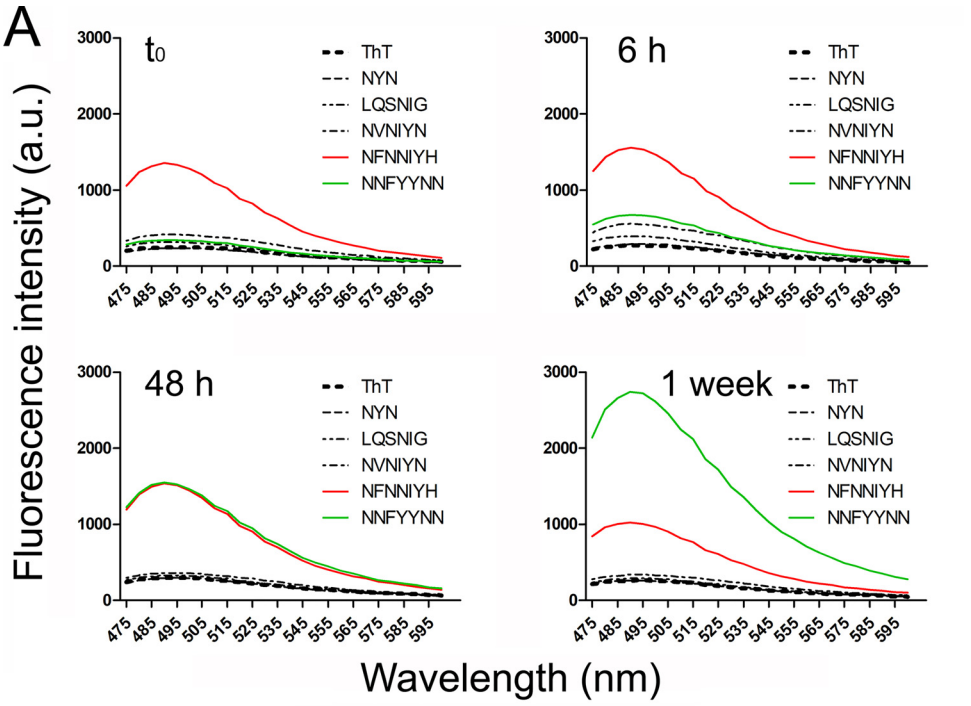

FIG 7 Peptide characterization. (A) ThT fluorescence analysis of the peptides after different incubation times. (B) Transmission electron microscopy images of the peptides. Scale bars, 500 nm.

conformational disorders occur when the load of protein aggregates surpasses the handling capacity of the cellular protein quality control machinery. Such proteostatic deregulation can be externally stimulated, as shown by the intracellular aggregation of the endogenous yeast Sup35 protein, which can be triggered by introducing in the cell aggregative seeds formed *in vitro* by the LCR of this protein (46). External actuation on *Plasmodium* proteostasis has been also shown when the function of the chaperone protein PfHsp110c was knocked down in the parasites and aggregation of LCR-containing proteins took place, which led to the pathogen's death (24). Interestingly, the antimalarial drug methylene blue had been found to promote the formation of amyloid β peptide (Aβ) fibrils (47), and the front-line antimalarial artemisinin has been recently described to kill malaria parasites by damaging proteins and inhibiting the proteasome (48). Indeed, artemisinin resistance has been associated with increased expression of unfolded protein response pathways (49). In bacteria, the cytotoxicity of protein aggregation has been successfully used to kill the pathogen without affecting the mammalian host (50).

Several experimental evidences sustain the possibility that protein aggregation could be harnessed to be developed into new antimalarial approaches: (i) the aggregation of proteins is a generic phenomenon (14); (ii) such aggregates are often cytotoxic (51, 52); (iii) aggregation-prone regions can be reliably predicted (53), and they can trigger the aggregation of complete proteins (54, 55); (iv) most *Plasmodium* proteins have predicted aggregation-prone stretches (9, 24); (v) seeding primes aggregation reactions (56, 57); and (vi) homologous seeding is more efficient than heterologous seeding (56–58), thus limiting the risk of peptide cross-reactivity with proteins from the host.

The presence in the blood circulation upon *Plasmodium* infection of abundant proteins containing prion-like domains suggests that malaria might have to be classified as an amyloidosis, which would call for a reevaluation of potential amyloid-related pathogenic mechanisms triggered by the parasite. However, since the *Plasmodium* proteins identified in 0.1% SDS-resistant aggregates are involved in many critical parasite processes, it is also reasonable to hypothesize that their aggregation might be harmful for the pathogen and therefore helpful for the survival of the human host. Although this might lead one to speculate that protein aggregation can result from an anti-parasitic action of the host, some experimental evidences suggest otherwise. Protein aggregation of *Plasmodium* proteins has been observed in *in vitro* cultures, which are free from any cells or molecules related to human antimicrobial defenses. In addition, murine malaria parasites contain *in vivo* abundant protein aggregates that do not affect the well-known life cycle of the pathogen within the mammalian host. Finally, we have also detected aggregated proteins in the *Plasmodium* stages of the mosquito, whose immune system is very primitive and not expected to exert antiparasitic actions similar to those found in humans.

Preliminary growth inhibition assays indicated that aggregative peptides present in presumably essential *Plasmodium* proteins and selected for their aggregative capacity do not affect the parasite's viability in *in vitro* cultures. Although a poor peptide entry into the cell might be responsible for the observed lack of activity, other alternative explanations must be considered. Intriguingly, the protein aggregation inhibitor rapamycin (59–61) had been observed to have antimalarial activity (62), and the antimalarial drugs curcumin and quercetin had been reported to inhibit the formation of Aβ fibrils (63, 64), suggesting the possibility that intracellular protein aggregates might actually have a functional role for the survival of the parasite. If a reduced protein aggregation can be associated with a decrease in parasite viability, then future antimalarial strategies based on the upsetting of the pathogen's proteostasis and therefore affecting multiple gene products could represent the entry to radically new therapeutic approaches that might minimize drug resistance evolution.

MATERIALS AND METHODS

Preparation of *P. falciparum* blood stages and female gametes. Human RBCs were obtained and prepared as described elsewhere (65). Cultures of the *P. falciparum* 3D7 and E5 strains were grown *in vitro* in human RBCs using previously described conditions (66). Synchronized cultures were obtained by ring-stage enrichment through 5% sorbitol lysis (67), and the medium was changed every 2 days

maintaining 3% hematocrit. Late-form stages were purified in 70% Percoll (GE Healthcare) (67, 68). Previously described protocols were used for the preparation of *P. falciparum* merozoites (69), gametocytes (70), and female gametes (71).

Briefly, to obtain *P. falciparum* merozoites, a highly synchronized culture was established by performing two sorbitol lyses (days 1 and 3), a Percoll cushion purification of highly mature schizonts (day 4), and another sorbitol lysis 5 h after Percoll. This 0/5-h ring culture was then grown for 24 h until trophozoites were obtained. At this point, pRBCs were separated from parasite-free RBCs by magnetic-assisted cell sorting (VarioMACS; Miltenyi Biotec), and trophozoites were grown and monitored hourly until segmented schizonts were observed (33 h after the second sorbitol treatment). Next, 10 μM E-64 protease inhibitor was added to the culture to avoid schizont rupture, and cells were grown for 9 h (42 h after the last sorbitol treatment). Finally, merozoites were obtained by passing the synchronized schizont culture through a 1.2-μm filter (Ministart syringe filter; Sartorius). *P. falciparum* gametocytes were obtained using the gametocyte-generating E5 subclone of the 3D7 strain, kindly provided by Alfred Cortés. Briefly, a culture containing 10% rings was grown in Roswell Park Memorial Institute 1640 culture medium (RPMI; Gibco, Paisley, UK), supplemented with 5 mg/ml AlbuMAX II (Invitrogen) to obtain RPMI-A, and with 50 mM *N*-acetylglucosamine to inhibit asexual replication and to select sexually committed ring-stage parasites. After 24 h, the medium was replaced daily for 2 weeks, without further addition of fresh blood. *P. falciparum* female gametes were obtained from stage V gametocytes by replacing the medium by *P. falciparum* activation medium (RPMI containing 0.2% $NaHCO_3$, 25 mM HEPES, 20% [vol/vol] heat-inactivated human serum, 100 μM xanthurenic acid [pH 8.0]) and incubating for 20 min at room temperature. *P. falciparum* sporozoites were commercially obtained (Sanaria, Inc., Rockville, MD).

Preparation of *P. berghei* and *P. yoelii* mosquito stages. The *P. berghei* parasite strain used was the transgenic line CTRP-GFP (72), expressing green fluorescent protein (GFP) only during ookinete stages. To obtain gametes and ookinetes, TO-Ola mice were simultaneously injected intraperitoneally with 200 μl of phenylhydrazine (6 mg/ml in 9% NaCl; 60 mg/kg [body weight]) to induce reticulocyte production and with 10^8 *P. berghei*-infected erythrocytes. To monitor the growth of the parasite, Giemsa-stained tail blood smears and exflagellation assays were prepared 72 and 96 h after inoculation. In a typical experiment, at day 3 postinfection, average parasitemias were 10 to 20% with all parasite blood stages (rings, trophozoites, schizonts, and gametocytes) present. To assess the percentage of mature gametocytes at days 4 to 5 postinfection, exflagellation assays were performed by mixing a tail blood drop with 15 μl of exflagellating medium: cold (19°C) RPMI (pH 8.4), containing 0.2% $NaHCO_3$, 25 mM HEPES, 50 mg/liter hypoxanthine, 2 mM glutamine, 5,000 U/ml penicillin, 5 mg/ml streptomycin, and 20% (vol/vol) heat-inactivated fetal bovine serum (Gibco, Paisley, UK). Exflagellating centers were counted microscopically at $\times$400 magnification. When the number of exflagellation centers per field was $>$10, mice were exsanguinated by cardiac puncture with a heparinized needle (30 U/ml blood). Blood was diluted 1:10 with exflagellation medium and incubated at 19°C. Gametes appeared after 20 min of incubation, whereas ookinetes were observed after 20 h. *P. berghei* oocysts were obtained by allowing parasites to develop in mosquito midguts. Briefly, 2-h-starved *A. gambiae* mosquitoes were allowed to feed for 20 min on mice infected with a high gametocytemia ($>$10 exflagellating centers/field at $\times$400 magnification) of *P. berghei* strain 507 (73), which constitutively expresses GFP in all parasite stages. After the blood meal, mosquitoes were maintained at 19°C for 7 to 21 days. At day 13, mosquitoes were dissected and midguts were resuspended in 200 μl of phosphate-buffered saline (PBS), proceeding immediately to fluorescence microscopy examination.

To obtain *P. yoelii* asexual stages, BALB/c mice were inoculated 2×10^7 red blood cells from *P. yoelii yoelii* 17XL-infected mice by intraperitoneal injection. Parasitemia was monitored daily by microscopic examination of Giemsa-stained thin blood smears. At day 5 after infection, mice where exsanguinated by cardiac puncture with a 10% EDTA-impregnated needle, and the blood was diluted 1:10 with RPMI-A immediately before proceeding to aggregated protein staining and fluorescence microscopy examination.

***In silico* analysis of the *P. falciparum* proteome.** The *P. falciparum* (isolate 3D7) reference proteome (ID UP000001450, release 2017_01), consisting of 5,369 proteins, was downloaded from UniProt (74). Protein sequences were screened with the PLAAC algorithm (75), using default parameters and the complete proteome as background, in order to identify potential prion-like domains, which rendered 342 proteins.

The abundance and aggregation propensity of each protein in the proteome were calculated and plotted as described elsewhere (76). Briefly, abundance (*C*) was calculated as the $\log_{10}$ of the protein concentration values obtained from PaxDb (77), which were normalized by rescaling them between 0 and 1 as follows:

$$C = \frac{\left(Ci - \min\left(Ci \ldots Cn\right)\right)}{\left(\max\left(Ci \ldots Cn\right) - \min\left(Ci \ldots Cn\right)\right)},$$

where C_{min} is the minimum value of protein concentration from the data set, C_{max} is the maximum value of protein concentration from the data set, and (*Ci*...*Cn*) is each value of protein concentration from the data set.

The aggregation tendency (*A*) was obtained using the TANGO algorithm, which estimates the cross-beta aggregation propensity in peptides and denatured proteins (78). For the estimation, TANGO parameters were set at pH 7.4, 37°C, and 0.25 mM ionic strength, using the output parameter "cross beta-aggregation," which was then normalized in the same manner by rescaling the values between 0 and 1 as follows:

$$A = \frac{\left(Ai - \min\left(Ai \ldots An\right)\right)}{\left(\max\left(Ai \ldots An\right) - \min\left(Ai \ldots An\right)\right)},$$

where A_{min} is the minimum TANGO cross beta-aggregation score from the data set, A_{max} is the maximum TANGO cross beta-aggregation score from the data set, and (*Ai*...*An*) is each TANGO cross beta-aggregation score from the data set.

Analysis of ProteoStat-stained amyloid deposits in live *Plasmodium* parasites. The *in vivo* intracellular formation of protein aggregates in the different *Plasmodium* stages was routinely determined with the ProteoStat aggresome detection reagent (Enzo Life Sciences, Inc.) according to the manufacturer's instructions. As a standard protocol, 200 μl of a *P. falciparum in vitro* culture (3% hematocrit, 4.5% parasitemia) were harvested and washed twice with 1 ml of 7.5 mg of bovine serum albumin (BSA)/ml of PBS (PBS/BSA); the resulting cell pellet was taken up in 200 μl of PBS/BSA containing 2 μg/ml Hoechst 33342 and ProteoStat (1:3,000 or 1:5,000 stock dilution for fluorescence microscopy or flow cytometry analysis, respectively) and incubated for 30 min in the dark at room temperature before being washed again twice with 1 ml of PBS/BSA. When needed, labeling of RBC membranes was performed simultaneously by including 5 μg/ml of wheat germ agglutinin functionalized with Oregon Green 488 (Invitrogen; λ_{ex} = 488 nm, λ_{em} = 510 to 550 nm). For microscopy, 10 μl of PBS/BSA washed cell suspensions were transferred into a Lab-Tek chambered cover glass (Nunc, Thermo Fisher Scientific) containing 180 μl of PBS/BSA and examined with an Olympus IX51 inverted system microscope or with a Leica TCS SP5 laser scanning confocal microscope using a ×63 immersion oil objective with 1.4 numeric aperture.

ProteoStat staining of *P. yoelii* and *P. berghei* asexual stages, *P. berghei* gametes, ookinetes, and oocysts, and *P. falciparum* sporozoites, merozoites, gametocytes, and gametes was performed as described above, using 200 μl of each preparation. Samples were viewed in a Zeiss Axioskop 2 Plus microscope fitted with an Axiovert CCD camera (Zeiss). Fluorescence was detected by excitation at 405 nm for Hoechst 33342 and 488 nm for both GFP and ProteoStat and emission collection in the ranges 415 to 500, 510 to 550, and 590 to 670 nm, respectively.

For flow cytometry, 10 μl of the cell suspension were mixed with 490 μl of sterile PBS in a disposable cytometer tube before being gated on a LSRFortessa flow cytometer (BD Biosciences, San Jose, CA) set up with the five-laser, 20-parameter standard configuration. Forward and side scatter were used in a logarithmic scale to gate the RBC population. Acquisition was configured to stop after recording 10,000 events. Hoechst 33342 and ProteoStat fluorescence levels were detected, respectively, by excitation with a 355 nm/60 mW and 488 nm/100 mW lasers, and emissions were collected with 450/50BP nm and 610LP-610/20BP bandpass filters.

Immunocytochemical detection of amyloid fibrils. pRBC culture smears were fixed on ice for 2 min using freshly prepared acetone:methanol (4:1). Rabbit anti-amyloid fibril OC antibody (AB2286; Merck Millipore, Darmstadt, Germany) and the secondary antibody, fluorescein-labeled AffiniPure donkey anti-rabbit IgG (711-095-152; Jackson ImmunoResearch Europe, Ltd., Cambridge, UK), were prepared at 1:200 and 1:100 dilutions, respectively, in PBS supplemented with 0.75% BSA. Smears were incubated with the primary antibody for 2 h, washed three times with PBS, incubated with the secondary antibody for 1 h, and then washed again three times with PBS. Finally, DAPI (4′,6′-diamidino-2-phenylindole; catalog no. 10236276001; Roche Applied Science, Foster City) was added to the smears at 1 μg/ml in PBS and, after a 30-min incubation, the slides were mounted with ProLong Gold antifade reagent (Life Technologies, Carlsbad, CA) and observed in a confocal microscope (TCS-SP5; Leica Microsystems, Wetzlar, Germany).

Flow cytometry sorting of ProteoStat-stained proteins in live *P. falciparum* blood stages. A 3D7 *P. falciparum* culture (3% hematocrit, 4% parasitemia), containing ca. 6×10^{12} parasites, was spun down (300 × *g*, 5 min) and washed once with RPMI. To disrupt erythrocyte membranes, the resulting pellet was taken up in 10 ml of lysis solution consisting of 1.5 mg/ml saponin in complete PBS containing 1× Mini protease inhibitor cocktail (cOmplete [Roche]; one tablet in 10.5 ml for 1× concentration) and then incubated for 15 min (4°C); finally, the free parasites were spun down (10,000 × *g*, 3 min, 4°C) and washed three times with complete PBS. To lyse *Plasmodium* cells, the samples were taken up in 1 ml of 1× cOmplete in H_2O, exposed to three freeze-thaw cycles (ethanol-dry ice bath for 2 min/37°C bath for 5 min), and forced 10 times through a 30-gauge needle, making fast strokes. The resulting homogenate was diluted in complete PBS, stained with ProteoStat at a final dye dilution of 1:5,000, and applied to a fluorescence-activated sorter (Aria SORP 5L) with an outlet nozzle of 130 μm. The 488-nm laser potency was adjusted to 100 mW, and the flow rate was set to the minimum (200 events/s) with a sheath pressure of 10 lb/in^2. ProteoStat positive events were detected using a band pass of 610/20 and 600 LP and harvested in 5-ml polystyrene cytometry tubes (659,108 positive events in 10 ml). To verify sorting, homogenate and postsorting ProteoStat positive and negative samples were loaded on an Amnis ImageStream^X Mark II imaging flow cytometer (Luminex Corp.). Sorted aggregates were kept at −20°C for 24 h before being dialyzed (benzoylated dialysis tubing, 2-kDa molecular weight cutoff) against 2 liters of ddH_2O (MilliQ system; Millipore) for 8 h, changing the water every 2 h. After dialysis, 12 ml of aggregate solution was recovered and lyophilized for 30 h, and the remaining pellet was dissolved directly in 100 μl of 1× Laemmli sample buffer and loaded in a 1.5-mm-thick 12.5% SDS-polyacrylamide gel electrophoresis (SDS-PAGE) run for 80 min at 40 mA. Colloidal Coomassie blue G-250-stained bands were excised and subjected to LC-MS/MS analysis (79). A full description of the LC-MS/MS protocol followed is provided in the supplemental material.

Isolation of aggregative proteins insoluble in 0.1% SDS. Aggregative proteins insoluble in 0.1% SDS were isolated as previously described (80). First, 40-ml portions of a *P. falciparum* preparation

containing approximately 5×10^9 late-form trophozoite- and schizont-stage parasites (24 to 36 and 36 to 48 h postinvasion, respectively) that had been purified from *in vitro* cultures in 70% Percoll were washed with sterile PBS and spun down ($300 \times g$, 5 min), and the the resulting cell pellet was stored at −20°C. To release cell contents, the pellet was thawed in 2 ml of radioimmunoprecipitation assay buffer (50 mM Tris-HCl [pH 9.4], containing 150 mM NaCl, 1% Triton X-100, 0.1% SDS, 2 mM EDTA, and 5% glycerol) supplemented with 1× cOmplete. The solution was homogenized on ice by pipetting constantly up and down for 30 min. Next, the lysate was spun ($300 \times g$, 2.5 min) to remove debris and unbroken cells, and the supernatant was carefully loaded on top of 1 ml of 40% sucrose and ultracentrifuged ($200{,}000 \times g$, 1 h) in order to pellet large insoluble aggregates. These were resuspended in 400 μl of SDS lysis buffer (PBS containing 2% SDS, 5 mM dithiothreitol, and 2 mM EDTA, supplemented with 1× cOmplete) and incubated at 37°C for 30 min, pipetting up and down every 2 min. The resulting lysate was spun down ($16{,}000 \times g$, 12 min), and the supernatant was recovered and concentrated using a 3-kDa cutoff Vivaspin 500 column ($15{,}000 \times g$, 30 min, room temperature). The concentrated lysate was fractionated in a 12.5% SDS-PAGE and stained with Coomassie brilliant blue R-250, and the material not entering the stacking gel was excised and subjected to LC-MS/MS analysis.

Characterization of peptide aggregation *in vitro* and *Plasmodium* growth inhibition assays. Selected peptides were purchased from CASLO ApS c/o Scion Denmark Technical University and diluted in dimethyl sulfoxide to obtain a ≥50 mM stock solution, which was further diluted to 150 μM in PBS (pH 7.4), filtered twice through a 0.22-μm filter to ensure reproducibility in the aggregation kinetics, and incubated at 37°C and 60 rpm/min (Eppendorf ThermoMixer C) for the times indicated before proceeding to ThT measurements and transmission electron microscopy sample preparation. At different times, ThT was mixed with the sample to a final concentration of 25 μM for both peptide and ThT. Fluorescence emission was collected in the range 470 to 600 nm using an excitation wavelength of 450 nm (Infinite M200 PRO multimode microplate reader; Tecan, Switzerland). For transmission electron microscopy analysis, a carbon-coated copper grid was deposited on top of a 50-μl drop of the peptide solution (150 μM in PBS, vortexed immediately before pipetting), which had been incubated for up to 1 week. After 30 min, the excess liquid was removed with filter paper, and the grid was placed on top of a water drop for 30 s and finally negatively stained for 2 min with 20 μl of 2% uranyl acetate. Samples were observed using a JEM 1010 transmission electron microscope (JEOL, Ltd., Japan). Images were acquired using a CCD Orius camera (Gatan, Inc.).

Plasmodium growth inhibition assays were performed as previously reported (65). Briefly, sorbitol-synchronized cultures of *P. falciparum* were diluted with human RBCs suspended in RPMI-A growth medium to give a final concentration of 1.5% parasitemia and 3% hematocrit with more than 90% of parasites at ring stage. A total of 150 μl of these pRBC preparations were pipetted to 96-well tissue culture plates, and the required amounts of peptide seeds were added from a 500 μM stock solution in PBS. Typically, cultures were grown for one replication cycle under 5% O_2, 5% CO_2, and 90% N_2 at 37°C for 48 h. For the determination of parasitemia, samples were diluted 1:100 in isotonic PBS and pRBC nuclei (the only nucleated cells present in the culture) were stained by addition of 0.1 μM Syto11 (Thermo Fisher Scientific, Inc.) in the final mixture before proceeding to flow cytometry analysis (81). Alternatively, microscopic counting of Giemsa-stained samples was performed (65). Growth inhibition in peptide-treated samples was defined as the percent decrease in parasitemia within the second generation of parasites relative to untreated control samples. Growth inhibition graphs and 50% inhibitory concentrations were obtained through sigmoidal fitting of growth inhibition data at different peptide concentrations.

Ethics statement. The human blood used in this work was commercially obtained from the Banc de Sang i Teixits (www.bancsang.net). Blood was not specifically collected for this research; the purchased units had been discarded for transfusion, usually because of an excess of blood relative to anticoagulant solution. Prior to their use, blood units underwent the analytical checks specified in the current legislation. Before being delivered to us, unit data were anonymized and irreversibly dissociated, and any identification tag or label had been removed in order to guarantee the nonidentification of the blood donor. No blood data were or will be supplied, and the blood samples will not be used for studies other than those made explicit in this research. The studies reported here were performed in accordance with the current Spanish Ley Orgánica de Protección de Datos and Ley de Investigación Biomédica and under protocols reviewed and approved by the Ethical Committee on Clinical Research from the Hospital Clínic de Barcelona (Reg. HCB/2018/1223, January 23, 2019).

All animal work was carried out in full conformity with Greek regulations consisting of the Presidential Decree (160/91) and law (2015/92) which implement the directive 86/609/EEC from the European Union and the European Convention for the protection of vertebrate animals used for experimental and other scientific purposes and the Presidential Decree 56/2013. The experiments were carried out in a certified animal facility license (EL91-BIOexp-02) and the protocol has been approved by the FORTH Ethics Committee and by the Prefecture of Crete (license number 93491, 30/04/2018).

SUPPLEMENTAL MATERIAL

Supplemental material is available online only.

SUPPLEMENTAL FILE 1, PDF file, 1.2 MB.

ACKNOWLEDGMENTS

X.F.-B. was funded by (i) Spanish Ministry of Science, Innovation and Universities (http://www.ciencia.gob.es/), grant numbers PCIN-2017-100 and RTI2018-094579-B-I00

(which included FEDER funds), and (ii) ERA-NET Cofund EURONANOMED (http://euronanomed.net/), grant number 2017-178 (NANOpheles). I.S.-K. was supported within the NANOpheles European project from Greek national funds cofinanced by the European Union (project number T8EPA2-00026). S.V. was funded by (i) Ministerio de Ciencia, Innovación y Universidades, Spain (http://www.ciencia.gob.es/), grant number BIO2016-78310-R, and (ii) Generalitat de Catalunya, Spain (http://agaur.gencat.cat/), grant number 2017-SGR-908. The funders had no role in study design, data collection and analysis, decision to publish, or preparation of the manuscript. ISGlobal and IBEC are members of the CERCA Program, Generalitat de Catalunya. We acknowledge support from the Spanish Ministry of Science, Innovation and Universities through the Centro de Excelencia Severo Ochoa 2019-2023 Program (CEX2018-000806-S). This research is part of ISGlobal's Program on the Molecular Mechanisms of Malaria, which is partially supported by the Fundación Ramón Areces.

REFERENCES

1. World Health Organization. 2019. World malaria report, 2019. World Health Organization, Geneva, Switzerland.
2. Mbengue A, Bhattacharjee S, Pandharkar T, Liu H, Estiu G, Stahelin RV, Rizk SS, Njimoh DL, Ryan Y, Chotivanich K, Nguon C, Ghorbal M, Lopez-Rubio JJ, Pfrender M, Emrich S, Mohandas N, Dondorp AM, Wiest O, Haldar K. 2015. A molecular mechanism of artemisinin resistance in *Plasmodium falciparum* malaria. Nature 520:683–687. https://doi.org/10.1038/nature14412.
3. Alonso PL, Tanner M. 2013. Public health challenges and prospects for malaria control and elimination. Nat Med 19:150–155. https://doi.org/10.1038/nm.3077.
4. Prudêncio M, Rodriguez A, Mota MM. 2006. The silent path to thousands of merozoites: the *Plasmodium* liver stage. Nat Rev Microbiol 4:849–856. https://doi.org/10.1038/nrmicro1529.
5. Cowman AF, Crabb BS. 2006. Invasion of red blood cells by malaria parasites. Cell 124:755–766. https://doi.org/10.1016/j.cell.2006.02.006.
6. Gardner MJ, Hall N, Fung E, White O, Berriman M, Hyman RW, Carlton JM, Pain A, Nelson KE, Bowman S, Paulsen IT, James K, Eisen JA, Rutherford K, Salzberg SL, Craig A, Kyes S, Chan MS, Nene V, Shallom SJ, Suh B, Peterson J, Angiuoli S, Pertea M, Allen J, Selengut J, Haft D, Mather MW, Vaidya AB, Martin DMA, Fairlamb AH, Fraunholz MJ, Roos DS, Ralph SA, McFadden GI, Cummings LM, Subramanian GM, Mungall C, Venter JC, Carucci DJ, Hoffman SL, Newbold C, Davis RW, Fraser CM, Barrell B. 2002. Genome sequence of the human malaria parasite *Plasmodium falciparum*. Nature 419:498–511. https://doi.org/10.1038/nature01097.
7. Eichinger L, Pachebat JA, Glöckner G, Rajandream MA, Sucgang R, Berriman M, Song J, Olsen R, Szafranski K, Xu Q, Tunggal B, Kummerfeld S, Madera M, Konfortov BA, Rivero F, Bankier AT, Lehmann R, Hamlin N, Davies R, Gaudet P, Fey P, Pilcher K, Chen G, Saunders D, Sodergren E, Davis P, Kerhornou A, Nie X, Hall N, Anjard C, Hemphill L, Bason N, Farbrother P, Desany B, Just E, Morio T, Rost R, Churcher C, Cooper J, Haydock S, van Driessche N, Cronin A, Goodhead I, Muzny D, Mourier T, Pain A, Lu M, Harper D, Lindsay R, Hauser H, James K, Quiles M, Babu MM, Saito T, Buchrieser C, Wardroper A, Felder M, Thangavelu M, Johnson D, Knights A, Loulseged H, Mungall K, Oliver K, Price C, Quail MA, Urushihara H, Hernandez J, Rabbinowitsch E, Steffen D, Sanders M, Ma J, Kohara Y, Sharp S, Simmonds M, Spiegler S, Tivey A, Sugano S, White B, Walker D, Woodward J, Winckler T, Tanaka Y, Shaulsky G, Schleicher M, Weinstock G, Rosenthal A, Cox EC, Chisholm RL, Gibbs R, Loomis WF, Platzer M, Kay RR, Williams J, Dear PH, Noegel AA, Barrell B, Kuspa A. 2005. The genome of the social amoeba *Dictyostelium discoideum*. Nature 435:43–57. https://doi.org/10.1038/nature03481.
8. Aravind L, Iyer LM, Wellems TE, Miller LH. 2003. *Plasmodium* biology: genomic gleanings. Cell 115:771–785. https://doi.org/10.1016/s0092-8674(03)01023-7.
9. Singh GP, Chandra BR, Bhattacharya A, Akhouri RR, Singh SK, Sharma A. 2004. Hyper-expansion of asparagines correlates with an abundance of proteins with prion-like domains in *Plasmodium falciparum*. Mol Biochem Parasitol 137:307–319. https://doi.org/10.1016/j.molbiopara.2004.05.016.
10. Feng ZP, Zhang X, Han P, Arora N, Anders RF, Norton RS. 2006. Abundance of intrinsically unstructured proteins in *Plasmodium falciparum* and other apicomplexan parasite proteomes. Mol Biochem Parasitol 150:256–267. https://doi.org/10.1016/j.molbiopara.2006.08.011.
11. DePristo MA, Zilversmit MM, Hartl DL. 2006. On the abundance, amino acid composition, and evolutionary dynamics of low-complexity regions in proteins. Gene 378:19–30. https://doi.org/10.1016/j.gene.2006.03.023.
12. Tartaglia GG, Cavalli A, Pellarin R, Caflisch A. 2005. Prediction of aggregation rate and aggregation-prone segments in polypeptide sequences. Protein Sci 14:2723–2734. https://doi.org/10.1110/ps.051471205.
13. Halfmann R, Alberti S, Krishnan R, Lyle N, O'Donnell CW, King OD, Berger B, Pappu RV, Lindquist S. 2011. Opposing effects of glutamine and asparagine govern prion formation by intrinsically disordered proteins. Mol Cell 43:72–84. https://doi.org/10.1016/j.molcel.2011.05.013.
14. Chiti F, Dobson CM. 2017. Protein misfolding, amyloid formation, and human disease: a summary of progress over the last decade. Annu Rev Biochem 86:27–68. https://doi.org/10.1146/annurev-biochem-061516-045115.
15. Olzscha H, Schermann SM, Woerner AC, Pinkert S, Hecht MH, Tartaglia GG, Vendruscolo M, Hayer-Hartl M, Hartl FU, Vabulas RM. 2011. Amyloid-like aggregates sequester numerous metastable proteins with essential cellular functions. Cell 144:67–78. https://doi.org/10.1016/j.cell.2010.11.050.
16. Seuring C, Greenwald J, Wasmer C, Wepf R, Saupe SJ, Meier BH, Riek R. 2012. The mechanism of toxicity in HET-S/HET-s prion incompatibility. PLoS Biol 10:e1001451. https://doi.org/10.1371/journal.pbio.1001451.
17. Chen Y, Dokholyan NV. 2008. Natural selection against protein aggregation on self-interacting and essential proteins in yeast, fly, and worm. Mol Biol Evol 25:1530–1533. https://doi.org/10.1093/molbev/msn122.
18. Monsellier E, Chiti F. 2007. Prevention of amyloid-like aggregation as a driving force of protein evolution. EMBO Rep 8:737–742. https://doi.org/10.1038/sj.embor.7401034.
19. Hou F, Sun L, Zheng H, Skaug B, Jiang QX, Chen ZJ. 2011. MAVS forms functional prion-like aggregates to activate and propagate antiviral innate immune response. Cell 146:448–461. https://doi.org/10.1016/j.cell.2011.06.041.
20. Si K, Choi YB, White-Grindley E, Majumdar A, Kandel ER. 2010. *Aplysia* CPEB can form prion-like multimers in sensory neurons that contribute to long-term facilitation. Cell 140:421–435. https://doi.org/10.1016/j.cell.2010.01.008.
21. Patino MM, Liu JJ, Glover JR, Lindquist S. 1996. Support for the prion hypothesis for inheritance of a phenotypic trait in yeast. Science 273:622–626. https://doi.org/10.1126/science.273.5275.622.
22. Muralidharan V, Goldberg DE. 2013. Asparagine repeats in *Plasmodium falciparum* proteins: good for nothing? PLoS Pathog 9:e1003488. https://doi.org/10.1371/journal.ppat.1003488.
23. Przyborski JM, Diehl M, Blatch GL. 2015. Plasmodial HSP70s are functionally adapted to the malaria parasite life cycle. Front Mol Biosci 2:34. https://doi.org/10.3389/fmolb.2015.00034.
24. Muralidharan V, Oksman A, Pal P, Lindquist S, Goldberg DE. 2012. *Plasmodium falciparum* heat shock protein 110 stabilizes the asparagine repeat-rich parasite proteome during malarial fevers. Nat Commun 3:1310. https://doi.org/10.1038/ncomms2306.
25. Acharya P, Kumar R, Tatu U. 2007. Chaperoning a cellular upheaval in

malaria: heat shock proteins in *Plasmodium falciparum*. Mol Biochem Parasitol 153:85–94. https://doi.org/10.1016/j.molbiopara.2007.01.009.
26. Pallarès I, de Groot NS, Iglesias V, Sant'Anna R, Biosca A, Fernàndez-Busquets X, Ventura S. 2018. Discovering putative prion-like proteins in *Plasmodium falciparum*: a computational and experimental analysis. Front Microbiol 9:1737. https://doi.org/10.3389/fmicb.2018.01737.
27. Toombs JA, Petri M, Paul KR, Kan GY, Ben-Hur A, Ross ED. 2012. De novo design of synthetic prion domains. Proc Natl Acad Sci U S A 109:6519–6524. https://doi.org/10.1073/pnas.1119366109.
28. Sabate R, Rousseau F, Schymkowitz J, Ventura S. 2015. What makes a protein sequence a prion? PLoS Comput Biol 11:e1004013. https://doi.org/10.1371/journal.pcbi.1004013.
29. Navarro S, Ventura S. 2014. Fluorescent dye ProteoStat to detect and discriminate intracellular amyloid-like aggregates in *Escherichia coli*. Biotechnol J 9:1259–1266. https://doi.org/10.1002/biot.201400291.
30. Usmani SM, Zirafi O, Müller JA, Sandi-Monroy NL, Yadav JK, Meier C, Weil T, Roan NR, Greene WC, Walther P, Nilsson KP, Hammarström P, Wetzel R, Pilcher CD, Gagsteiger F, Fändrich M, Kirchhoff F, Münch J. 2014. Direct visualization of HIV-enhancing endogenous amyloid fibrils in human semen. Nat Commun 5:3508. https://doi.org/10.1038/ncomms4508.
31. Jena KK, Kolapalli SP, Mehto S, Nath P, Das B, Sahoo PK, Ahad A, Syed GH, Raghav SK, Senapati S, Chauhan S, Chauhan S. 2018. TRIM16 controls assembly and degradation of protein aggregates by modulating the p62-NRF2 axis and autophagy. EMBO J 37:e98358. https://doi.org/10.15252/embj.201798358.
32. Wang G, Dinkins M, He Q, Zhu G, Poirier C, Campbell A, Mayer-Proschel M, Bieberich E. 2012. Astrocytes secrete exosomes enriched with pro-apoptotic ceramide and prostate apoptosis response 4 (PAR-4): potential mechanism of apoptosis induction in Alzheimer disease (AD). J Biol Chem 287:21384–21395. https://doi.org/10.1074/jbc.M112.340513.
33. Nunes da Silva R, Costa CC, Santos MJG, Alves MQ, Braga SS, Vieira SI, Rocha J, Silva AMS, Guieu S. 2019. Fluorescent light-up probe for the detection of protein aggregates. Chem Asian J 14:859–863. https://doi.org/10.1002/asia.201801606.
34. Raju I, Kumarasamy A, Abraham EC. 2011. Multiple aggregates and aggresomes of C-terminal truncated human αA-crystallins in mammalian cells and protection by αB-crystallin. PLoS One 6:e19876. https://doi.org/10.1371/journal.pone.0019876.
35. Franke-Fayard B, Fonager J, Braks A, Khan SM, Janse CJ. 2010. Sequestration and tissue accumulation of human malaria parasites: can we learn anything from rodent models of malaria? PLoS Pathog 6:e1001032. https://doi.org/10.1371/journal.ppat.1001032.
36. Kayed R, Head E, Sarsoza F, Saing T, Cotman CW, Necula M, Margol L, Wu J, Breydo L, Thompson JL, Rasool S, Gurlo T, Butler P, Glabe CG. 2007. Fibril specific, conformation dependent antibodies recognize a generic epitope common to amyloid fibrils and fibrillar oligomers that is absent in prefibrillar oligomers. Mol Neurodegener 2:18. https://doi.org/10.1186/1750-1326-2-18.
37. Díaz-Caballero M, Navarro S, Fuentes I, Teixidor F, Ventura S. 2018. Minimalist prion-inspired polar self-assembling peptides. ACS Nano 12:5394–5407. https://doi.org/10.1021/acsnano.8b00417.
38. Adda CG, Murphy VJ, Sunde M, Waddington LJ, Schloegel J, Talbo GH, Vingas K, Kienzle V, Masciantonio R, Howlett GJ, Hodder AN, Foley M, Anders RF. 2009. *Plasmodium falciparum* merozoite surface protein 2 is unstructured and forms amyloid-like fibrils. Mol Biochem Parasitol 166:159–171. https://doi.org/10.1016/j.molbiopara.2009.03.012.
39. Low A, Chandrashekaran IR, Adda CG, Yao S, Sabo JK, Zhang X, Soetopo A, Anders RF, Norton RS. 2007. Merozoite surface protein 2 of *Plasmodium falciparum*: expression, structure, dynamics, and fibril formation of the conserved N-terminal domain. Biopolymers 87:12–22. https://doi.org/10.1002/bip.20764.
40. Yang X, Adda CG, Keizer DW, Murphy VJ, Rizkalla MM, Perugini MA, Jackson DC, Anders RF, Norton RS. 2007. A partially structured region of a largely unstructured protein, *Plasmodium falciparum* merozoite surface protein 2 (MSP2), forms amyloid-like fibrils. J Pept Sci 13:839–848. https://doi.org/10.1002/psc.910.
41. Marques J, Moles E, Urbán P, Prohens R, Busquets MA, Sevrin C, Grandfils C, Fernàndez-Busquets X. 2014. Application of heparin as a dual agent with antimalarial and liposome targeting activities towards *Plasmodium*-infected red blood cells. Nanomedicine 10:1719–1728. https://doi.org/10.1016/j.nano.2014.06.002.
42. Jayakumar R, Kusiak JW, Chrest FJ, Demehin AA, Murali J, Wersto RP, Nagababu E, Ravi L, Rifkind JM. 2003. Red cell perturbations by amyloid beta-protein. Biochim Biophys Acta 1622:20–28. https://doi.org/10.1016/s0304-4165(03)00101-6.
43. Murali J, Koteeswari D, Rifkind JM, Jayakumar R. 2003. Amyloid insulin interaction with erythrocytes. Biochem Cell Biol 81:51–59. https://doi.org/10.1139/o03-009.
44. Boyle MJ, Langer C, Chan JA, Hodder AN, Coppel RL, Anders RF, Beeson JG. 2014. Sequential processing of merozoite surface proteins during and after erythrocyte invasion by *Plasmodium falciparum*. Infect Immun 82:924–936. https://doi.org/10.1128/IAI.00866-13.
45. Lu C, Zheng X, Zhang W, Zhao H, MacRaild CA, Norton RS, Zhuang Y, Wang J, Zhang X. 2019. Interaction of merozoite surface protein 2 with lipid membranes. FEBS Lett 593:288–295. https://doi.org/10.1002/1873-3468.13320.
46. King CY, Diaz-Avalos R. 2004. Protein-only transmission of three yeast prion strains. Nature 428:319–323. https://doi.org/10.1038/nature02391.
47. Necula M, Breydo L, Milton S, Kayed R, van der Veer WE, Tone P, Glabe CG. 2007. Methylene blue inhibits amyloid Aβ oligomerization by promoting fibrillization. Biochemistry 46:8850–8860. https://doi.org/10.1021/bi700411k.
48. Bridgford JL, Xie SC, Cobbold SA, Pasaje CF, Herrmann S, Yang T, Gillett DL, Dick LR, Ralph SA, Dogovski C, Spillman NJ, Tilley L. 2018. Artemisinin kills malaria parasites by damaging proteins and inhibiting the proteasome. Nat Commun 9:3801. https://doi.org/10.1038/s41467-018-06221-1.
49. Mok S, Ashley EA, Ferreira PE, Zhu L, Lin Z, Yeo T, Chotivanich K, Imwong M, Pukrittayakamee S, Dhorda M, Nguon C, Lim P, Amaratunga C, Suon S, Hien TT, Htut Y, Faiz MA, Onyamboko MA, Mayxay M, Newton PN, Tripura R, Woodrow CJ, Miotto O, Kwiatkowski DP, Nosten F, Day NPJ, Preiser PR, White NJ, Dondorp AM, Fairhurst RM, Bozdech Z. 2015. Population transcriptomics of human malaria parasites reveals the mechanism of artemisinin resistance. Science 347:431–435. https://doi.org/10.1126/science.1260403.
50. Bednarska NG, van Eldere J, Gallardo R, Ganesan A, Ramakers M, Vogel I, Baatsen P, Staes A, Goethals M, Hammarström P, Nilsson KP, Gevaert K, Schymkowitz J, Rousseau F. 2016. Protein aggregation as an antibiotic design strategy. Mol Microbiol 99:849–865. https://doi.org/10.1111/mmi.13269.
51. Bucciantini M, Giannoni E, Chiti F, Baroni F, Formigli L, Zurdo J, Taddei N, Ramponi G, Dobson CM, Stefani M. 2002. Inherent toxicity of aggregates implies a common mechanism for protein misfolding diseases. Nature 416:507–511. https://doi.org/10.1038/416507a.
52. Bucciantini M, Calloni G, Chiti F, Formigli L, Nosi D, Dobson CM, Stefani M. 2004. Prefibrillar amyloid protein aggregates share common features of cytotoxicity. J Biol Chem 279:31374–31382. https://doi.org/10.1074/jbc.M400348200.
53. Belli M, Ramazzotti M, Chiti F. 2011. Prediction of amyloid aggregation *in vivo*. EMBO Rep 12:657–663. https://doi.org/10.1038/embor.2011.116.
54. Ventura S, Zurdo J, Narayanan S, Parreno M, Mangues R, Reif B, Chiti F, Giannoni E, Dobson CM, Aviles FX, Serrano L. 2004. Short amino acid stretches can mediate amyloid formation in globular proteins: the Src homology 3 (SH3) case. Proc Natl Acad Sci U S A 101:7258–7263. https://doi.org/10.1073/pnas.0308249101.
55. Ivanova MI, Sawaya MR, Gingery M, Attinger A, Eisenberg D. 2004. An amyloid-forming segment of β2-microglobulin suggests a molecular model for the fibril. Proc Natl Acad Sci U S A 101:10584–10589. https://doi.org/10.1073/pnas.0403756101.
56. Sabaté R, Espargaró A, de Groot NS, Valle-Delgado JJ, Fernàndez-Busquets X, Ventura S. 2010. The role of protein sequence and amino acid composition in amyloid formation: scrambling and backward reading of IAPP amyloid fibrils. J Mol Biol 404:337–352. https://doi.org/10.1016/j.jmb.2010.09.052.
57. Krebs MR, Morozova-Roche LA, Daniel K, Robinson CV, Dobson CM. 2004. Observation of sequence specificity in the seeding of protein amyloid fibrils. Protein Sci 13:1933–1938. https://doi.org/10.1110/ps.04707004.
58. Wright CF, Teichmann SA, Clarke J, Dobson CM. 2005. The importance of sequence diversity in the aggregation and evolution of proteins. Nature 438:878–881. https://doi.org/10.1038/nature04195.
59. Wyttenbach A, Hands S, King MA, Lipkow K, Tolkovsky AM. 2008. Amelioration of protein misfolding disease by rapamycin: translation or autophagy? Autophagy 4:542–545. https://doi.org/10.4161/auto.6059.
60. Ravikumar B, Duden R, Rubinsztein DC. 2002. Aggregate-prone proteins with polyglutamine and polyalanine expansions are degraded by autophagy. Hum Mol Genet 11:1107–1117. https://doi.org/10.1093/hmg/11.9.1107.

61. King MA, Hands S, Hafiz F, Mizushima N, Tolkovsky AM, Wyttenbach A. 2008. Rapamycin inhibits polyglutamine aggregation independently of autophagy by reducing protein synthesis. Mol Pharmacol 73:1052–1063. https://doi.org/10.1124/mol.107.043398.
62. Bell A, Wernli B, Franklin RM. 1994. Roles of peptidyl-prolyl *CIS-trans* isomerase and calcineurin in the mechanisms of antimalarial action of cyclosporin A, FK506, and rapamycin. Biochem Pharmacol 48:495–503. https://doi.org/10.1016/0006-2952(94)90279-8.
63. Espargaró A, Ginex T, Vadell MD, Busquets MA, Estelrich J, Muñoz-Torrero D, Luque FJ, Sabate R. 2017. Combined *in vitro* cell-based/*in silico* screening of naturally occurring flavonoids and phenolic compounds as potential anti-Alzheimer drugs. J Nat Prod 80:278–289. https://doi.org/10.1021/acs.jnatprod.6b00643.
64. Yang F, Lim GP, Begum AN, Ubeda OJ, Simmons MR, Ambegaokar SS, Chen PP, Kayed R, Glabe CG, Frautschy SA, Cole GM. 2005. Curcumin inhibits formation of amyloid beta oligomers and fibrils, binds plaques, and reduces amyloid *in vivo*. J Biol Chem 280:5892–5901. https://doi.org/10.1074/jbc.M404751200.
65. Urbán P, Estelrich J, Cortés A, Fernàndez-Busquets X. 2011. A nanovector with complete discrimination for targeted delivery to *Plasmodium falciparum*-infected versus noninfected red blood cells *in vitro*. J Control Release 151:202–211. https://doi.org/10.1016/j.jconrel.2011.01.001.
66. Cranmer SL, Magowan C, Liang J, Coppel RL, Cooke BM. 1997. An alternative to serum for cultivation of *Plasmodium falciparum in vitro*. Trans R Soc Trop Med Hyg 91:363–365. https://doi.org/10.1016/s0035-9203(97)90110-3.
67. Lambros C, Vanderberg JP. 1979. Synchronization of *Plasmodium falciparum* erythrocytic stages in culture. J Parasitol 65:418–420. https://doi.org/10.2307/3280287.
68. Radfar A, Méndez D, Moneriz C, Linares M, Marín-García P, Puyet A, Diez A, Bautista JM. 2009. Synchronous culture of *Plasmodium falciparum* at high parasitemia levels. Nat Protoc 4:1899–1915. https://doi.org/10.1038/nprot.2009.198.
69. Le Roch KG, Zhou Y, Blair PL, Grainger M, Moch JK, Haynes JD, de la Vega P, Holder AA, Batalov S, Carucci DJ, Winzeler EA. 2003. Discovery of gene function by expression profiling of the malaria parasite life cycle. Science 301:1503–1508. https://doi.org/10.1126/science.1087025.
70. Saliba KS, Jacobs-Lorena M. 2013. Production of *Plasmodium falciparum* gametocytes *in vitro*. Methods Mol Biol 923:17–25. https://doi.org/10.1007/978-1-62703-026-7_2.
71. Ruecker A, Mathias DK, Straschil U, Churcher TS, Dinglasan RR, Leroy D, Sinden RE, Delves MJ. 2014. A male and female gametocyte functional viability assay to identify biologically relevant malaria transmission-blocking drugs. Antimicrob Agents Chemother 58:7292–7302. https://doi.org/10.1128/AAC.03666-14.
72. Vlachou D, Zimmermann T, Cantera R, Janse CJ, Waters AP, Kafatos FC. 2004. Real-time, *in vivo* analysis of malaria ookinete locomotion and mosquito midgut invasion. Cell Microbiol 6:671–685. https://doi.org/10.1111/j.1462-5822.2004.00394.x.
73. Janse CJ, Franke-Fayard B, Mair GR, Ramesar J, Thiel C, Engelmann S, Matuschewski K, van Gemert GJ, Sauerwein RW, Waters AP. 2006. High efficiency transfection of *Plasmodium berghei* facilitates novel selection procedures. Mol Biochem Parasitol 145:60–70. https://doi.org/10.1016/j.molbiopara.2005.09.007.
74. UniProt Consortium. 2015. UniProt: a hub for protein information. Nucleic Acids Res 43:D204–D212. https://doi.org/10.1093/nar/gku989.
75. Lancaster AK, Nutter-Upham A, Lindquist S, King OD. 2014. PLAAC: a web and command-line application to identify proteins with prion-like amino acid composition. Bioinformatics 30:2501–2502. https://doi.org/10.1093/bioinformatics/btu310.
76. Carija A, Pinheiro F, Iglesias V, Ventura S. 2019. Computational assessment of bacterial protein structures indicates a selection against aggregation. Cells 8:E856. https://doi.org/10.3390/cells8080856.
77. Wang M, Weiss M, Simonovic M, Haertinger G, Schrimpf SP, Hengartner MO, von Mering C. 2012. PaxDb, a database of protein abundance averages across all three domains of life. Mol Cell Proteomics 11:492–500. https://doi.org/10.1074/mcp.O111.014704.
78. Fernandez-Escamilla AM, Rousseau F, Schymkowitz J, Serrano L. 2004. Prediction of sequence-dependent and mutational effects on the aggregation of peptides and proteins. Nat Biotechnol 22:1302–1306. https://doi.org/10.1038/nbt1012.
79. Moles E, Urbán P, Jiménez-Díaz MB, Viera-Morilla S, Angulo-Barturen I, Busquets MA, Fernàndez-Busquets X. 2015. Immunoliposome-mediated drug delivery to *Plasmodium*-infected and noninfected red blood cells as a dual therapeutic/prophylactic antimalarial strategy. J Control Release 210:217–229. https://doi.org/10.1016/j.jconrel.2015.05.284.
80. Kryndushkin D, Pripuzova N, Burnett BG, Shewmaker F. 2013. Non-targeted identification of prions and amyloid-forming proteins from yeast and mammalian cells. J Biol Chem 288:27100–27111. https://doi.org/10.1074/jbc.M113.485359.
81. Davis BH. 2001. Diagnostic utility of red cell flow cytometric analysis. Clin Lab Med 21:829–840.

Detection of protein aggregation in live *Plasmodium* parasites

Arnau Biosca,[a,b,c] Inés Bouzón-Arnáiz,[a,b,c] Lefteris Spanos,[d] Inga Siden-Kiamos,[d] Valentín Iglesias,[e,f] Salvador Ventura,[e,f] Xavier Fernàndez-Busquets[a,b,c]

[a]Barcelona Institute for Global Health (ISGlobal, Hospital Clínic-Universitat de Barcelona), Rosselló 149-153, ES-08036 Barcelona, Spain

[b]Nanomalaria Group, Institute for Bioengineering of Catalonia (IBEC), The Barcelona Institute of Science and Technology, Baldiri Reixac 10-12, ES-08028 Barcelona, Spain

[c]Nanoscience and Nanotechnology Institute (IN2UB), University of Barcelona, Martí i Franquès 1, ES-08028 Barcelona, Spain

[d]Institute of Molecular Biology and Biotechnology, FORTH, N. Plastira 100, 700 13 Heraklion, Greece

[e]Institut de Biotecnologia i de Biomedicina, Universitat Autònoma de Barcelona, ES-08193 Bellaterra, Spain

[f]Departament de Bioquímica i Biologia Molecular, Universitat Autònoma de Barcelona, ES-08193 Bellaterra, Spain

Supplemental Material

Supplemental Methods

LC-MS/MS analysis. Trypsin digestion of proteins in gel slabs was performed in a ProGest^{TM} automatic digestor (Genomic Solutions). Each sample was washed with 25 mM NH_4HCO_3 and acetonitrile (ACN), reduced in 20 mM DTT (60 min, 56 °C), alkylated in 50 mM iodoacetamide (30 min, 30 °C, protected from light) and digested with 80 ng of porcine trypsin (Trypsin Gold, Promega) for 16 h at 37 °C. The resulting peptides were extracted from the gel matrix with 10% formic acid (FA) and ACN, and dried in a SpeedVac concentrator.

Mass spectrometry was performed in a NanoAcquity HPLC system (Waters) coupled to an OrbitrapVelos mass spectrometer (Thermo Scientific). Dried extracts were taken up in 1% FA and an aliquot was injected into the liquid chromatography system equipped with a reverse phase C18 column (75 μm internal diameter, 25 cm length, 1.7 μm particle NanoAcquity BEH column, Waters), with a mobile phase 1-40% B gradient in 30 min followed by a 40-60% B gradient in 5 min (A: 0.1% FA in water; B: 0.1% FA in ACN) and a flow rate of 250 nl/min. Eluted peptides were ionized in an emitter needle (PicoTipTM, New Objective) with an applied spray voltage of 2 KV. A 300-1,700 m/z range of peptide masses was analyzed in data dependent mode where a full scan was acquired with a resolution of 60,000 full width at half maximum at 400 m/z. Within this range, the 15 most abundant peptides (≥500 counts) were selected from each scan and fragmented in the linear ion trap using collision-induced dissociation (38% normalized collision energy) with He as the collision gas. The scan time settings were: Full MS: 250 ms (1 microscan) and MSn: 120 ms. Generated *.raw data files were collected with Thermo Xcalibur (v. 2.2).

A database was created by merging all human protein entries present in the Swiss-Prot database with all entries for *P. falciparum* (isolate 3D7) present in the Uniprot database (January 2016). A small database with common laboratory protein contaminants was also added and *.raw data files obtained in the LC-MS/MS analyses were used to search with SequestHT search engine using Thermo Proteome Discover (v. 1.4.1.14) against the aforementioned database. Both target and a decoy database were searched to obtain a false discovery rate (FDR), and thus estimate the number of incorrect peptide-spectrum matches that exceeded a given threshold, applying preestablished search parameters (enzyme: trypsin; missed cleavage: 5; fixed modifications: carbamidomethyl of cysteine; variable modificacions: oxidation of methionine; peptide tolerance: 10 ppm and 0.6 Da for MS and MS/MS spectra, respectively). To improve the sensitivity of the database search, the semi-supervised learning machine Percolator was used in order to discriminate correct from incorrect peptide spectrum matches. Percolator assigns a q-value to each spectrum, which is defined as the minimal FDR at which the identification is deemed correct (0.01, strict; 0.05, relaxed). These q values are estimated using the distribution of scores from decoy database search.

Supplemental Figures

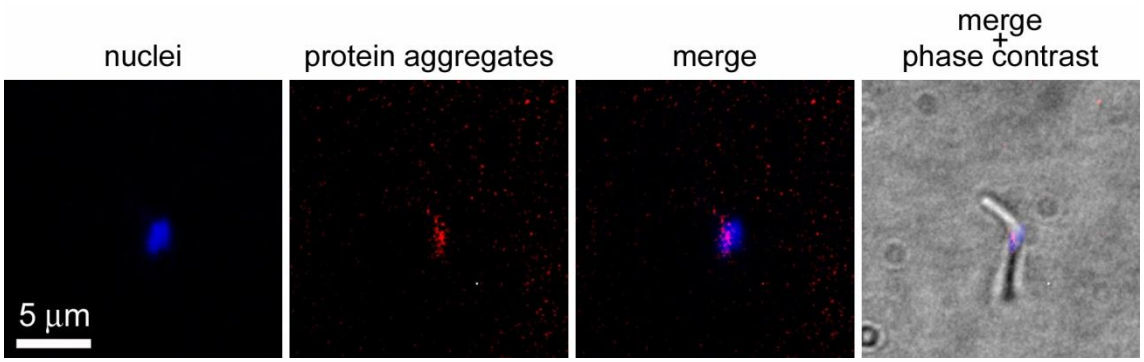

Fig. S1. ProteoStat® staining of *P. falciparum* sporozoite.

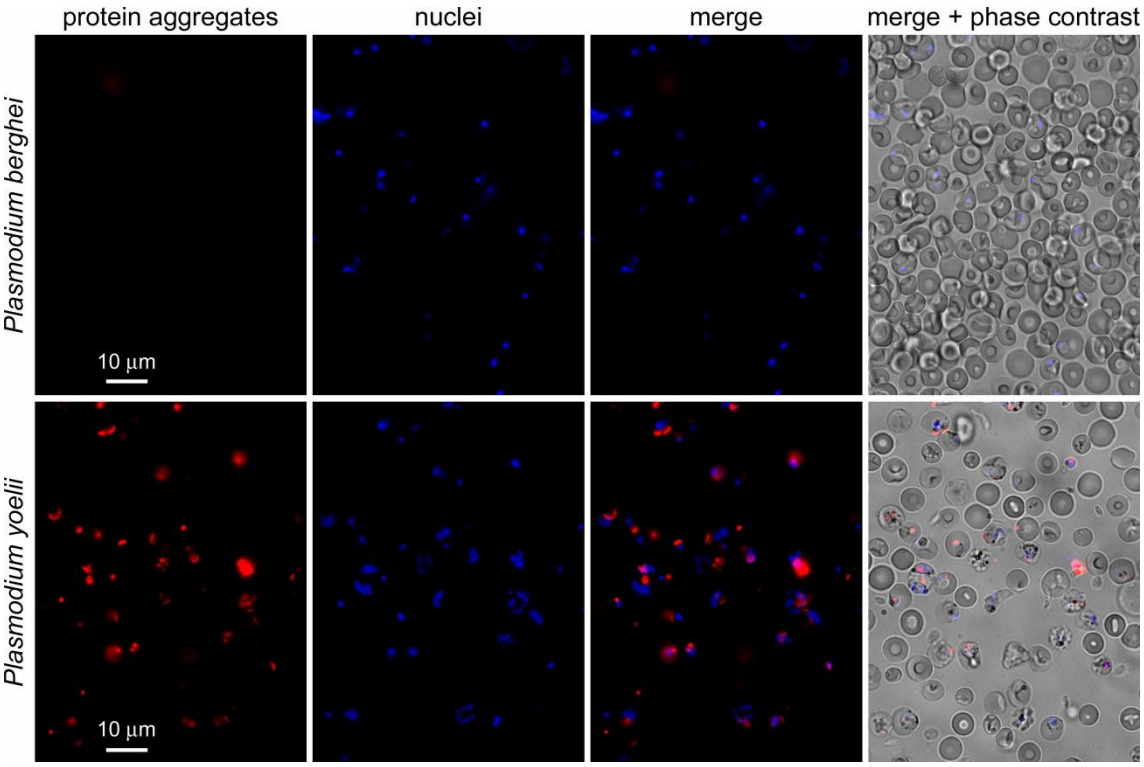

Fig. S2. ProteoStat® staining of *P. berghei* and *P. yoelii* blood stages.

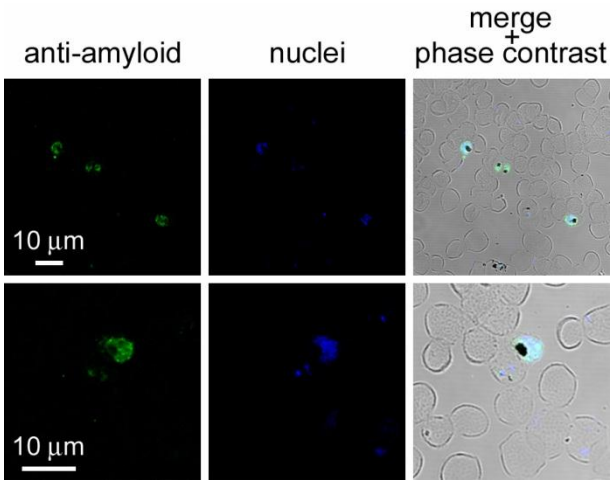

Fig. S3. Anti-amyloid Ab staining of pRBC cultures.

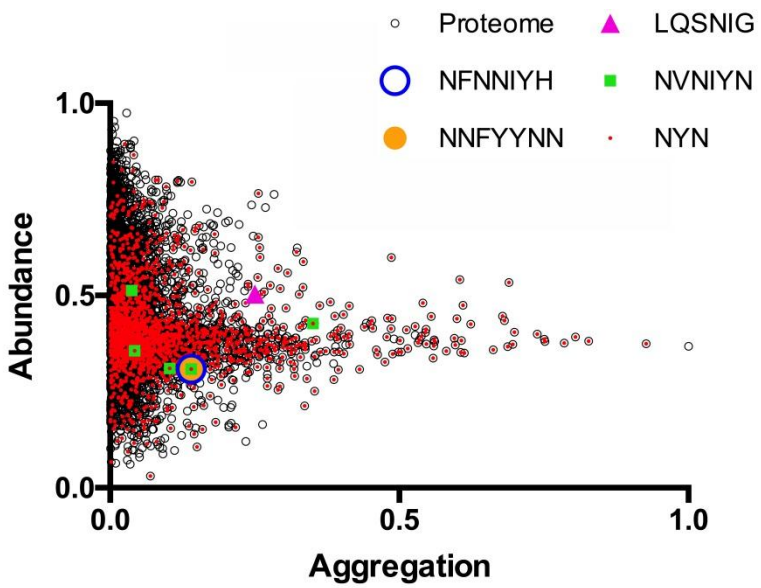

Fig. S4. Two axes dot plot for the peptide aggregation and abundance values.

Table S1. Proteins identified in the ProteoStat®-stained aggregates sorted by flow cytometry.

Accession	Description	Score	Coverage	# Proteins	# Unique peptides	# Peptides	# PSMs	# AAs	MW [kDa]	pI
Q8I0U8	Merozoite surface protein 1	233.03	25.29	1	35	35	269	1720	195.6	6.51
Q8I0P6	Elongation factor 1 alpha	141.51	54.63	1	15	18	192	443	48.9	9.06
Q8IB24	Heat shock protein 70	137.58	36.04	1	19	19	189	677	73.9	5.67
C0H571	High molecular weight rhoptry protein 2	121.15	20.46	1	25	25	187	1378	162.6	8.27
Q8IKK7	Glyceraldehyde-3-phosphate dehydrogenase	108.86	51.63	1	13	13	125	337	36.6	7.69
Q8IC05	Heat shock protein 90	108.83	32.21	1	19	19	139	745	86.1	5.01
Q8IDQ9	Phosphoethanolamine N-methyltransferase	69.79	42.48	1	8	8	77	266	31.0	5.60
Q76NM3	L-lactate dehydrogenase	68.38	41.46	1	10	10	50	316	34.1	7.55
Q8I395	High molecular weight rhoptry protein 3	60.21	17.06	1	11	11	81	897	104.8	6.67
C6KTA4	Pyruvate kinase	49.25	22.70	1	9	9	80	511	55.6	7.55
O77309	Cytoadherence linked asexual protein 3.2	48.24	16.10	1	19	19	104	1416	167.4	7.15
Q8I4X0	Actin-1	47.04	37.77	1	9	12	72	376	41.8	5.34
Q8I2X4	Heat shock protein 70	40.66	23.16	1	11	11	44	652	72.3	5.31
Q8IIV2	Histone H4	40.40	39.81	1	4	5	38	103	11.4	11.22
Q8I0V4	Endoplasmin homolog, putative	35.34	16.44	1	9	9	48	821	95.0	5.41
Q8IKW5	Elongation factor 2	30.60	15.50	1	8	8	42	832	93.5	6.80
Q8ILZ1	Rhoptry-associated protein 1	23.72	16.62	1	9	9	33	782	90.0	7.11
Q6LFH8	Ornithine aminotransferase	23.71	11.84	1	4	4	29	414	46.0	6.89
Q7KQL5	Tubulin beta chain	20.87	7.64	1	3	3	24	445	49.7	4.83
C0H4V6	14-3-3 protein	19.25	19.47	1	4	4	21	262	30.2	4.92
C6KT18	Histone H2A	16.50	22.73	1	2	2	18	132	14.1	10.29
Q8I6U8	Glycophorin-binding protein	16.28	54.00	1	5	5	22	824	95.8	5.14
Q8I492	Mature parasite-infected erythrocyte surface antigen	13.61	7.46	1	5	5	20	1434	168.2	4.78
Q8I3M5	Karyopherin beta	12.47	2.94	1	3	3	13	1123	127.3	4.92
Q7KQK6	GTP-binding nuclear protein	9.65	17.76	1	3	3	14	214	24.9	7.94
Q8I2Z8	Probable ATP-dependent 6-phosphofructokinase	7.53	3.03	1	3	3	14	1418	159.4	6.76
C6KT34	Cell division cycle protein 48 homologue, putative	6.59	4.11	1	3	3	14	828	92.3	5.08

Q8IDV0	Elongation factor 1-gamma, putative	6.43	5.35	1	2	2	9	411	47.7	7.39
Q8IKR1	V-type H(+)-translocating pyrophosphatase, putative	6.07	7.81	1	3	3	14	717	76.4	6.54
Q8IKC8	Exported protein 2	6.05	9.76	1	2	2	4	287	33.4	5.27
Q8IIG6	Phosphoglycerate mutase	5.91	8.80	1	2	2	4	250	28.8	8.28
Q8IBA0	Receptor for activated c kinase	5.00	9.60	1	2	2	2	323	35.7	6.71
Q8I4R5	Rhoptry neck protein 3	4.96	0.99	1	2	2	10	2215	263.0	9.20
Q8IIV1	Histone H2B	4.56	14.53	1	2	2	10	117	13.1	10.26
Q8IBV7	Histone H2B	2.71	15.45	1	2	2	2	123	13.8	10.80
Q7K6A4	S-adenosylmethionine synthase	2.62	11.69	1	3	3	10	402	44.8	6.74
C0H5F4	Reticulocyte binding protein 2 homolog b	1.84	0.91	1	2	2	6	3179	374.0	5.27
Q6ZLZ9	Tubulin alpha chain	1.81	5.08	1	1	2	6	453	50.3	5.06

Accession: UniProtKB protein accession number.

Description: UniProtKB protein name.

Score: Sum of the scores of the individual peptides, which are based on the number of fragment ions that are common to two different peptides with the same precursor mass and its correlation with a default threshold score.

Coverage: Percentage of amino acids found in the analyzed peptides compared to the total number of amino acids in the entire sequence of the protein.

 # Proteins: The number of identified proteins in a protein group (all proteins that are identified by the same set of peptides).

 # Unique peptides: The number of peptide sequences unique to a protein group.

 # Peptides: The number of distinct peptide sequences in the protein group.

 # PSMs: The total number of identified peptide sequences for the protein.

 # AAs: The total number of amino acids of the entire sequence of the protein.

MW [kDa]: The molecular weight of the protein calculated as the sum of the molecular weight of each amino acid without considering posttranslational modifications.

pI: The isoelectric point of the protein.

Table S2. Proteins from the *P. falciparum* proteome containing a prion-forming domain identified by the PLAAC algorithm.

Uniprot accession	Protein description	PrLD score	PrLD sequence
Q8IJP9	ADA2-like protein	289.599	SASNNNMINNKVMNSAGMMSSNGDMNYNLNYMNYMNNTNNINMPGSGGGSGVNRMTTVPINHVMNFPN SYMSGANMPSQVPQNMHFDAIENMHDMKQTPQQMKHKTSQLNSSANQGDINNNAKQVGGLPANFMQNQ MHPQYQYQQQVHMQQLVQQQNVHGYNNMMQSNNQQKFPNQPGAHKQSNASILKMPPFSSLNSGDQRSSY SIAQKLPRHVMDTNNNVPSINNNNSSSNNNNNPRHSSSNMPSLNNPNQFNSVSLKFPYKGSSPQPLNSINNNNN PNQPNQQNHQNQPNHMPNISAQQNMQNVNNNNNNPSVVQQMNVNHPIMQHNMIQQNQNNMHNLAPN KPNESQSMFPLGASSNQQGNMQNIASPNKQKMQPLFQQGGQQIIAPNQKGINTASISGSISRQPNQGTGQIPISH QNIQQFYHNNSGQMFPQQPPFLQRVSTTPQHVPQQQVPYEWMNNPYMHHQYMLQQCQLTPQQLFMHQQK QQNNMLHHQQQQQQQLQHQQMQQQQLHQQQIQQQQLHQQQIQQQQLHQQQIQQQQIQQQQLQQQQL QQQQIQQHQLQQQQQQQQQGNIPPLSARQSKQGILQMQSQNNISHLPPNLEQHFQQQNISELQHHQQQMQ NVSAQHSSISTFEPNAQQTMYQG
O96124	Erythrocyte membrane protein 3	220.166	QQNTGLKNTPSKGQQNTGLKNTPNERQQNTGLKNTPSEGQQNTGLKNTPSEGQQNTGLKNTPNERQQNTGLK NTPSEGQQNTGLKNTPIEGQQNTGLKNTPSEGQQNTGLKNTPNERQQNTGLKNAANKGQQNTGLKNTPSKGQ QNTGLKNTPNERQQNTGLKNTPNERQQNTGLKNTPSEGQQNNDLKNTPNERQQNTGLKNTASKGQQNTGLKN APNERQQNTGLKNTPSEGQQNTGLKNTPSEGQQNTGLKNTPNERQQNTGLKNTASKGQQNTGLKNAPNERQQ NTGLKNTPSEGQQNTGLKNSASKGQQNTGLKNTPSEGQQNNDLKNAPNERQQNTGLKNTPSEGQQNTGLKNTP SEGQQNTGLKNTPSGGQQNTGLKNTPNERQQNTGLKNTPSEGQQNTGLKNTPNERQQNTGLKNAANKGQQNT GLKNTPNEGQQNTGLKNTPSEGQQNTGLKNTPSEGQQNTGLKNTPSEGQQNTGLKNTPNERQQNTGLKNAANK GQQNTGLKNTPNEGQQNTGLKNTPSEGQQNTGLKNTPSEGQQNTGLKNTPSEGQQNTGLKNAANKGQQNTGL KNTPSGGQQNTGLKNTPNEGQQNTGLKNTPSEGQQNTGLKNTPSEGQQNTGLKNTPNERQQNTGLKNTPSEG QQNTGLKNTPSEGQPNTGLKNTPNEGQQNTGLKNTPSEGQQNTGLKNAANKGQQNTGLKNTPNEGQQNTGLK NTPSEGQQNTGLKNTPSEGQQNTGLKNTPSEGQQNTGLKNAANKGQQNTGLKNTPNERQQNTGLKNTPNEGQ QNTGLKNTPSEGQQNTGLKNTPSEGQQNTGLKNTPSEGQQNTGLKNTPSEGQPNTGLKNTPNEGQQNTGLKNT PSEGQQNTGLKNAANKGQQNTGLKNTPSEGQQNTGLKNTPSEGQQNTGLKNAANKGQQNTGLKNTPSEGQQ NTGLKNTPSEGQQNTGLKNAANKGQQNTGLKNTPSEGQPNTGLKNTPNEGQQNTGLKNTPSEGQQNTGLKNTP NEGQQNTGLKNTPSEGQQNTGLKNTPNEGQQNN
Q8I398	Nucleoporin NUP100/NSP100, putative	188.444	MFNQNFNNSNLNKGNFQDSNNLLKNKNMFMQNSSQNNNIFGTFNQNNNTNKSLFGNSNLQSNIGNTDNSLFG GSKIQQPNNALVNKSIFNLGGSSGTSTGLSGGKSIYDNMNSQSNLNTKNIFGSTNVSNNTQGNMGGNSLFMNAN NQNNLNMKNIFGSSSGLNNQTSNLGNKSIFGGLQPSNQTTPSNNIFGNMSSNQTNSSNIFGNLSSTSQNKSNSIFG GLGTSTNQSTGGGLFGNTGATSQNKTGGIFGGLSSTNQASTSSTSMFGGLSSNQAKPTNSLFGGLSSGATSNTGTQ QSGNLFGSASGIGQSKTVGGIFGNLSSTNQASTSSSNMFGGLSSNQAKPTSSLFGGLSSGTTTNTSTQQSGNLFGSA TGLGQNKTGGGIFGTLPSANQTSTTSSNMFGGLSTNQAKPTSSLFGGMSSGTTGITTNTTAQSGNLFGGTGTSQN

			KTGNLFGALPGANQTSTTSNIFGGLSSAQSKPTSNIFGTMGTVSATTTAASTSSNIFGSTGGLNQSKPSTGNVFGSL QTMTQPGSTNMFGTTQGTSQGLTSTNMFSSSTVPGSSQNKFTNMFGTLSGTTGSTPMGTLTTPNSTTTATTGLT GTGVGGTSGTSNIFGNVSGGSSFGNLSANKNIFGSTGTGMTLSTASTSLSPSVGTSLGQNLGGAMTSTLNTNLTTP GFGQSGGSNIFGNLGGTVTSNIGSTITPTPSSS
Q8I5B3	Protein transport protein SEC13	181.666	NNNNMNYTGNVNVDSASYMHDNTNASNLNMNYPNGSNSLINPNNNLSHQGPYQNKDTFHRSSQGNFAAYNN STQQQQQYSNVNSTGSQMNNVQAGNTVSNNVISNFANNNTNQMKGPPGQMNEPPGQMNGPPSQMNGPPS QMNGPPSQITVPPTPPAYLTMQNSKKNNTSNLTPNMNNIPPPTAPPLVVNNSHGASGPYAPSNFSQQPHGVSAP FGVPSSSPPAQQQVGGSVTNMSVSSNINNNKSTFGGPPPPLPSTSTTPIIPAAGSSNFPKASTSSLQQQVHGPFPNV NMSRSSFAINSQMPPSFSHPNNNNNNNNNNNINNNNNNSGMMPPRPSQYSNNLNLNPLSTSVPPPAFSSDTQ GMQNKNSITSNFNNNSNNSFSNFNSHMNQANLPPPNPSVMNPSKPVGSTYGSISGGYNVPHAPNMMNDSNVK PQNQQYGYSNYNMPPRQNTHMNN
Q8IKA0	Nucleoporin NUP116/NSP116, putative	162.687	QAYIAHNTSSRKFGAQNMSGGTYQAQNTSGGMYEAQNTSGGIYGAQNTLRETYGAQNTSGGIYQAQNTSGGM YEAQNTSGGIYGAQNTLRETYGAQNTSGGIYGAQNTSGGIYGAQNTLRETYGAQNTSSGTYQPQNTSSGTYQPQ NTSSGTYRPQNTSSGTYQPQNTSSGAYQPQNTSSGTYQPQNTSSGTYQPQNTSSGTYQPQNTSSGTYQPQNTSS GTYQPQNTSSGTYQPQNTSSGTYQPQNTSSGTYQPQNTSSGTYQPQNTSSGTYQPQNTSSGIYGTQNMSSGING TKNMSSGIYGTQNMSSGIYGA
Q8I5H4	Polyadenylate-binding protein	134.684	QQRFRMHPIRHHMNNPLNTPMQYASPQSPQLQFSQNTLSYGRPVITAFNQNNLISWRHQQAAQQQAVHQQA VHQQAAQQQLNFNTNLRGQINQMRLYTQNNMMNNNLNQNKPNAQLHHNQQYVPNALAQNGQQQPNLNA AGQHNAQQLQQQGNNQLLNNNMRNMNNRANRNMGNLGNMNNQKQLPLNINNKQQNAASQANQMNHQ AQPQGAQAQQKNPQQMQQVPQGNNFKFTAQARNRMELPNKNANKVNTMNNNMNVNFNNNSTLTAAALAS APPSMQ
Q8IIS9	Polyadenylate-binding protein-interacting protein 1, putative	132.364	QNNMSFNNLMWNNYYQDISGGTTFNSNNLLNNMNNTPGSNNNNNIMINNTNSLLHNMNGINNNSSNNIMNI AGSNTMSSSNNNNSVNSGVVLLGVSSGNMNNMDNNDQDKMNTTTNNNNNTNNNNNNNNNNNSNNNICN NSLHGAKSNSNHNNIHDNNNNNNNMHAGNINNISQTIGGMSSNDGPFINQGMMPGITNLRSSHFMSNSSANFM NNSENSNGPFHPMDGTHAHQNFQPNGSLIAHHNFYVNHHPYILNNHPNPLPGPQPIFAPPLPYTNTLTSTGNTTG AGGVHHDMPFAQHTSVYGSFSNNPANLIASGASISSQKSPSLSINPYNFLSCSLPTPPPQLPHTGPLSMTSLDPHFM STGNNSHMKLPYTNNMCPHPGRRSIYNHFSHAHISNSNNMNDNNFDPTNSNNNNNNNNNNNNNNNNGNNN NNGNNNTMAANLNYNFNTFNHPNNNNSCALVLNNDNNSTNNIHLNQGLNSNTLNLNNTGNVICVNNPMHLN TSGNMTHHHMNNMHMNHGMIINNNIGKQKKSISMNHNNTDNNNNNNNNNNNNNINNNNNNVKQQFNNYR EGKNSLKGNMMNSNVCINNNYNHYNSPNNNNNNNNNNNNNKKHSRYNSISNLNNAYNAAYNINTTGNNVNNIS SNNSKNIYNSKGVKREGYNSEDNDNTAGNYYLKNGNPIMNVANTNNTNNTNNANNANNANNTNNTNNANNA NNTNNTNNANNTNNTNNA
Q7K740	Circumsporozoite (CS) protein	127.901	QPADGNPDPNANPNVDPNANPNVDPNANPNVDPNANPNANPNANPNANPNANPNANPNANPNANPNANPNANP NANPNANPNANPNANPNANPNANPNANPNANPNVDPNANPNANPNANPNANPNANPNANPNANPNANPN ANPNANPNANPNANPNANPNANPNANPNANPNANPNANPNKNNQGNGQGHNMPNDPNRNVDENANANS

			A
Q8IKG1	Uncharacterized protein	124.990	NNSNNGNENGNNNNGNGNGNGNGNCNGNGNGNGNGNGNGNCNGNGNGNGNGNGNGNGNGNGNGNC NGNGNGNGNGNGNGNGNCNGNGNGNGNGNGNGNGNGNGNGNGNGNGNGNCNGNGNGNGNGNGNG NGNGNGNGNGNGNGNVNGNGNGNGNGNGNGNCNGKCNGNGNGNGNGNGNGNDNGNGNGNNENGNG NGNGNGNGNNENGNDNNG
Q8IJD3	Uncharacterized protein	116.566	QQQQQQQQQQQQQQQQQQQQQQQQQQQQQQQQQQQQQQQQQQQQQQQQQQQQQQQQQQQQQQQQQQ QQQQQHNNNNIIGNHVNYNMGGVQ
O97255	Uncharacterized protein	96.651	QPTDLASNSNASSSYQATNTNIQNMNLNNLNHNLVNDMNQPLYTNLNTIINPPFNNQLANAVINLPLDQQVVQP LGQQVGQPLGQAINYQVIPPPQTIGQQLAEPINQQLNHQLSQQMNQQMNQQMNQQISHQMNAQLDQQMN HQMNHQMSHQMNQQLNHQMNQQLNHQMNQQLNQQLNQQLNQQLNQQLNQPLSMTMNQPFNHPALYN NTNKPLNPSLYVVSNMMNNNYNGN
Q8I519	Erythrocyte membrane protein 1 (PfEMP1)	95.571	QNRSDGSSSVHVGGGSGGGGGSGGGGGSGGGGGSGGGGGSGGGGGSGGGGGSGGGGGSGGGGGSGGGGG SGGGGGSGGGGGSGGGGGSGGGGGSGGGGGSGGGGGSGGGGGSGS
Q8I207	Uncharacterized protein	95.427	SPSTASTSTSLRSASTASTASTLRSASTASTASTASTASTASTASTASTASAASTTRSASAASTTRSASAASTTRSAS AASTTRSASTASTARSASTASTASAASAASTTRSASAASTTRSASAASTTRSASAASTTRSASAASTASTASTGSTSTT QSPSTSTSTTQSPSTSTSTTQSPSTSTSTTQSPSTGSTSGSTTRLPSTGSTIRFPSTGSS
Q8I5Z0	Zinc finger protein, putative	93.329	NTNNPPNTDNNNNNNNNADNRNNDNDNNNTNNNNNNNNNNNNNNGGSNNSSGSTNNNGGNNSANNHTN NNNNNNNNNNNNSNNNSNNNNSNNNNNNNSNNNSNNNNHSSSSNNAPNSSHANNNHSNDNNINNNYRN NHVHTCISNNSYHRNSGNTNNFSNNMHSSYNNIINGIYNYQNNSRNLNNSSSFGRTNILQDNSHHENMSNMAN QNNNFEAIVQNLFQRNVNTLGRENNPSLFSSRNEQLRLNNNHNIMNNNNTNNNNNNNNNNNNNNNNNNNN NNNGNNNNHCSHGDTYFYNYLRYSVNNNGRNHNNSGS
Q8ILR9	Protein PF14_0175	90.871	QQLSAHSLQQQMYPQQMTSQVHSSFHAQKIKQQLQQQMNHQQINKHQMNQQQMNKQQMNQQQINQQQ MNQQQINQQQINQQQINQQQINQQQINQQQINQQQINQQQINQQQINQQQINQQSMSKYPYQAQ
C6KTC8	Phospholipase, putative	89.089	GQQNDSVGQQNDSVGQQNDSVGQQNDPVGQQNDSVGQQNDPVGQQNDPVGQQNDYVGQQNDSVGQQN DYVGQQNDYVGQQNDPVGQQNDSVGQQNDYVGQQNDPVGQQNDPVGQQNDPVGQQNDSVGQQNDYVG QQNDPVGQQNDYVGQQNDYVGQQNDPVGQQNDPVGQQN
O96221	Protein transport protein SEC31	84.834	PSPNVYQNNMYNNNNNNNNININSSSNNNNNNNNNKVLSSMHHPMQQFNQCNVNKMYTSTSNIINNNTMN SNFKSVIPPPLPMNTQMNNSTSSIQPPPSVPPTKFHTQIINNTMNSRSSIATTTKNYPTSNLNSVIPTSMNNMNTNI SHGNNVTPPYMSQTNVAVPNMNNNNNNNNTMNPTYPSLPKFPNYNLNSQVQQNSIIPEKQLTSPMFSSNSYGN INKTHTTNNAVPPPPNVTSSVVTPPMPSNQLNNTRSSFADIQNVVSPPRNKNQSISSTANLNYQHDNQFNKRECM EQPVYPMTNQSSMFSMNNTMQKKNVPGGFQDNTSQMNYGMQPTGSPPPSSLSTTSPIAGALTVTPGMPVPW PIPTTTQQLGSTTQSTAN
Q8IJG6	Chromodomain-helicase-DNA-binding protein 1 homolog,	82.683	QNMSMRPQMGMNKNCGGGLHNSYQKSLLSSYNMNNMSMNHLMNNSMNRYNSLNNNNYPHQDMNQTN MHMTNIKSALQNNNNNNNNDMKGNNMKQNGYMNNNNMNYQRNDMLMRNNSNSFNMAGNFYPYMNN NNNNNNSNNSSNNNNNNNNNSNNNNSNNNNSNNNNNSNNNSSYYGASSVMGLNSNTNNMMNNTSLNNN

	putative		FNNNNNNNMGAENNNKTMSLLNKTGGGSLDNNNTSHQPMKSLQSTINLNNRNINNMNNVSGNNNSNSINSNNI NSNSVFNNNNSKGVGSFISNPSMN
Q8ID65	Uncharacterized protein	80.531	NNVPTFVNMSSALNTNNIFNTNALTANNIFNKNNVFGTNTSTNLFGTNKNSTLNPIPAISTGGTFNSNIFSSGTSNIF GTNNNTSTNVFNNNNMTNNVSTNIFGTTNTQPSSMFNTGGTNNSLIGTTTNTSFSALNNKNTLNNMSTMNNMN TMNNMNTLNNNIISSSSNIFNKDKLFGSSGTPNIFNNNNTLSNTANTFGSTTNTSNIFSKNIANSTSGNLFGNTGTT NNMFNTSNNNLFNNNNNNNNNNNNNNNSFRNSLYSSNNNSLNISNSLINNNNNINMMGSSGFPNRSTNTSNL FGLTTTTNNNNNNMTNNILNKSSQNVSSNLFGNNNNSSNNIFSSMNTSSQGNKINTYDNKNLFSSNLNNNTSSMLK DNNFASWGNNKNQMMNNNSFVLNNLNTSTFGSNKFGINTQNNNSNTLFNNNPSGVIGVGNNYANIIGNNMS NANNNNNNVSSSSSSLFSSNNMFNTNSNNNMFGSKNGLLGTSNNNNVSNNLLLNNNTSNNNIFNNKLFQNTNN NFISGTNTNITKNTFSVNTNMPNNNIFQNNNFSVNKNISQISNFNNISSNNNNNNIFQQKNTTSNFNSVFNSSNKN TLFSR
Q8IJA3	Conserved Plasmodium protein	78.121	QLNAHNRNPMNNKAMYQPMFDNQPGMMMQRSASYSNIMPFVKGMNNNDYSNYMQYNKMGMNMNMN MNQMPQQGFPNFRNMGSNVGPNMGSPMGSPMGPSMGSPMGPSMGSPMGPNMGSPMSSPMGSHMGPN LNPNFFPQQSRQYSYSVSPTYQQNMPNFNNFSNRHMPSMSDLYFARQYSGMKFGDMNNSPFDSQKPYKF
Q8IJF0	Conserved Plasmodium membrane protein	76.663	SQMLNLQINMYNMYEQQKMMLQYGNINAQGNYMNGQTNNVMNGQGNNYMNGQTNNVMNGQGNNYM NGQKNNVMNGQGNNYTNSQMNNYMNIQTNNCMNGQENNYLNSQTNNYMNIQTNNCMSGQENNYLNSQT NNYMNIQTNNYMNIQTNNCMSGQENNYLNSQTNNYMNIQTNNYMNIQTNNYMNGQENNYMNGQTNNFM NDQTNNYMNSQVHTEIPYRPNENAQTSSQIMNG
C6KTC9	RNA-binding protein, putative	70.247	NGNNNNNNNNNNNINNNNNINNNNNNNNNNIVNNNNNNNVNNNNNNELSNHHSYELNFYDHMNSNVNTFPS HYSTHNGSTSSLLYGSNNFPTQLNHINQMNTMNQLNQMNTMSQLNQMNSMNQLSQLNPLNQLNPLNQLNQL NPLNQLNQLNPMNQLNQLNPMNQLNQLNQMSQLNQLNQMSQLNQLNQMSQLNQLGHMNQVNYFTNQMS VIQDYTNSISNMNHINSYGSN
Q8I3J0	Hsc70-interacting protein	69.280	PGGMPGGMPGGMPGGMPGGFPGGFPGGMPGGMPGGFPGGMPGGMPGGMPGGMPGGMPGGMPSGM PGGMPSGMPGGMPGGMPGGMPDLNSPEMKELFNNPQFFQMMQNMMSNPQ
Q8I562	Clustered-asparagine-rich protein	67.567	AVPNVSINNNNNNNNSNTFFQKNNMNNTNFSQGSTNYGSNYNSENFQGNNNMNNYNFYNNNSSNNNNNNQ TNTQNNFMNRNMKNKNMNNNNNNNNNSNNNMMMNMNFNNNQQMNNNPMLNQNNFMLNNNNNYNN NAKNVNDMYRDGEMSPNHLNNNNNNINNNNNNNNNNNNNNNNNNNVMFRQNNSHLAQMYQAN
Q8I487	Skeleton-binding protein 1	67.286	QNPEQNPEQNAQQNAQQNAQQNAQQNAQQNAQQNAQQNTQQNTQQKTQQNPQQNAQQNTQQNTQQ QS
Q8IJW6	Asparagine-rich antigen	65.462	NNQNNMINLGFHDGFGTNGLMKTQLNNQMTNQMTNQMTNQMTNQMTNQMTNQMTNQMTNQMTNQMTNQ MTNQVNNQMTNQMTNQMNNQMKNQVNSHINSQVAGHMNANMFNGNNSNGTNMLGNMNMLNNMVN SNMDNNVNNNYSNNYPGSGNNGLNNMTSCVMNNNGG
O96223	Conserved Plasmodium protein	63.846	NGGVNQYDNHMDQMNQMNQTNQMNQMNQMNQTNQMNQMNQMNQMNQTNQMNQTNQMNQTN QMNQTNQMNQTNQMNQMNIQHQRNSVNAPNIYIQNFDQNCDIYYNNNGKSNGNLNVQQSDNAHNP
Q8ID39	Uncharacterized	63.816	GTQNPVPPPPAPPLTNNQGENNIPTDNRNNENKKLMNTNIKMNQQVDNNNNNNNNNNNNLGSAMNTPMNN

	protein MAL13P1.336		MNKGGPRNNVNNSEHMREHSNHTVNRFAPMGQYANSKNNNMNNVHNVNNVNNVNNVNNVNNVNNMNN MNNMNNMNNNMNNMNNNMNNNMNNNMNNMNNMNSMNSMNNMNNMNSMNNMNNMNNMNNNNNNK FNENNILYKGTNYNRNVKNLGQNNNEGNTNMKHGHNNNRGQGNNNNNNNNNNFNRRN
Q8IKV6	Rhoptry neck protein 2	63.783	GPGGDYPNLYQNIYGNEKNPNIFPGSPRNINVYSVHHIPNNGANGGLNSGANGGLNNGANDGLNNGANGGLNN GANGGLNNGANGGLNNGMNNGMNNGMNNGMNNGMNNGMNNGMNNGMNNGTNGGLNNGMNNGMNNGM NNGMNNGIHDDLYNSENSTFNNGLNNSGRTGLNNAYPHNGMLNNGTEYNVHYGNSDSNNTN
Q8ILC9	Uncharacterized protein	62.573	NYNMNNNMGNHMNNNMGNHMNNNMGNHMNNHISNHMNNHISNHMNNQLNNNIYVNNRVGIGYMSN SVNQHNHMSPHMNNTINVHNNNNNNNNSNNNNNNNNNNNNNNNNNNSSSGSNCVNNTLRNNLMKNNFNQ FNRMVNNNSINIHTSSSNINNNMNNYNIHLTHQKINSNNNNINNNNLNMNGKLNYHQMSNKVHGTVPIPMNV HMGGTSISNINHMNNINNMNNMNNINNMGSSNRMGTSPINHPIPHKKGGTHMSNQITRNAMNKMLSNPINV DNKMNVLNRKNSCTVNFNMNNPMVSNMNNYMNSNNMNRNSLPNNICSGGTIMPNVMSKGKIKDTAINNNS FRNNNNINNMNNMNSMNHMNSMNHMNSMNHMNNVNHMNNMNNVNSMMNNRMSEQN
Q8IJ39	Conserved Plasmodium protein	61.347	QLQTSTQSLKQNLHTHNKNNSMSTNQQTIQNKHTGQHQQNLLNNNNSLGQYTQNQIQPNTSQNTASSTSSSVT GKADTNNINNASQNNQNNYISKQLYHNSNYYNINSSSFNIPPGFNMSQDKEQNNNYLNNNITTNNNNTNVSAYR NNWNSINEKNLNHYNLNYNYNRSNKNSFNYTSNFNSNVYNGNRDNNNNFFNYNNFSYALQTPPGLQNYYQNTQ YQQQNNYNNRNYNYSAYNNN
Q8ILQ0	Spliceosome-associated protein, putative	59.163	MNNFYPPNPHQPTSSNYLQAQVGHPTNIPMNARGSTSFMIPPKINNRIGNILPSNISSNLPPNIPPNLPPNFPPNFP PNLPPNLPPTLPPTLPPTLPPTLPPNLPPTLPPTLPPNLPPTLPPTLPPNLPPNLPPNFPPTLPPNFPPTLPPNFPPTLPP NFPPGFPPNLPPNFPPTLPPNIPPGFPPNIPPNLPPNIPSYS
Q8I3R4	Zinc finger protein, putative	58.714	NQNQNQHQNQHQNQHQNQHQNQHQNQHQNQHQNQHQNQHQNQHQNQHQNQHQNQHQNQHQNQHQNQ
Q8IHM0	Erythrocyte membrane protein 1 (PfEMP1)	58.317	APPPPPPPQPPPPPPQPARPAEDQIEHDHRARSDGGQRQRPLPLPPVQQPPVQQPPVQQPPAQPPQQPPQQPP QPPPPAPEGGGLGRSLPRADRNG
C0H4T9	CCR4-associated factor 1	58.107	NNMNNNNNNNNNNNNNNNNNNNNNNNNNNNNNNSNNNNSNNNNSNNNNNSNNNNNNNNNNNNSN NNNNNSNNNNNNNNNNNNNNNNSNNNNYNNSNNNNNNHS
C0H5J6	Protein transport protein Sec24A	57.023	MQPYDYNRGLNNNNTANYNNQNNANAPINNPFLHNNDIGNNNNNMKTNEGPYNAPTYYNPGQHQQQQQQQ QQQGPPLHQGYQHSGVYGMNQGNYKTNNIGENMYNQDGHNNTSYINQGQPYRNVTSQFIPVSSNNTLKAGG NMLGYDNMGNINHVQP
Q8IHX6	Conserved Plasmodium protein	56.779	MNNNNNNKYNNDIHNSINKNGSTNINNNMNMPNNIMSNIANNRGSIQSNINNIPRPMNNINNVHSNINIPSSR NISSNINMANSRNVSSNMNMTNNVGINNNMNINNNVNRTSSINVPNNMGRTSNINLSNNMSRTNNLNMNNN INSANNMNMPNNMNASNNNMNISSNVNRTSNVNRTSNMNIPNNMNIPNNMNIPNNMNMPNNMNIPNNM NIPNNMNIPNNMNIPNNMNMPNNMNMPNNINMPNN
Q8IL74	CCAAT-binding transcription factor, putative	56.513	NGNNSNNMNSQIMNTLNNSTNDLNLLYRSSNNNNNNNNNNTYNNINNNNVDDFNNSSINLQNNIYMNQNKY FNNKDFNISNNNYMPPNGIISNNIYPSNNFSNRHMSMYSNRGMNTTQGNNNSNNNNNNNNNSSSFNNSSSF NNSSSNNSSSNNNNSSNYNSSCSNNNSSSNNNNSSTSSNNNGNNNKNNYNNNYNNS

Q8IEF0	Pre-mRNA-processing factor 40, putative	56.068	SSGPNVSGGPNMPGGSNMPGGPNMPGGSNMPGGPNMPGGSNMPGGPNIPGGPSPPSIPQIPNLPTIPGMPNILNLPNLPNLSNFPNFPGLPNIPNLPGIVPHNINNSHFMSANPMNPIGMPFMPGLLPNMNTCDYYHKNLMPMHPGYDNYNNIMYGQPNNLGMPIPPNNM
C0H489	Protein transport protein Sec24B	55.446	NNNYINNNNNNYNNNNNNNYNNYNNDGQLINNLSQVTLNNNYNYNNQSVSSPFDQKNNDQNFYSAARQKSQYMNPHINNKNITNNANNANNFINDNTSTQSNVQNYNINQTNYTNNNNNINNINSNNINNINNNNNIYSNCNSYYNNQPTNTNTHFYSNNTKENAPVTSQMTSFNMNGQVEKNNLNNKTYNNMNESPNNMNQSYNYNNLHNNVSNQTNYQNNYYPNNSQPVNVTQNS
Q8I4U7	Uncharacterized protein	55.167	NNMNNMNNINMNSMPHKNSFMGNDGINNMNSMNNNNNNNNNNVNNNNNNVSNNNNNNVSNNNNNNVNFMDNMGNNNNNNNNNNNPMNKYNNYMMNRNVLNNMGGTNPLYNNMYNMKFPYMNNDMMNYNYNINSFQNMNYDKMNKSMFKRYPNFMGGYPYNNMNPYNNFNAFNMNYQQNDQMNQLPNMQGGYKSKLMNDNLSNYQSFNNNNVKQNHHDNNNNDNNNN
Q8IKH2	Transcription factor with AP2 domain(S)	54.992	QGSNILMNGPQGNNNNMNNSNSNNNNNSGSNNNSNNNNNNNNNTNNNNNSGSNNNSNNNNNMNNNKNNNNNNNNSNSGNSNSSQNQHMYLSSHNNDIFENNNNNSNSGNNDSNNNNQSN
O96201	Conserved Plasmodium protein	54.465	QNADQYQDQNKNHKQDQRQDQNKSHKQDQLHDQNQNQGQLHDQNQNQGQLHDQNQNQGQLHDQNINQGQLQNQNQNYYQNYYQNHYQNDHQNDHQNDHQNDHQNHYQNNHQNDHQNDHQNDHQNDHQNHYPYQYQDQG
Q8ID21	Uncharacterized protein	54.347	NNNPTNMMTYNNSNYVNTCDHINNRAMGNYNQNVFVPNNYNNPNNNTQNYDSINNSLTHYNNSSEGRTLYNNNNTNMGHYNNTNNFRNYDQGNNRNVTAQMNYHMYNNMSNNNMSNNNIPNNNMPNNNVPNNNMPNNNVPNNNMPNNNVSTLHHRMNALHPQPNNHHYNPAYNEHLNNSYNQQNNNTLYNEQNNAEQNSSNTYNYNKNSETYNKNN
C0H4C9	Uncharacterized protein	53.796	NQNRNRNQNRNQIQNQIQNQIQNQIQNQIQNQIQNQNQNQSQNQNQNQIQNQNQIQNQSQNQSQNQS
C0H5B1	Eukaryotic translation initation factor 4 gamma	52.658	QNNNDNMNTNEDNNNNNNNNNNGVFSNYQNNNMNRNNSINIKRNLNNNNNINNNMNKMGSQDKNQNSNNNFYMNYNYQNRKNSMNNNMNNNMNNNMNHNMNNNMNHNMNNNMNHNMNNNMNHNMNNNMNNNINSLDSDMSPNYHAHVKMSMMNYNNNESNTANPNQMNFEQTNNDNMKRENNNMNNYGYDDNTVHVNNNTPSTDFFSRAVGYNNNYLNNNNNMNSAVNNNSSNGNNM
Q8I0U8	Merozoite surface protein 1	51.956	GASAQSGASAQSGASAQSGASAQSGASAQSGASAQSGTSGPSGPSGTSPSSRSNTLPRSNTSSGASPPADAS
Q8IBB9	GPI-anchored micronemal antigen	51.673	NQQQNVNNNEKLNNNNNNNNNQQVNNNNNNNNNQQVNNNNNNNNNNQVNNNNNNNNNNQVNNNNYNNNNQVNNNNNNNNQQVNNNNNYNNQLNNNNFNNNLQ
Q8IKS5	Uncharacterized protein	51.183	SNNNNNNMNDINQQNIPNFYMMNNNQTPHLHQTTNAYATIPPINNHQIQTQPTNTVQYIQPNYEQVITQVDQNRNLFNQQLVGSTVMQNMTPQGVNTLNYPATINTVCVPQTISNTNNTTSQQVQYIPQTQAYAPYNNVQNTTIYERNYVPQIAQNTMTNNVVQQYVPSTTTMVQENVQNTPSSQ
O77375	DNA-directed RNA	51.160	SPTQSPKSPTSVMHSPFSPFDHQNQQPVDATNLLFSPKNNNIMNYNVFSPKPNINNNVIQSPNIYSPNPMLDIFSP

	polymerase subunit		KPQINHNIYSPSYSPTSPTYNANNAYYSPTSPKNQNDQMNVNSQYNVMSPVYSVTSPKYSPTSPKYSPTSPKYSPTS PKYSPTSPKYSPTSPKYSPTSPKYSPTSPKYSPTSPKYSPTSPVAQNIASPNYSPYSITSPKFSPTSPAYSISSPVYDKSGV VNAHQPMSPAYILQSPVQIKQNVQDANMFSPIQQA
Q8I2S1	Cyclin-dependent kinases regulatory subunit	49.910	GTSRRHNHNNNNNNNNNNNNNNNNNNNNNNNNNNNNNNNNNNNNNNNNNNNNNNNNNNNNNNNNN NNNNNNNNNNNNNNNNNNNNNNNNNNN
Q8II02	Uncharacterized protein	49.273	SQGTLSNDGSNNMNNNNVNNNNVNNNNVNNNNVNNNNVNNNNVNNNNMINNNMNNNNMNNNNMNN NNMNNINVNNSNMNNNINNNMNNNNNVNASNILLGASALTGAAISGQNQNGINNNQNVVNNNTNNGTIQN SIMLNNSSS
C0H4L6	Uncharacterized protein	48.327	NNNNNNNNNNNNNKNDNDNNNNDNNNNNNNNDNNYNNDNNNDNNNESRSSSKNNKIKNNNSKGNNHN NNQDNNEKNNDDHNNGGDHDGNGSGQNSGNSNTRNNNNNNNNNNNNNNNNNNNSSNNNNNSSNNNNNS SNNNNNNNNNNNNKKNNNNNSSSSNNNNHNANNNSS
Q8IJI4	10b antigen, putative	48.318	NNQSGMNQQNVMNQQKVMNQPNAMNFPNNMNHPNNMNHPNNMNHPNNMNHPNNMNHPNNMNHP NNMNHPNNMNHLNNMNHPNNINQPNLINYQYPMNHVQHINHPDNRNKMNNPNIPNYPNVNVSAP
Q8I4N5	Erythrocyte membrane protein 1 (PfEMP1)	48.295	ANAEGGGQKGARGPNGGTEGANSGKGAQQQQEQQQEQQQEQQQQQQQQQQPHSTDSSSSPPSSNP
Q8IHX8	Conserved Plasmodium protein	48.211	NYNNPNLNNQNMNNFNFSSRNVNSYPNLNNFNFTSRNMNNHNLNNFKNGYLSPNLNNINYGTRNMRVTPFNS PGLNMGRPYMFTPRQYPQMNNVNMNVNGMGYMNNVNSMNNVNSMNNVNSMNNVNSMNNVNNMNNR NNNQFSNYFNNMPTVGNINKGNIESNCFNNTNVNNALLQNTNFNNNSNNSGA
Q8I418	Guanidine nucleotide exchange factor	47.913	NPMGGYNTMGGNNPMGGYNPMGGNNPMGGYNPMGGNNTMGGNNPMGGYNPMGGYNPMGGYNPMG GYNPMGGNTNEANAFNLPS
Q9TY95	Serine-repeat antigen protein	47.835	SQTGNTGGGQAGNTGGDQAGSTGGSPQGSTGASPQGSTGASPQGSTGASQPGSSEPSNPVSSGHSVSTVSVSQ TSTSS
Q8IIQ7	Asparagine-rich antigen	47.692	NRNNNNNFSNIRQGNNNMNNIMNNYNGNNNNNSNNNNNNNNSSNNNHMSNNNNNNNNMYNHMNNNN PFFNDNNKNMKMDMMKNVGNTINNNMNQNFNYNNIKGSYLNNNQQVGGSNVHMNHQNNMLNDKMN NNAFNFKNQNYLNNNHMNKQSIADNNNNNNNNNNNINNTQSG
Q8ILJ3	Lipase, putative	47.544	NNNNNNNNNNNNDNMNDNHNNNNDDNNNDDNNNDNNNNINNNINNNNNNINNNINNNNNNNNNND NNNNDNNNNNNNNNNNNNNNNNNNNNNNNNNNNNNNNNDNNNNNNDNNNNNNNDNNNNNNDNNNNNN DNNNNNNNDNVDNNNNNNNNNNNVDNNQ
Q9U0K8	Uncharacterized protein	47.530	SNMNGNVNGNMNGNVNGNMNGNVNGNVNGNMNGNMNGNMNGNVNGNMNGNMNGNMNGNMNG NVNGNVNGNVNGNVNGNVNGNVNGNVNGNINENMNNLFNDCMYYNQHSNNEHDNNVNGNNNINSNNNN NNGNN
Q8I567	mRNA methyltransferase,	47.373	SNSAASPSPSPSPSIPFNNNRGSKIGNSTYNQNFLNNNSSYNKQPNNLGASNYPYINKNYTSPNNYVVNNNVNPSYIP MNFNNVNISPNVPYNNNNNYNYGAYPNVNNNMIHNNNINNMDGKNNYSYDNNLKNVHMNEYTSFMGMKSY

	putative		PVAPPPNINHMININQNNIHAYNNTNNNNNNNNNNNIYMNNKFNDMKNIPPPPLPNNNIPNVPNIPSPPSLPN NTYHFNANNQINAFAPQYN
Q8IB09	Asparagine-rich antigen	46.853	QQLANSKFVNNNIYPNYNNMNDMTNNNNNNNNNNNNNNNNNNNNNNNNNNNNNNNNNNNNNNNNSNN NNDYVHNNINVSTSLGCATGSVMSQGSSTNNMNYNLRNYESKNFNSYQNGIISDNSNSNNNSNNNNNNNNNN NNTNSSSSNG
Q8I383	Zinc finger protein, putative	46.448	SNMSNNNINANMNVVNNANVNVAHMNHMMLNNMNHMHNMNHMNNININHMNNMNHMNNININHINVNM NSFMNGNMNHMTPLNHMNNMNMHLNLNHMNNMNSMNSMNSMNSMNNMNNMNNMNSININMNNM NSMNSMNNVSSVNNVNHMNFNMNHMNFNMNHMNNHNNNNNNNNNNCSNSMIPSVMNTS
Q9TY98	Conserved Plasmodium protein	46.292	QNVGNVFQQSYGNVDESMGRNGSIDGFSMPPSGGLNNVSVQNNANIQNNANIQNNANIQSNANIQNNANIQS NANIQSNANIQSNANIQSNVNSHGGTNRQNNINNVNFFENNAYTQQTSYGGWANPS
Q8I3X9	Uncharacterized protein	45.295	NGTFFQMGDMNFVNYDRNYMNGQDYPTNNQTNYMNGQDYPTNNQTNYMNGQDYPTNSQTNYMNRQDYP TNSQTNYMNRQDNLTNSQTNYMNRQDNLTNSQTNYMNRQDNLTNSQTNYMNRQDNLTNSQTNYMNRQDY PTNS
Q8IHQ0	Conserved Plasmodium protein	44.680	NNSNNNNNNNNSNNNNNSNNNNNSNSNSNSNNNTNSNSNSNSNSNNNTNSNNNSNSNSNNNNSNNNTTT NNSSSSNNSNNNNYYHNN
Q8I403	Uncharacterized protein	44.483	NNNNSTNYNGSNYNGSNYNGSNYNGSNYNGNGNNTSNNNNYYGNNYNNNNNNNNNNNNNNNNNNNNNN NSSSSSSGSAAG
Q8IIJ3	Uncharacterized protein	44.310	MQGPIAISSDGNNSPLANQIVTPNVYGSPNSISPINMTNNIAPLTSNPSPTPPSPLPQSLGTSISPTTTTTTTTNIAGGA PIGSPNIMSQGMVGGVATPPGVQVPNNAIPFNPMNPTNLMPLNQIGQNPAFNIHPTASNLRGDPGNVNYN
Q8ILA7	Ataxin-2 like protein, putative	44.227	ANNVSNNYQSSNNISKNMPAQNISNTLVNLPYIPMIPPNITTVTNHNNNMNNNNNVNNNNNINNNNNNINNSN NINNNNNINNNNIISSNNNISSNNIISSNNNISSNNNISSNNNNNITNSGYIENPIYYNPYMRNYFSPHNNNSSLHISS NNPYFFNLPSTNMDTNFTSNKNMNIYPMRNPHVVQNNHMNFPHMHSYMHSNINYAINNNSINLMANPNIANT NMNVPGTFPPDFLLMNAHKYVNSQPVPMPFFPQVPYPNYYASSHGMSPT
Q8IKB6	Histone deacetylase, putative	43.850	PNNMYNQNNMYNQNNMYNQNNMYNQNNMYYPNNMYNQNNMYNQNNMYNPNNMYYQNNMYNQNN MYNQNNMYYPNNMCNPNYLYNDNNNN
Q8IC12	E3 ubiquitin-protein ligase, putative	43.195	NNNNPPDMDTYNSNISVMNNMNSMNNMNNNMESNMRTDVNVHHNNMNRRNSFNNSSNLQHTYNNNYN QYDHKNSNDSYTRNERRNSLNNYNFRKPSLNPNNEFYNNNDYSSDLINSHPINYSNVPESNYNMNHPIHHMNSAS HGMSNNTSHGMSNNTSHGMSNNTSHGMSNNTSHGMSNNTSHGMSNNTSHGMSNNTSHGMSNNTSHSMNNTSHSMNN TSHSMNNPSHHINHSSHNVMNKNCGNKRNYTSNNSGDYNESVKSNNYYNHAGNNTNYYNSN
C6KSW2	Uncharacterized protein	43.131	MNFNTNNNNNNNDNDSSNNNNNSNNNNNSNNSNNNINNNNSNNSNNNNNNNNNNNNNNNNNNKNN NNNSNNNNNSYNNNNSNNNNNAQITYGENIYSTSNYQNNN
Q8IJZ4	E3 ubiquitin-protein ligase, putative	43.003	SRSGPNSRNDNNNNDGNNNSNNTNSRHYNYRNMNNFGYRTNIPRSRRNNHNNNNNNDDGSNNNRHNSSNS NNNNNNTRSSHVRGEHDNFFNDFMLFRNMYQQIFNPSFRAADAEVHFTAAVGSSNNSNDINRHNNNRNNTTT PTTNNNNNNNNNNNNNNNNNNNNNHMGNRNSSRNN

P50498	Merozoite surface antigen 2	41.877	PSTGAGGSAGGSAGGSAGGSAGGSAGSGDGNGADAEGSSSTPATTTTTKTTTTTTTTTNDAEASTSTSSENP NHKNAETNPKGKGEVQEPNQANKETQNNSNVQQDSQTKSNVPPTQDADTKSPTAQPEQAENSAPTAEQTESPE LQSAPENKGTGQHGHMHGSRNNHPQNTSDSQ
Q8I3V8	Pre-mRNA-splicing factor CWC2, putative	41.783	PPSQILLNTPPPPSGQPPTGIQNVSHNSPPVPPTCPPPPTPPAPPGQPTQSNYPSQYYNMYNNMSVENYMGYPYY YSQYYNVGPHQSNA
Q8I5A3	Asparagine-rich protein, putative	41.777	MNYNNLNHNNTMFASRTSSSRNNNNNININSNINVNNNNNNNNNVNNNNNNNININNNGSNNMYLLKNKSLNRN GSILSNLNFLNTNNYNNNNNDNNNNININNNNNININNNNNMLSSASVNLNNANLNNINSNTINNNTNMNSTNIMN NNILSNNILSNNNVNNTNKDFLANNFNLKKNTHYASLTSNGNNMNLLNEQFISYNSNTENINNMNSNNMNSNN MNSNNMNSNIMNSNNMNSNNMNSNNMNSNNMNSNNNHINNNHINNHHINNHHINNHHSNNHHINNHHI NNHPGNHNMNAHA
Q8IAU1	ATP-dependent RNA helicase DBP1, putative	41.607	NNFNNRFNNNNNNNMDNRNFHMNNNMHMNNNNNNNNNNPFNNNKGPFSNYNQQHHNPFNNKNNSAFN NNNNNPGTLAFGNNPFNNNMYPNNNNNNNNNNFPFNNNNNPFNNN
C0H5H1	Uncharacterized protein	40.726	NNNNNNGGGSSSGSSDNNNNNNNNRGGNNNNQYYGNNNNNNNNNNSNNNNNNNNNNNNSNNSNNSNN NNYN
O77328	Serine/threonine protein kinase, putative	40.696	SSSNNMNGNNNMNGNNNMNGNNNMNGNNNMNGNNNMNGNNNMNGNNNMNDNNNMNGNNIMNG NNIMNGNNNINRNNIMNGNNIMNGNNNINRNNIMNRNN
Q8IHQ2	CCAAT-box DNA binding protein subunit B	40.473	SQAYDSHNNNNDNNNNNNNNNNNNNNNNNNNNNNNSDNNNNSSSNNNTTNDSTTTNNNTNSSTYNGT QNNTNLSNNNNSNNSNNSFNMSSFFSKGANSNDSQRNYN
Q8IIC8	Uncharacterized protein	40.426	NNANKNNNVPSGNNPNNQTTNPANNNNNNNNLNKDNYVQIFGDLLKNMNIPSNNNNNNNNNNNNNNNNN NNNNNNSSNNNSSSNNNNSSSNNNNSSNNNNNNAKAANPM
C0H4U5	Uncharacterized protein	40.117	QQQYKNNLMQNNMNFALNKKGNMNLPPPPPNNLGMQPNNVTMANQNMNYKQNNFPFVNNYKNMPNNLT QNLQNSMTNIPMNVNPNIPNNMMNPYMNGAYNNNFRNNMYQQNIPLPPP
Q8IIT5	Conserved Plasmodium protein	39.876	SSQSKSSSQLSSPLSSPLSSPSPSSSPSSSPSSSPSSSPSSSPSPSSSPSPSSSPSSSPSSSPSSPPSP
O96158	Conserved Plasmodium protein	39.054	GGMASGMTNNVTSSITNNMTSSMTNNMASGMTSSMTNNMASGMTSSITNNMTSSMTNNMASGMTSSITN NMTSSMTNNMASSMTSSMTNNMTSSMTNNMTSSMTNNMLNNMN
Q8IB67	Histone acetyltransferase GCN5	38.946	SNNNNNNNNNESNNNNNNNESNNNNNNNNNNESNNNNNNNESNNNNHGNNNNSSNNNNNNNNNNNN NNNNNNNNNNNNNNNNNNNNN
Q8IJB2	Uncharacterized protein	38.849	QNGGQNGNQNGSQNEGQNEGQNEGRVQSQDQRQNQSQDQRQNQSLDQRQDQRQDQRQDQRQYQS
Q8I218	Erythrocyte membrane protein 1, PfEMP1	38.833	GPPPPRAPRQSLARSADNPSPRPAPPGGPQPPSGTPDAGGARAETGPSPQQPPKPPAGNGGVA
O97306	Uncharacterized	38.790	SQGNNNYNIPKNFNNNNNNNNNSKFINYNSQQYYPSHQQQQQQHQQQQQQQQQQTLIQTQ

	protein		
Q8IAX8	DNA/RNA-binding protein Alba 1	38.471	NSRPFRRGGFRPRFYRGFRGGRGGFLRRGGYRGFGDRVYEPRSSFRGGRGSGYGGNFGRGGYRSGGGMGGGFR GGFRGGFRGGRDGGYRGGNRGGSRSGFRGGRGGFRGGRALS
Q9U0H1	DNA polymerase	38.412	NYTNQQSVVSQQSVVSQQSVVSQQSVVSQQSVVSQQSVVSQQSVTSQSTQSSQANQPNHTNQSTHMN
Q8I5D0	WD repeat-containing protein, putative	37.584	ASRNDSPNDSRDSHNRNNDNNDNNNNNNKNNNNNNNNNNNNNNNNNNNNKNNSNTGGGGNNNNNNN NNNNNNNNNNNNNNNNNNNNNNNNN
Q8I5J1	Transcription factor with AP2 domain(S)	37.477	NSNNNNNNINSNNNINSNNNNNNNNNNNNNNNSNNNINSNSNNNNNNNHNNNNNHNNHNNNHNNNHNN NHNNNHNHNNHNNHNNNNHNNQSCNNAS
Q8ILZ7	CUGBP Elav-like family member 2, putative	36.841	MNPLNNNMNNMDNMNNMDNMENMDNFDNNNNNNNNSSYMQSHAFKNMNMDNFNRYSMNMNFNMQ NNNNNQRNNNNNNNGNNNNDNNNNNNINNNNSNGNNNNNSSSNNNSP
Q8I339	Cysteine repeat modular protein 1	36.077	NNNVNTNTNMKNNNQGNILSNMNNNNNNQGNILSNMNNNNNNQGNILSNMNNNNNNQGNILSNMNNN NNNQGNILSNMNNNNNNNGNILSNMNNNNNNQ
Q8IKU1	Co-chaperone p23	35.876	MGMNSFGGMGGMPDMSQFGNMGGLGNMGGLGNMGGLGNMGGLGNMGGLGNMGGLGNMGGLGNMG GMGDLDFSKLGNMGGDMPNFAGLGGMDQFKNMPNMNNMN
C0H5M9	Histidine-rich protein III	35.369	SQAHAGDAHHAHHVADAHHAHHVADAHHAHHVADAHHAHHVADAHHAHHAHHAANAHHAANAHHAANA HHAANAHHAANAHHAANAHHAANAHHAANAHHAANAHHAANAHHAANAHHAADANHG
C6KT67	Nuclear polyadenylated RNA-binding protein NAB2, putative	35.343	PNPRFVGDNPNPFMQPPTMMNNQEMSSYNMNNMPNFYQGNYVVGSKNMMDNSNNFISNNMNNNFVNSR YQNNIQPKNGKFLQNINNTSVSSSVNFMNTNRFNNNVNNNNYGFQKNNMINNNSNTNVVGTVPMDEQINNT QNFIKQNNNNMRNQQTFFSNTHNENNVNTHQYFTPKGNKQQ
C6KSN1	Uncharacterized protein	35.336	NNNQCGNVYNGINGGSIDNINNMNNMNNMNNMNNMNNMNNMNNMNHMNNMNNMNNMNHMNNM NNMNNMNHMNNMNNMNHMNNINYNNNDGSTYNNYNNFTRNNQNS
Q8I1V7	Erythrocyte membrane protein 1, PfEMP1	35.280	QGVGAGGADFLPATSSVATALAPGAVPSRPSLQLLSGVGVPGEPGMAPGVKSIPVPPLGVGVGGIPGVGALGGGA LGPGGPVGLDGVPGQAQPLTLLRPGVLGNGLQSPQS
Q8I1V6	Erythrocyte membrane protein 1, PfEMP1	35.280	QGVGAGGADFLPATSSVATALAPGAVPSRPSLQLLSGVGVPGEPGMAPGVKSIPVPPLGVGVGGIPGVGALGGGA LGPGGPVGLDGVPGQAQPLTLLRPGVLGNGLQSPQS
Q8I3A3	Ubiquitin specific protease, putative	35.243	SNSTNSTRRNYNRNNNNNNNNKNNNNNNNNNNNNNNNNNNNNSRNNNNNNNNNNNNNNNNNNNNNNNN NNNHNNNN
C6KSV9	SWI/SNF-related matrix-associated actin-dependent regulator of chromatin	35.168	MNYPQLVNNNNINTFQNFGNNINYINNNMQNPPYMVNMDIPNNVMHYNGQDNYNNLYNQQVTYPPQYMM NSNPYYNETMSSQNNMNQMYNMTAHMEQCPNGNFYNFNNNNNNNNNNNF
Q8IE71	Uncharacterized protein	35.082	NNNNNNNNNNNNNNNNNNNNNNNNNNNNNNNNNNNNNNNNNNNNNNNNNNNNNNNNNNNNN
Q8IE31	Uncharacterized	35.069	SGGSNNNSGNNNNNNNNNISNNNNNNNSNNNGNVNGGNHHLMSNLMTNNNMNLTNNNNNNNNNNNNN

	protein		NNNNNNNNNN
O97292	WD repeat-containing protein, putative	34.983	PVGGVSTSNNNLMSMRGRRLTRSTRNNGNNNNNNNNNNNNRSSINNRSSNNNRSSNNNSSSNNNNSSNNNRSSNNNSSSNNRSGHRLTRGGN
Q8IEE4	Transcription factor with AP2 domain(S)	34.876	MNHNNINSNNNNINSHNNNMNNNNDNMNNMNNNNNNINNMNNNNNNINNMNNNNNNINNMNNNNNNNMNNMNNNNNNINNNNNNNNHNNNSSNG
Q8IJJ2	Conserved Plasmodium protein	34.839	NTNNNTNNNTNNNANNNANNNANNNANSNANNNANYNTNSNANSNANYNTNNNTNNNNNNNNNN
Q8IB94	E3 ubiquitin-protein ligase, putative	34.785	ASGLPIGDSNNSSNYNNNSNNNNNNNNNSNSNNNNNNNSNNNNNNNNNNNNNNNNNNNNNSNSNNERSRLFMSNQNRNVHHNNN
C0H552	Uncharacterized protein	34.437	NNTNNNNNNNNNNNNNNNNNNNNNNNNNNNNNNNNNNNNNNNNNNNNNNNNNNNNNNNNNNNNN
Q8IDZ7	Uncharacterized protein	34.192	NQTNQTNFINHMNQTNQTNFINHMNQTNQTNQTNQTNQTNFINHMNQTNQTNQTNQTNQTNQTNQTNHMN
Q8I5W9	Uncharacterized protein	34.113	GTNNNNGKSQNDSQSSSQSDSQSSSQSSSQSGSQRGSQSDSQNESQSDSQSDSQSDSQSDSQSDNQS
O96166	Serine repeat antigen 2	33.923	QQPTLPTLAQETQPQQQQQQKEVGSGIGAEQKVESARPGAEVSQSDVERAGRSSGTGGSVGTKISPGSQGQGKVAGPQLPRLPQLPQSFEQSRNQQSSPVTPKRNGISPTNAKSPESVLPPAQS
Q8I1X5	Pre-mRNA-processing-splicing factor 8, putative	33.710	PQNVPNGFINNIGNIPYNNMNAFPPNMPKLPTNMPFLPPNMPILPPHLQHMPNVLPHLQNMPNVPPHLASFPNMINLPNLPPHMHNLPPNMHSLPPHMHNLPPNMHSLPPNMNYIPPGINNYMPNMMNMPPPYMMKMPNM
Q8IDP7	Uncharacterized protein	33.322	NNNADNNNNNNSNNNNNNNSNNNDNHNNDNNNNDNNSNGNNNNNNNNNNNNNNNNNNNNNNNNNNSNNDNGDNNRNN
Q8IKA2	Uncharacterized protein	33.219	MNNNDYNNNINMNTLNNIQNLNIPIQNNGNKFMNNNDIPMNNNNSQQFNMTSNNLIQNNTFQNGYNQTIDFSNIGGSNINVNPIMNNDTFHTYNNNNNVENCYNNLQSYNNNYNIQGYNNNNNIQGYNNNNNNIQDYNNNNNIQCFNNNNIQAYNNQPNLSALPNFN
Q8IM23	Fibrillarin, putative	33.194	MTDSFRGGSGNFKRNSNNFGKGNNNAVRKGSNWKGFNGGRGGGGGGRGGGGGGRGGGGGGRGGGGGRGGGGRGN
C0H5K2	Uncharacterized protein	32.811	NGNSVPQSNTQNELHGMNNTSNMNNQNIIPQNNHYYGNDVNYPKPNYSNNNYNYMAYHKMSCLNYVYPYNPYRNKNYPYGNLPNIYYPDGYYANYCYPNYYYPIYYYPNYYYPNNYYAYNNFPHNNFRHNNIPHNNFRHNNIPHNNFLPNNFPHNNIPHNNFPPNNFPHNNYANNN
Q8IBZ8	Cg1 protein	32.435	NGLSPNSMGTSANISPQNSMTTPNNTSDTKGVSSSNTLSSPNTLSSSNRLSSPNTLSSPNTLSSSNRLSSPNTLSSSNTLPSSNTLSSSNTLSSSNTLSSPNTLSSSNTFSSAPNLFPSSFNVSYTPFYITSLSAYFSSSAHHMP
O97260	Zinc finger protein, putative	32.209	NNNNSSNNNNNSNNSSNNNSNNNSNNNSNNNNSNNSNNNNNNTNRNMSSNNNRNNNNTNESSGNN

C0H4W5	Protein kinase 1	32.131	PGNNNMIVQGMINSNNNNNRDNNGDNNSSNNNSSNNNSSNNNSSNNNSSNNNSSNNNSSNNNSSNNNSSSSSSS
Q8IKH4	Uncharacterized protein	31.858	NNNNSFNSMNQNNNFTNFMNINNYHGNTTLLPPQQNIQNNDVHPSNSYGNINMMNNNNSLYSNNSNYYVNSITNDVNYSMINNFNSFHNNTTEYMVPQTTYNNSLGDNGTRTTTYPNVGLNNLNVYQNMYNENNMNNTNNNIFQEYPNNIMPPYNLSNNIGHNSYSYTAYNYTNVVSNLNNN
Q8IB40	C-13 antigen	31.844	NSNFTRPNSSINNEYAQQQGGSFFYNDKSKGYMSNTHNNMNNNVNNNMNNNMNNNMNNNMNNNMNNNMNNNMNNNMNNNMNNSMARHNSN
Q8ILU8	Ribonucleoprotein, putative	31.761	ATGRGIPLNNYVPMQNNFNNPLGNPMGNMPTGMVLNTGTNKNLNPAINPNIRLPNMGINNQRPIMPPISMQINQNPPHNNANQAKGLPPGVPQLPFPPNVNPPAE
Q8ID63	Uncharacterized protein	31.733	NNNNNNNNNNNNNNNNNNNNINNNNSNNNNNNNNNNNNNNNNNNNNNNNNNNNNNNNNNNNNYYN
O97253	Uncharacterized protein	31.624	NGMSNKNNMNNMNNMNNTNNMNNTNNTNNINNTNNINNTNNMNNTNNTNNTNNTNNMNNMNNTNNMNNTNNMNNMNNN
Q8II32	Uncharacterized protein	31.492	QTQNIQTDNVKTQNAQPDNVQTQNAQPDNVQTQNAQPDNVQTQNAQPDNVQTQNAQPDNTQ
Q8IL08	Uncharacterized protein	31.393	GNTQNNSVSNNLFGSNITNVNSNMSLNSKSLFDNSMNNQKSNIFSSVKPNESLFSSNNNNNNSNSSTTVASGPSNIFGAPLSNTQQSPFSKTTNNTFGNLNIDSNNNNNNNNNNMIITGNGANNNTGLNFNSSNITNSVTQMNVNNQTFNNPLNNVVQN
Q8IKJ2	Uncharacterized protein	31.334	NNSSNNNNNNNNNINSNNNNNNNNSNININSNNNNNSNNNNNSNNNSNNKSNNKSNNKSNNKSNNKSNYNNNSSNNNRNNNNNYYYYDNNNNYDNNYNISNNYNDNSSSSDNSN
Q9U0H8	Uncharacterized protein	31.296	AFNPNNHNNNNNNNNNNNINSNNSNNNSNNNNNNNNNNNNNNNNNNNNNNNNNVVYFNNNNNNNCSNNPSSSNN
Q8I0W8	Deoxyribodipyrimidine photo-lyase, putative	31.172	QNNVYLPSQNNVYLPSQNNVCPPLQNNVYLPSQNNVCPPLQNNVCPPSQNKACPSSQNNVCPSSQNNVCPSSQNNVCPSSQNNVCPSSQNNVCPPSQNNVPP
Q8IKL6	Uncharacterized protein	31.159	NNAHNNTHNNTHNNTNNNTHNNTNNNTNNNTNNNTNNNTNNNTHNNTNNNTNNNTHNNTNNNRHNNRHNNRHNNSQNNLLINAQNNTN
Q8I573	Uncharacterized protein	31.013	MGRSSRNRSSNSSSRSSFLSRPGSRDMNRGNNTSAQNYSGSLGQHQSNKSGGFLSNMMGTVASGMASGVGFGVAQRAVDSILGARHVEVSHVNSNVDNQQLNQAAA
Q8IEC5	Uncharacterized protein	30.926	NNSSSISNHNNNNNNTHNHNNNNNNNNNNNNNNNNNNNNNNNNNNNNNNNNNNNNNNNNSSSSCSNRRAFSTN
Q8IHP9	Sporozoite and liver stage asparagine-rich protein	30.675	NNTPQSYNTPQSYNTPQSYNTPQSYNTTQNYNTTQNYNTTQNCNTTQNYNTTQNYNTTQHNNN
C6KSN0	Uncharacterized protein	30.660	SARNTTSSSSSISTTCYNNNNNNDNNNGNNNDNNNGNNNGNNNDNNNGNNNGNNNDNNNGNNHNNNHNNNHNNNNSYNSNN

Q8IKY0	Transcription factor with AP2 domain(S), putative	30.505	SSNMNNNNNMKNFNNTNINAYQQNNYNNNYCTNYTTSYQRNVHSSNYNNTGYNNNNNNNNFNNNNNFNNNNNFNNNNNFNNNNNFNNN
Q8I3Z1	MATH and LRR domain-containing protein PFE0570w	30.497	SAQNGGYLRAGSNNLSNNKMNNQGGNHINVKRVLTNNLNMNNMNNNNNNNNNNNNNNNNNNNNNNNNNNNNNNNNNNN
Q8I5D5	NIMA related kinase 1	30.297	SNNNNMNNMSNMNNMSNMNNMSNMNNMSNMNNMSNMNNMSNMNNMSNMNNMNNMSNIKNNYSNQNNISNNNYTYMAMQ
Q8IHR4	Dynamin-like protein	30.270	NTNQFNQSSKHNPNMSQGSSANMSMYLNDGSSSMSKRNPMMHNRNMSPSSMNTNMMKQTNMLGQKMGNSPSSYMQQGHMN
Q8IEM0	HORMA domain protein, putative	30.197	SNQYSNAHNNYMSNVISNNNNNINNNNNCGTGYQQPKHNIVNYNQENKNGEISQGVSQGVSQGVSQGVSQGVSQGVSQGVSQGVSQ
Q8I259	Uncharacterized protein	30.050	GNNNIHMNSNNNNNNNNNNNNNNNNNNNNNNNNNNNNNNNNNNNNNNNNNNSSSGNNNTNKPGN
Q8IJR7	Uncharacterized protein	30.026	NMSNMSNISNTSNVFFPSITNTSNYNN
C0H4L9	Uncharacterized protein	29.745	QTYTQQHEHSYNHTIGQSYSQQYEHPYNQTNGQSYPQQHEHPYNQPYNEMYVQPYDTSNYQSYNQMYGQYYDNTNFETYNQMYNQHYDNANYQTYNQIDDNKNNPN
Q8IKP3	DNA-directed RNA polymerase III subunit RPC5, putative	29.652	NNNNNNNNDNNNNNNNNNNNNNNNNNNSNNNNNNNYNYYNNNYNNNYNNNYNNNYNNNNNLNNLNSN
Q8IBU8	Uncharacterized protein	29.514	NNAANNNMNNAPTNVMHNTSNSLMNNAPTNVINNTSNSLMNNAPTNVINNTSNSLMNNAPTNVINNTSNNLMNNAPTNVINNTSNSLMNNAVSQLINNGTNHMINNGTNHMMNN
Q9TY99	Knob-associated histidine-rich protein	29.121	QHQHQHQAPHQAHHHHHHGEVNHQAPQVHQQVHGQDQAHHHHHHHHHQLQPQQPQGTVANPPSN
Q8IDX9	MSP7-like protein	29.105	SQTSPAPQGTSGLQGEKVPGALSSVSQTSSPDVSSRSEQPQTMPESPRPEGTSTESQPRGSTESDASNKNGSQTNVRTISNSSNSITSPQTTQPSNNQNNTVSTTS
A0A143ZVM5	Histidine-rich protein II	29.029	AHHAHHAADAHHAHHAADAHHAHHAADAHHAHHAHHAADAHHAHHAADAHHAHHAADAHHAHHAADAHHAHHAADAHHASDAHHAHHAAYAHHAHHASDAHHAADAHHAAYAHHAHHAADAHHAADAHHATDAHHAADAHHAADAHHAADAHHATDAHHAHHAADAHHATDAHHAHHAADAHHAAAHHATDAHHAAAHHATDAHHAAA
Q8ILS4	NOT family protein, putative	28.802	NNYNTTQSALATSEATSNNNNINNNNSSSNNNNNNNNNNSSSNNNNNNNNNNNNNNNNNNNNSN

A0A146LZZ4	Uncharacterized protein	28.591	MNNMNNNMNNVNNVNNVNNVNNVNNMNNNMNNNMNNNMNNNINDMNNVNNINQINNSNNINQINNVNNIN QINNSNNMNHINNSNNMNHINNSNNMNHINNSNNMNHINNSNNMNHINNANNFNMNNNMENPCEANNFNQNMSS
O97291	Microtubule and actin binding protein, putative	28.516	NNNDNYSYYNSYNNSHNNSHNNSHNNSHNNSHNNSHNNSHNNSHNNSHNNSHNNSHNNSHNNSHNNSHN NSHNNSHNNSHNNS
C6KTB7	E3 ubiquitin-protein ligase protein PFF1365c, putative	28.466	GNDNVSNNNNNNNNNININSSSNNNNNNSSSNNNNNNSSNNNNNSSNNNNNSSSSNNNNVRNSNN
C6KT01	Pyridoxal kinase	28.420	NGNMNGHMNGHMNGHMNGHMNGHMNGHMNGHMNGHMNGHMNGHMNGHMNGHTNGHMNGHM NDHMNGHMNGHTNDHMNGHTNDHMNGHTNDHMNGHTN
Q8IIK7	Uncharacterized protein	28.387	MANANYNNARKYDNRAYNNNTNNRKPVSATKPSNNGPVRSNPSGNNTTNNTNNNVNSGMAKAGMDKYQQR CNVAYNNYDNTKSSNPNNNANNNLNNKKFNNETQIKSNPHSDTRMNNAGTTNNSSNPPSKPQASTNNN
Q8IKZ0	Uncharacterized protein	28.376	NNNGNTNENMNTNINANINTNINMNTNINMNRNINNNNNNNNNNNNNNNNNNNNNNNNNNNNNNNNNGI GDNNNNINNVNISNNAYPNDPFNNANNS
C6KSX7	AP-3 complex subunit beta, putative	28.059	NNQTNDAIHSNNNNNNNNNNNNNNNNNINNNNNNINNNNNNINNNNNNINNNNNNINNNNNNINNNNNN NINNNNNNINNNNNNN
C6KSM6	Uncharacterized protein	28.003	QNNNHMDNNMNNNMNNNMNNNMNNNMNNNMNNNIINNQFYNNVNSSMVNNTYGLPKYNKEDMSRNI MNNMGGIFSMNYGNNNNNNNNNNNNNNNNNNN
Q8IM09	Uncharacterized protein	27.922	SNGLMNTNNNINNSNNNNNFNNNNNYNNNFNNYNNNNNYNNIYNNNTPFDMNFSNFNNNLNNNINNVQA NLGNGPNYMNTSGNNFNG
Q8IC48	Uncharacterized protein	27.904	APQNNVQNKPRQNIQNQHEKNVQSKAPQQNIQNRAPQKNKQNNTPVQNTISKSQVQNRVNKSPVQNDYSKH NGRGPNQMNRPNPNRHVAQPLR
Q8IAP4	GTPase-activating protein, putative	27.886	NNNNNNNNNNNVNNNYSGNPNLDNSLKLYATNQKEQQNNLEGIRGSMYDNNNSYNNMYAYNNEHYMDNQ HNAYGNRMSNPNNYLNSNGNNNNNNNGYGYGYGFNNKSSFSNNNFN
Q8ILZ2	WD repeat-containing protein, putative	27.869	NSNNNNNNNTIPSTQHFRLFINNPLSNNLTAVESNVPNRRSNSVGHNLYTYINNMLYNPNNTLNFNRDMNVVN MMGRTFDISRIGNTRNTNAQNYQNNMDNRNADCNNENQTMNEQNEGYYLNVEVIPGSMHLQDNVQNGQSV NIQNGQSVNIQNGQSVNIQNGQSVNIQNGQSVNIQNDQ
Q8ILG1	Acid phosphatase, putative	27.570	NNNNNNNNENNNNNISNNNNNISNNNNNNISNNNNNSSNNNNNNCSNNNNSSSNNNNSSSNNKNNNLNSN LNSNNNNNIYQ
Q8I517	Uncharacterized protein	27.552	NNSNDTNNSNNSNDTNNSNNSNDSNNSNNSNNSNNSNNSNNSNNSNNSNNSNSNSPN
Q8IDK4	Uncharacterized protein	27.515	NNYHNANHNANHNANNNANNNANHNANHNANHNANHNANHNANHNTNHNTNHSSNHSSNQN
Q8IIM8	Ubiquitin domain-	27.309	QAGLQIENALNMNNNNNNNNNNNSNRPGGAFRMEDILNNLNNLNNLSNPNNTTDNNNNNNNNNANPGNNL

	containing protein DSK2, putative		NSFLQSPELLQAFQQVMSSNRNLGNFNFPNANMN
Q8I2T2	Ubiquitin-like protein, putative	27.295	SNNNNNRMHNNMNTNFYSYNNDPIYRNNNMHGMNQPINNNNNYYYPNQFFRNSTYHNSTSNMNINADMYGSTNNVNNNANRNNYYPLPYDIRNSANRTNLQQ
Q8ID94	Uncharacterized protein MAL13P1.304	27.100	MNNNNNNNNNSNNNNNSNNNNNGNSNNNFFSGKGNALSAYQNKILNIKSNNNNAHHFVNKNVPTYSPPNIIMANKKGGNFNNTSGNIINRYNVENNNHRNTYHPSNNNTRNSVNFLNKNILYGNNNNNNNNNNNNINITNISNNNNNINITNISNNNNINITNISNNNKQPISSNQHPYQQKQSHHHNNS
Q8IEN8	Uncharacterized protein	26.967	NNSSSNNNNNNNIYSNNYNRNHNMFNNNNNFLQNHSKNSFSKGFGIQNNANVYNQHYNNNINQRTDNYNYNYHNNNNNNINSSNVNQQYGSRN
Q8IIJ7	Conserved Plasmodium membrane protein	26.929	QSNIPINNTNQNINGSPINTTTTNNNNNNENNNNNENNNNNENNNNNENNNNNENNNNNENNNNNENNNNNENNNNNENNNNENNNNNENNNNNENNNNNENNNNNNHHNHNHNHNQNNHHNQNINYPNPQN
Q8I5Y7	High mobility group protein B3, putative	26.923	ANVQNMQNIKNIQNIQNMQNMQNIQNGHINNNHISYGANSNVATMHHTNNTHMAHINYNYYDQTNIGNNNNNNYTMNMSLPANQNITDKPAMELIPTINVLHPYANNFNGNVCNTSTNVINNNMNINNMNSMNNINNININNNHNSSSGSSAIAPP
C6KST7	Uncharacterized protein	26.876	PNVSMSINGNTIQPPNNNNNNNNNNNNNNNNNNNVVSNMNMLNNLGPSSGPITLNGFNNNMNSSMNSNNNSTN
Q8IAW5	Uncharacterized protein	26.456	NSSNGESNRYSNAMDNANYYNTTNNMNNMSNMSNMSNLNNMNNMSNMNNMNNMSNMSNMNNRLYLLNKRSSLNNNYSPNNIKPLYNQQYSNKNLYNTLNHNQNPLNQ
Q8IIW4	CCR4-NOT transcription complex subunit 1, putative	26.381	NMNNMNNMNNMNNMNNMNNMNNVNNVNNVNNMNNMNNMNNMNNMNNMNNININNMNNMNNVQSVNIQHNNNNYN
Q8I2G4	Gametocytogenesis-implicated protein	26.232	QNNDYNQNNDYNQNNDYNQNNDYNQNNDYNQNNDYNLNSGYNLNSGYNLNSGYNLNSGYSLNSGYSLNNVYNQYSNNIENSGNILNNGFFGSSTNNNNRS
Q8I2P8	Protein kinase, putative	25.994	NMYNNNVNNMNNVNNMNNMNNMNNVNNVNNMNNMNNVNNMNNMNNVNNMNNMNNMNNMNNVNNMNNVNSLNHMN
Q8IHV8	Conserved Plasmodium protein	25.985	NNNNNDNNNNNNNNNNNNNNNNNNNSNGDNNNNNNNNNNGDNCNNNNDNHNNNDNNNSNNNNNNN
O96165	Serine repeat antigen 3	25.856	GSQNPKNSSSTTPASGSQKGSSSESPGSSVEKQSQESNKESTNGGNVVSQGTPANTFGQNSNNPSDSPQGTSTLPSPP
Q8IHT5	Transcription factor with AP2 domain(S)	25.809	QSSKMVQMDPMMQMDLRIQMDPRMQMDPRMQMDPKVQMDSMNQMDPMNQSNQINQINQISQINQISQINQISQINQINQINQINQINQSNQMNHINYINQSN
Q8IBQ3	Uncharacterized protein	25.657	SHRSNYSNYYYYSHQSHNQDVNQSHNQDVNQTHNQDINHMYSQDGNQIYSQDINQIHNQDGNQSYNHPSHHTSQQQINTPSYYNYNVNLSSFYSS
Q8I3L3	Structural maintenance	25.413	GNNLNNGNNLNNGNNLNNGNNLNNGNNLNNGNNLNNGNILNNGNNLNNGNNLNNGNNLNNGNILNNGNN

	of chromosomes protein 6, putative		LNNGNILNNGNNFN
C0H4R8	Serine/threonine protein kinase, FIKK family	25.312	NRNNNNYNGNINKNNNNIHGNRNSNNIHGNRNSNNIHGNRNSNNIHSNRNSNNTHSNRNSNNTHSNRNSNNSNRNNYNSFVVPGNMNSNNN
C6KSY0	Transcription factor with AP2 domain(S)	25.304	SQNNDMSQNNDMSQNNDMSQNNDILQNNDMSQNNDMSQNNDMSQNNDMSQNNDMSQNNDILQNNDILQNNDILQNNDILQNNDMSQNNDMSQNNDMSQNNNTP
Q8IC35	Erythrocyte membrane-associated antigen	25.119	MSHYNNNDNNNNNNNNNNNNNNNNNNNNNNSHNNNYNNQPHSNNYYYNNKSNDNLNNNKTSSSSYAPNFKRETSDDISNNNINYNNTNYNNTNYNNTNYNNNNYN
Q8IAW3	U1 small nuclear ribonucleoprotein C	25.096	PQNFLGFLNNRNINNPLGNPMMNYMNPNMYMKYNPMKSYHSYSMRSSHPYRLNIHNNKYSRAGYVPPSHHKYSVNPMHNNYHQAHNNYSYPNSINPSNQINYSNNYGSNNFNNSN
C0H4Q1	Uncharacterized protein	24.938	QNDTTTTTTTNNNNNNNNNNNNNNNNNNINNNNINNNNINNNNNNNNNNNINNNNINNNNINNNNNNNNNNNNYYDRTNDGNFSNG
O96236	DNA-directed RNA polymerase subunit beta	24.913	SNNNSNNSNNNMNNMSNMSNMSNIRSSISSNLSFSSNIGSSNVLDTLPDSPINNTYNNNNNININSSSNNYSLHGAASVTSSTPSSTTIFSSGQTAGSSNSN
O96234	Conserved Plasmodium protein	24.909	GPLYNNHHNNHNNHSNHNNHINHNNHSNHNNHNNHNNHNNHSNHSNHNNRNHNYYNNYYLYTNYQKHKNNKIPPPPSGPPPNNIKYNNVHPNNYNPPPPPPGTLQTFNTN
Q8IE57	RNA-binding protein, putative	24.806	QNQNMLLQNINKINNNNNNNNNSNNNNNNMINNVINNTINNMHNYNNNPYNKPPPPPPGAPPQSLYMQNN
Q8IK98	Uncharacterized protein	24.763	GNNNGNNQNNGGNNKKYNDGNNNGNNQNNGGNNKKYNDGNNNGNNQNNGGNGYDSGDSNNS
C6KSP3	Uncharacterized protein	24.753	NNNNNNDDPDNNNNNNSNYNTGTTPLTNTAMTGVKGKNTNSNNNNNNNNNNNNNNNNNNNNNNNKSNRMYGMATSSN
Q8IIS4	Transcription factor with AP2 domain(S)	24.751	SAHNANNNNNNNNNGNGNSNKNTKNIKNNTNGTNSTTNSTNNANGNNNNNNNNNGNNNNYTGG
Q9U0I0	Uncharacterized protein	24.746	NNNNNNVNNMNSVNNINSVSSVNNINSVNNINSVSSVNNMNSVNNMNSVNNMNSVNNMNSVNNMNSVNNMNSVSSVNSVNSVISMNNNMNNQNTLLKNFNNSISSNNLHNKNMNHLNFMNNNMTSYNNMPINVDNSNVLNNNNHMGN
Q8I569	CCR4-NOT transcription complex subunit 4, putative	24.552	NNNNNNNNNNNINRGDNNYMNNINLTNMNEMNNINDMNNINNNNNDDNNNNNDNNNNDNNNDNDNNNDNNNNNNNNNNNNNNNNNNNNNNYYYYISNNYNNNYSSSGS
B9ZSJ1	Uncharacterized	24.328	NYPRQDSQTNHYGRYTSRTNNQPRQDNQTNYYSRYTSRSNNPPRQDSQTSYYGRYTSRTNNQHRS

	protein		
C0H5D9	Uncharacterized protein	24.176	SNPPSSQALSTDPPSSNPPGSNAYSIDPQNNNPYSNNLYSSNLYSSNLYSSNLYSSNFYSSNLYSSNLHSSNLHSSNLDSSNLHSSNAP
Q8I3U0	Transcription factor with AP2 domain(S)	24.064	NGNNNENSNNNNNDYNNNNNNNNNNNNDYNNNNNNNNNDYNNNNNNNDYNNNNNNNDYNNNNKNYNNNKNYNNNKNYNNNNNDDNQSNDDNQNN
Q8I5X5	Uncharacterized protein	23.925	NNGNNNNNDNNDNNDNNYNDNNNNNNNNNNNNNNNNNNNNNNNNNNNNNNNNNHDNNNNMDYYNYGG
C0H4Y0	Ubiquitin conjugation factor E4 B, putative	23.863	ANSNSYLNATTRNNRTSNGSSNSVANLNYSSLNNNNNNNNNNNNNNNNNNNNNSNNFNDSSFNSDNNS
Q9U0H2	Uncharacterized protein	23.850	MASQNVKMASQNVKMDNQNVKMASQNVKMSSQNVKMSSQNVKMSSQNVKMSSQNVKMSSQNVKMSSQNVKMSSQNVKMSSQNVKMSSQNVKMSSQNVKMSSQNVKMSSQNVKMSSQNVKMSSQNIQMNSHN
Q8IKF6	Uncharacterized protein	23.691	GVGHTNNNSQKNNTYNLHNHLQNELFNLPNHLQNNLMFNNNNNKSQLHQLQNSQNQNNVHQHIQNQNASNQQINQSYN
Q8I3B3	Uncharacterized protein	23.687	NNNMNNNSGTNINTNANTNNNMWNLQNNNLGNNTFFGNNNMTNQNDLNKNNSLFGNSPNNMMKTTGFFNNNTIGNHPNDINKTGNLFGNNTGLNSSTDIMKNNSFFGSSINTQNDLNKNNMNNNNNNNNNSNSFFGSAFG
Q8IDB9	Zinc finger protein, putative	23.671	NNMNIHMNNHVNSNINNHVNNNMNNHMNNNMNNHMNNNNNNNNNNMNNHINNNINNHMNNNINNHTNNNMNNYINHNMNNHYSNYSYGTYDNRSMQ
C6KSW5	Eukaryotic translation initiation factor 3 subunit L	23.625	NNNNNNNNNNNNNNNNNNNNNNNNNNNNNNNNYYYYHKNKQNKQDKQDKQNKLNRQNKQNKQNHLNRHNNQNKPNHQNNMHAQVAAS
Q8ILL5	Uncharacterized protein	23.614	NSTQGYNNNNNNNNNNNNNISNHNNNYYSTHANITQFNADMNNSNNQNNTTAPCSNEHMSSNNNNNNN
C0H5G5	Transcription factor with AP2 domain(S)	23.438	NMFNNMYNNVNNNINGNNINGNNINGNNIIGNNINGNNINGNNINGNNINNNNINSNNINSNNINSNNINSNNINSNNINSNNINSNNINSNNINSNNINSNNINSNIYNNMYNMNYKNNVISSNNNYINNINNEQHSNPMNYNTYG
Q8IBR9	Exported serine/threonine protein kinase	23.361	SNNMVSNDMLNNMPNNMLNNMSNIMSNNMSNNMSNNMLNNMSNNMSSNMSSNMARNVSNNMSSNFISSNLSNSFISNNMSSN
Q8IEC6	Uncharacterized protein	23.219	GNNMIYNNSYNTQMHNNNNMQANYSVPVDISCNNSISNYNSTMVVNNNKENNININGNNNDNINGNNNDNSNGNNNDNSNGNNNDNNSDNNNNNINGNNNDNNNDNNNDNNNDNNNDNNNDNNNDNNNNNNSCNDYNYNYNYNYNYN
O97267	Circumsporozoite-and TRAP-related protein	23.089	PPGSPSESTPGSPSESTPGSPSESTPGSPSESTPGNPSESTPGSPSESTPGNPSESTPGSPSESTPGSPS
C6KTF9	Erythrocyte membrane	23.004	AGSRTTRAADGAEPTRDDGNGDGAGGAPAKSGGSGATTTSSGSICVPPRRRRLYVGGLTKWAEKQSSQGGGAPQ

	protein 1, PfEMP1		VSPSATASSGSQS
C0H566	Zinc finger protein, putative	22.860	MNNNYLNNNYMNNNCMSNNYMNNNCMSNNYMNSNCMNNNYMNSNCMGNHYIRNHCTGNNCIGNNIYS GGYNTLRNYISNNNNNNNSSSNNNSNSNNNNNNNVYNYSSVNNLNNVDNMNNS
Q8IK00	Uncharacterized protein	22.855	SSNDNNRGHNNNSDDNNGGDNNNGGDNNNGGDNNNGGDNNNGGVNTNGGDNNNGGDNNNGGDNTNS SN
C0H570	RNA-binding protein, putative	22.853	NQNNVVMNNNNNMHNNMNNNKIIQPYKMPMYNPNAYPPHPFYMNNNFAPYNNMPPANAYQNN
Q8IFP4	Erythrocyte membrane-associated antigen	22.838	SYGMNNPYKAKNNNNNNNSNNNNNNSNNNNNNNNNNSQHHYYYYNNNNCSNYNNPYNYYNNN
Q8IE18	RNA-binding protein, putative	22.838	NNSMQDNNKRNSMHNNNGMNKNRGGGNKGFFGKKFSSNSNNYNNNNNNGNNYNNNNNNNNYNNNNNNN NGNNFN
Q8IKS2	Ferlin, putative	22.594	NTSSQHGNVTNNYDGYNNGAYEMGMYNMETYNIKNNDNNNNNNNYNNYNNNSYNNNNYYYNNYAAPYTSYN NNVLQNDTRNNVRYNHSNNMMINNMYKNNIYNASQFGVINYNNYNN
Q8IKY8	Chloroquine resistance marker protein	22.587	QSTQSKTHSTQSKTQSTQSKTHSSQSKTHSSQSKTHSSQSKTQSTQSKTQSTQSKTQSTQRKTQSTQSKTHSTQSKT QSTQSKTHSTQS
Q8II45	Ubiquitin-like protein, putative	22.571	NMNSTSPTNNTSSDLMNTINMINSLSNLGNYNTPYGNIVGENTTTNNSKNYAHNNNNKDNNIDSASGSIPPYYM DQSFFMEAMNFLRNTTNNDIVNNNNNNNNSSSNNNRFNNALFNNTPLNNNFSNFMNVLQNVGAGNGYIPSGR TNNTNENQAP
O77314	Uncharacterized protein	22.561	SNVSSYTSSSSFNSYNLSGTHQRDGYNYNMRGYKSYGNYGNYENCGNCVNPMNNTNNMNNMNNHNNMINTY YGGYKSSGNYYNKSYNSNNNNNNNSNNSYYDNNA
Q8I2F2	Uncharacterized protein	22.458	QQHKVQPPKVQQQKVQPPKSQQQKVQPPKSQQQKVQPPKVQQQKVQPPKVQKPKLQNQKGQKQVSPKAKG NNQA
Q8I284	Asparagine-rich antigen Pfa35-2	22.302	NNNNNNDDNNNNNDKSNSMNNNFGNYHNNNSNSNSHYNNYHHNNNYHHNNNYHHHNNYHHHNNYHHH NNYHHNNYHGNNHFNNYHHNNMNSYNEGRTIPNNSYSGKNSYNNNMG
Q8IBF6	Transcription factor with AP2 domain(S)	22.076	SSNYNYDNNNGYSNESSDNYNNGYNDSTDNNNGYNSNSSYNSNNNEDDNNNNNNNDENCDNNNNHNNNNY NNNNNYGNNNNNNNNNKDNNNNDGNGSSNNNNN
Q8I3L5	Zinc finger protein, putative	22.053	NNNGNMEHNTNATSNIMSSFNLAQVQTLCNQGNEASNSYNTMNDMIYKEGNMNGNMHGNMHGNMHSNM HSNMYGSMYGSMYGNMHENMSVFMNGNMNILMNVPMNEYMNAHMNTNINNNQFYNLNNP
Q8ILJ6	Uncharacterized protein	21.827	SQNNHGYNNGYNNVYKNSGCSTVITNNNNNNNNNNNNIYNNNINNVNNNIYNNSSIYNNSNIYNNSSIYNNSNI YNNSNIYNNNIYNNNIYNNNIYNNNIYNNNLYNNNLYNNNVYNNNLYNNNIYNSNNNSSIYNNTHNN
Q8IBH8	Uncharacterized protein	21.779	SYSTSGLYNNNNMNNMNNMNNMNNNMNTVGNYMISSNNTNNMYNMNNMYNMNNMYNMNNS
Q8I590	Uncharacterized	21.777	NNQYNNCDNNQYNNHDNNQYNNHDNNYDNNQYNNHDNNQYYYNPNNQYYNNQYFNNNYSQYHNS

	protein		
Q8I239	Phosphatidylinositol-4-phosphate 5-kinase	21.772	NNMNGDNINGDNNNNHNNINGDNNNNHNNINGDNNNNNHNNINGDNNNNHNNINGDNNNNNHNNINGDNNNNHNNINGDNNNNHNNSHNNNSHNNNNKAENSLGQP
Q8IKT9	Uncharacterized protein	21.764	NNPQNLNNIANNMTNPPNYGYNTYRRYNSLSRTYHQNNINYDININTFQNATTINNPNAPPCVGNMNNLNNINNMNNVNNVNNVNNINNLNNVNNINNNYTFLKTQPRNSLSIDNSKRMSFNRNSYISNVPTNNYNNNFYNQINMSSTTNN
Q8IL84	Metacaspase-like protein	21.569	MNNMNNMNNMNNVNNMNNVNNMNNVNNMNNMNNVNNMNNMNNVNNMNNVKSMYNNNNNSNVYYRISRQN
Q8ILI4	WW domain-binding protein 11, putative	21.529	NNSYNYMNYYYNYANNYINSYNYNPLNHGPYNPMYYYNYNNIKGNNQTTNLTNNNNSLISSYNHSNMNMMNYYGTNSNNGN
C0H5F7	Uncharacterized protein	21.488	NYNNDMNNYQHDMNNYNNDNNDYNHYMNNYQHDVNNYQHGVYNYQHDVNNYQHGVYNYQHDVNNYQHDVNNYQQDVNNYQHDVNNYQHDVNNYNHCVNNYNHCVNNYNHEGSNDSTDNKYNGNNNYNGHNNHHGDSDHNADNNYNDNNYLNPSGRNNNSSNNDGGN
Q8IJW2	Uncharacterized protein	21.329	NNMNNVNNVSNMNNKNNMNNMNNMNNMNNMNNMNNMNNMINMNNMNNMINMNNVNHMNNINHMNNLNRMNNINHMNNINHMNNINHMNNINHMNNINHMNN
C6KSS4	Spindle assembly abnormal protein 6, putative	21.196	NNMNNMNNMNNININNMNNMNNMNNMNNMNNMNNININNMNNININNMNNININNINNMNNNYKNMLGNNNNNNNN
C0H530	Ran-binding protein, putative	21.141	GGSNMYPNNNNNNNNNNNNNNSNNIINNNNSSNSCGINNTLGFTTGSTNNPNTLLNNNMNNFATPS
Q8IJ76	Early transcribed membrane protein 10.2	21.004	PSYYPTTGPNPNTHGPPSRRISTSRSSGSSNRSSSGTSTRSKGPSSPLRDSSGRSSGRSTTP
Q8IM33	Uncharacterized protein	20.960	NNNNNNNNNNNMSSNSSTNNKSPNSDLNNISSYSGSNNLSSNSDSNNLLSNSDSNNLSSNSDNNNVSSNSDSNNLLSNSDSNNLLSNSDNNNVSSNSDNNNVSSNS
C0H5J2	Uncharacterized protein	20.939	NNMNNMNNININNMNNININNMNNMNNMNNVNNMNNMNNININNMNNVNNMNNININNMNNVNSNNSNNN
Q8I515	RNA-binding protein, putative	20.871	SQSFGNMKNFNININMNSTNNHNNNNNNYNNNNYNNNNNNNSNNNNNNNNNNNCNNNNYN
Q8IAY2	Uncharacterized protein	20.710	NTNSNNNNNNNNININNNNNNININININNNNNNNNNNNININININNNNNNNNNNSQ
Q8IIG8	Uncharacterized protein	20.697	QNGLSVHQAINNNNNNIYHNNNNIYPNNNNNMYHSNNNMYHSNNNNNNMYYNNNKYYTYEHASSNVNPSSYFAAEQNEAPYNFTINNKNNNIGTNYNFPSVNNNTHGHMYN
Q8IE65	Uncharacterized protein	20.586	SSNNHNNDSSNNHNNDSSNNHNNDSSNNHNNDSSNNHNNDSSNNHNNNSSNNHNNDSSNNHNNNSSNNHN

C0H4S8	Uncharacterized protein	20.557	NNASSVYRNYNVSNGNEHTNFNNNVSASHANFSYKPMRNNNNNNNNNMRGDNNSMRGGYSMRNDQRNDQRNDQRNDQRN
O96228	Conserved Plasmodium membrane protein	20.529	QNGMIQSVNDGDKNSNFNNNNNNNINGDSNNNNINGDSNNNNINGDSNNNNINGDSNNNNINGDSNNNNINGDSNNNNINGDSNNNYHNNYHNNYRNNYHNNYRNNN
C6KSP9	RNA-binding protein, putative	20.521	PTHMNNNMMNINNININNNNNNNNRMHPNNSINYRNMNNHNNNPHYQHNYNNSNMNNPNNNS
Q8IHW1	Conserved Plasmodium protein	20.427	PTTMQAAAALNQSLMYPNNAISTEYPQYHMFNGMNSMYGGIPQYYGGMNIPMNPYYDPYG
B9ZSJ6	Phosphatidylinositol 4-kinase, putative	20.426	MNNNNNNKMNNNNNNKMNNNNNNKMNNNNNNKMNNNNNNKMNNNNNNKMNNNNNNKMNNNNNNKMNNNNNNKMNNNNNNKMNNNNNN
Q8I3S3	mRNA-binding protein PUF1	20.239	NSNNNNNNINGNINNNINGNINNNINGNINNNMNGNINNNMNGNINNNIHSNINNNSNNNNSNNNSNNNN
Q8I5I4	Nucleus export protein BRR6, putative	20.007	GSNYALSIGGYRSNNDYNSTYPNLNNNYNHLNNNNNNNMSPYPYYPFYPIIPQPINYNNSGNPNMDIPIMNCMPSQNKFYRNSSFNRNAYTNSFMNN
Q8IDI3	Inner membrane complex protein 1f, putative	19.991	NNNNNNNNNNNNSNNSNNSNYFYNGRNSSINNAFAYKQYYDSNKNGNNQHRLSHPSNMVHNINNSRTRSPS
Q8I5J9	Inner membrane complex protein 1h, putative	19.943	NNNMNSNNMNNNMNPFQTTNFMMPLMNCFQQNPDPNTLKNSENGIPNMNMSPTILRPINSRDTPNNNMNPQEHIKNNITPYPNNSLNSNFTNYNMPQNLYSQIENLPHAHNLPDGFQWQYPDGVSNNP
C0H4X0	Uncharacterized protein	19.936	NSHSHSNSHSNSHSHSNSHSNSHSHSNSHSNSHSHSNSHSHSHSNSHSNSHSHSSTQNSLYHDTNQAN
Q8IK01	Inner membrane complex protein 1c, putative	19.918	QNNIYQQANSFNQFNENAYNQNAFNRSYELLNKQSSVKSQNNASGENFSQMNFYNQYSGANFEQERSIQASNFEPSGSMQ
Q8I3L2	Uncharacterized protein	19.764	PQRFLQQNQYTKYTNNNHQNVTATNNDNNELTNCSINFNNYYQHQNNGNNSINNNNNNNNNNNNNNSIQ
Q8IAN4	DNA repair and recombination protein RAD54, putative	19.751	SMSSISNNNMKNGNDMNNTNNNTNNNTNNNTNNNTNNNINSNINNNINNNINSNINNNINSNMNNNTNLRCGSRGNQNDASGYVGN
C6KSN4	Uncharacterized protein	19.745	MGYMNNVNNINSMNSMNNINSINSMNNMNTMNSMNSMHNMNSMNSMYNMNSMNSMNSLNNVNNM
O96205	Conserved Plasmodium protein	19.732	GNNLTNTNMMPNNMSTMSIPNMNVNHMNVNHMNVNNMNINNMNINNMNVPNRNMPNRNIPNMMHVDSQNNLYNSGYNSKPSGN

Q8IIR0	Pre-mRNA-processing factor 6, putative	19.641	NFNNSASSQSGHKTPIGLGYQSSLGVQTPLGLRTPYGLQNSLSGLKTPLSGLQNSLSGLKTPLSGLQNSLSGLKTPLSGLQNSLSGLKTPLSGLQTPYMRNPSSLFGMDTPLINNNIKSNMSISGLNTPFTLSGYNTPLSASNVSGYNTP
Q8IBX7	Uncharacterized protein	19.338	STSYQDVNNFANAQNTQPITNQQYFYPLIPQYPFATTAYNPNINYPSMIPVNNNYNNYNN
Q8IES7	Uncharacterized protein	19.294	QNINQNINQNINQNINQNINQNINHNINQNINHNINQNINQNINQNINQNINQNINQNINQ
Q8II83	Uncharacterized protein	19.161	MNNVNSVNSVNSVNNMNNVNNMNNVNNMSNMNNMNNVNNMNNMNNININVNNININVNNMNNIPNGYYNN
Q8I4Y0	Kinesin-13, putative	19.075	NNNNNNNNDNNDNNNDNNNNNNNDSSSMVNNMINHMINNNININNNINVNNNNNNNNNNNNNSHNNHLPQPNYA
Q8II18	Zinc finger protein, putative	19.065	NSNYPPTYYPFHTTNNNNNNNNNNNNNNNNNNNNNNKHVYSYLYNDQQIHQINNNIHQNASNA
Q8I5I9	Transcription factor with AP2 domain(S)	19.037	NNNNKNNNNNNNNNNNNNNSNDNNNNRNGNNNIINPFFLYNKMFCMNNNANNFNNGNIINNFTNNGMAHNHNPNMNINSFRNNNM
Q8II04	Uncharacterized protein	18.997	QRSQDYLRNDMNNMNNMNNMNNMNNMNNINHINNINHMNNMNDMNNMNDMNNMNNMNNMNNINHMNNMNNMNNMNDMNKQNS
Q8I391	Uncharacterized protein	18.922	GMASSYNHMNKNVHSQNYTRMGDHSMDSPNYMNKYNMNNRHNSNEASTNRQPFPQYGPINTPPSINKKNAHSNNNNNNNNNKYINDNYYNNNSMIPNKYSPDGRYSPSN
Q8IBL9	Uncharacterized protein	18.406	APPPYAGDNTASVNPHIPNFHSGVMNRNSISPIYPTSIRSNNMINNNMMNADGTVLPANMNHPNNMLNVTNNMMVSPHPMNN
O97236	Uncharacterized protein	18.405	PNQNINISTQNISTSNDNINNNTQSINNNNINNNYINSNNNYINSNNINNNNNNNNINICGQPFNNYLYSNLNNNVSQQLPPNLSQVLNKNQILNQGN
Q8ILQ6	Uncharacterized protein	18.334	MNNMNNMNNMNNVNNMNNMNNVNNMNNMNNVNSMNNMNNIYSNINNVQLNVRNNFYNAIPSA
Q8I3U2	Sporozoite surface antigen MB2	18.257	NQNYDNPNNDNPNYDNQNYDNQNYNNPNYDHPNYDNQNYDNQNYNNPNNDYSTSQLYNSDNLQM
Q8IL57	Serine/threonine protein kinase, putative	18.254	NSSTNSLYSNGNSTTISNSNTTNMNNNVNNNVNSNVNNNVNNNVNNNVNNNMHNNIMNNVYNNMSNN
Q8IBF4	Uncharacterized protein	18.141	NNQNNYKSNQYVNEHNGNHGNNENDNNDNNNNNKNDNNNNDTTNNNNNNDNNDNNNNNNNNNNNNNNNNNSG
Q8IBH6	Uncharacterized protein	18.139	NANMNSLSNTSNVNINNNNNNNNNNSNGSIRSSGYNLIDNNINYSNHNNNNHNNNHNNNNYYYYNNMNS
C0H5J5	Polyadenylate-binding protein, putative	18.068	QYLAPQYLNIDRMNNSYNSPPPPPPPMSCHGNESSNYANNEMYSIQNTMPNNRYNSRVSTNDVHQSFINTQYGHFPYNFFKNNEQGPYMQRSYNKTYNNMGKT

Q8IB63	Uncharacterized protein	17.990	NNNYDNNNNNNNDNNNNNNNNDNNNNNNNDNNNNNNNDNNNNNNYDNNSKQSFSQKNSSENYDNGSGS
Q8II67	Phosphatidylinositol-4-phosphate 5-kinase, putative	17.981	QRYINHNNYNNHNNYNNHNNHNNYNIHNNHSNNHNNHSNNHNNHSNNHNNHSNNHNNHNNHMDDYQKYPSPNNTNM
Q8IDE5	NLI interacting factor-like phosphatase, putative	17.931	NNRNSYFNNNNNNKNNNNNSSNNNNNNNNKPFNNMTFSLNKYLNPYVNYNKTNINSRNINSSYHMGNKNKLLNKNRNMKNNANPHGSSNNNNNNNNNNNNNTYYNS
Q8ILL7	Uncharacterized protein	17.907	NNNNNNNKNINHNNNNNKNINHNNNNHNNNHNNNHNNNHNNNHNNNHNNNHNNNHNNNNNHNN
Q8IJW3	Histone deacetylase 2	17.820	NMNDAQHIHGSNNINDAQHIHGNNSMNDAQHINDNNSINDAQHINGNNSMNDAQHINGNNSMNDAQHINGNNSMNDAQLINGSNNTN
Q8I5C7	Multidrug resistance-associated protein 2	17.763	NHTAQRSNDNTPNNNNTDNNNTSDNNNTSNNNNTSDNNNTSDNNNTSDNNNTSNNNNTDNNNTSNN
Q9U0J0	Replication protein A1, large subunit	17.760	NNNNMNNMSNVNNMSNVNNVNNVNNVNNVNNVNNVNNVNNVNNVSNNNSVIMDHPSGNYNHENDPNNHHNYNNHNNYHTYDRHVNPSNNHQHYNN
Q8I538	Uncharacterized protein	17.742	ASSNNNNNFGNNNNFGNNNSCGNNNSCGNINHFGNNNSCGNINHFGNNNSCGNNNSCGNNNNFGNN
Q8IIS3	Mechanosensitive ion channel protein	17.728	GYNNNNNNNNNNNNNIQSNYNINRNINNNMNINTQQPKINYPPHGNNNFPTHHLRYNRNKPLQYTSPP
Q8I358	Exoribonuclease, putative	17.664	NSLSNNHPQIYSFTKYNQSRNQETNHHYHNPNHYSNDPRLNNAYHYNNKVRDNMQNYNNSANYNYTKTPKNYNYHHNQNFQDQNYNNNFPNLSHKNNNMYQMP
Q8IL17	Erythrocyte membrane-like protein	17.423	SALSFAGQNMDASNNYNQGDISGNNNIMKGGQDLYNNPNNTSFQMNSLNFNEKQNNNNNNNFNIGEMSNFNNQNKNHANS
O77374	Uncharacterized protein PFC0810c	17.382	NMNLATNTNNAMGNITNDSNIINTNNNNNTSDINNNNTSDINNNNTNNINNNNTNNINNNNTNNINNNNTNNTNNNSNNNNNNN
Q8IAR6	26S proteasome regulatory subunit RPN10, putative	17.340	SNNNNNNNESNNNNNESNNNNNESNNNNNESNNNNNESNNNNNESNNNNNESNNNNNGNTCGNNNNNS
C6KSR4	Uncharacterized protein	17.304	NNNMNGGNVNSIFNNPMNGGNVNNIFNNPMNGRVSTNINTYNHSNTTNAHINNHSNNVNPHNTNDPSA
Q8IHX4	RNA-binding protein, putative	17.151	SNYNNGMFSNATYNNYTYNNAIFSNNVYNNKTATNSIQNINIHGNNNIHGNNNVHGNNNVHGNNNVHGNNNVHGNNN
Q8IJL2	Eukaryotic translation	17.131	NSTQNNTIINNNNNNNNNMNGINNNIPMNSINNNIPMNSINNNIPMNSINNNIHMNSINNINVGMSYVNNMN

	initiation factor subunit eIF2A, putative		NKMMNNNNNNNNLTNPTSYS
Q8I0W7	ATP-dependent RNA helicase DDX23, putative	17.060	NQHQQHQQHQQHHHHNNNNNNNNISCNDNSDHNSNLNSNLNSNLNSNLNSNLNSNLSSNHISNNNLHNNHHPN
Q8IAK9	Uncharacterized protein	16.771	PRNPNIPYVRFPHHQWGQGMMYGRPYYPWVPFMGDGRGYNFYNPHQHMVYGRPYYWVPPPPA
Q8IJ85	Asparagine-rich antigen	16.748	NNMNNMNNMNNINNVNNINNMSNINNMSNINNMSNINNMSDINNVNSLPSINNNNNNNNQSGNTNIYNPN
Q8I5U3	Uncharacterized protein	16.730	MGANNMHNEINSNNNNNNNDNNNNNNNDNNNNNNNIEQYRQSTTIINTPNQNMFDNNNNFNNSVDNINSYNEIIFHQNVQNYITPNGTTKDNIQNGLQNNMQQCSQS
Q8IL69	Uncharacterized protein	16.627	SNMQNINSSNFMGNFNSINNSMNNRNDLYNLNPFMSMQSMNQDMNNRNNYPFEPRGSNYGN
Q8IEL1	Uncharacterized protein	16.610	NTNTNTNTNTNTNTNTNTNTNTNTNTNTNTNTNTNTNINTNTNTNTNTNTNTNTHTNTNTNTNTNTNTNTN
Q8IC42	Uncharacterized protein	16.568	PAGRNYSLGNLSTGTTSQGSTSSRHYSLGGQPSSSGRSFSGSKYNTSNLASSSTTESSVSGLNTNEAHV
Q8IKN5	Uncharacterized protein	16.562	NNQNNQNYQHNQHNNIYNHSNNNYNNNMYHNNDRNIKTNMETYGNKFVSNNYNNKNNYMSKMSGFGNPYFNQNPVQ
O96239	DEAD/DEAH box helicase, putative	16.467	MPGNENMNMSGNENMNMSVNENMNMSVNENMNMSGNENMNMSGNENMNMSGNENMNMSGNENMNMSGNENMNMSGNENMNMSGN
Q8IK89	Trailer hitch homolog, putative	16.324	SSNDRNMNNRRYYNNRPNYNFHYNNRNYNNNQNNNNNNNNNNNYKYRNYRNYERSNYVIGELQSQPNPA
O97251	EB1 homolog, putative	16.136	SRGMNNSMVNNNINNLNNNVNNSTNVNINNSVSNNVNNYMNSNMYSGNTTSTTTLITTTSSNNNNNSNN
Q8IBV5	Uncharacterized protein	16.116	NANFSSQNGENNLNFYNNNNNNNNRSYTNYTNNMNDEINNQYNLFYNINNENNNNNNNNNNNYYYNNNYNNNNN
Q8IJ86	Mitochondrial preribosomal assembly protein rimM, putative	16.069	GGSALTGSFSSTMKNMLQNNVLQGKAYCNNGNMDNNTKSNSSDGSSSDGSSSDGSSSDGNSSDGSSSSSSNYKNTQSYS
Q8I5P8	Conserved Plasmodium membrane protein	16.051	SGNNENNNNNNNDGHNNNNNDSHNNNNNDGHNNNYDHNNDSTLENTNLPQNSYNNNGNNGNNSS
C0H4R0	Uncharacterized protein	16.025	NMNNSSNSKAYNNNMRDTSSSNTSMSDTISSNTNSSHTNSSHTTSSNTTSSHTHSRHTHSRRTHSSHTTNSDTNSSNNNKSSSNSA
Q8I355	FHA domain protein,	15.880	ARGNNLNMCNNNNQQNVNNQININNNNNNNNNNTHNSINSIDEANINLNSTTSEQNLTLSNIPINNNIKNDQAH

	putative		NNNNNNNNNTNNMTNGNISNNANSQNIL
Q8IJ54	Merozoite surface protein 6	15.696	QATYQFPSTSGGNNVIPLPIKQSGENQYTVTSISGIQKGANGLTGATENITQVVQANSETNKNPTSHSNSTTTSLNN NILGWEFGGGAPQNGAA
C6KSS5	Protein PFF0380w	15.667	QRGQNLQRGDNLQRGDNLQRGDNLQRGDNLQNGDNLQNGDNLQRGDNLQNGENLQSGENLQSGENLQSG
Q8I552	Uncharacterized protein	15.593	NNNNNINSNNINSNNINSNNINSNNINSNNINSNNINSNNSNNSNNINSNNSNNINNIGSAINSNN
Q8ILV4	Uncharacterized protein	15.476	NNNINNNNNINNNNNINNNNNINNYNNSNNSNGVAGADEHNNINSHNNQNITHNFTNNSSNDLGYNHNQN
C0H5I1	Uncharacterized protein	15.443	PQKQYNHIYTNQSNISHNIHNTYYSQNAYQNENYYYQYLNYPHVANFNMMMMNTTNPVLYNNNNNNNNN
Q8IBL4	Uncharacterized protein	15.313	PPPPPPTSLYNNNNDNNNDNDNNNNNNNITNSHMGEYNDNHSDEDNNNNNNNNFSYNNSRVNTNNSAYRGK NNNMQN
C6KSN9	Transcription factor with AP2 domain(S)	15.297	ASQYNNNNNDNNNDNNDNNNNNNNDNNNYGNTMVQNEFNRYFMNNNNYMVMNNNMHTNNMLNN
Q8I1Z1	Alpha/beta hydrolase, putative	15.262	GNNKSSNNNNNNNNNNNNSCSSSSNNSMSLNMKTLSSYTLKNKNTQGNSNHDNNNNNNNNNCNNSNSNS
Q8IKK6	Uncharacterized protein	15.132	NNHNNNNNLYSNNMNSNNMNSNNINSNNINSNSIYSNNIYSNNIYSNNIYSNNTYSNNTYSNN
C6S3D0	Conserved Plasmodium protein	15.106	NMNPNNNNNNNKNNDNNNNNNKNNDNNNNNNKNNDNNNNNNKNNDNNNNNNKNNDNNNNNNKNND NNNNNNKNNDNNNG
Q8I5K3	Histone-lysine N-methyltransferase, H3 lysine-4 specific	15.054	NPNNSNISYGVKNSNISYDANNSNISYDANNSNISYGVNNSNISYGADNSNISHSFNNSNISHSFNNSNISHSANNS NISHSANNSNS
O77327	Splicing factor 3B subunit 1, putative	14.602	NMSTPYISNNMSTPYISNNMNTPYISNNMNTPYISNNMNTPYISNNMNTPYISNNMNTPYIPNN
O97239	Protein dopey homolog PFC0245c	14.519	MTGNQTSSTKDVGGMVNNAIRQNIEQNNMIHPNQINNNNNNNNNNNNNVYNFNDFTNSMNQPN
C0H5L5	Uncharacterized protein	14.192	SNMSNSNMSNSNLSNFNVSNSNVSNSNVSNFNVSNFNVSNFNVSNFNVSNTHEPNFNMTYSHVPNINQP
O77318	Uncharacterized protein	14.179	NNPTNNLTDNPTNNSTDNPTNNSIDNPTNNSIDNPTNNSIDNPTNNSIDNPTNNSIDNPTNNSIDNPTNNSTDNPI NSPNYQQVTQSN
Q8I5Y2	Conserved Plasmodium protein	14.020	NNTMNYGINNTMNYGINNNMNYDVNNTMNYDVNNTMNYDVNNTMNYGINNNMNYDINNNMNYDINNTM NYDVNNTMNYNINNPMYYDINNPINYQMNNTNISNINNPINYQMNIPLDYQMIPNNNINNIHNNNNNINNSIYF QNNN

Q8I3R5	Carbon catabolite repressor protein 4, putative	13.965	NNNNNNNDNNSSNNNNNNNNINSGTHNVNNTNMVVHMNNSTTNFYNLYDMDNNNNNNVANFHLQN
Q8IID2	Calcium-dependent protein kinase 7	13.955	NQNENQNENQNENQNENQNENQNENQNENQNENQNENQNENQNENQNENQNENQNENQNENQNENQN ENQKNNNN
Q8ILI1	Uncharacterized protein	13.733	NNNDNNNDNNNDNNNDNNNDNNNDNNNDNNNDNNNDNNNDNNNDNNNYQNNYQNNDNNQN
C0H4S0	AAA family ATPase, putative	13.711	NNVNNVNNVNNVNNVNNVNNVNNVNNVNNVNNVNNVNNVNNVNNVNNVNNVNNVNNVNNVNNVNNV NNVNNVNNVNM
Q8IBL5	Uncharacterized protein	13.571	QMDGNNNNMYSSMYSSMYSSMHSNMHSGIHNNIHNNIHHNIHNNIHHNIHNNIHNNMHSNMHNNMHNN MHNNMHNNIHSNNFINCNNALLINEYNNFSKSGMLLNNSNNNHNNNNNNNNNNNGVSN
Q8IM32	Uncharacterized protein	13.558	NSANNNNNNNNNNNNDNNNNNNDDNNNDDDNNNDDDNNNNNDNNNNGNGDHNNNSNNNKGGDGGD NNN
Q8I2R3	Uncharacterized protein	13.530	NNVNSINNMNSINNMNSINNMNSINNMNSINNMNSINNINHMSNMNNMNSINSLNSMNNMNSINSLNSMN N
Q8IEE5	DNA replication licensing factor MCM4	13.263	MGTPRRRLGQQNNNNNSPFALSSSNIFGSNNEIFGSNFMHTPMSSRRTKNSKSFLNSMLNESRYLNQSNAGSQ
Q8I235	Kinesin-8, putative	13.252	NTTGRGDQKMNVNQINNNINVNNHVTVNNNNNNNNNNNGSVNNHIQVHEGSNNHGVSSLSPVHQNG
Q8IIF4	Protein kinase	13.069	NNNNNNNYYYYYNNNQIYMNNCYMNNKYNNMNMEHMKNYYNNGYNNEYYNHINLSNIPYNNIQLQNGHFH NINMNNQNMIPFQNINNTLYASNQ
C0H5A4	U1 small nuclear ribonucleoprotein A, putative	12.992	PSSYVNGAGKNMDSAGNIIPNINNNIQYHMPIPNNMPYGVNPNYNIHNNKMINNPKNMYNAPYPLNMNTIPIN SYGGA
Q8IJH4	Dynein heavy chain, putative	12.888	NSNTATTTTTTTNNNNNNNNNDNITINNSGASQINNTNNDNNNITIDNQNNYGNEPGDSNKNYHKQNSQNMN
O97298	Uncharacterized protein	12.842	NTYGNNNTYGKDNTYGNNNTYGKDNTYGNNNTYGKDNTYGNNNTYGKDNTYGNNNTYGNNNTYGNNNTYG
Q8I4T6	THO complex subunit 2, putative	12.479	QSTSRTSVHNVNADVNVTMNPFNNSTPVHIPSNPPFAPMPKNIYNPNAYPIVQNTINPPP
Q8ILJ1	Uncharacterized protein	12.467	NNNNINNNYPYGTHLNTNNYGLRNLNSSYLNANGQNVSNVPGTTLIKNANVNNLNYSYASNN
Q8IDT2	Uncharacterized protein	12.399	PQQNNNKNMSHSQKFNEYIPMNGFRSIYHNNNMNNGNGYYTNTFNKHNSNLYTHQNNMYGRNN
Q8I1N6	AP2/ERF domain-	12.226	NSQVNESSAPASNYKGGGVQFYMNLDTTNLLAASLMTNNIINNLNNQGNGDNSHVNNNYNSNA

	containing protein PFD0985w		
Q8ID46	Uncharacterized protein	12.200	QYNNYDHNNSNYMMNANMEKANVNANVNANVNANANANIYSYNSENNNIPGKQINNITNNNKNNYNNNN
Q8IIH0	Uncharacterized protein	12.123	MSNRNINNNINNNISNNISNNMNSNINNNLNNNLNNNLNNNINNNINDNMNNCQNGNFYGTYNNQ
Q8IKT0	Uncharacterized protein	10.683	MMHPFNFVPQLDNKINVVSMQPFQMYVPNNNAVIPQSFSSDHTTQHYSQPIYFEPLPPIYVKNQLLPSPILVQMP TTVVVQNESQPAMVLNQPPSN
Q8I2Y5	RNA-binding protein musashi, putative	9.763	QNNQNYVKKNQNFNYYQKNNLNNRNNFVRRTPMYHHENEAPNTFNYPVSFVPNVYTNVPHGYQLNYPGNLDS FNAFYNNPRY

PrLD score: Sum of PLAAC LLRs in full region of Viterbi parse containing CORE region, being LLRs the max sum of PLAAC log-likelihood ratios (base 4) in a window of 60 amino acids size.

Table S3. Proteins identified in 0.1% SDS-resistant aggregates.

Accession	Description	Score	Coverage	# Proteins	# Unique Peptides	# Peptides	# PSMs	# AAs	MW [kDa]	pI
C6KTB7	Putative E3 ubiquitin-protein ligase protein PFF1365c	609.25	22.75	6	170	189	245	10287	1205.3	7.96
Q8I525	Conserved Plasmodium protein	558.96	35.62	42	163	184	236	5767	691	5.81
C0H5J9	Uncharacterized protein	540.29	60.84	1	110	112	169	2605	290.8	5.25
O77384	Protein PFC0760c	512.91	43.22	37	127	142	212	3394	402.7	4.83
C6KST7	Uncharacterized protein	508.51	31.25	56	146	158	197	6077	720.1	7.01
Q8IES7	Uncharacterized protein	458.05	19.15	2	122	146	190	9271	1111.1	9.00
C6KSY0	Transcription factor with AP2 domain(S)	384.99	34.51	18	110	116	161	4109	485.3	6.18
Q8I5L6	Clathrin heavy chain	325.36	51.38	11	75	86	118	1997	232.8	6.39
O97239	Protein dopey homolog PFC0245c	320.00	26.88	12	82	93	128	3933	467.6	7.23
C0H4C4	Uncharacterized protein	307.38	21.60	15	90	99	128	5639	671.6	7.47
Q8IKF6	Uncharacterized protein	277.51	37.88	1	66	72	109	2558	295.6	5.35
Q8IM09	Uncharacterized protein	272.83	14.24	2	72	84	106	7182	851.3	8.73
Q8ILB9	Dynein-related AAA-type ATPase	261.37	14.03	1	79	85	110	8105	970.4	7.87
O96205	Conserved Plasmodium protein	250.75	25.06	86	74	86	111	3990	477.6	8.27
Q8IBY8	Uncharacterized protein	246.97	32.89	18	66	80	104	2910	350.5	5.85
C0H5D0	Uncharacterized protein	232.79	24.49	3	56	69	91	3438	402.2	8.21
O96204	Conserved Plasmodium membrane protein	216.36	22.15	2	62	71	93	4091	493.9	8.27
Q8I3M5	Karyopherin beta	213.73	56.28	1	43	43	70	1123	127.3	4.92
Q8IE50	Myosin C	203.68	33.43	6	57	60	73	2160	250.1	8.63
C0H5A0	Uncharacterized protein	180.24	18.41	69	40	48	65	3525	418.3	7.06
Q8ILA2	Uncharacterized protein	143.76	21.99	2	42	49	61	2269	270.3	8.25
Q8I5S6	Eukaryotic translation initiation factor 3 subunit A	139.86	38.63	2	38	43	63	1377	166	6.81
C0H4L9	Uncharacterized protein	132.37	19.49	3	30	34	49	2129	256.8	7.08
Q8IJG6	Chromodomain-helicase-DNA-binding protein 1 homolog	126.51	14.39	1	34	40	45	3328	381	6.33
C0H4L1	Importin-7	125.66	39.63	1	37	38	46	1229	145.4	5.30
Q8IIW4	CCR4-NOT transcription complex subunit 1	124.50	16.29	2	36	41	57	3371	391.7	7.05

C6KT82	SNF2 helicase	121.59	23.87	2	30	43	58	2719	315.4	6.98
Q8IB24	Heat shock protein 70	119.94	56.43	10	30	31	40	677	73.9	5.67
Q9U0K8	Uncharacterized protein	119.91	20.41	1	30	33	44	1960	230	6.90
C0H4K4	Uncharacterized protein	115.74	16.75	1	36	44	51	3559	425	8.81
Q8IJP6	Uncharacterized protein	102.35	16.15	1	26	34	44	2279	267.8	7.83
Q8I259	Uncharacterized protein	96.36	17.92	1	25	29	36	2221	254.8	5.68
Q8I4X0	Actin-1	93.76	78.46	1	19	24	43	376	41.8	5.34
Q8ILJ1	Uncharacterized protein	93.06	28.37	2	32	33	36	1477	175.7	7.30
C6KSQ6	Probable DNA repair protein RAD50	90.92	17.53	1	28	33	37	2236	267.8	8.59
Q8I548	Uncharacterized protein	89.62	18.74	1	23	23	29	1681	192.7	5.54
C0H4P4	Uncharacterized protein	89.12	9.81	1	29	36	39	4944	598.9	7.84
C6KSR4	Uncharacterized protein	88.82	15.70	2	31	36	43	2414	280.2	5.19
C6S3C9	Serine/threonine-protein phosphatase	87.16	13.62	1	17	23	32	2166	254	5.83
C0H530	Ran-binding protein	85.84	27.30	1	24	26	31	1198	139.1	6.37
Q8IC05	Heat shock protein 90	78.93	34.36	6	20	22	27	745	86.1	5.01
Q8IE65	Uncharacterized protein	78.43	7.99	70	21	24	32	3519	418.8	6.76
C0H5B3	Uncharacterized protein	78.11	11.11	1	18	25	30	3411	408.6	8.82
Q9U0I0	Uncharacterized protein	74.47	20.26	2	25	27	34	1298	150.2	6.61
C6KSS4	Spindle assembly abnormal protein 6	73.26	29.50	1	18	20	27	861	101.2	6.33
Q8ILG6	Coatamer beta subunit	73.02	17.30	1	14	15	24	1370	159.9	6.23
Q8IHU4	Uncharacterized protein	71.02	12.13	1	23	25	27	2738	324.6	5.92
Q8ILA8	Uncharacterized protein	66.47	16.16	69	16	22	27	1788	210.6	8.60
C6KTD2	Putative histone-lysine N-methyltransferase 1	66.28	6.40	6	18	32	34	6753	795.5	8.59
Q8IIS4	Transcription factor with AP2 domain(S)	66.04	12.20	1	17	19	23	1828	206.7	5.99
Q9U0N1	Glutamic acid-rich protein	61.96	30.01	1	11	13	22	673	79.7	4.93
Q9TY99	Knob-associated histidine-rich protein	61.17	25.08	1	9	9	20	654	71.3	9.09
C6KT67	Nuclear polyadenylated RNA-binding protein NAB2	59.94	22.26	1	15	16	24	786	91.1	8.90
Q8IKZ7	Calponin homology domain-containing protein	59.02	12.99	2	17	21	28	1986	237.9	6.76
Q8IEF5	Exportin-1	52.98	20.45	5	16	16	22	1232	142.9	5.96
Q8ILT5	Protein SEY1 homolog	52.51	28.82	2	19	20	23	937	110.5	7.55

Q8IL84	Metacaspase-like protein	51.27	10.30	1	14	16	22	2020	237.7	9.22
Q8ID39	Uncharacterized protein MAL13P1.336	50.92	20.15	1	12	15	22	685	78.5	9.38
Q8I492	Mature parasite-infected erythrocyte surface antigen	50.00	25.87	1	15	19	30	1434	168.2	4.78
Q8IL42	Guanine nucleotide exchange factor	47.93	10.22	33	19	24	32	3384	404.3	6.51
A0A143ZY62	Uncharacterized protein	45.83	7.89	1	10	22	29	4358	529	8.47
Q8ILS4	NOT family protein	45.67	3.78	1	10	13	17	4466	519.5	7.25
Q8ILC9	Uncharacterized protein	44.77	6.58	1	11	23	27	5757	682	8.68
C0H4V6	14-3-3 protein	44.22	73.66	7	12	15	16	262	30.2	4.92
Q8IHY4	Uncharacterized protein	43.80	8.14	7	12	19	22	2849	335.7	5.99
Q8I398	Nucleoporin NUP100/NSP100	43.05	8.33	1	11	13	18	2112	235.4	8.28
Q8I2I8	Uncharacterized protein	42.59	10.28	3	10	10	15	1342	159	6.95
Q8IKK7	Glyceraldehyde-3-phosphate dehydrogenase	42.52	45.70	1	12	12	17	337	36.6	7.69
C0H5A6	Uncharacterized protein	41.36	5.38	1	10	19	24	6147	737.2	9.06
Q6LFH8	Ornithine aminotransferase	40.57	38.65	1	12	12	15	414	46	6.89
Q8I0P6	Elongation factor 1 alpha	39.46	41.99	4	12	14	16	443	48.9	9.06
Q8I4U7	Uncharacterized protein	38.17	5.33	1	7	8	12	1989	231.2	6.32
Q8IDI3	Inner membrane complex protein 1f	37.83	12.44	1	9	14	17	1318	151.4	8.81
Q8IBP4	Phosphoinositide-binding protein	37.39	7.39	3	9	12	14	2166	258.3	6.74
C0H4K3	Uncharacterized protein	37.12	4.62	1	8	10	13	3268	393.2	7.52
Q8IAW0	Importin subunit alpha	36.63	27.16	1	9	10	12	545	61.1	5.30
Q8I4T6	THO complex subunit 2	36.16	6.11	1	6	9	13	2932	348.5	8.51
Q8I3Z1	MATH and LRR domain-containing protein PFE0570w	35.70	3.99	16	5	27	29	10061	1186.8	7.49
O77312	Exportin-1	35.18	16.51	1	10	12	16	1254	147.8	5.97
Q8I414	Uncharacterized protein	34.97	4.91	1	7	13	14	3134	370	5.44
Q8I562	Clustered-asparagine-rich protein	34.94	32.36	1	9	9	15	445	51.5	8.60
Q9U0J0	Replication protein A1, large subunit	34.56	17.03	1	10	14	16	1145	134.1	7.03
C6KTB9	Choline/ethanolaminephosphotransferase	33.72	28.64	1	9	9	11	391	45.1	9.36
Q8I5G0	Uncharacterized protein	32.30	9.59	1	11	14	14	1501	178	5.57
Q8IAY9	Importin beta	32.08	18.24	1	8	8	11	877	99.9	4.97
Q7KQL5	Tubulin beta chain	32.06	34.61	11	10	10	12	445	49.7	4.83

Q8ILV2	60S ribosomal protein L10	32.02	39.73	3	6	9	13	219	25.2	9.95
Q8IB94	E3 ubiquitin-protein ligase	31.39	2.34	73	8	15	18	8591	1004.5	5.30
Q7K6A4	S-adenosylmethionine synthase	31.19	32.09	1	11	12	14	402	44.8	6.74
Q6ZLZ9	Tubulin alpha chain	30.78	23.62	7	7	8	10	453	50.3	5.06
Q8IKM7	Uncharacterized protein	30.24	10.29	1	10	12	13	1632	191.9	7.08
Q8IDD4	Serine/threonine protein kinase	29.63	6.40	1	6	17	17	4044	475.4	8.90
Q8I3V8	Pre-mRNA-splicing factor CWC2	29.51	17.57	1	8	11	14	848	98.3	5.71
Q76NM3	L-lactate dehydrogenase	29.04	36.08	1	6	6	8	316	34.1	7.55
A0A143ZZV5	Uncharacterized protein	28.47	3.05	1	5	11	13	6034	720.5	8.68
Q8IKR2	Uncharacterized protein	28.44	15.50	1	7	7	12	684	77.8	5.29
Q8IKW5	Elongation factor 2	28.30	15.63	1	8	8	11	832	93.5	6.80
C0H5L6	Uncharacterized protein	27.16	4.88	1	6	9	11	2868	346.6	7.30
O96201	Conserved Plasmodium protein	25.75	10.63	1	8	11	13	1844	214.5	7.33
Q8IKJ2	Uncharacterized protein	25.33	2.83	1	4	9	11	3251	388.6	8.70
Q8IKL1	Uncharacterized protein	25.08	9.95	1	7	8	9	1357	161.1	6.42
Q8IIQ6	Vacuolar protein sorting-associated protein 35	24.75	8.48	1	5	5	8	1050	123.4	6.39
Q8I3I6	AP complex subunit beta	24.63	18.95	1	8	9	10	929	106.1	6.04
Q8IKY0	Transcription factor with AP2 domain(S)	23.91	12.31	1	5	8	12	715	84.4	7.39
Q8I5C6	Uncharacterized protein	22.95	7.47	1	5	7	10	990	117.4	5.95
Q8IAZ5	Vacuolar protein sorting-associated protein 9	22.87	5.35	1	4	8	10	1833	214.6	6.61
Q8I5Y3	Eukaryotic translation initiation factor 3 subunit C	22.69	15.65	1	8	12	14	984	115.9	5.38
Q8II83	Uncharacterized protein	22.56	6.88	19	6	9	11	1789	212.7	6.21
Q8IKH8	40S ribosomal protein S3	22.44	28.05	1	4	5	7	221	24.7	10.18
Q8ID46	Uncharacterized protein	22.19	2.61	16	4	8	10	4136	494.4	5.85
Q8IKR4	Uncharacterized protein	22.03	4.81	1	7	10	11	2391	283	7.23
Q7KQK6	GTP-binding nuclear protein	21.75	38.79	2	7	7	8	214	24.9	7.94
Q8IHW8	Conserved Plasmodium protein	21.53	6.46	16	4	11	13	2213	265.1	8.81
C6KSZ7	Uncharacterized protein	20.74	5.66	1	6	11	13	2528	303.9	6.47
Q8I2Z8	Probable ATP-dependent 6-phosphofructokinase	20.72	6.84	1	5	7	10	1418	159.4	6.76
C6KT34	Cell division cycle protein 48 homologue	20.40	11.23	1	6	7	9	828	92.3	5.08

Q8IBL5	Uncharacterized protein	19.81	5.53	1	9	11	11	2190	260.6	5.71
Q8IJL2	Eukaryotic translation initiation factor subunit eIF2A	19.60	5.03	1	4	9	9	2405	280.6	8.62
Q8I5W6	Conserved Plasmodium protein	19.26	3.07	9	5	10	11	4469	533.3	9.01
C6S3H2	Uncharacterized protein	17.83	4.40	1	5	8	10	1955	229.4	6.46
C6KTB3	Transportin	17.66	7.15	1	4	5	8	1147	132.8	5.29
Q8IBJ1	Ubiquitin carboxyl-terminal hydrolase	17.48	3.61	1	2	7	8	3183	372.9	7.91
Q8IJW6	Asparagine-rich antigen	17.44	5.89	1	5	6	7	1597	182.6	6.23
Q8I3F9	Formin 1	17.09	5.98	1	3	10	11	2675	309.3	8.18
O96221	Protein transport protein SEC31	16.78	5.57	1	5	6	7	1471	166.6	6.93
C0H5J0	Uncharacterized protein	16.63	5.30	1	4	10	12	3281	394.3	8.75
Q8I1X5	Pre-mRNA-processing-splicing factor 8	16.47	4.02	2	5	6	6	3136	366.2	8.66
Q8ILL3	60S ribosomal protein L5	16.16	26.19	1	6	7	7	294	34	9.77
Q8I447	DNA mismatch repair protein MSH6	16.01	4.07	1	2	3	4	1350	156.3	6.40
O97225	Spindle pole body protein	14.99	5.93	1	3	7	8	2226	267.8	7.49
Q8IJS7	PRE-binding protein	14.91	13.17	1	3	8	9	1139	131.5	9.16
Q8IBZ0	Uncharacterized protein	14.82	4.10	2	3	11	11	3267	407.1	9.85
Q8IKF0	Eukaryotic initiation factor 4A	14.67	24.37	1	5	6	6	398	45.3	5.69
Q8I2I3	Gamma-tubulin complex component	14.38	7.47	1	3	6	6	1512	180.4	8.15
C0H5I8	Uncharacterized protein	13.85	7.21	1	3	6	7	1596	191.3	6.29
Q8IBN5	40S ribosomal protein S5	13.72	34.36	1	4	4	7	195	21.8	9.61
Q8I467	Cofilin/actin-depolymerizing factor homolog 1	13.64	30.33	1	3	3	4	122	13.7	7.78
C0H5H6	Uncharacterized protein	13.16	1.34	1	2	6	7	5988	696.6	7.77
Q8I445	Uncharacterized protein	12.81	13.31	1	5	6	9	924	112.6	6.38
Q8IK03	Uncharacterized protein	12.75	3.07	1	2	5	7	2050	243	8.92
Q8I2Y3	Uncharacterized protein	12.50	4.65	1	4	6	6	1826	215.2	5.99
A0A143ZWQ6	Uncharacterized protein	12.42	3.44	2	4	8	9	3459	420.2	8.51
Q8ILX0	Uncharacterized protein	12.12	4.97	1	2	7	9	3218	390.4	9.16
Q7K6A5	Multidrug resistance protein 1	12.08	5.43	6	4	7	9	1419	162.1	8.84
Q8IIG8	Uncharacterized protein	12.06	4.23	1	2	3	4	1749	208.5	6.02
C6KT18	Histone H2A	11.72	51.52	17	4	4	6	132	14.1	10.29

Q8ILJ7	Phosphoenolpyruvate carboxylase	11.67	6.36	1	2	3	4	1148	133.9	7.81
Q8I586	Asparagine and aspartate rich protein 1	11.51	1.16	1	1	5	7	5439	645.9	6.43
C0H4A6	Ribosomal protein L15	11.48	11.22	1	2	2	3	205	24.1	11.25
C0H4K6	E3 ubiquitin-protein ligase	11.22	1.93	1	1	7	7	3893	460.1	6.58
Q8IKN7	Uncharacterized protein	11.06	17.35	1	4	4	4	340	40	9.57
Q8I5L0	Cell cycle associated protein	10.83	3.11	1	3	6	6	2705	323.9	9.22
Q8I403	Uncharacterized protein	10.60	3.43	1	2	7	7	2535	297.4	6.51
Q8ILL9	Serine/threonine-protein phosphatase	10.47	6.26	1	1	3	4	959	112.5	6.96
Q8IL08	Uncharacterized protein	10.39	3.20	1	2	4	5	3001	346.7	8.79
Q8ILH0	rRNA (Adenosine-2'-O-)-methyltransferase	10.22	4.50	69	2	7	8	2779	332.7	8.35
O97289	Peptidase	10.08	5.31	1	2	3	3	1074	125.8	6.60
Q8ILQ6	Uncharacterized protein	9.94	6.27	1	4	9	9	2201	262.1	6.77
A0A143ZVW7	Uncharacterized protein	9.69	4.59	1	5	6	6	1852	217.4	6.84
Q8II24	Heat shock protein 70	9.50	6.49	1	2	3	7	663	73.3	6.84
Q8I1N6	AP2/ERF domain-containing protein PFD0985w	9.47	1.84	1	1	6	7	3473	399.9	5.97
Q7KQK2	PfpUB Plasmodium falciparum polyubiquitin	9.43	64.3	2	1	5	6	381	42.8	7.58
Q8IHR4	Dynamin-like protein	9.36	6.45	1	3	4	5	837	96.3	8.16
Q8IC40	Uncharacterized protein	9.35	3.80	1	3	6	7	1843	220.3	7.96
Q76NN8	Calcium-transporting ATPase	9.34	2.77	1	2	2	3	1228	139.3	7.24
Q8ILL2	60S ribosomal protein L7-3	9.24	21.2	1	3	4	4	283	32.7	10.15
Q8I3L4	Acyl-CoA synthetase	9.14	8.77	11	1	4	5	673	76.8	8.21
Q8I240	Bromodomain protein	8.89	4.55	1	1	6	6	2285	268	6.21
Q8IDN6	Protein transport protein SEC61 subunit alpha	8.87	8.69	1	2	2	2	472	52.2	8.63
Q8IAV6	Uncharacterized protein	8.83	5.09	19	1	5	6	2651	314.3	8.09
Q8IE09	60S ribosomal protein L23	8.64	23.74	1	3	3	3	139	15	9.86
Q8IBZ6	Cg2 protein	8.64	3.33	3	1	6	6	2729	325.3	7.75
C0H5I2	Uncharacterized protein	8.57	3.51	1	2	5	5	1594	190.2	8.53
C0H4C6	Uncharacterized protein	8.54	1.82	16	1	5	6	2975	355	5.35
C0H4R8	Serine/threonine protein kinase, FIKK family	8.22	2.06	1	2	3	4	1457	171.7	6.47
Q8IKZ6	Multidrug resistance protein 2	8.13	3.42	16	1	4	5	1024	118.9	9.14

C0H570	RNA-binding protein	7.88	13.15	1	2	2	2	289	33.6	9.10
Q8IC35	Erythrocyte membrane-associated antigen	7.86	5.13	1	1	7	9	2299	264.8	8.60
Q8IDB8	HVA22-like protein	7.73	11.76	1	2	2	3	153	18.4	9.31
Q8I431	60S ribosomal protein L4	7.73	10.71	1	3	4	4	411	46.2	10.49
Q8I444	Small ubiquitin-related modifier	7.68	19.00	1	2	2	3	100	11.1	4.91
Q8IIE0	Conserved Plasmodium protein	7.50	1.20	1	1	3	4	1832	217.6	7.69
Q8ILR9	Protein PF14_0175	7.49	2.53	69	2	7	7	4662	548.5	8.73
C0H571	High molecular weight rhoptry protein 2	7.45	2.03	1	1	2	2	1378	162.6	8.27
Q8IEL8	Vacuolar protein sorting-associated protein 18	7.37	3.53	1	3	5	5	1672	198.2	7.72
Q8IM32	Uncharacterized protein	7.33	2.48	5	1	5	6	2820	338.2	5.27
C6KT03	Kinetochore protein NDC80	7.27	2.71	1	1	1	2	591	69.8	5.57
Q8I583	Sentrin-specific protease 1	7.23	7.60	1	1	3	5	1026	123.1	7.77
Q8I6U8	Glycophorin-binding protein	7.18	26.70	1	2	2	3	824	95.8	5.14
Q8I3B4	DEAD/DEAH box helicase	7.17	5.05	13	3	7	8	2536	300.7	6.93
Q8IJM0	26S proteasome regulatory subunit p55	7.09	19.06	1	3	4	4	467	55.2	5.85
C0H5G3	60S ribosomal protein L18-2	7.04	12.83	1	2	2	2	187	21.4	11.14
Q8IJI6	Conserved Plasmodium membrane protein	7.00	2.37	1	2	9	10	6934	829.7	9.09
Q8IDL5	Uncharacterized protein	6.95	1.53	5	1	6	6	3855	460.6	7.53
Q8IDQ9	Phosphoethanolamine N-methyltransferase	6.94	15.04	1	3	3	3	266	31	5.60
Q8IDH5	Thioredoxin-related protein	6.94	13.94	1	3	3	3	208	24	9.38
O77313	N-ethylmaleimide-sensitive fusion protein	6.89	7.15	5	1	3	4	783	89.1	6.71
Q8I3L2	Uncharacterized protein	6.85	4.16	1	1	1	2	481	55.8	7.53
Q8I531	Transcription factor with AP2 domain(S)	6.85	1.79	1	1	4	5	2577	299.2	6.32
Q8I5M3	Uncharacterized protein	6.79	4.34	1	1	4	4	1061	122.7	6.57
Q8IEQ3	Uncharacterized protein	6.69	5.86	1	1	2	2	478	56.8	9.51
C6KSN4	Uncharacterized protein	6.68	2.32	1	1	5	6	2368	280.3	9.20
Q9TY94	ATP-dependent RNA helicase UAP56	6.67	10.94	2	4	4	4	457	52.2	6.00
Q8I538	Uncharacterized protein	6.64	2.43	1	1	3	3	1812	212.6	5.07
Q8I207	Uncharacterized protein	6.49	5.54	1	2	3	3	560	60.2	8.56
Q8I5C2	Myosin d	6.44	4.53	1	2	6	6	2231	265.8	8.32

Q8IAM0	Glutamate dehydrogenase	6.30	4.29	1	1	4	4	1397	160.3	6.74
O97313	40S ribosomal protein S3a	6.29	18.32	1	4	4	4	262	30	9.77
Q8IJP9	ADA2-like protein	6.21	2.37	1	1	4	4	2578	300.1	8.65
Q8IKQ9	Signal peptide peptidase	6.19	4.13	1	2	2	3	412	47.5	8.81
C6KST5	T-complex protein 1 subunit zeta	6.07	7.92	33	1	3	4	543	61.5	6.92
Q8IJ32	Dynamin protein	5.97	9.17	1	1	2	4	709	81.5	6.43
C6KSR5	Coatomer alpha subunit	5.90	2.05	1	2	2	2	1512	176.8	8.34
Q8IJ92	Uncharacterized protein	5.90	6.53	1	1	5	6	919	109.2	8.59
Q8IAX8	DNA/RNA-binding protein Alba 1	5.88	4.44	1	1	1	2	248	27.2	10.58
Q8IJC6	60S ribosomal protein L3	5.86	14.77	2	3	4	4	386	44.2	10.20
Q8IKM5	60S ribosomal protein L27	5.86	15.07	1	2	2	2	146	16.7	10.23
Q8IBC1	Uncharacterized protein	5.66	2.73	1	1	3	3	1907	228.7	6.77
Q8IFP1	Pre-mRNA-splicing helicase BRR2	5.64	1.60	1	1	3	4	2874	337.7	5.80
C6KSW6	Leucine-rich repeat protein	5.64	3.17	25	2	5	5	1864	220.2	5.77
Q8IIS9	Polyadenylate-binding protein-interacting protein 1	5.53	3.39	1	1	6	7	3334	381.6	7.05
Q8IIB7	Ethanolamine kinase	5.48	4.73	1	1	1	1	423	49.9	5.81
Q8IIW0	Chromatin remodeling protein	5.40	5.19	1	3	6	7	1426	167.3	6.55
Q8IET9	Uncharacterized protein	5.39	1.17	2	2	3	3	2743	325	8.31
B9ZSJ4	Reticulocyte binding protein homologue 1	5.35	3.97	49	2	12	14	2971	357.4	8.03
Q8IL02	40S ribosomal protein S2	5.34	19.12	1	5	5	5	272	29.9	9.99
Q8IHR6	Coatomer subunit gamma	5.34	3.84	1	2	3	3	1068	124.3	6.86
Q8IIV2	Histone H4	5.34	29.13	2	3	3	3	103	11.4	11.22
Q8IKH2	Transcription factor with AP2 domain(S)	5.32	6.27	1	1	3	3	813	92	8.41
Q8IM66	26S proteasome regulatory subunit RPN6	5.28	4.20	1	1	2	2	666	78.3	6.28
Q8IE06	Uncharacterized protein	5.25	6.79	1	1	6	6	1001	113.5	9.19
Q8IHT5	Transcription factor with AP2 domain(S)	5.24	0.69	1	1	1	2	1604	186	5.27
Q8IE71	Uncharacterized protein	5.21	2.41	1	2	3	4	1661	200.9	9.29
P62344	Calcium-dependent protein kinase 1	5.18	6.11	1	1	2	3	524	60.8	7.58
O97282	T-complex protein 1 subunit epsilon	5.13	8.04	1	1	3	3	535	59.1	5.99
C6KT76	Phosphotransferase	4.83	3.65	1	1	1	1	493	55.2	7.09

Q8IDR3	Myosin-A	4.79	7.95	1	2	3	4	818	92.2	8.16
Q8IKR1	V-type H(+)-translocating pyrophosphatase	4.77	1.53	1	1	1	2	717	76.4	6.54
Q8IJJ2	Conserved Plasmodium protein	4.76	1.93	1	1	2	2	1761	210.2	6.51
Q8I427	Cell differentiation protein	4.75	4.75	1	2	2	2	652	73.4	5.25
C6KT21	Uncharacterized protein	4.68	8.88	1	1	6	6	743	89.4	6.65
O77380	CPSF (Cleavage and polyadenylation specific factor), subunit A	4.64	2.68	1	1	4	4	2870	338.3	7.68
O77393	Uncharacterized protein	4.58	3.96	1	1	7	8	2423	293.5	9.47
Q8I517	Uncharacterized protein	4.58	0.61	1	1	1	1	2309	276.4	8.18
Q8IBF2	EMP1-trafficking protein	4.58	16.49	1	2	4	5	2110	244	6.95
O97298	Uncharacterized protein	4.51	0.94	1	1	3	3	3096	372.5	8.95
Q8I1U7	Structural maintenance of chromosomes protein 3 homolog	4.50	4.95	1	1	4	4	1193	141.1	6.87
O97250	60S ribosomal protein L7	4.45	5.45	33	1	2	3	257	30.5	10.35
Q8IEA1	Uncharacterized protein	4.42	0.96	1	1	3	3	3347	404.7	8.54
O96220	T-complex protein 1 subunit theta	4.42	11.07	1	1	3	3	542	60.9	7.69
O77385	Cdc2-related protein kinase 4	4.37	5.09	1	1	4	4	1553	182.1	8.15
Q8IE79	Vacuolar protein sorting-associated protein 52	4.34	4.21	1	1	3	3	1353	161.9	5.83
Q8IKS1	Uncharacterized protein	4.26	4.46	1	1	2	3	1077	126	6.74
O96124	Erythrocyte membrane protein 3	4.25	19.83	1	1	5	5	2441	273.5	8.85
C6KSY6	60S ribosomal protein L19	4.24	13.19	1	2	3	3	182	21.6	11.31
Q8ILS9	Uncharacterized protein	4.23	4.86	4	1	8	8	3026	357.4	8.91
Q8I5M6	Conserved Plasmodium protein	4.20	1.97	1	1	3	3	2134	256	6.57
Q8IIT6	Dna2/nam7 helicase family member	4.17	2.34	1	1	2	2	1024	120.1	8.22
Q8IB51	60S ribosomal protein L22	4.16	10.07	1	1	1	1	139	16.4	10.15
C6KSK8	Erythrocyte membrane protein 1, PfEMP1	4.13	2.95	1	1	4	4	2879	333.3	6.65
O96258	40S ribosomal protein S26	4.12	19.63	1	2	2	2	107	12.5	10.98
Q8I3U0	Transcription factor with AP2 domain(S)	4.10	3.66	1	1	5	5	2378	276.3	5.78
Q8IAU1	ATP-dependent RNA helicase DBP1	4.10	3.08	1	1	2	2	941	108.6	9.04
O77382	Kinesin-5	4.08	6.24	2	1	7	7	1619	191.7	6.79
C0H4N8	NIMA related kinase 4	4.08	6.77	1	1	2	2	310	36.3	9.26
Q8IC19	Uncharacterized protein PF07_0021	4.06	3.44	1	1	2	2	989	118.3	7.96

Q8I0W8	Deoxyribodipyrimidine photo-lyase	4.03	7.82	1	1	6	6	1113	129.1	9.10
O77372	Uncharacterized protein	3.93	1.67	1	3	8	10	4981	592.9	8.95
C6KSN9	Transcription factor with AP2 domain(S)	3.93	2.48	1	2	3	3	1979	229.5	6.18
Q8I295	4-hydroxy-3-methylbut-2-enyl diphosphate reductase	3.86	1.31	1	1	1	2	535	62.4	9.31
Q8IDK7	Glutamate--tRNA ligase	3.84	3.48	1	1	2	2	863	101.4	8.75
C0H4Y0	Ubiquitin conjugation factor E4 B	3.83	1.21	1	1	1	1	1326	154.5	6.11
Q8IKZ0	Uncharacterized protein	3.83	1.71	1	1	2	2	1641	190.9	5.19
O96185	Uncharacterized protein PFB0460c	3.82	2.33	1	1	3	4	2573	308	6.39
B9ZSI1	Uncharacterized protein	3.82	1.97	1	1	3	5	1823	219.3	8.76
C0H4U1	RNA-binding protein	3.78	3.23	1	1	2	3	1176	140	6.67
O77328	Serine/threonine protein kinase	3.76	1.39	1	1	3	3	1650	193.7	9.09
Q8IFN3	Uncharacterized protein	3.67	9.66	1	2	3	7	476	58.3	9.82
Q8IFN0	Uncharacterized protein PFD1115c	3.67	4.84	1	1	5	6	1612	190.8	7.81
Q8IEU9	Erythrocyte membrane protein 1, PfEMP1	3.64	1.32	1	1	5	5	3346	385.5	5.85
C0H5E3	Uncharacterized protein	3.56	2.55	1	1	3	3	1214	145.5	5.53
Q8ILJ0	Uncharacterized protein	3.50	10.65	1	1	2	2	526	62	8.72
Q8I5V7	Uncharacterized protein	3.47	3.18	1	1	3	3	849	102.9	9.45
Q8ID63	Uncharacterized protein	3.46	0.43	1	1	1	1	3265	386.1	8.56
O77360	ATP-dependent RNA helicase DHX57	3.34	2.82	1	1	4	4	2269	267.1	8.18
C0H4T0	AP-3 complex subunit delta	3.32	2.42	1	1	2	2	1609	193	8.43
Q8I5Y7	High mobility group protein B3	3.32	1.05	1	1	2	2	2284	266.9	6.68
Q8IJ60	Methionine--tRNA ligase	3.29	4.95	1	1	3	3	889	104.1	7.61
C0H5D8	Uncharacterized protein	3.28	2.22	16	1	4	6	2115	252.5	8.35
Q8IK82	Bromodomain protein	3.27	2.19	1	1	1	1	729	85.7	7.17
Q8I3I5	Eukaryotic translation initiation factor 3 subunit E	3.24	3.48	1	1	1	1	517	61.4	7.34
Q8I2G2	Cytoadherence linked asexual protein 9	3.10	5.22	1	1	3	3	1340	160.3	8.78
Q8I5F9	Ubiquitin-activating enzyme E1	3.06	2.19	1	1	1	1	1140	131.7	5.78
C6KTA4	Pyruvate kinase	3.06	4.31	1	1	1	1	511	55.6	7.55
Q8IJZ5	Uncharacterized protein	3.02	3.02	1	1	7	7	3013	357.8	8.85
Q8I542	Calcyclin binding protein	3.01	12.28	1	1	2	2	228	26.6	8.27

Q8ILH5	Uncharacterized protein	3.01	2.70	1	1	2	3	1445	172	6.18
C0H5F0	DNA polymerase theta	3.00	5.79	1	1	3	3	1244	147.3	8.18
Q8ILN8	40S ribosomal protein S25	2.98	11.43	1	1	1	1	105	11.7	10.11
Q8I3T9	60S ribosomal protein L2	2.94	5.00	1	1	1	1	260	28	10.48
Q8ID75	Uncharacterized protein	2.91	1.07	1	1	1	1	1024	124.7	6.18
Q8I3V1	Glideosome-associated protein 40	2.86	2.41	1	1	1	1	456	51.8	7.91
Q8I390	Coatomer subunit beta	2.85	4.06	1	1	2	2	1010	118.2	5.55
C6KT23	60S ribosomal protein L27a	2.82	6.08	1	1	1	1	148	16.7	10.54
Q8IL22	Histidine--tRNA ligase	2.82	5.74	1	1	2	2	1132	133.6	7.74
Q8I2V4	Regulator of chromosome condensation	2.78	3.46	1	1	5	5	3381	395.9	6.89
O77322	Uncharacterized protein	2.77	2.51	1	1	2	2	1711	202	8.12
Q8I404	Uncharacterized protein	2.75	4.09	1	1	1	1	782	94.1	5.49
Q8I2A9	Vacuolar protein sorting-associated protein 51	2.66	3.24	69	1	3	3	1634	197	6.73
Q8IJD0	Merozoite capping protein 1	2.63	3.82	1	1	1	1	393	43.9	9.70
Q8ILQ9	ATP-dependent RNA Helicase	2.58	0.77	1	1	1	1	1041	124.7	9.52
Q8IEM5	mRNA-decapping enzyme 2	2.58	2.81	1	1	2	2	1173	137.4	9.04
Q8IJR6	Autophagy-related protein 18	2.54	2.37	1	1	1	1	380	43.5	9.22
Q8I391	Uncharacterized protein	2.46	3.51	1	1	2	2	1197	139.9	8.72
Q8I406	Phosphatidylinositol 4-kinase	2.46	3.59	1	1	3	3	1559	182.6	5.39
Q8ILP8	Tetratricopeptide repeat family protein	2.45	4.58	1	1	2	3	1245	147.9	6.99
Q8IJI1	Conserved Plasmodium membrane protein	2.43	5.23	1	1	1	2	325	37.1	6.29
C0H4F4	Uncharacterized protein	2.38	5.79	1	1	1	1	328	39.8	9.26
Q8IB79	Uncharacterized protein	2.34	1.88	1	1	1	1	373	45.1	5.77
Q8I3W4	Aspartate--tRNA ligase	2.30	1.68	1	1	1	1	1128	134.7	8.88
Q8I3B0	60S ribosomal protein L32	2.27	9.16	1	1	1	1	131	15.5	11.06
Q8I1X1	Lysine decarboxylase	2.27	2.73	1	1	3	3	2415	280.6	6.64
Q8IIL3	Uncharacterized protein	2.26	4.60	1	1	8	10	2480	295.2	7.99
Q8II57	Structural maintenance of chromosome protein	2.26	1.65	16	1	3	4	1818	214.5	7.46
C0H4Y1	Uncharacterized protein	2.22	3.19	1	1	2	2	752	88.4	9.74
Q8IDM0	Uncharacterized protein	2.21	2.49	1	1	2	4	1847	221.4	8.34

Q9U0N4	Multidrug resistance-associated protein 1	2.21	1.48	1	1	1	1	1822	214.3	8.73
C0H5H4	Uncharacterized protein	2.16	5.77	1	1	4	6	1474	174.4	5.78
Q8IAX5	40S ribosomal protein S16	2.12	22.92	1	1	2	2	144	16.3	10.24
Q8IKB6	Histone deacetylase	2.11	0.89	1	1	1	1	2251	268.8	8.98
Q8IE74	Uncharacterized protein	2.08	0.92	1	1	4	4	5415	658.6	9.32
Q8IHP3	MAEBL	2.06	2.09	1	1	2	3	2055	243.1	8.85
Q8IFL8	Uncharacterized protein	2.04	2.23	1	1	1	1	314	36.7	6.19
C0H491	Uncharacterized protein	2.03	3.49	18	1	7	8	3211	383.6	8.51
Q8IEA7	Uncharacterized protein	1.95	3.33	1	1	3	3	1442	170.6	8.78
O77395	40S ribosomal protein S15A	1.89	6.15	1	1	1	1	130	14.9	9.99
Q8I2U0	Uncharacterized protein	1.89	1.23	1	1	1	1	486	58.7	8.22
Q8IB82	Uncharacterized protein	1.77	2.59	3	1	3	3	1276	154.8	9.06
Q8IE17	Protein kinase	1.76	3.23	1	1	2	3	557	66.8	8.47
Q8IM10	40S ribosomal protein S8	1.75	5.05	1	1	1	1	218	25	9.98
Q8IAY6	Superoxide dismutase [Fe]	1.75	3.03	1	1	1	1	198	22.7	6.79
Q8IBU8	Uncharacterized protein	1.73	1.13	1	1	2	3	2206	258.2	6.51
C0H4X6	Lipase maturation factor	1.69	17.46	1	1	4	6	590	71.2	8.43
Q8I3X9	Uncharacterized protein	1.67	2.80	1	1	2	2	1644	198.6	9.51
C6KSV0	Histone H3	1.65	11.76	8	2	2	2	136	15.4	11.14
Q8ILM9	Uncharacterized protein	1.62	2.09	74	1	4	4	1630	195.2	8.16
Q8I480	RING finger protein PFE0100w	0	1.97	1	1	1	1	1272	151.5	9.00
Q8IHP1	Serine/threonine protein kinase	0	3.36	1	1	4	4	1429	170.6	8.92
Q8ILZ2	Uncharacterized protein	0	1.63	1	1	6	6	4405	526.4	8.90
Q8IM30	PPR repeat protein	0	1.32	1	1	1	1	608	71.5	8.53
Q8IIV1	Histone H2B	0	35.90	2	1	3	3	117	13.1	10.26
Q8I505	Conserved Plasmodium protein	0	3.78	69	1	2	2	450	54.8	8.05
Q8II53	Serpentine receptor	0	3.49	1	1	1	1	773	94.4	7.94
Q8I501	Rab specific GDP dissociation inhibitor	0	13.07	1	1	2	2	459	52.3	7.01
Q8IIU8	40S ribosomal protein S4	0	4.60	1	1	1	1	261	29.8	10.08
Q8IL48	tRNA binding protein	0	18.41	1	1	2	2	402	46.4	7.27

C6KTD8	DNA polymerase epsilon catalytic subunit A	0	0.65	1	1	1	1	2907	344.4	8.37
C0H536	Uncharacterized protein	0	1.54	1	1	1	1	1166	138.2	8.92
Q8I495	Erythrocyte membrane protein 1, PfEMP1	0	4.76	1	1	2	2	2207	251.3	5.31
Q8I2P1	Uncharacterized protein	0	0.98	1	1	1	1	1225	144.9	8.34
Q8I3B7	Protein RER1	0	12.94	1	1	1	1	201	24.2	9.17
C0H4P2	Uncharacterized protein	0	1.86	1	1	4	5	3489	420.4	8.54
C6KT12	AP-2 complex subunit alpha	0	4.61	1	1	3	6	1236	145.3	8.65
C6KTC6	Nicotinate phosphoribosyltransferase	0	4.66	1	1	1	1	665	77.1	7.64
Q8ID65	Uncharacterized protein	0	2.59	1	1	2	2	1813	207.2	8.90
O97333	Uncharacterized protein	0	1.26	1	1	1	1	398	48	9.07
O77308	ABC transporter B family member 4	0	1.17	1	1	1	1	1365	161.1	9.42
Q8IAX1	Uncharacterized protein	0	1.36	1	1	1	1	515	61.5	8.53
Q8IEJ4	Uncharacterized protein	0	3.39	1	1	4	4	2361	277.5	7.80

Accession: UniProtKB protein accession number.

Description: UniProtKB protein name.

Score: Sum of the scores of the individual peptides, which are based on the number of fragment ions that are common to two different peptides with the same precursor mass and its correlation with a default threshold score.

Coverage: Percentage of amino acids found in the analyzed peptides compared to the total number of amino acids in the entire sequence of the protein.

Proteins: The number of identified proteins in a protein group (all proteins that are identified by the same set of peptides).

Unique peptides: The number of peptide sequences unique to a protein group.

Peptides: The number of distinct peptide sequences in the protein group.

PSMs: The total number of identified peptide sequences for the protein.

AAs: The total number of amino acids of the entire sequence of the protein.

MW [kDa]: The molecular weight of the protein calculated as the sum of the molecular weight of each amino acid without considering posttranslational modifications.

pI: The isoelectric point of the protein.

Paper 2

Letter of acceptance in BMC Biology

BMCB-D-21-01108R3

The protein aggregation inhibitor YAT2150 has potent antimalarial activity in Plasmodium falciparum in vitro cultures.

Inés Bouzón-Arnáiz; Yunuen Avalos-Padilla; Arnau Biosca; Omar Caño-Prades; Lucía Román-Álamo; Javier Valle; David Andreu; Diana Moita; Miguel Prudêncio; Elsa M. Arce; Diego Muñoz-Torrero; Xavier Fernàndez-Busquets

Dear Dr. Fernàndez-Busquets,

Many thanks for submitting your revised manuscript, which we are now very happy to accept for publication in BMC Biology. Your manuscript files have now been passed to our Production team, who will prepare the article for publication. They will be in touch regarding the next steps, including the article proofs. I have asked our Production team to additionally contact you to set a publication date for the manuscript.

If your press office has plans for media promotion around this article please let us know at press@biomedcentral.com.

We are glad for the opportunity to publish your paper, and hope to work together again in the future.

Please do not hesitate to let us know if you have any questions.

Kind regards,

Vitor

Vitor Sousa, PhD
Senior Editor, BMC Biology
https://bmcbiol.biomedcentral.com/

Title

The protein aggregation inhibitor YAT2150 has potent antimalarial activity in *Plasmodium falciparum in vitro* cultures.

Short title

Protein aggregation as an antimalarial target.

Author list

Inés Bouzón-Arnáiz,[1,2,3] Yunuen Avalos-Padilla,[1,2,3] Arnau Biosca,[1,2,3] Omar Caño-Prades,[1,2,3] Lucía Román-Álamo,[1,2,3] Javier Valle,[4] David Andreu,[4] Diana Moita,[5] Miguel Prudêncio,[5] Elsa M. Arce,[6] Diego Muñoz-Torrero,[6] Xavier Fernàndez-Busquets,[1,2,3]*

Affiliations

[1]Barcelona Institute for Global Health (ISGlobal, Hospital Clínic-University of Barcelona), Rosselló 149-153, 08036 Barcelona, Spain.

[2]Nanomalaria Group, Institute for Bioengineering of Catalonia (IBEC), The Barcelona Institute of Science and Technology, Baldiri Reixac 10-12, 08028 Barcelona, Spain.

[3]Nanoscience and Nanotechnology Institute (IN2UB), University of Barcelona, Martí i Franquès 1, 08028 Barcelona, Spain.

[4]Department of Experimental and Health Sciences, Pompeu Fabra University, Barcelona Biomedical Research Park, Dr. Aiguader 88, 08003 Barcelona, Spain.

[5]Instituto de Medicina Molecular, Fac. Medicina Univ. Lisboa, Av. Prof. Egas Moniz, 1649-028 Lisboa, Portugal.

[6]Laboratory of Medicinal Chemistry (CSIC Associated Unit), Faculty of Pharmacy and Food Sciences, and Institute of Biomedicine (IBUB), University of Barcelona, Av. Joan XXIII, 27-31, 08028 Barcelona, Spain.

*Corresponding author. Email: xfernandez_busquets@ub.edu

Abstract

Background: By 2016, signs of emergence of *Plasmodium falciparum* resistance to artemisinin and partner drugs was detected in the Greater Mekong Subregion. Recently, the independent evolution of artemisinin resistance has also been reported in Africa and South America. This alarming scenario calls for the urgent development of new antimalarials with novel modes of action. We investigated the interference with protein aggregation, which is potentially toxic for the cell and occurs abundantly in all *Plasmodium* stages, as a hitherto unexplored drug target in the pathogen.

Results: Attempts to exacerbate the *P. falciparum* proteome's propensity to aggregation by delivering endogenous aggregative peptides to *in vitro* cultures of this parasite did not significantly affect their growth. In contrast, protein aggregation inhibitors clearly reduced the pathogen's viability. One such compound, the bis(styrylpyridinium) salt YAT2150, exhibited potent antiplasmodial activity with an *in vitro* IC_{50} of 90 nM for chloroquine- and artemisinin-resistant lines, arresting asexual blood parasites at the trophozoite stage, as well as interfering with the development of both sexual and hepatic forms of *Plasmodium*. At its IC_{50}, this compound is a powerful inhibitor of the aggregation of the model amyloid β peptide fragment 40, and it reduces the amount of aggregated proteins in *P. falciparum* cultures, suggesting that the underlying antimalarial mechanism consists in a generalized impairment of proteostasis in the pathogen. YAT2150 has an easy, rapid, and inexpensive synthesis, and, because it

fluoresces when it accumulates in its main localization in the *Plasmodium* cytosol, it is a theranostic agent.

Conclusions: Inhibiting protein aggregation in *Plasmodium* significantly reduces the parasite's viability *in vitro*. Since YAT2150 belongs to a novel structural class of antiplasmodials with a mode of action that potentially targets multiple gene products, rapid evolution of resistance to this drug is unlikely to occur, making it a promising compound for the post-artemisinin era.

Keywords: *Plasmodium falciparum*, protein aggregation, YAT2150, amyloid pan-inhibitors, malaria, antimalarial drugs

Background

The available arsenal of antimalarial drugs is insufficient to progress towards eradication of the disease, a scenario that is worsened by the rampant evolution of resistance by *Plasmodium*. This situation calls for immediate efforts to discover new antimalarials of easy and cost-affordable production, having several molecular targets in the pathogen and acting through new antiparasitic mechanisms not shared by currently used drugs.

The deadliest species of the malaria parasite, *Plasmodium falciparum*, is exceptionally rich in proteins containing long glutamine/asparagine (Q/N) repeats [1], which are low complexity regions with a propensity to form insoluble intracellular aggregates [2]. It has been recently reported that protein aggregation occurs abundantly in all *Plasmodium* stages in both vertebrate and mosquito hosts [3]. Because the presence of protein deposits (either amorphous aggregates, large amyloid fibrils or small soluble oligomers with little or no fibrillar content) within a cell is generally associated with cellular stress and toxicity [4], this distinctive phenotype of malaria

parasites could potentially be harnessed to develop new therapeutic strategies based on the perturbation of the pathogen's proteostasis. Protein aggregates expose hydrophobic residues and unpaired polypeptide backbone structures that interact promiscuously with other molecules and critical factors of the proteostasis network [5]. Moreover, large intracellular deposits can displace membrane structures and may cause their breakdown [6]. As a result, protein aggregation is usually considered toxic for the organism undergoing it. Indeed, proteinaceous assemblies such as amyloids and prions were initially discovered in neurodegenerative diseases and were quickly attributed to an anomalous state of otherwise properly folded proteins. Many pathologies are related to a defect in protein folding and the ensuing aggregation of partially folded intermediates, including Alzheimer's [7], Parkinson's [8] and Huntington's disease [9], amyotrophic lateral sclerosis [10], transmissible spongiform encephalopathies like Creutzfeldt-Jakob disease [11] and scrapies [12], and spinocerebellar ataxia [13]. The cytotoxicity of protein aggregation has also been identified at the root of the evolutionary tree, and bacterial susceptibility to protein misfolding has been proposed as the target of future antibiotics [14].

However, a deeper study of the aggregation process of many amyloids and prion-like proteins has shown that, in some cases, protein aggregation is not associated with a toxic process. Examples of functional amyloids can be found in prokaryotes, where they can be involved in virulence, extracellular matrix assembly and biofilm formation [15]. In higher organisms, functional amyloids are present in the eggshell of some insects and fish [16,17] and as a component of silk [18]. In humans, amyloids participate in the storage of peptide hormones [19] and melanin polymerization [20], and have also been proposed to play a role in long-term memory potentiation [21]. Functional roles in

malaria parasites for Q/N repeats have been suggested as tRNA sponges [22] and in immune evasion and antigenic variation [23].

Intriguingly, some commonly used antimalarial drugs have been reported to affect protein aggregation. For instance, artemisinin resistance is associated with an increased expression of genes involved in the unfolded protein response [24], in agreement with the hypothesis that artemisinin's antimalarial activity damages proteins and inhibits the proteasome [25]. Inhibition of the *P. falciparum* proteasome has been shown to have potent gametocytocidal activity [26,27], suggesting that impairing protein disposal is deleterious for the parasite as a result of the potential toxicity of an increase in unfolded, aggregation-prone proteins. On the other hand, a significant antimalarial drug-based body of evidence hints at the striking possibility that protein aggregation might be functional for malaria parasites. Oligomerization of the amyloid β (Aβ) peptide is inhibited by methylene blue and curcumin [28,29], and the latter compound also prevented amyloid fibril formation, while another antimalarial, quercetin, showed potent anti-Aβ peptide aggregation activity [30]. A number of quinoline antimalarials (e.g. quinine, chloroquine, amodiaquine, quinacrine, mefloquine and primaquine) have been reported to inhibit scrapie-associated prion protein accumulation both *in vitro* [31] and inside cells [32-37]. Quinacrine directly dissociated amyloid plaques in the brain of a 5XFAD transgenic mouse model of Alzheimer's disease [38]. Certain 4-aminoquinoline-based heterodimeric compounds with antiplasmodial activity in the μM range [39] are strong amyloid pan-inhibitors [40]. Rapamycin, recently shown to reduce the *in vitro* growth of *P. falciparum* with a half maximal inhibitory concentration (IC_{50}) around 2 μM [41], was previously described to decrease protein aggregation *in vivo* by stimulating autophagy [42] and through protein synthesis inhibition [43,44]. Also, part of the alleged antimalarial properties of green tea have been tracked down to the

flavonoid epigallocatechin-3-gallate [45], which disaggregates the amyloid fibrils formed by the intrinsically unstructured merozoite surface protein 2 [46], a component of the coat present on the *P. falciparum* stage that invades a naïve red blood cell (RBC).

Given this proliferation of results pointing at both stimulation and inhibition of protein aggregation being deleterious for malaria parasites, we have explored here both hypotheses.

Results

Effect of endogenous aggregative peptides on *P. falciparum* cultures

Previous studies have established that seeding exacerbates protein aggregation reactions [47], and that homologous seeding is much more efficient than heterologous seeding [48]. Considering the potential cellular toxicity of protein aggregation, we set out to test the hypothesis that endogenous *Plasmodium* peptides with high aggregative capacity could behave as nucleating agents and further increase the already high protein aggregation inside the parasite, which might compromise its viability. In our previous work, 0.1% sodium dodecyl sulfate (SDS)-resistant protein aggregates obtained from late stage *P. falciparum*-parasitized RBC (pRBC) culture homogenates had been analyzed by liquid chromatography with tandem mass spectrometry (LC-MS/MS) [3]. From the pool of 369 proteins identified, 10 peptides with high aggregation propensity were selected (Additional file 1: Table S1). When incorporated to *in vitro* pRBC cultures none of the peptides had a significant effect on parasite growth up to concentrations ≥125 μM.

To improve the likely poor entry of aggregative peptides into pRBCs, the 6 sequences from Additional file 1: Table S1 that exhibited the highest tendency to form

amyloid fibrils *in vitro* according to thioflavin T (ThT) fluorescence and transmission electron microscopy (TEM) imaging ([3] and Additional file 1: Fig. S1) were elongated at their N-terminus by the cell-penetrating peptides (CPPs) TP2 (PLIYLRLLRGQF), LMWP (VSRRRRRRGGRRRR), and TAT (GRKKRRQRRRPQ). The peptides were also labeled with fluorescein to allow their detection inside target cells. According to preliminary flow cytometry data, the CPPs by themselves did not show a significant entry into non-infected RBCs (Additional file 1: Figs. S2-S4), despite all three peptides having been described to enter cells by non-endocytic mechanisms [49-51], although intake increased between 3- and 6-fold for pRBCs. Aggregative peptides conjugated to TAT resulted in a cell entry into pRBCs generally lower than for TAT alone, whereas conjugation to LMWP and TP2 increased in most cases the intake by pRBCs. Penetration into non-parasitized erythrocytes remained roughly constant for LMWP- and TAT-elongated peptides but decreased for TP2-conjugated peptides relative to free TP2. The best results were obtained using TP2, with TP2-LQSNIG entering 17% of pRBCs. Peptide intake was mainly in late erythrocytic *Plasmodium* stages, in agreement with the observed lack of penetration into naïve RBCs. Late forms are known to have an increased permeability to extracellular components [52], suggesting that it was this characteristic, rather than CPP activity, the main drive to make CPP-aggregative peptides enter pRBCs.

Conjugation of self-aggregative peptides to fluorescein-labeled CPPs had different effects on their *in vitro* aggregation capacity (Fig. 1A), which generally decreased but remained relevant in most cases. Conjugation to TAT resulted in the most significant drop in aggregation, with only TAT-LISFIL and TAT-LYWIYY retaining >30% of their self-aggregative potential. On the other hand, LMWP was the least intrusive CPP in this regard, whereby only LMWP-LISFIL showed a clear drop of ca. 50%

aggregation relative to CPP-free LISFIL. Conjugation to TP2 offered the most disperse results, with some peptides like TP2-NVNIYN and TP2-LISFIL losing most of their aggregative capacity and others such as TP2-LYWIYY clearly increasing it. When incorporated to *in vitro P. falciparum* growth inhibition assays, CPP-conjugated aggregative peptides did not have a significant impact on the viability of the parasite unless very high amounts were used (Additional file 1: Table S2). Peptide concentrations up to 200 μM resulted in parasitemias similar to those of untreated controls, the best result being obtained with some LMWP-elongated peptides, which at 20 μM induced a modest growth inhibition around 10%.

To further increase the presence inside pRBCs of endogenous *P. falciparum* aggregative peptides, a previously described protocol for the transfection of ghost RBCs [53] was adapted to preload these with peptides prior to *Plasmodium* infection (Fig. 1B). In our *in vitro P. falciparum* culture conditions, ghosts were successfully invaded by the parasite, which could grow inside them at a rate undistinguishable from assays where intact RBCs were used as host cells (Additional file 1: Fig. S5). Aggregative peptides conjugated to fluorescein-labeled CPPs exhibited in general a better intake by ghost RBC suspensions relative to regular RBCs (Fig. 1C), except for some TP2-conjugated peptides, whose entry into ghosts remained low. These peptide-loaded RBCs could be infected by *P. falciparum*, being the proportion of peptide-containing pRBCs significantly larger in ghost-enriched cultures, especially for TAT- and LMWP-conjugated peptides (Fig. 1D). Overall, using ghosts as host cells resulted in between 5 to 20% of *Plasmodium*-infected cells containing exogenously added peptides as determined by flow cytometry analysis, which was deemed sufficient to assess the effect on parasite growth of peptide-treated samples relative to untreated controls.

When incorporated at 10 µM into ghost RBC preparations to be used for *in vitro P. falciparum* growth inhibition assays, LMWP-conjugated aggregative peptides had the largest impact on the viability of the parasite (Table 1). This result was consistent with the observations that LMWP had a good entrance in ghosts (Fig. 1C) and that it was the least disruptive CPP for the aggregation of *Plasmodium* peptides (Fig. 1A). LMWP-NFNNIYH was the most active peptide, reducing *Plasmodium* growth to ca. 66% that of the untreated control. Among the other CPP-conjugated peptides, only TP2-LYWIYY had a significant effect leading to a ca. 85% parasite growth relative to the control. Remarkably, some CPP-free and fluorescein-free aggregative peptides did also decrease parasite viability in ghost-pRBC cultures, such as GLVFFI and YLFFIS, which resulted in 79.4 ± 0.9% and 77.5 ± 12.3% growth, respectively (Additional file 1: Table S3). These two peptides had a relatively low cytotoxicity in human umbilical vein endothelial cells cultures (Additional file 1: Table S4), suggesting that their effect on *P. falciparum* might represent a genuine antiplasmodial activity.

As mentioned above, the 10 peptides chosen for this proof-of-concept study of the potential toxicity of endogenous protein aggregation for *Plasmodium* were selected from late-stage cultures. This form of the pathogen has grown to completely fill the host RBC cytosol, and therefore contains the highest amount of parasite protein of all the blood stages, which did facilitate the identification of a larger number of potentially active aggregative peptides. However, this strategy might target proteins that are expressed late in the intraerythrocytic cycle, and therefore the induction of aggregation could occur when the parasite is about to egress its host cell, minimizing the potential antiplasmodial effect of uncontrolled protein aggregation. To identify aggregative peptides in proteins expressed early in the blood cycle, we isolated protein aggregates from early-stage pRBC culture homogenates resisting dissolution in the presence of

0.1% SDS. LC-MS/MS analysis of this sample resulted in the identification of 33 *Plasmodium* proteins (Additional file 1: Table S5), of which 23 were also present in the pool of 369 proteins isolated from late blood stages [3]. These 23 proteins were not highly aggregative, but they were relatively abundant in the parasite (Additional file 1: Fig. S6). Of the 23 proteins analyzed for their abundance and aggregation propensity, the most aggregation-prone was E3 ubiquitin-protein ligase (Uniprot ID: C0H4K6). When this large protein (3893 amino acids) was run through the WALTZ algorithm [54], which identifies amyloid-forming amino acid sequences, 46 peptides with high aggregation propensity were identified (Additional file 1: Table S6). Two of these, KDLLF and KVVNI (WALTZ aggregation scores 96.32 and 96.99, respectively), formed amorphous aggregates *in vitro* (Additional file 1: Fig. S7) and were present in 10 and 9 *P. falciparum* proteins, respectively (Additional file 1: Table S7). Because aggregation-prone regions can promote the aggregation of the proteins containing them [55], peptides present in early blood stages and in a large number of *Plasmodium* proteins are likely to stimulate protein aggregation for a longer time and over a wider fraction of the proteome. Regular RBCs were essentially impermeable to fluorescein-labeled KDLLF and KVVNI, which however were found in a significant fraction of ghost RBCs in non-parasitized and, especially, in *P. falciparum*-parasitized cultures (Fig. 2). In ghost pRBCs, these exogenously added fluorescein-labeled peptides localized inside the parasitophorous vacuole, and not in the RBC cytosol (Additional file 1: Fig. S8). Within the vacuole, the peptides distributed in both the parasite's cytosol and in the digestive vacuole, according to confocal fluorescence microscopy colocalization data with markers of these two cellular compartments. However, in *in vitro* growth inhibition assays done in peptide-containing ghost pRBC preparations,

parasite viability was not significantly impaired by either peptide up to a concentration of 10 µM (Additional file 1: Table S8).

Effect of amyloid pan-inhibitors on *P. falciparum* cultures

The failure to clearly reduce *Plasmodium* viability through exposure of the parasite to low concentrations of a few selected endogenous self-aggregating peptides does not exclude the possibility that a deleterious effect on the parasite could be eventually achieved through stimulation of uncontrolled protein aggregation. Although we assume that the cytosolic localization described above can be extrapolated to most aggregative peptides delivered to *Plasmodium*, a fraction of them likely end up in other cellular subcompartments such as the digestive vacuole, thus reducing their effective cytosolic concentration and their potential stimulatory effect of protein aggregation. At this point, we decided to explore in parallel the alternative hypothesis that protein aggregation might have a functional role for *Plasmodium*. With that aim, we characterized in *P. falciparum in vitro* cultures the effect of a recently described family of β-sheet blockers that behaved as protein aggregation pan-inhibitors [40]. Interestingly, some of these compounds are 4-aminoquinolines, a chemical family that includes well-known antimalarial drugs like amodiaquine and chloroquine. Indeed, some of these 4-aminoquinoline derivatives had been described to possess antimalarial activity [39]. As controls we included other known β-sheet intercalators such as ThT, Congo Red, and YAT2150 [56], the active component of the commercial protein aggregation detection reagent ProteoStat® (Fig. 3).

The results obtained indicated that, *in vitro*, YAT2150 had a potent antiplasmodial activity with an IC_{50} of 90 ± 2 nM, comparable and even superior to that of most

aminoquinoline amyloid pan-inhibitors previously described (Table 2). This compound, a bis(styrylpyridinium) salt, belongs to a chemical family where no antimalarial drugs have been described so far, which motivated us to characterize its activity in deeper detail. YAT2150 was also strongly active against the chloroquine-resistant W2 strain (IC_{50} of 90 ± 1 nM), and several artemisinin-resistant strains (Fig. 4) with IC_{50} values ranging from 90 to 160 nM. When added to ring stages at its IC_{80}, YAT2150 arrested the life cycle of the pathogen at trophozoite stage (Fig. 5), whereas when the drug was delivered to cultures containing late *Plasmodium* forms, the parasites were able to complete their intraerythrocytic maturation and egress the pRBC, although their growth inside the new invaded RBCs became arrested at early trophozoite stage. In human umbilical vein endothelial cell cultures, the YAT2150 concentration required for the reduction of cell viability by 50% (CC_{50}) was determined to be 3.4 µM (Additional file 1: Table S9), which resulted in a selectivity index (CC_{50}/IC_{50}) of 37.8. *In vivo*, YAT2150 started inducing adverse effects in female and male mice at 10 and 17 mg/kg respectively.

Upon binding protein aggregates (e.g. those formed by the model amyloidogenic peptide Aβ fragment 1-40, Aβ40), YAT2150 is a fluorescent molecule with respective absorbance and emission maxima at 500 and 610 nm (Fig. 6A). The fluorescence properties of YAT2150 allowed for a straightforward flow cytometry analysis of its targeting to erythrocytes (Fig. 6B), which revealed a remarkable specific targeting to pRBCs vs. non-parasitized RBCs in all blood stages, although in a significant proportion of early ring forms the fluorescent signal was below the set cytometer threshold. Confocal fluorescence microscopy imaging confirmed the presence of YAT2150 staining in all blood stages of *P. falciparum in vitro* cultures (Fig. 6C). pRBC fluorescence increased along the intraerythrocytic cycle of the parasite, with individual

merozoites being strongly stained. The subcellular location of the signal was always observed inside the parasitophorous vacuole and not in the RBC cytosol. Confocal fluorescence microscopy colocalization analysis (Fig. 7A) and correlative light and electron microscopy data (Fig. 7B) confirmed the presence of YAT2150 mainly in the parasite's cytosol, particularly in association with endoplasmic reticulum regions.

Effect of YAT2150 on protein aggregation

According to *in vitro* ThT fluorescence assays, 0.1 µM YAT2150 is a strong inhibitor of the aggregation of Aβ40, and even at 10 nM, well below its IC_{50} in *P. falciparum* cultures, YAT2150 prevented Aβ40 fibrillogenesis to a large extent (Fig. 8A). This is in agreement with the hypothesis that inhibition of protein aggregation might be the main mechanism responsible for the antimalarial activity of this compound. To discard the possibility that the decrease in ThT fluorescence observed in Aβ40 aggregation assays resulted from a steric hindrance imposed to ThT binding of amyloid fibrils by the presence of YAT2150, we used TEM to examine Aβ40 samples treated with YAT2150 (Fig. 8B). TEM images showed that the amyloid fibril aggregates of YAT2150-containing samples were smaller and more fragmented than those present in control untreated Aβ40, supporting the role of this compound as an amyloid aggregation inhibitor. YAT2150 at concentrations >90 nM was also found to disassemble preformed Aβ40 fibrils (Additional file 1: Fig. S9). Both *in vitro* aggregation inhibition and disaggregation assays show the presence of characteristic amorphous aggregates at 0.1 µM YAT2150, which might represent an intermediate species between mature Aβ40 fibrils and the disassembled protofibrillar structures found at higher drug concentrations. These aggregation inhibition and disaggregation activities were also

observed with the six aggregative peptides from Fig. 1 present in *P. falciparum* proteins (Additional file 1: Fig. S10).

Once confirmed the *in vitro* activity of YAT2150 as inhibitor of the aggregation of a model amyloidogenic peptide like Aβ40 and of aggregative peptides present in *P. falciparum* proteins, we investigated if this effect could also be occurring in live parasites. To explore if there was a correlation between the observed *in vitro* antimalarial activity of YAT2150 and a disruption of protein homeostasis in the treated parasites, we performed Western blots and dot blot assays using protein extracts of YAT2150-treated *P. falciparum* cultures where the presence of ubiquitinated proteins and amyloid fibrils was examined (Fig. 9). Under physiological conditions, the predominant route for misfolded and aggregated protein clearance involves ubiquitination and proteasome-mediated degradation [57]. At the concentration of 90 nM, its IC_{50} *in vitro*, YAT2150 treatment of *P. falciparum* cultures led to a reduction along time in the fraction of ubiquitinated proteins above 250-kDa (Fig. 9A), which is enriched in protein aggregates, in agreement with an inhibitory effect on protein aggregation.

To directly probe the level of protein aggregation in live *Plasmodium* cells following YAT2150 treatment, we developed a ThT-based method to measure protein aggregation in parasite cultures. ThT fluorescence of culture extracts, normalized to have equal protein content, exhibited a reduced emission spectrum in samples that had been treated for only 90 min with 90 nM YAT2150, the compound's *in vitro* IC_{50} (Fig. 9C). After 4 h of treatment, the decrease in ThT fluorescence was more evident, even for cultures treated with the IC_{10} of YAT2150 (27 nM). This reduced signal could still be clearly detected after 30 h of 90 nM treatment (Additional file 1: Fig. S11). These results indicating a relevant decrease in aggregated protein load in live parasites following

YAT2150 treatment at physiologically relevant concentrations are supportive of a mode of action of this drug consisting on the inhibition of protein aggregation in the pathogen.

According to dot blots using an amyloid structure-specific antibody, exposure of parasites for 90 min to >3 μM YAT2150 inhibited amyloid fibril formation (Fig. 9E), but resulted in a concomitant increase in ubiquitinated proteins (Fig. 9D). These results suggested a causal effect between decreasing protein aggregation and a deleterious effect on the parasite ultimately leading to a rapid generalized deregulation of proteostasis.

Artemisinin, one of the most potent antimalarials in use, has been described to cause protein damage/unfolding and to inhibit folding of newly synthesized proteins, likely inducing protein aggregation [25]. When *P. falciparum* cultures were treated with artemisinin and YAT2150 combined at different ratios, the resulting fractional inhibitory concentration values were always higher than 1.5 (Fig. 9F), which indicated an antagonistic action of both drugs [58]. Thus, parasite viability was higher than expected for drug synergism, supporting the hypothesis that YAT2150 has protein aggregation inhibitory activity that antagonizes the antimalarial effect of artemisinin, and vice versa. In Fig. 4 we tested the effect of YAT2150 in 3D7 *P. falciparum* parasites harboring the K13 mutations associated to artemisinin resistance M579I and R561H [59], and in the multiresistant Cam 3.II strain, which, besides being resistant to chloroquine and sulfadoxine/pyrimethamine, it had been modified to carry the K13 mutations R561H and R539T [59]. The results did not show a significant IC_{50} increase relative to the corresponding parental strains except for M579I (*p* value of 0.02; all other *p* values > 0.15), in agreement with a mode of action for YAT2150 different from that of artemisinin.

YAT2150 did not block the formation of hemozoin (Additional file 1: Fig. S12), thus confirming that its antimalarial mechanism is different from that of the widely used quinoline drugs like chloroquine. This result is in agreement with the calculated IC_{50} of YAT2150 in the chloroquine-resistant *P. falciparum* W2 strain (Fig. 4A), undistinguishable from its activity in the chloroquine-sensitive 3D7 strain.

Activity of YAT2150 on *Plasmodium* gametocytes and liver stages

The recent appreciation that efficient antimalarial strategies will require the interruption of parasite transmission from the human host to the vector [60] has prompted the search for transmission-blocking drugs [61]. Targeting gametocytes, the sole stage of malaria parasites present in the blood circulation capable of transmitting the infection to the mosquito vector following their ingestion by a blood-feeding *Anopheles* female, can ease exposure of the pathogen to drugs and reduce the likelihood of the emergence of resistance [62]. However, although eliminating gametocytes is one of the main approaches being explored to disrupt the life cycle of *Plasmodium*, drugs active at this critical step are scarce [63]. YAT2150 efficiently blocked the development of *P. falciparum* early and mature stage V gametocytes *in vitro* with respective IC_{50} of 95 ± 3 nM and 103 ± 3 nM (Fig. 10A), close to that obtained for the asexual blood stages. For the amyloid pan-inhibitor aminoquinoline DONE3TCl the IC_{50} values on early and late gametocytes were 285 ± 56 nM and 78 ± 12 nM, respectively.

Finally, targeting the liver stage of malaria parasites is a key therapeutic and prophylactic antimalarial strategy because its blockade would impair the subsequent RBC invasion, thus preventing progression to symptomatic disease. Therefore, we assessed the *in vitro* activity of YAT2150 against hepatic infection by *Plasmodium.* To

this end, we employed a well-established infection platform based on the use of luciferase-expressing rodent malaria *Plasmodium berghei* parasites and the human hepatoma cell line Huh7. Our results showed that YAT2150 significantly inhibited the infection of hepatic cells by *P. berghei*, with an estimated IC_{50} of 0.78 µM (Fig. 10B). DONE3TCl, used as a control in this experiment, revealed only very modest activity at 1.5 µM and was toxic against the Huh7 host cells at concentrations ≥2 µM (Fig. 10B), confirming the specificity of YAT2150's hepatic stage antiplasmodial activity.

Discussion

Perhaps the main threat to malaria elimination and its eventual eradication is the evolution by the parasite of resistance to every drug deployed against it [64]. Drug resistance arises with the spontaneous emergence of mutations or gene duplications conferring reduced drug susceptibility, which are then selected by the presence of low local drug concentrations insufficient to suppress the growth of resistant clones. Although novel regimens and strategies for the better use of existing antimalarial drugs are required, the deployment of novel compounds is an urgent need, given the paucity of their appearance in the clinical arena. Among the most desirable properties of future antimalarials in order to minimize the risk of resistance evolution are (i) a low IC_{50} to allow for the safe administration of lethal doses to the parasite, (ii) classification into a chemical group where no antimalarials have been described so far to minimize the risk of adaptation of existing resistance mechanisms, and (iii) a target present in several stages of the pathogen and which is not a single-gene product to reduce the chances that resistance can appear rapidly.

The potential toxicity for the cell of protein aggregates, the high amount of aggregation-prone proteins in *Plasmodium*, and the specificity of seeding in protein

aggregation reactions, suggested that, *a priori*, the specific exacerbation of the propensity of the parasite's proteome to aggregate could be exploited for therapeutic purposes. However, aggregative peptides present in *P. falciparum* proteins were not observed to have significant toxicity for the parasite when exogenously incorporated to *in vitro* cultures at clinically relevant concentrations. This result indicates that the targeting of a few gene products where the peptides are present does not suffice to significantly impair *Plasmodium* viability, although an effective prevention of aggregation by the parasite chaperones cannot be ruled out. Actually, the cytoplasmic *P. falciparum* heat shock protein 110 (PfHsp110c) has been proved to be 15 to 30 times better than its yeast or human orthologs at preventing aggregation of Q/N repeat-enriched proteins in mammalian cells [65]. However, disruption in *P. falciparum* of the ubiquitin-dependent protein disposal pathway through inhibition of ubiquitin E3 ligase has been proposed as an antimalarial strategy [66]. The same enzyme has been identified here as a protein with a high propensity to aggregate and therefore a potential target for antiplasmodial approaches based on overloading the parasite's proteasome. Further research is required to explore this possibility in deeper detail.

On the other hand, the use of pan-inhibitors of protein aggregation leads to a disruption of proteostasis affecting multiple gene products, and it is therefore unlikely to elicit rapid evolution of resistance. This alternative strategy did dramatically reduce the viability of the malaria parasite. Several compounds with diverse chemotypes that inhibit protein aggregation have been shown to possess antimalarial activity in *in vitro P. falciparum* cultures. In this scenario, evolution of resistance by the pathogen would be further complicated by the need to evolve different ad hoc resistance mechanisms for each individual drug if these were used in combination. For those molecules belonging to chemical families where currently used antimalarials belong, resistance might be

achieved with relative rapidity through the adaptation of already existing resistance mechanisms. As an example of this, resistance to the aminoquinolines chloroquine and piperaquine has been associated with distinct sets of point mutations in the *P. falciparum* chloroquine resistance transporter *Pf*CRT, an efflux pump evolved by the parasite to expel chloroquine [67]. However, resistance would be slowed down significantly for those molecules belonging to chemical families where no antimalarials have been described so far, such as YAT2150, a double styrylpyridinium salt with an IC_{50} in *P. falciparum* cultures of ca. 90 nM. The sensitivity to YAT2150 of the chloroquine-resistant W2 strain and the results of hemozoin formation assays indeed indicate that the antimalarial mode of action of YAT2150 is not related to that of chloroquine.

YAT2150 specifically targets pRBCs vs. non-parasitized RBCs and binds aggregates in all *Plasmodium* stages, including early blood forms, and therefore its inhibitory effect on protein aggregation can be manifested at the start of the intraerythrocytic cycle, thus maximizing its antimalarial activity. *P. falciparum* overall ubiquitination increases as parasites mature from ring through trophozoite and schizont to merozoite forms [68], mirroring the observed increase in YAT2150 fluorescence along the blood stage cycle, in agreement with a scenario where protein aggregation mounts to reach its maximum with merozoite egress. The reduced signal observed in a significant fraction of early ring stages suggests that protein aggregates are required for merozoite invasion of the RBC but are lost in the process, which would set the aggregation clock of the pathogen back to zero at the moment of parasitizing a new erythrocyte.

Besides its activity against *Plasmodium* asexual blood stages, YAT2150 displays marked activity against the sexual and hepatic phases of the malaria parasites' life cycle, paving the way for the exploration of this compound as a potential multi-stage

antiplasmodial therapy. Other attractive characteristics of this compound are an easy, rapid and inexpensive synthesis, long room temperature storage, and its fluorescent emission when binding protein aggregates in the pathogen, which offers an added malaria diagnosis potential. YAT2150 can then be defined as a malaria theranostic agent.

Artemisinin, which in live parasites induces protein aggregation [24,25], has been described to inhibit *in vitro* the aggregation of amyloid peptides [69,70]. However, our data showing a sensitivity of artemisinin-resistant strains to YAT2150 similar to that of the corresponding parental non-resistant lines, strongly suggests that the antimalarial modes of action of both drugs are not related. Actually, in *P. falciparum* cultures we have observed an antagonistic action of artemisinin and YAT2150, suggesting that their main effects on the pathogen are opposed and therefore their combined use should *a priori* not be recommended. However, by 2016 the emergence of artemisinin and partner drug resistance in *P. falciparum* was detected in the Greater Mekong Subregion [71], and recently the independent evolution of artemisinin resistance has also been reported in Africa [72] and South America [73]. This alarming scenario calls for the urgent development of new drugs like YAT2150 with little-exploited targets in the malaria parasite.

The heme group released from hemoglobin as *Plasmodium* feeds on it has also been shown to promote the aggregation of proteins in the cell [74,75], which could explain the reduced presence of protein aggregates in early ring stages of the parasite. The potent blocking of the aggregation of Aβ40 and of aggregative peptides present in parasite proteins by YAT2150 at concentrations inhibiting parasite growth in *in vitro* cultures, suggests that this drug initially causes in live parasites inhibition of protein aggregation, which is presumably functional for *Plasmodium*. This hypothesis is

supported by the observed inhibition of protein aggregation in *P. falciparum* cultures at the compound's physiologically relevant IC_{50}. At the same concentration, YAT2150 disassembles *in vitro* preformed aggregates/fibrils of Aβ40 and of aggregative peptides found in *P. falciparum* proteins, in agreement with the existence of functional protein aggregates that are required for parasite survival. The cytosolic localization of the protein aggregation inhibitor YAT2150 in *Plasmodium* rough ER regions, where proteins are being synthesized, is consistent with the likely role of this drug in disrupting a yet to be described parasite's aggresome.

Our data obtained at high YAT2150 concentrations show a reduction of amyloid fibril content, which is mirrored by a simultaneous massive increase in ubiquitinated proteins, suggesting the existence in *Plasmodium* of functional amyloidogenic protein regions that, if disrupted by amyloid inhibitors, eventually assemble into amorphous aggregates. We propose that this interference with the as yet unknown role of certain aggregative proteins eventually triggers adverse physiological alterations in the parasite ultimately leading to a generalized deregulation of proteostasis. This scenario would conciliate the apparently contradictory observations regarding the effect of some antimalarials on protein aggregation in the pathogen.

Conclusion

The data presented above suggest that further increasing protein aggregation in the already aggregate-overloaded *Plasmodium* cell does not significantly affect the viability of the parasite, whereas aggregation inhibition has clear deleterious effects for it. This finding strongly suggests that certain functional protein aggregates can be crucial for the survival of malaria parasites and for the progression of their pathological effects.

Because some of these presumably functional protein assemblies might have an amyloid nature according to the results obtained with endogenous aggregative peptides identified in the pathogen's proteome, the description of malaria as an amyloidosis should probably be considered. This might spur the search for new antiplasmodials whose mode of action is the inhibition of protein aggregation in the parasite, such as YAT2150, whose promising characteristics can make it the spearhead of a new generation of antimalarial drugs for the post-artemisinin era.

Methods

Except where otherwise indicated, reagents were purchased from Sigma-Aldrich Corporation (St. Louis, MO, US), and reactions were performed at room temperature (RT; 22 to 24 °C). Peptides labeled on their N-terminal ends with 5(6)-carboxyfluorescein succinimidyl ester mixed isomers (5/6-FAM) were purchased from CASLO ApS, c/o Technical University of Denmark (Kongens Lyngby, Denmark), or synthesized in-house (see below). All the peptides used in this work were aminated in their C-terminal ends. Aggregation-prone sequences fused to cell-penetrating peptide motifs were prepared as described below. Except otherwise stated in the figure and table legends, all assays were replicated in at least three independent experiments maintaining the same experimental conditions. The most representative biological replicate is shown.

Synthesis of peptides elongated with cell-penetrating motifs

P. falciparum aggregation-prone peptides linked to the CPPs LMWP (VSRRRRRRGGRRRR) [76], TAT (GRKKRRQRRRPPQ) [51], or TP2

(PLIYLRLLRGQF) [77] were produced by solid-phase synthesis in Prelude (Gyros Protein Technologies, Tucson, AZ, US) or Liberty Blue instruments (CEM, Matthews, NC, US). Five-fold excess of fluorenylmethoxycarbonyl (Fmoc)-amino acids dissolved in *N*,*N*-dimethylformamide (DMF) were coupled in the presence of 2-(1*H*-benzotriazol-1-yl)-1,1,3,3-tetramethyluronium hexafluorophosphate (5-fold molar excess) and *N*,*N*-diisopropylethylamine (10-fold molar excess). After coupling and washing with DMF, Fmoc removal was done with 20% piperidine in DMF. Upon completion of the synthesis, the peptide resin was deprotected as described above, washed with dichloromethane and DMF and, if required, reacted with 5/6-FAM activated with *N*,*N'*-diisopropylcarbodiimide (10-fold molar excess of both reagents). Then the peptides were side-chain deprotected and cleaved from the resin with 95% (v/v) trifluoroacetic acid (TFA), 2.5% (v/v) triisopropylsilane and 2.5% (v/v) water. Two-hundred mg of each peptide-resin were treated with 5 ml of cleavage cocktail for 2 h at RT. Resin was removed by filtration and peptides in TFA solution were isolated by precipitation with cold diethyl ether and centrifugation (2 × 10 min at 2000× g); supernatant was removed and the peptide pellet was dried. Next, the crude peptide was taken up in water for high performance liquid chromatography (HPLC) and mass spectrometry (MS) analyses. HPLC analysis was performed with C18 columns (4.6 × 50 mm, 3 μm; Phenomenex, Torrance, CA, US) in a Shimadzu LC-2010A liquid chromatograph (Shimadzu Corporation, Kyoto, Japan). Solvent A was 0.045% TFA in H_2O, and solvent B was 0.036% TFA in acetonitrile. Elution was carried out with linear gradients (10-50% for LMWP- and TAT-peptides and 30-65% for TP2-peptides) of solvent B into solvent A over 15 min at 1 ml/min flow rate, with UV detection at 220 nm. MS was performed in a LC-MS 2010EV instrument (Shimadzu Corporation) fitted with an XBridge column (4.6 × 150 mm, 3.5 μm; Waters Corporation, Milford, MA, US). Peptides were eluted

with the same linear gradients used for HPLC of solvent B into solvent A (A: 0.1% formic acid in H_2O; B: 0.08% formic acid in acetonitrile).

Preparative HPLC runs were performed on a Luna C18 column (21.2 mm × 250 mm, 10 μm; Phenomenex), using the same linear gradients as for HPLC and MS of solvent B (0.1% TFA in acetonitrile) into A (0.1% TFA in H_2O), as required, with a flow rate of 25 ml/min. Fractions with >95% homogeneity were further characterized by electrospray mass spectrometry using a XBridge column C18 (Waters Corporation) and a gradient at 1 ml/min of solvent A (0.1% formic acid in H_2O) into solvent B (0.08% formic acid in acetonitrile), with 220 nm detection. Those with the expected HPLC homogeneity and mass were pooled, lyophilized, and used in subsequent experiments.

Synthesis of YAT2150 (dibromide salt)

All reagents and solvents were obtained from commercial suppliers and used without further purification. Automatic flash column chromatography was performed on a CombiFlash Rf 150 (Teledyne Isco) with prepacked RediSep Rf silica gel cartridges. Melting points were determined in open capillary tubes with a MFB 595010M Gallenkamp melting point apparatus. IR spectra were run on a Perkin Elmer Spectrum RX I spectrophotometer. Absorption values are expressed as wavenumbers (cm^{-1}). 500 MHz ^{1}H / 125 MHz ^{13}C NMR spectra were recorded on a Bruker Avance Neo 500 MHz spectrometer, at the *Centres Científics i Tecnològics* of the University of Barcelona (CCiTUB). The chemical shifts are reported in ppm (δ scale) relative to dimethyl sulfoxide (DMSO) solvent signals (DMSO-d_6 at 2.50 and 39.5 ppm in the ^{1}H and ^{13}C NMR spectra, respectively), and coupling constants are reported in Hertz (Hz). Assignments given for the NMR spectra have been carried out on the basis of DEPT

and COSY $^{1}H/^{13}C$ (gHSQC sequences) experiments. High resolution mass spectra were carried out at the CCiTUB with a LC/MSD TOF Agilent Technologies spectrometer.

A mixture of 1,10-dibromodecane (1.50 g, 5.00 mmol) and 3,4-dimethylpyridine (1.2 ml, 1.14 g, 10.7 mmol) was heated at 120 °C for 3 h. Then, isopropanol (5 ml) was added and the reaction mixture was stirred under reflux for 1 h. The mixture was allowed to cool down to RT, the resulting brown residue was washed with ice-cold Et_2O (2 × 40 ml), the supernatant was removed and the remaining brown sticky oil was dried *in vacuo*, taken up in MeOH (1 ml) and treated with cold Et_2O (2 × 40 ml), drawing off the liquids. After drying the residue *in vacuo*, 1,1'-(decane-1,10-diyl)*bis*(3,4-dimethylpyridin-1-ium) dibromide (2.48 g, 96%) was obtained as a brown oil that solidified on standing; mp: 69-71 ºC; IR (ATR) *v*: 3443, 3396, 3027, 2988, 2921, 2851, 1635, 1512, 1483, 1471, 1391, 1224, 1143, 1031, 870, 838, 710, 597, 559 cm^{-1}; ^{1}H NMR (500 MHz, DMSO-d_6) δ: 1.20-1.32 [m, 12H, 3'(8')-H_2, 4'(7')-H_2, 5'(6')-H_2], 1.89 [tt, $J = J' = 7.5$ Hz, 4H, 2'(9')-H_2], 2.40 (s, 6H, pyridinium 3-CH_3), 2.52 (s, 6H, pyridinium 4-CH_3), 4.50 [t, $J = 7.5$ Hz, 4H, 1'(10')-H_2], 7.95 (d, $J = 6.0$ Hz, 2H, pyridinium 5-H), 8.85 (dd, $J = 6.0$ Hz, $J' = 1.5$ Hz, 2H, pyridinium 6-H), 8.96 (br s, 2H, pyridinium 2-H); ^{13}C NMR (125 MHz, DMSO-d_6) δ: 16.3 (2 CH_3, pyridinium 3-CH_3), 19.6 (2 CH_3, pyridinium 4-CH_3), 25.4 (2 CH_2), 28.3 (2 CH_2), 28.7 (2 CH_2) [C3'(8'), C4'(7'), C5'(6')], 30.5 [2 CH_2, C2'(9')], 59.7 [2 CH_2, C1'(10')], 127.9 (2 CH, pyridinium C5), 137.6 (2 C, pyridinium C3), 141.5 (2 CH, pyridinium C6), 142.8 (2 CH, pyridinium C2), 157.6 (2 C, pyridinium C4); HRMS-ESI+ *m/z* calculated for $[C_{24}H_{38}N_2]^{2+}/2$: 177.1512, found 177.1513.

A solution of 1,1'-(decane-1,10-diyl)*bis*(3,4-dimethylpyridin-1-ium) dibromide (514 mg, 1.00 mmol) and 4-(diethylamino)benzaldehyde (390 mg, 2.20 mmol) in *n*-butanol (5 ml) was treated with six drops of piperidine and the reaction mixture was stirred

under reflux for 4 h, and then concentrated under reduced pressure. The resulting black oily residue was purified by automatic flash column chromatography (CH_2Cl_2 / 7 N ammonia solution in MeOH 9:1), to provide 1,1'-(decane-1,10-diyl)*bis*{Aminake, , Thiostrepton and derivatives exhibit antimalarial and gametocytocidal activity by dually targeting parasite proteasome and apicoplast} dibromide (351 mg, 42%) as a red oil that solidified on standing; mp: 173-174 ºC; IR (ATR) *v*: 3399, 2975, 2927, 2853, 1641, 1574, 1520, 1479, 1404, 1351, 1311, 1260, 1219, 1186, 1128, 1076, 1011, 958, 807, 572 cm^{-1}; ^1H NMR (500 MHz, DMSO-d_6) δ: 1.13 [t, J = 7.0 Hz, 12H, $N(CH_2\text{-}CH_3)_2$], 1.21-1.31 [m, 12H, 3'(8')-H_2, 4'(7')-H_2, 5'(6')-H_2], 1.87 [tt, $J = J'$ = 7.5 Hz, 4H, 2'(9')-H_2], 2.48 (s, 6H, pyridinium 3-CH_3), 3.43 [q, J = 7.0 Hz, 8H, $N(CH_2\text{-}CH_3)_2$], 4.37 [t, J = 7.5 Hz, 4H, 1'(10')-H_2], 6.74 [d, J = 9.0 Hz, 4H, phenylene 3(5)-H], 7.08 (d, J = 16.0 Hz, 2H, pyridinium C4-C*H*=CH), 7.64 (d, J = 9.0 Hz, 4H, phenylene 2(6)-H]), 7.88 (d, J = 16.0 Hz, 2H, pyridinium C4-CH=C*H*), 8.26 (d, J = 6.5 Hz, 2H, pyridinium 5-H), 8.66 (dd, J = 6.5 Hz, J' = 1.5 Hz, 2H, pyridinium 6-H), 8.73 (br s, 2H, pyridinium 2-H); ^{13}C NMR (125 MHz, DMSO-d_6) δ: 12.5 [4 CH_3, $N(CH_2\text{-}CH_3)_2$], 16.5 (2 CH_3, pyridinium 3-CH_3), 25.5 (2 CH_2), 28.4 (2 CH_2), 28.7 (2 CH_2) [C3'(8'), C4'(7'), C5'(6')], 30.5 [2 CH_2, C2'(9')], 43.9 [4 CH_2, $N(CH_2\text{-}CH_3)_2$], 58.9 [2 CH_2, C1'(10')], 111.3 [4 CH, phenylene C3(5)], 113.4 (2 CH, pyridinium C4-*C*H=CH), 119.8 (2 CH, pyridinium C5), 122.1 (2 C, phenylene C1), 130.8 [4 CH, phenylene C2(6)], 132.9 (2 C, pyridinium C3), 140.5 (2 CH, pyridinium C6), 142.4 (2 CH, pyridinium C4-CH=*C*H), 143.3 (2 CH, pyridinium C2), 149.5 (2 C, phenylene C4), 152.4 (2 C, pyridinium C4); HRMS-ESI+ *m/z* calculated for $[C_{46}H_{64}N_4]^{2+}/2$: 336.2560, found: 336.2550.

For its use in the assays reported below, the final product, YAT2150, was dissolved in DMSO to obtain a 9 mM stock solution.

In vitro peptide aggregation assays

Peptide stocks prepared in DMSO were diluted in phosphate buffered saline (PBS) at a final concentration of 150 µM. After vigorous vortexing, peptides were incubated at 37 °C and 1400 rpm in a ThermoMixer® (Eppendorf, Hamburg, Germany) for 48 h. After that time, peptides were further diluted in triplicates to 25 µM in PBS, ThT was added at the same final concentration in PBS, and fluorescence emission was collected from 470 to 600 nm using an excitation wavelength of 450 nm (Infinite Nano+ multimode microplate reader, Tecan Trading AG, Männedorf, Switzerland). A blank measurement of each sample was done before adding ThT.

Fluorescein-labeled peptides were diluted in PBS at 150 µM and incubated for 24 h at 37 °C and 1400 rpm. After this time, peptides were further diluted in triplicates in PBS to a final concentration of 15 µM, to which the protein aggregation detection reagent ProteoStat® (Enzo Life Sciences, Inc., Farmingdale, NY, US) was added at 1:1000 final dilution, and transferred to a 96-well black plate (Greiner Bio-One, Madrid, Spain). ProteoStat® fluorescence was quantitated (Tecan Infinite 200 PRO, Tecan Trading AG) using respective excitation and emission wavelengths of 550 and 600 nm. The fluorescence of a ProteoStat®-only control was also measured and subtracted from the sample values.

For the *in vitro* analysis of Aβ40 aggregation, one mg of Aβ40 (GenScript Biotech, Piscataway, NJ, US) was dissolved in 500 µl of 1,1,1,3,3,3-hexafluoro-2-propanol (HFIP; Honeywell Fluka-Thermo Fisher Scientific, Waltham, MA, US) under vigorous stirring for 1 h and sonicated for 30 min in an ultrasound bath. Afterwards, the solution was stirred for 1 h and maintained at 4 °C for 30 min. Aliquots were prepared, HFIP was evaporated under a nitrogen stream for a few seconds and the dry peptide was

stored at –20 °C. Prior to use, these Aβ40 aliquots were dissolved in DMSO and sonicated for 10 min to ensure minimal aggregation. To assess the effect of YAT2150 on the formation of amyloid fibrils, Aβ40 DMSO solutions were diluted to 25 µM in PBS containing different concentrations of YAT2150, and incubated for 24 h at 37 °C and 1400 rpm. Alternatively, to test the effect of YAT2150 on already formed amyloid fibrils, Aβ40 DMSO solutions were diluted to 25 µM in PBS and incubated as above in order to allow fibril formation. Then, YAT2150 was added at different concentrations and the mixture was incubated in the same conditions for another 24 h. The final samples always contained less than 5% DMSO to avoid interference of this solvent on Aβ40 amyloid fibril formation. Finally, ThT treatment was performed as described above. The analyses of aggregation inhibition and disaggregation performed with aggregative peptides present in *P. falciparum* proteins were conducted in the same way.

P. falciparum growth inhibition assays

P. falciparum parasites of the 3D7 (MRA-102, chloroquine-sensitive) and W2 (MRA-157, chloroquine-resistant) strains (both from Malaria Research and Reference Reagent Resource Center, Manassas, VA, US), and Cam 3.II (chloroquine and sulfadoxine/pyrimethamine resistance), Cam 3.II + K13 R561H, Cam 3.II + K13 R539T, 3D7 + K13 R561H and 3D7 + K13 M579I strains (all carrying artemisinin resistance, developed and authenticated by Stokes et al. [59] and kindly donated by Prof. David A. Fidock), were 5% sorbitol-synchronized as described elsewhere [78] in order to obtain a culture enriched in ring stage parasites. After the synchronization process, a new culture at 1.5% parasitemia and 2% hematocrit was established and 150-µl aliquots of it were transferred to 96-well plates. The required amounts of peptides,

antimalarial drugs or amyloid pan-inhibitors were added to each well at different concentrations and in triplicates. For synergy assays of YAT2150 and artemisinin, serial dilutions of both compounds were prepared at different concentration ratios (1:0, 0:1, 1:1, 1:2, 2:1, 1:5 and 5:1) as explained elsewhere [79]. A positive growth control of untreated parasites and a negative growth control of parasites treated with a lethal dose of chloroquine (1 µM) were also included. Parasites were grown for 48 h, a complete replication cycle, in standard culturing conditions (5% O_2, 5% CO_2, and 90% N_2 at 37 °C). After the incubation period, 3 µl of culture from each well were mixed with 197 µl of PBS containing 0.1 µM Syto 11 (Thermo Fisher Scientific), to obtain a final concentration of ca. 1-10 × 10^6 cells/ml. Parasitemia was assessed by flow cytometry using a LSRFortessa flow cytometer (BD Biosciences, San Jose, CA, US) set up with the 4 lasers, 20 parameters standard configuration. The single-cell population was selected on a forward-side scatter scattergram. Syto 11 fluorescence signal was detected by exciting samples at 488 nm and collecting the emission with a 530/30 nm bandpass filter. Growth inhibition was calculated taking as reference values both the growth rate of the untreated culture and the growth rate of the culture treated with chloroquine. Growth inhibition data was transformed through sigmoidal fitting and used to determine the compound's concentration required for the reduction of *P. falciparum* viability by 50% (IC_{50}).

To assess the synergistic effect of YAT2150 and artemisinin, IC_{50} values for each individual compound in the mixtures were calculated and plotted in an isobologram ("x" value = YAT2150 IC_{50} and "y" value = artemisinin IC_{50}). Fractional inhibitory concentration (FIC) values were calculated by dividing the IC_{50} of one of the compounds in the mixture by the IC_{50} of the same compound in the 1:0 or 0:1 ratio mixtures.

For stage of growth inhibition analysis, *P. falciparum* cultures were synchronized at ring or trophozoite stages by repeated treatment with 5% sorbitol or 70% Percoll (GE Healthcare, Chicago, IL, US) [78,80], respectively. Half of each culture remained untreated and the other half was treated with the IC_{80} [27] of YAT2150. At different time points, culture samples were stained with Giemsa and the number of ring, early and mature trophozoites and schizonts was counted by microscopic examination of at least 100 pRBCs for each sample. Pictures were taken with a Nikon Eclipse 50i microscope equipped with a DS-Fi1 camera (Nikon Corporation, Tokyo, Japan).

Quantitative analysis of protein aggregation in live *P. falciparum* cultures

P. falciparum cultures enriched in early stages were treated with the IC_{10} (27 nM) and IC_{50} (90 nM) of YAT2150 or left untreated. After 90 min, 4 h and 30 h, a Percoll purification was done in order to isolate parasitized cells from uninfected RBCs. After Percoll purification, the pellets of late stage parasites and a control non-infected RBC suspension containing the same proportion of cells than the purified cultures were resuspended in 50 µl of lysis buffer (4.5 mg/ml NaCl in water supplemented with EDTA-free protease inhibitor cocktail, PIC, Hoffman-La Roche, Basel, Switzerland; 1 PIC tablet/10 ml water) and incubated overnight, at 4 °C under stirring, with the objective of releasing their inner content. After this time, lysed samples were spun down and the protein content in the supernatant was quantified with the bicinchoninic acid assay (Thermo Fisher Scientific), following the manufacturer's instructions. 30 µg of protein from each supernatant were further diluted with PBS to a final volume of 70 µl and plated on a 96-well black plate in triplicates. ThT fluorescence was measured as described above.

Flow cytometry for cell targeting studies

A non-synchronized *P. falciparum* 3D7 culture was stained with 1 μM YAT2150 and 2 μg/ml of the DNA dye Hoechst 33342. Five μl of this culture were mixed with 500 μl of PBS and analysed in a LSRFortessa flow cytometer set up with the five-laser, 20-parameter standard configuration. Forward and side scatter were used in a logarithmic scale to gate the RBC population. Acquisition was configured to stop after recording 30,000 events. Hoechst 33342 and YAT2150 fluorescence levels were detected, respectively, by excitation with 350 and 561 nm lasers, and emissions were collected with 450/50BP nm and 600LP-610/20BP bandpass filters. The fraction of pRBCs containing fluorescein-labeled peptides was also assessed by flow cytometry, in this case exciting with a 488 nm/60 mW laser and collecting the emission with a 525/50BP nm bandpass filter. To avoid fixation artifacts, all the flow cytometry data presented in this work were obtained with live cells.

Peptide loading into ghost RBCs

Ghost RBCs loaded with various peptides were generated as previously described [53]. Briefly (Fig. 1B), regular RBCs were washed twice using three times their volume of ice-cold 1× PBS by centrifugation at 200× g for 10 min at 4 °C. After the second washing, the supernatant was removed and the RBC pellet taken up in one volume of ice-cold lysis buffer, 1 mM ATP, 5 mM K_2HPO_4 in double deionized water (ddH_2O; MilliQ system, Millipore Corporation, Burlington, MA, US), containing 10 μM of the peptide to encapsulate. RBCs were incubated with the lysis buffer at 4 °C with gentle stirring for 1 h, when the generated ghost RBCs were spun down and half of the total

volume of the sample was substituted by resealing buffer. The final concentration of the buffer after mixing with the sample was 150 mM NaCl, 5 mM $MgCl_2$, 1 mM ATP and 1 mM glutathione. Ghost RBCs were incubated with the resealing buffer for 1 h at 37 °C with gentle stirring. Finally, the samples were washed four times with three times their volume of Roswell Park Memorial Institute 1640 medium (RPMI, Gibco®, Thermo Fisher Scientific) containing L-glutamine and sodium bicarbonate, and supplemented with 5.95 g/ml 2-(4-(2-hydroxyethyl)piperazin-1-yl)ethanesulfonic acid (HEPES). The ghost RBC pellet was taken up in an equal volume of RPMIc: RPMI containing 5 mg/ml Albumax II (Invitrogen, Waltham, MA, US) and 2 mM L-glutamine, and finally stored at 4 °C until further use.

Infection of ghost RBCs or RBCs with *P. falciparum* was performed by establishing a new culture using late-stage parasites purified in 70% Percoll as described elsewhere [78,80]. Parasites were added to peptide-loaded ghost RBC cultures (Fig. 1B) or regular RBC cultures containing the same proportion of peptide. After 72 h of incubation as described above, the viability of *Plasmodium* cells was assessed by staining parasites in the culture with 2 µg/ml Hoechst 33342 and analyzing the parasitemia by flow cytometry as described above. The % of growth inhibition was calculated comparing the parasitemia in the treated sample with the parasitemia of an untreated control culture, according to the formula: 100 – % survival, where % survival was calculated as follows:

$$\frac{\text{sample \% parasitemia} - \text{initial \% parasitemia}}{\text{final \% parasitemia of untreated control} - \text{initial \% parasitemia}} \times 100,$$

where parasitemia was calculated as:

$$\frac{\text{number of pRBCs}}{\text{total number of parasitized} + \text{naïve RBCs}} \times 100$$

Fluorescence microscopy

For YAT2150 staining, a *P. falciparum* 3D7 culture was incubated in RPMIc for 30 min at 37 °C with 4.5 µM of the compound and 4 µg/ml of Hoechst 33342. For colocalization studies, 0.5 µM of ER Tracker™ Green (BODIPY™ FL Glibenclamide, Thermo Fisher Scientific) was included in the solution. Cells were placed in an 8-well LabTek™ II chamber slide system (Thermo Fisher Scientific), rinsed with warm PBS and diluted 1:20 for their observation in a Leica TCS SP5 confocal microscope (Leica Camera, Mannheim, Germany) equipped with a 63× objective of 1.4 NA. Hoechst 33342 was excited with a diode laser at 405 nm, ER Tracker Green with the 488 nm line of an argon laser, and YAT2150 with a diode-pumped solid-state laser at 561 nm. The corresponding fluorescence emissions were collected in the ranges of, respectively, 415-460, 490-590, and 600-700 nm. The subcellular localization in ghost pRBCs of fluorescein-labeled aggregative peptides was done in cultures that had been grown in ghost RBCs loaded with 10 µM peptides labeled in their N-ter ends with 5/6-FAM. Colocalization was evaluated as above but in this case using 0.5 µM of either ER Tracker™ Red (BODIPY™ TR Glibenclamide, Thermo Fisher Scientific) or LysoTracker™ Red DND-99 (Thermo Fisher Scientific) in addition to Hoechst 33342. Emissions of ER Tracker Red and LysoTracker Red (both excited with a diode-pumped solid-state laser at 561 nm) were collected between 590-680 nm whereas the peptide signal (following excitation at 488 nm) was detected in the 490-550 nm range. To avoid crosstalk between the different fluorescence signals, sequential line scanning was performed. To quantify Manders' overlap coefficient [81], images were analyzed using the Just Another Colocalization Plugin (JACoP, [82]) in the Fiji software [83]. To avoid fixation artifacts, all the fluorescence microscopy data presented in this work were obtained with live cells.

LC-MS/MS analysis of aggregative proteins from ring stage parasites

For the isolation of aggregative proteins from ring stage parasites, 80 ml of a *P. falciparum* preparation containing approximately 4×10^9 early stage parasites that had been sorbitol-synchronized from *in vitro* cultures were washed with sterile PBS and spun down (300× g, 5 min), storing the resulting cell pellet at −80 °C until performing LC-MS/MS analysis as previously described [3].

Dot blots and Western blots

Cultures of the *P. falciparum* 3D7 strain were sorbitol synchronized in ring stages, and after 24 h were treated for 90 min with YAT2150 concentrations ranging from 33 nM to 33 µM, or for 24 h with 90 nM YAT2150. After that time, cultures were spun down and pellets were washed once with ice-cold PBS supplemented with EDTA-free PIC (1 PIC tablet/10 ml PBS). For anti-ubiquitin Western blots, PBS was also supplemented with 20 mM *N*-ethylmaleimide. Washed parasite pellets were treated with 0.15% saponin at 4 °C for 15 min and washed again by centrifugation (10,000× g, 15 min, 4 °C) with appropriately supplemented PBS until no hemoglobin was observed in the supernatant. Protein extracts were quantified with the bicinchoninic acid assay. For dot blots, 4-µl drops of saponin extract containing 0.5 or 1 mg/ml protein were spotted on a nitrocellulose membrane. Once protein extracts were completely absorbed by the membranes, these were incubated for 3 h in blocking solution: 5% milk powder in tris-buffered saline (0.15 M NaCl, 20 mM tris-base, pH 7.6) supplemented with 0.1% Tween-20 (TBS-Tween). The blocked membranes were washed 3 × 5 min with TBS-Tween and incubated overnight at 4 °C with rabbit polyclonal anti-amyloid fibrils OC

antibody (AB2286, Millipore Corporation) diluted 1:500 in blocking solution or with mouse monoclonal anti-spectrin α/β (S3396, Sigma-Aldrich Corporation) diluted 1:10,000 in TBS-Tween. For Western blots, 15 μg of saponin-extracted proteins were incubated for 5 min at 95 °C diluted in Laemmli solution (0.14 M SDS, 0.125 M tris-HCl, pH 6.8, 20% glycerol, 10% 2-mercaptoethanol, 3 mM bromophenol blue) and resolved by SDS-polyacrylamide gel electrophoresis in 12% bis-tris acrylamide (Bio-Rad Laboratories, Inc., Hercules, CA, US) gels run at 80 V until samples entered the resolving gel and at 120 V afterwards. Proteins were transferred from the gel to polyvinylidene difluoride membranes activated with methanol. After transference, membranes were blocked with blocking solution for 1 h at RT, washed 3 × 5 min with TBS-Tween and probed overnight at 4 °C with rabbit polyclonal anti-ubiquitin antibody (#3933, Cell Signaling Technology, Inc., Danvers, MA, US) diluted 1:1,000 in blocking solution, or with mouse monoclonal anti-spectrin α/β diluted 1:10,000 in TBS-Tween. Then, membranes were washed 5 times with TBS-Tween and incubated for both dot blot and Western blot during 1 h with either goat anti-rabbit (#12-348, Upstate Biotechnology, Inc., Lake Placid, NY, US) or goat anti-mouse (#145660, Amersham Life Science, Inc., Amersham, UK) IgG-horseradish peroxidase conjugate diluted 1:10,000 in TBS-Tween. After 4 washes with TBS-Tween and one last wash with TBS, peroxidase substrate (ECL Prime Western Blotting Detection Reagent, Amersham Life Science, Inc.) was poured on the membrane and chemiluminescent signal was measured in a LAS 4000 reader (ImageQuant TL, GE Healthcare, Chicago, IL, US) at different exposure times.

Transmission electron microscopy (TEM)

A carbon-coated copper grid was deposited for 30 min on top of a 50-µl drop of 25 µM peptide solutions prepared as explained above. Then, the excess liquid was removed with filter paper and the grid was placed on top of a ddH_2O drop for 30 s and finally negatively stained for 2 min with 20 µl of 2% uranyl acetate. Samples were observed using a JEM 1010 transmission electron microscope (JEOL Ltd., Tokyo, Japan). Images were acquired using a CCD Orius camera (Gatan, Inc., Pleasanton, CA, US).

Correlative light and electron microscopy (CLEM)

A 0.5% parasitemia RBC culture was prepared for CLEM by allowing its binding to concanavalin as described [84]. Briefly, a µ-*Dish 35 mm, High, Grid-500* (ibidi GmbH, Gräfelfing, Germany) was coated for 20 min at 37 °C with a 50 mg/ml concanavalin A solution in ddH_2O and wells were rinsed with pre-warmed PBS before parasite seeding. *P. falciparum*-infected RBCs washed twice with PBS were deposited into the dish and incubated for 10 min at 37 °C; afterwards, unbound RBCs were washed away with three PBS rinses. Seeded RBCs were then incubated with 3 µM YAT2150, and nuclei were counterstained with 2 µg/ml Hoechst 33342. The preparation was observed with a Zeiss LSM880 confocal microscope (Carl Zeiss, Jena, Germany), with respective λex/em for YAT2150 and Hoechst 33342 of 405/415-520 nm and 561/565-600 nm. Images were obtained from areas corresponding to a specific coordinate of the dish-grid by tile scans that were stitched into larger mosaics. A bright field image facilitated the recognition of the grid coordinates from the plate where the cells selected for CLEM were located. After confocal image acquisition, cells were washed three times with TEM fixation buffer (2% paraformaldehyde and 2.5% glutaraldehyde in PBS) for 5 min each. Then, the fixation buffer was changed to 1% osmium tetroxide and 0.8% potassium

ferricyanide in fixation buffer and incubated at 4 °C for 45 min, followed by three 5-min washes with ddH_2O. Then, a dehydration procedure was performed by gradually increasing ethanol concentration: 50% (10 min), 70% (10 min), 80% (10 min), 90% (5 min, 3×), 96% (5 min, 3×), and 100% (5 min, 3×). At this point, the plastic part of the dish was carefully separated from the crystal part containing the samples, which was embedded in Spurr resin by successive incubations with different proportions of resin/ethanol, starting with 1/3 for 1 h, 1/1 for 1 h, 3/1 for 1 h and 1/0 overnight. After the embedding procedure, a BEEM® capsule containing polymerized Spurr resin was filled with a small volume of liquid resin in order to obtain an interphase in which the dish was placed. The BEEM® capsule was incubated at 70 °C for 72 h, and the crystal part of the dish was removed by alternatively immersing samples in liquid nitrogen and boiling water. When the crystal was broken, cells remained attached to the resin, which was further cut in a microtome with a diamond blazer in order to obtain 100 nm-thick resin slides, which were mounted on a carbon-coated copper grid and negatively stained with 2% uranyl acetate for 2 min and washed with ddH_2O for 1 min. Samples were observed in a JEM 1010 transmission electron microscope. Images were processed for CLEM analysis using the CORRELIA plug-in [85] in the Fiji software (version 2.0.0-pre-8) [83].

Hemozoin formation assay

In vitro hemozoin formation assays were performed as explained elsewhere [86,87] with minor modifications. A stock of 4.5 mg/ml hemin chloride in DMSO was further diluted to obtain a solution of 0.036 mg/ml in 0.1 M acetate buffer (pH 4.8) containing 0.015 mg/ml of Tween-20. This solution was distributed in Eppendorf tubes, and chloroquine

or YAT2150 were added at different concentrations. An untreated hemin sample and controls containing drugs but not hemin were also prepared. To monitor the initial turbidimetry and free hemin, absorbance was measured, respectively, at 630 nm and 415 nm (Infinite Nano+ multimode microplate reader) in triplicates, and tubes were vortexed and incubated protected from light in a ThermoMixer® (37 °C, 2 h, 700 rpm). After 2 h, samples were left at RT for 1 h in the dark and then centrifuged (10 min, 21,300× g) to precipitate hemozoin crystals. The supernatant of each sample was recovered and plated in triplicates (150 µl/well, 96-well plates) and absorbance was read again. The amount of free hemin in each sample was calculated ($A_{415} - A_{630}$) and subtracted from the free drug control.

Gametocyte assays

Cultures of the *P. falciparum NF54-gexp02-Tom* strain (developed and authenticated by Portugaliza et al. [88] and kindly provided by Prof. Alfred Cortés), were maintained in standard conditions in RPMI medium supplemented with 0.5% Albumax II and 2 mM choline, synchronized in ring stages with sorbitol lysis, and diluted to 2% parasitemia. To trigger sexual conversion, choline was removed from the medium and cultures were maintained in the same conditions for 48 h after synchronization (cycle 0). In the next cycle (cycle 1), parasites were treated with 50 mM N-acetylglucosamine (GlcNac) in order to kill asexual parasites, and maintained in RPMI supplemented with 10% human serum. Medium was refreshed daily and GlcNac was kept during 4 days. To determine the effect of YAT2150 and DONE3TCl in early gametocytes, the culture was distributed in triplicates (200 µl/well, 96-well plates) and drugs were added in cycle 1 and maintained for 48 h in the culture. Controls of untreated parasites as well as of

parasites treated with a lethal dose of chloroquine were prepared. Gametocytemia was monitored daily by light microscopy until the majority of parasites (~ 90%) could be identified as stage V gametocytes. At that point, Giemsa smears of each well were prepared and mature gametocytes were manually counted (10,000 cells were counted for each replica by two investigators blinded to group assignment). To test the effect of YAT2150 and DONE3TCl on mature gametocytes, cultures were grown for 14 days, when the majority of the parasites could be identified as stage V gametocytes. Afterwards, the culture was treated for 48 h with the drugs and the gametocytemia determined as above.

In vitro activity against *P. berghei* hepatic stages

The *in vitro* activity of YAT2150 and DONE3TCl against the liver stages of *P. berghei* (obtained from Leiden University Medical Centre, Leiden, The Netherlands) infection was assessed as previously described [89]. Briefly, Huh7 cells (Cenix BioScience GmbH, Dresden, Germany) were routinely cultured in RPMI supplemented with 10% (v/v) fetal bovine serum, 1% (v/v) glutamine, 1% (v/v) penicillin/streptomycin, 1% non-essential amino acids, and 10 mM HEPES. For drug screening experiments, Huh7 cells were seeded at 1×10^4 cells/well of a 96-well plate and incubated overnight at 37 °C with 5% CO_2. Stock solutions of test compounds (10 mM) were prepared in DMSO and serially diluted in infection medium, i.e., culture medium supplement with gentamicin (50 μg/ml) and amphotericin B (0.8 μg/ml), in order to obtain the test concentrations. On the day of the infection, the culture medium was replaced by serial dilutions of test compounds and incubated for 1 h at 37 °C with 5% CO_2. Next, 1×10^4 firefly luciferase-expressing *P. berghei* sporozoites, freshly isolated from the salivary glands of female infected *Anopheles stephensi* mosquitoes (reared from eggs originally obtained from the

Radboud University Medical Centre, Nijmegen, The Netherlands), were added to the cultures, plates were centrifuged at 1800× g for 5 min at room temperature and incubated at 37 °C with 5% CO_2. To assess the effect of each compound concentration on cell viability, cultures were incubated with Alamar Blue (Invitrogen, Waltham, MA, US) at 46 h post infection, according to the manufacturer's recommendations. The parasite load was then assessed by a bioluminescence assay (Biotium, Fremont, CA, US), using a multi-plate reader, Infinite M200 (Tecan, Männedorf, Switzerland). Nonlinear regression analysis was employed to fit the normalized results of the dose-response curves, and IC_{50} values were determined using GraphPad Prism (GraphPad software, version 6.0, La Jolla, CA, US).

In vitro toxicity assays

Human umbilical vein endothelial cells (HUVEC; CRL-1730 American Type Culture Collection, Manassas, VA, US) were plated at 5000 cells/well in 96-well plates and grown in Medium 199 with Earle's salts supplemented with 10% fetal bovine serum (FBS) and 1% penicillin/streptomycin for 24 h at 37 °C in 5% CO_2. After that, the medium was substituted by 100 µl of drug-containing culture medium without FBS, and incubation was resumed for 48 h. 10 µl of 4-[3-(4-iodophenyl)-2-(4-nitrophenyl)-2*H*-5-tetrazolio]-1,3-benzene disulfonate labeling reagent (WST-1) was added to each well, and the plate was incubated in the same conditions for 2 h. After thoroughly mixing by pipetting up and down, the absorbance of the samples was measured at 440 nm using a Benchmark Plus microplate reader (Bio Tek, Agilent Technologies, Santa Clara, CA, US). WST-1 in the absence of cells was used as blank and samples were prepared in triplicate for each experiment. Percentages of viability were obtained using non-treated cells as control of survival. The compound's concentration required for the reduction of

cell viability by 50% was defined as CC_{50}. The *in vitro* selectivity index was defined as CC_{50}/IC_{50}.

In vivo toxicity assays

In vivo assays were done at the animal facility of the *Parc Científic de Barcelona* (PCB). BALB/c female and male mice (BALB/cAnNRj, seven weeks old, Janvier Laboratories, Le Genest-Saint-Isle, France) were maintained with unlimited access to food and water under standard environmental conditions (20-24 °C and 12/12 h light/dark cycle). Three 100-µl doses of a drug solution prepared to administer 0.0959, 0.3069 and 0.9822 mg YAT2150/kg were tested in a total number of 6 mice/drug dose. First, the lowest dose was intravenously injected to one female and one male mouse. An oxygen stream of 4% isoflurane was used to anesthetize the mice, which were then maintained during the whole injection procedure (less than 3 min) with 2.5% isoflurane. After the administration, mice were observed and different parameters related to their behavior (lethargy, motility alterations, seizures, coma, automutilation, aggressiveness, vocalizations, stereotyped movements) and physical conditions (pain, respiratory disturbances, tachycardia or bradycardia, dehydration, hair loss, body weight loss, dermatitis, bad hygiene, pruritus, tearing) were followed. If after 48 h no deleterious effects were observed, the following dose was administered to two other male and female mice. All mice were observed for 14 days after treatment in order to detect long-term side effects.

In silico analysis

Protein abundance and aggregation propensity were calculated and plotted as elsewhere described [90]. Briefly, abundance (C) was calculated as the $\log_{10}$ of the protein concentration values obtained from PaxDb [91], which were normalized by rescaling them between 0 and 1:

$$C = \frac{(Ci - \min(Ci \dots Cn))}{(\max(Ci \dots Cn) - \min(Ci \dots Cn))},$$

where (*Ci...Cn*) is each value of protein concentration from the dataset, *Cmin* is the minimum value of protein concentration from the dataset, and *Cmax* is the maximum value of protein concentration from the dataset.

Aggregation tendency (A) was obtained using the TANGO algorithm, which estimates the cross-beta aggregation propensity in peptides and denatured proteins [92]. For the estimation, TANGO parameters were set at pH 7.4, 37 °C and 0.25 mM ionic strength, using the output parameter "AGG," which was then normalized in the same manner by rescaling the values between 0 and 1:

$$A = \frac{(Ai - \min(Ai \dots An))}{(\max(Ai \dots An) - \min(Ai \dots An))},$$

where (*Ai...An*) is each value of protein aggregation from the dataset according to the "AGG" parameter of TANGO, *Amin* is the minimum value of protein aggregation from the dataset, and *Amax* is the maximum value of protein aggregation from the dataset.

Peptide aggregation scores were obtained with the WALTZ algorithm [54], designed to predict amyloidogenic regions inside proteins. The values expressed correspond to the average score per residue given by the algorithm.

Statistical analysis

All statistical analyses were performed using GraphPad Prism 9 (GraphPad software, version 9, La Jolla, CA, US). The normal distribution of the obtained data was assessed by various normality tests (Shapiro-Wilk, Anderson-Darling, D'Agostino-K and Chen-Shapiro) and a two-sided test of variance was performed. Afterwards, samples were analyzed by two-sided Student's *t* test. All tests were accomplished at the 0.05 significance level cut-off.

Reference List

1. Pallarès I, de Groot NS, Iglesias V, Sant'Anna R, Biosca A, Fernàndez-Busquets X *et al*. Discovering putative prion-like proteins in *Plasmodium falciparum*: a computational and experimental analysis. Front Microbiol. 2018;9:1737.

2. Halfmann R, Alberti S, Krishnan R, Lyle N, O'Donnell CW, King OD *et al*. Opposing effects of glutamine and asparagine govern prion formation by intrinsically disordered proteins. Mol Cell. 2011;43:72-84.

3. Biosca A, Bouzón-Arnáiz I, Spanos L, Siden-Kiamos I, Iglesias V, Ventura S *et al*. Detection of protein aggregation in live *Plasmodium* parasites. Antimicrob Agents Chemother. 2020;64:e02135-19.

4. Chiti F, Dobson CM. Protein misfolding, amyloid formation, and human disease: a summary of progress over the last decade. Annu Rev Biochem. 2017;86:27-68.

5. Olzscha H, Schermann SM, Woerner AC, Pinkert S, Hecht MH, Tartaglia GG *et al*. Amyloid-like aggregates sequester numerous metastable proteins with essential cellular functions. Cell. 2011;144:67-78.

6. Klaips CL, Jayaraj GG, Hartl FU. Pathways of cellular proteostasis in aging and disease. J Cell Biol. 2018;217:51-63.

7. Mroczko B, Groblewska M, Litman-Zawadzka A. The role of protein misfolding and tau oligomers (TauOs) in Alzheimer's disease (AD). Int J Mol Sci. 2019;20:4661.

8. Zhu G, Harischandra DS, Ghaisas S, Zhang P, Prall W, Huang L *et al*. TRIM11 prevents and reverses protein aggregation and rescues a mouse model of Parkinson's disease. Cell Rep. 2020;33:108418.

9. Troncoso-Escudero P, Hetz C, Vidal RL. Therapeutic potential of insulin-like growth factor 2 in Huntington's disease: controlling proteostasis to alleviate the load of misfolded protein. Neural Regen Res. 2021;16:1564-1565.

10. McAlary L, Yerbury JJ, Cashman NR. The prion-like nature of amyotrophic lateral sclerosis. Prog Mol Biol Transl Sci. 2020;175:261-296.

11. Cassard H, Huor A, Espinosa JC, Douet JY, Lugan S, Aron N *et al*. Prions from sporadic Creutzfeldt-Jakob disease patients propagate as strain mixtures. mBio. 2020;11:e00393-20.

12. Leighton PLA, Nadolski NJ, Morrill A, Hamilton TJ, Allison WT. An ancient conserved role for prion protein in learning and memory. Biol Open. 2018;7:bio025734.

13. Chen ZS, Huang X, Talbot K, Chan HYE. A fine balance between Prpf19 and Exoc7 in achieving degradation of aggregated protein and suppression of cell death in spinocerebellar ataxia type 3. Cell Death Dis. 2021;12:136.

14. Bednarska NG, van Eldere J, Gallardo R, Ganesan A, Ramakers M, Vogel I *et al*. Protein aggregation as an antibiotic design strategy. Mol Microbiol. 2016;99:849-865.

15. Van Gerven N., Van der Verren SE, Reiter DM, Remaut H. The role of functional amyloids in bacterial virulence. J Mol Biol. 2018;430:3657-3684.

16. Podrabsky JE, Carpenter JF, Hand SC. Survival of water stress in annual fish embryos: dehydration avoidance and egg envelope amyloid fibers. Am J Physiol Regul Integr Comp Physiol. 2001;280:R123-R131.

17. Tsiolaki PL, Louros NN, Iconomidou VA. Hexapeptide tandem repeats dictate the formation of silkmoth chorion, a natural protective amyloid. J Mol Biol. 2018;430:3774-3783.

18. Römer L, Scheibel T. The elaborate structure of spider silk: structure and function of a natural high performance fiber. Prion. 2008;2:154-161.

19. Maji SK, Perrin MH, Sawaya MR, Jessberger S, Vadodaria K, Rissman RA *et al*. Functional amyloids as natural storage of peptide hormones in pituitary secretory granules. Science. 2009;325:328-332.

20. Fowler DM, Koulov AV, Alory-Jost C, Marks MS, Balch WE, Kelly JW. Functional amyloid formation within mammalian tissue. PLoS Biol. 2006;4:e6.

21. Heinrich SU, Lindquist S. Protein-only mechanism induces self-perpetuating changes in the activity of neuronal *Aplysia* cytoplasmic polyadenylation element binding protein (CPEB). Proc Natl Acad Sci U S A. 2011;108:2999-3004.

22. Frugier M, Bour T, Ayach M, Santos MA, Rudinger-Thirion J, Theobald-Dietrich A *et al*. Low complexity regions behave as tRNA sponges to help co-translational folding of plasmodial proteins. FEBS Lett. 2010;584:448-454.

23. Verra F, Hughes AL. Biased amino acid composition in repeat regions of *Plasmodium* antigens. Mol Biol Evol. 1999;16:627-633.

24. Mok S, Ashley EA, Ferreira PE, Zhu L, Lin Z, Yeo T *et al*. Population transcriptomics of human malaria parasites reveals the mechanism of artemisinin resistance. Science. 2015;347:431-435.

25. Bridgford JL, Xie SC, Cobbold SA, Pasaje CF, Herrmann S, Yang T *et al*. Artemisinin kills malaria parasites by damaging proteins and inhibiting the proteasome. Nat Commun. 2018;9:3801.

26. Czesny B, Goshu S, Cook JL, Williamson KC. The proteasome inhibitor epoxomicin has potent *Plasmodium falciparum* gametocytocidal activity. Antimicrob Agents Chemother. 2009;53:4080-4085.

27. Aminake MN, Schoof S, Sologub L, Leubner M, Kirschner M, Arndt HD *et al*. Thiostrepton and derivatives exhibit antimalarial and gametocytocidal activity by dually targeting parasite proteasome and apicoplast. Antimicrob Agents Chemother. 2011;55:1338-1348.

28. Necula M, Breydo L, Milton S, Kayed R, van der Veer WE, Tone P *et al*. Methylene blue inhibits amyloid Ab oligomerization by promoting fibrillization. Biochemistry. 2007;46:8850-8860.

29. Yang F, Lim GP, Begum AN, Ubeda OJ, Simmons MR, Ambegaokar SS *et al*. Curcumin inhibits formation of amyloid b oligomers and fibrils, binds plaques, and reduces amyloid *in vivo*. J Biol Chem. 2005;280:5892-5901.

30. Espargaró A, Ginex T, Vadell MD, Busquets MA, Estelrich J, Muñoz-Torrero D *et al*. Combined *in vitro* cell-based/*in silico* screening of naturally occurring flavonoids and phenolic compounds as potential anti-Alzheimer drugs. J Nat Prod. 2017;80:278-289.

31. Georgieva D, Schwark D, von Bergen M, Redecke L, Genov N, Betzel C. Interactions of recombinant prions with compounds of therapeutical significance. Biochem Biophys Res Commun. 2006;344:463-470.

32. Murakami-Kubo I, Doh-Ura K, Ishikawa K, Kawatake S, Sasaki K, Kira J *et al*. Quinoline derivatives are therapeutic candidates for transmissible spongiform encephalopathies. J Virol. 2004;78:1281-1288.

33. Kocisko DA, Baron GS, Rubenstein R, Chen J, Kuizon S, Caughey B. New inhibitors of scrapie-associated prion protein formation in a library of 2000 drugs and natural products. J Virol. 2003;77:10288-10294.

34. Kocisko DA, Caughey B. Mefloquine, an antimalaria drug with antiprion activity *in vitro*, lacks activity *in vivo*. J Virol. 2006;80:1044-1046.

35. Korth C, May BC, Cohen FE, Prusiner SB. Acridine and phenothiazine derivatives as pharmacotherapeutics for prion disease. Proc Natl Acad Sci U S A. 2001;98:9836-9841.

36. Klingenstein R, Löber S, Kujala P, Godsave S, Leliveld SR, Gmeiner P *et al*. Tricyclic antidepressants, quinacrine and a novel, synthetic chimera thereof clear prions by destabilizing detergent-resistant membrane compartments. J Neurochem. 2006;98:748-759.

37. Doh-Ura K, Iwaki T, Caughey B. Lysosomotropic agents and cysteine protease inhibitors inhibit scrapie-associated prion protein accumulation. J Virol. 2000;74:4894-4897.

38. Park S, Kim HY, Oh HA, Shin J, Park IW, Yoon S *et al*. Quinacrine directly dissociates amyloid plaques in the brain of 5XFAD transgenic mouse model of Alzheimer's disease. Sci Rep. 2021;11:12043.

39. Sola I, Castellà S, Viayna E, Galdeano C, Taylor MC, Gbedema SY *et al*. Synthesis, biological profiling and mechanistic studies of 4-aminoquinoline-based heterodimeric compounds with dual trypanocidal-antiplasmodial activity. Bioorg Med Chem. 2015;23:5156-5167.

40. Espargaró A, Pont C, Gamez P, Muñoz-Torrero D, Sabate R. Amyloid pan-inhibitors: one family of compounds to cope with all conformational diseases. ACS Chem Neurosci. 2019;10:1311-1317.

41. Martínez-Flórez A, Galizzi M, Izquierdo L, Bustamante JM, Rodriguez A, Rodriguez F *et al*. Repurposing bioenergetic modulators against protozoan parasites responsible for tropical diseases. Int J Parasitol Drugs Drug Resist. 2020;14:17-27.

42. Ravikumar B, Duden R, Rubinsztein DC. Aggregate-prone proteins with polyglutamine and polyalanine expansions are degraded by autophagy. Hum Mol Genet. 2002;11:1107-1117.

43. King MA, Hands S, Hafiz F, Mizushima N, Tolkovsky AM, Wyttenbach A. Rapamycin inhibits polyglutamine aggregation independently of autophagy by reducing protein synthesis. Mol Pharmacol. 2008;73:1052-1063.

44. Wyttenbach A, Hands S, King MA, Lipkow K, Tolkovsky AM. Amelioration of protein misfolding disease by rapamycin: translation or autophagy? Autophagy. 2008;4:542-545.

45. Sannella AR, Messori L, Casini A, Francesco VF, Bilia AR, Majori G *et al*. Antimalarial properties of green tea. Biochem Biophys Res Commun. 2007;353:177-181.

46. Chandrashekaran IR, Adda CG, MacRaild CA, Anders RF, Norton RS. EGCG disaggregates amyloid-like fibrils formed by *Plasmodium falciparum* merozoite surface protein 2. Arch Biochem Biophys. 2011;513:153-157.

47. Jarrett JT, Lansbury PT, Jr. Seeding "one-dimensional crystallization" of amyloid: a pathogenic mechanism in Alzheimer's disease and scrapie? Cell. 1993;73:1055-1058.

48. Krebs MR, Morozova-Roche LA, Daniel K, Robinson CV, Dobson CM. Observation of sequence specificity in the seeding of protein amyloid fibrils. Protein Sci. 2004;13:1933-1938.

49. Ruseska I, Zimmer A. Internalization mechanisms of cell-penetrating peptides. Beilstein J Nanotechnol. 2020;11:101-123.

50. Xu J, Khan AR, Fu M, Wang R, Ji J, Zhai G. Cell-penetrating peptide: a means of breaking through the physiological barriers of different tissues and organs. J Control Release. 2019;309:106-124.

51. Kauffman WB, Fuselier T, He J, Wimley WC. Mechanism matters: a taxonomy of cell penetrating peptides. Trends Biochem Sci. 2015;40:749-764.

52. Goodyer ID, Pouvelle B, Schneider TG, Trelka DP, Taraschi TF. Characterization of macromolecular transport pathways in malaria-infected erythrocytes. Mol Biochem Parasitol. 1997;87:13-28.

53. Govindarajalu G, Rizvi Z, Kumar D, Sijwali PS. Lyse-reseal erythrocytes for transfection of *Plasmodium falciparum*. Sci Rep. 2019;9:19952.

54. Maurer-Stroh S, Debulpaep M, Kuemmerer N, Lopez dlP, Martins IC, Reumers J *et al*. Exploring the sequence determinants of amyloid structure using position-specific scoring matrices. Nat Methods. 2010;7:237-242.

55. Ventura S, Zurdo J, Narayanan S, Parreño M, Mangues R, Reif B *et al*. Short amino acid stretches can mediate amyloid formation in globular proteins: the Src homology 3 (SH3) case. Proc Natl Acad Sci U S A. 2004;101:7258-7263.

56. Patton WF, Yarmoluk SM, Pande P, Kovalska V, Dai L, Volkova K *et al*.. Dyes for Analysis of Protein Aggregation. PCT/US20 10/003061[WO2011/065980 A2]. 3-6-2011. 30-11-2010.

57. Johnston HE, Samant RS. Alternative systems for misfolded protein clearance: life beyond the proteasome. FEBS J. 2021;288:4464-4487.

58. Bell A. Antimalarial drug synergism and antagonism: mechanistic and clinical significance. FEMS Microbiol Lett. 2005;253:171-184.

59. Stokes BH, Dhingra SK, Rubiano K, Mok S, Straimer J, Gnädig NF *et al*. *Plasmodium falciparum* K13 mutations in Africa and Asia impact artemisinin resistance and parasite fitness. eLife. 2021;10.

60. Alonso PL, Brown G, Arevalo-Herrera M, Binka F, Chitnis C, Collins F *et al*. A research agenda to underpin malaria eradication. PLoS Med. 2011;8:e1000406.

61. Delves MJ, Ramakrishnan C, Blagborough AM, Leroy D, Wells TNC, Sinden RE. A high-throughput assay for the identification of malarial transmission-blocking drugs and vaccines. Int J Parasitol. 2012;42:999-1006.

62. Delves MJ. *Plasmodium* cell biology should inform strategies used in the development of antimalarial transmission-blocking drugs. Future Med Chem. 2012;4:2251-2263.

63. Recht J, Ashley EA, White NJ. Use of primaquine and glucose-6-phosphate dehydrogenase deficiency testing: divergent policies and practices in malaria endemic countries. PLoS Negl Trop Dis. 2018;12:e0006230.

64. Menard D, Dondorp A. Antimalarial drug resistance: a threat to malaria elimination. Cold Spring Harb Perspect Med. 2017;7:a025619.

65. Muralidharan V, Oksman A, Pal P, Lindquist S, Goldberg DE. *Plasmodium falciparum* heat shock protein 110 stabilizes the asparagine repeat-rich parasite proteome during malarial fevers. Nat Commun. 2012;3:1310.

66. Jain J, Jain SK, Walker LA, Tekwani BL. Inhibitors of ubiquitin E3 ligase as potential new antimalarial drug leads. BMC Pharmacol Toxicol. 2017;18:40.

67. Kim J, Tan YZ, Wicht KJ, Erramilli SK, Dhingra SK, Okombo J *et al*. Structure and drug resistance of the *Plasmodium falciparum* transporter PfCRT. Nature. 2019;576:315-320.

68. Green JL, Wu Y, Encheva V, Lasonder E, Prommaban A, Kunzelmann S *et al*. Ubiquitin activation is essential for schizont maturation in *Plasmodium falciparum* blood-stage development. PLoS Pathog. 2020;16:e1008640.

69. Xu J, Zhao C, Huang X, Du W. Regulation of artemisinin and its derivatives on the assembly behavior and cytotoxicity of amyloid polypeptides hIAPP and Ab. ACS Chem Neurosci. 2019;10:4522-4534.

70. Bao Q, Luo Y, Li W, Sun X, Zhu C, Li P *et al*. The mechanism for heme to prevent Ab(1-40) aggregation and its cytotoxicity. J Biol Inorg Chem. 2011;16:809-816.

71. Phyo AP, Ashley EA, Anderson TJC, Bozdech Z, Carrara VI, Sriprawat K *et al*. Declining efficacy of artemisinin combination therapy against *P. falciparum* malaria on the Thai-Myanmar border (2003-2013): the role of parasite genetic factors. Clin Infect Dis. 2016;63:784-791.

72. Uwimana A, Legrand E, Stokes BH, Ndikumana JM, Warsame M, Umulisa N *et al*. Emergence and clonal expansion of *in vitro* artemisinin-resistant *Plasmodium falciparum kelch13* R561H mutant parasites in Rwanda. Nat Med. 2020;26:1602-1608.

73. Mathieu LC, Cox H, Early AM, Mok S, Lazrek Y, Paquet JC *et al*. Local emergence in Amazonia of *Plasmodium falciparum k13* C580Y mutants associated with *in vitro* artemisinin resistance. eLife. 2020;9:e51015.

74. Travassos LH, Vasconcellos LR, Bozza MT, Carneiro LA. Heme and iron induce protein aggregation. Autophagy. 2017;13:625-626.

75. Vasconcellos LR, Dutra FF, Siqueira MS, Paula-Neto HA, Dahan J, Kiarely E *et al*. Protein aggregation as a cellular response to oxidative stress induced by heme and iron. Proc Natl Acad Sci U S A. 2016;113:E7474-E7482.

76. Ye J, Liu E, Gong J, Wang J, Huang Y, He H *et al*. High-yield synthesis of monomeric LMWP(CPP)-siRNA covalent conjugate for effective cytosolic delivery of siRNA. Theranostics. 2017;7:2495-2508.

77. He J, Kauffman WB, Fuselier T, Naveen SK, Voss TG, Hristova K *et al*. Direct cytosolic delivery of polar cargo to cells by spontaneous membrane-translocating peptides. J Biol Chem. 2013;288:29974-29986.

78. Lambros C, Vanderberg JP. Synchronization of *Plasmodium falciparum* erythrocytic stages in culture. J Parasitol. 1979;65:418-420.

79. Fivelman QL, Adagu IS, Warhurst DC. Modified fixed-ratio isobologram method for studying *in vitro* interactions between atovaquone and proguanil or

dihydroartemisinin against drug-resistant strains of *Plasmodium falciparum*. Antimicrob Agents Chemother. 2004;48:4097-4102.

80. Radfar A, Méndez D, Moneriz C, Linares M, Marín-García P, Puyet A *et al*. Synchronous culture of *Plasmodium falciparum* at high parasitemia levels. Nat Protoc. 2009;4:1899-1915.

81. Manders EMM, Verbeek FJ, Aten JA. Measurement of co-localization of objects in dual-colour confocal images. J Microsc. 1993;169:375-382.

82. Bolte S, Cordelières FP. A guided tour into subcellular colocalization analysis in light microscopy. J Microsc. 2006;224:213-232.

83. Schindelin J, Arganda-Carreras I, Frise E, Kaynig V, Longair M, Pietzsch T *et al*. Fiji: an open-source platform for biological-image analysis. Nat Methods. 2012;9:676-682.

84. Avalos-Padilla Y, Georgiev VN, Lantero E, Pujals S, Verhoef R, Borgheti-Cardoso LN *et al*. The ESCRT-III machinery participates in the production of extracellular vesicles and protein export during *Plasmodium falciparum* infection. PLoS Pathog. 2021;17:e1009455.

85. Rohde F, Braumann UD, Schmidt M. Correlia: an ImageJ plug-in to co-register and visualise multimodal correlative micrographs. J Microsc. 2020;280:3-11.

86. Herraiz T, Guillén H, González-Peña D, Arán VJ. Antimalarial quinoline drugs inhibit b-hematin and increase free hemin catalyzing peroxidative reactions and inhibition of cysteine proteases. Sci Rep. 2019;9:15398.

87. Huy NT, Uyen DT, Sasai M, Trang DT, Shiono T, Harada S *et al*. A simple and rapid colorimetric method to measure hemozoin crystal growth *in vitro*. Anal Biochem. 2006;354:305-307.

88. Portugaliza HP, Llorà-Batlle O, Rosanas-Urgell A, Cortés A. Reporter lines based on the *gexp02* promoter enable early quantification of sexual conversion rates in the malaria parasite *Plasmodium falciparum*. Sci Rep. 2019;9:14595.

89. Ploemen IH, Prudêncio M, Douradinha BG, Ramesar J, Fonager J, van Gemert G-J *et al*. Visualisation and quantitative analysis of the rodent malaria liver stage by real time imaging. PLoS ONE. 2009;4:e7881.

90. Carija A, Pinheiro F, Iglesias V, Ventura S. Computational assessment of bacterial protein structures indicates a selection against aggregation. Cells. 2019;8:856.

91. Wang M, Weiss M, Simonovic M, Haertinger G, Schrimpf SP, Hengartner MO *et al*. PaxDb, a database of protein abundance averages across all three domains of life. Mol Cell Proteomics. 2012;11:492-500.

92. Fernandez-Escamilla AM, Rousseau F, Schymkowitz J, Serrano L. Prediction of sequence-dependent and mutational effects on the aggregation of peptides and proteins. Nat Biotechnol. 2004;22:1302-1306.

93. Viayna E, Sola I, Bartolini M, De Simone A., Tapia-Rojas C, Serrano FG *et al*. Synthesis and multitarget biological profiling of a novel family of rhein derivatives as disease-modifying anti-Alzheimer agents. J Med Chem. 2014;57:2549-2567.

Declarations

Acknowledgments

We are grateful to Prof. Alfred Cortés for the donation of the *P. falciparum* strain used in gametocyte assays, and to Prof. David A. Fidock for the donation of artemisinin-resistant lines. ISGlobal and IBEC are members of the CERCA Programme, *Generalitat de Catalunya*. We acknowledge support from the Spanish Ministry of Science, Innovation and Universities through the *"Centro de Excelencia Severo Ochoa 2019-2023"* Program (CEX2018-000806-S). This research is part of ISGlobal's Program on the Molecular Mechanisms of Malaria which is partially supported by the *Fundación Ramón Areces*.

Consent for publication

Not applicable.

Funding

This work was supported by grants PCIN-2017-100, RTI2018-094579-B-I00 and PID2021-128325OB-I00 (XF-B), and SAF2017-82771-R and PID2020-118127RB-I00 (DM-T), funded by *Ministerio de Ciencia e Innovación/Agencia Estatal de Investigación* (MCIN/AEI/ 10.13039/501100011033), which included FEDER funds; (ii) ERA-NET Cofund EURONANOMED (http://euronanomed.net/), grant number 2017-178 (XF-B); and (iii) *Generalitat de Catalunya*, Spain (http://agaur.gencat.cat/), grant numbers 2017-SGR-908 (XF-B) and 2017-SGR-106 (DM-T). Work at Pompeu Fabra University was supported by the "La Caixa" Banking Foundation (https://fundacionlacaixa.org/, grant HR17-00409), and by grant AGL2017-84097-C2-2-R and the "María de Maeztu" Program for Units of Excellence in R&D from the Spanish Ministry of Science, Innovation and Universities. The funders had no role in study design, data collection and analysis, decision to publish, or preparation of the manuscript.

Availability of data and materials

All data generated or analysed during this study are included in this published article and its supplementary information files.

Authors' contributions

XF-B conceptualized the research. IB-A performed the experiments. JV synthesized peptides. EMA synthesized YAT2150. OC-P performed Western and dot blots. LR-A performed aggregative peptide assays. YA-P performed confocal fluorescence microscopy analysis. DM performed hepatic stage assays. IB-A, AB, DA, DM-T, MP and XF-B provided methodology. DA, DM-T, MP and XF-B supervised the work. XF-

B and IB-A wrote the original draft, which was reviewed and edited by all authors. All authors read and approved the final manuscript.

Competing interests

A patent application (EP21382949.2) has been filed to protect some of the results presented in the paper, which includes as inventors IB-A, AB, DM-T and XF-B. All other authors declare they have no competing interests.

Ethics approval and consent to participate

The human blood used in this work was from voluntary donors and commercially obtained from the *Banc de Sang i Teixits* (www.bancsang.net). Blood was not collected specifically for this research; the purchased units had been discarded for transfusion, usually because of an excess of blood relative to anticoagulant solution. Prior to their use, blood units underwent the analytical checks specified in the current legislation. Before being delivered to us, unit data were anonymized and irreversibly dissociated, and any identification tag or label had been removed in order to guarantee the non-identification of the blood donor. No blood data were or will be supplied, in accordance with the current Spanish *Ley Orgánica de Protección de Datos* and *Ley de Investigación Biomédica*. The blood samples will not be used for studies other than those made explicit in this research.

For *in vivo* assays, in the presence of toxic effects including, among others, >20% reduction in weight, aggressive and unexpected animal behavior or the presence of blood in feces, animals were immediately anesthetized using a 100 mg/kg ketamine plus 10 mg/kg xylazine mixture and sacrificed by cervical dislocation. The PCB animal facility has the relevant authorizations as approved establishment of breeding, supplier

and user (B9900044 and REGA code: ES080190036527) to work with vertebrate animals used for experimental and scientific purposes. The animal care and use protocols followed adhered to the specific national and international guidelines in accordance with the current Catalan (D 214/1997/GC) and Spanish laws (RD 53/2013; order ECC/566/2015) and the corresponding European Directive (2010/63 EU).

Figures and Tables

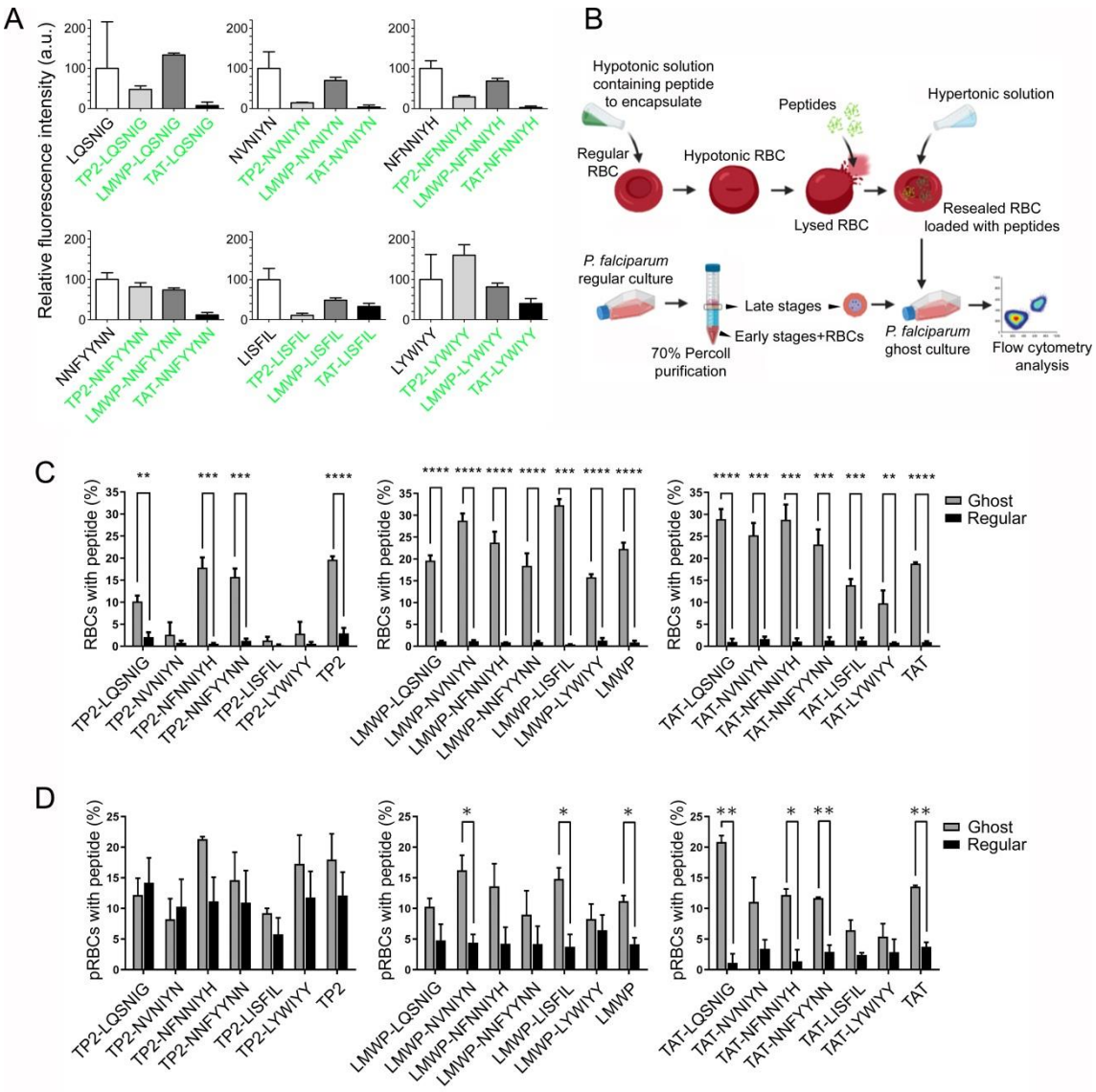

Fig. 1. Loading of aggregative peptides into ghost RBCs. (**A**) ProteoStat® *in vitro* aggregation assay of aggregative peptides conjugated to fluorescein-labeled CPPs. The control normalized to 100% aggregation corresponds to the unconjugated, fluorescein-free aggregative peptides. a.u.: arbitrary units. Graphs show the mean ± SEM of three independent experiments. (**B**) Scheme of peptide loading into *P. falciparum* ghosts. (**C**,**D**) Flow cytometry analysis of the targeting of fluorescein-labeled CPP-conjugated aggregative peptides in ghost and regular RBC suspensions. (**C**) Fraction of RBCs positive for fluorescein-labeled peptides. (**D**) Colocalization analysis of *Plasmodium* and fluorescein-labeled peptides 72 h post-infection. The parasitemias achieved in all cases were within the expected values for regular *P. falciparum* cultures. Bars represent the means ± SEM of at least two independent experiments where 30,000 events were recorded in the flow cytometer. *: $p \leq 0.05$; **: $p \leq 0.01$; ***: $p \leq 0.001$; ****: $p \leq 0.0001$.

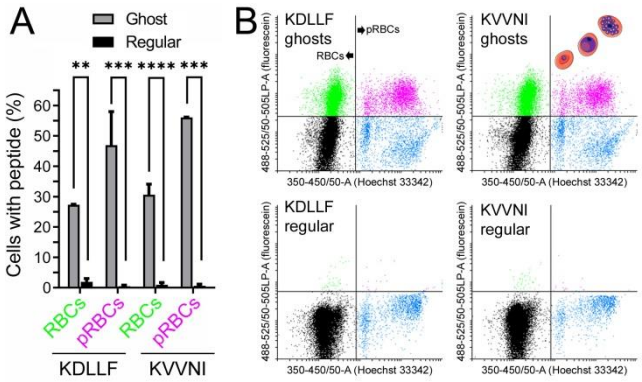

Fig. 2. Flow cytometry analysis of the presence of the fluorescein-labeled peptides KDLLF and KVVNI in ghost RBCs. (**A**) Bar graph of the aggregated data. Bars represent the means ± SEM of at least two independent experiments where 30,000 events were recorded in the flow cytometer. **: $p \leq 0.01$; ***: $p \leq 0.001$; ****: $p \leq 0.0001$. (**B**) Representative examples of flow cytometry plots to illustrate for both peptides their presence inside ghost vs. regular RBCs and pRBCs. The cartoons in the upper right plot roughly indicate from left to right the cell populations corresponding to ring, trophozoite and schizont forms.

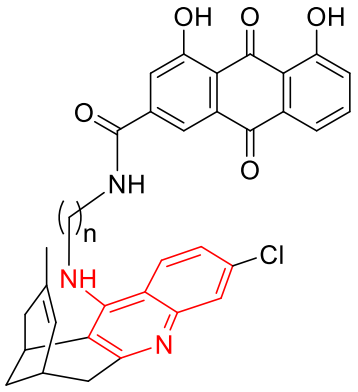

HUP5ANTRA, n = 5
HUP7ANTRA, n = 7
HUP10ANTRA, n = 10

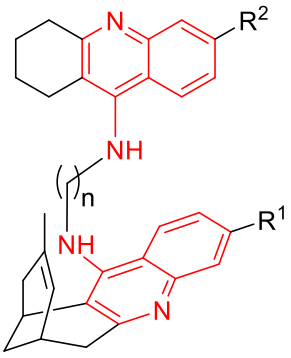

HUP7TH, n = 7, R^1 = Cl, R^2 = H
HUP8TH, n = 8, R^1 = Cl, R^2 = H
HUP9TH, n = 9, R^1 = Cl, R^2 = H
HUPH10TH, n = 10, R^1 = R^2 = H

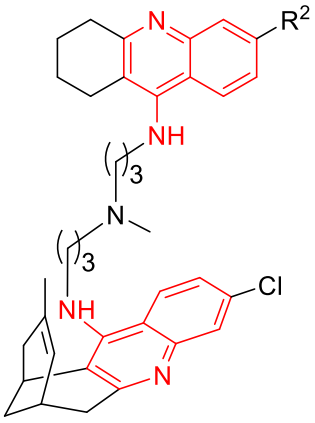

HUPNTH, R^2 = H
HUPNTCl, R^2 = Cl

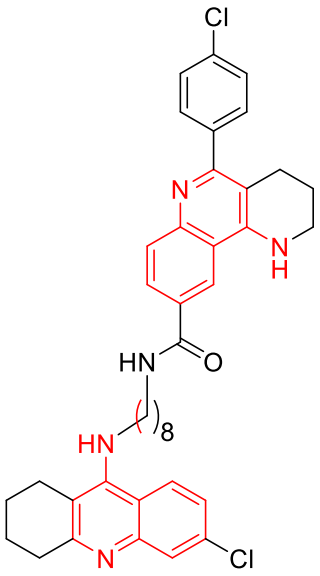

DP128

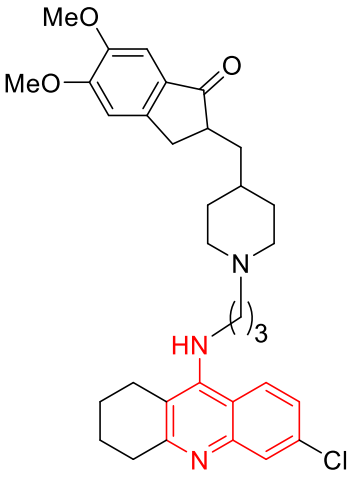

DONE3TCl

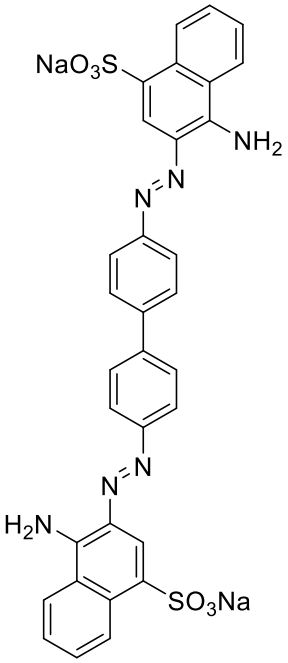

Congo Red

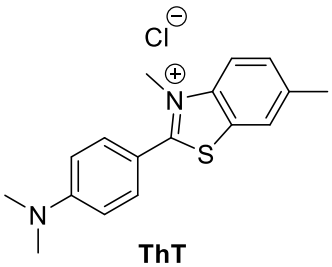

ThT

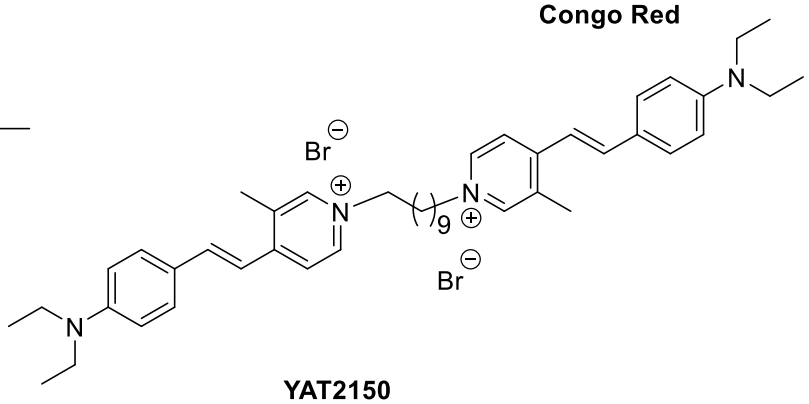

YAT2150

Fig. 3. Chemical structures of amyloid pan-inhibitors and β-sheet intercalators that were tested for *in vitro* antimalarial activity. The 4-aminoquinoline scaffold that is present in amyloid pan-inhibitors is colored in red.

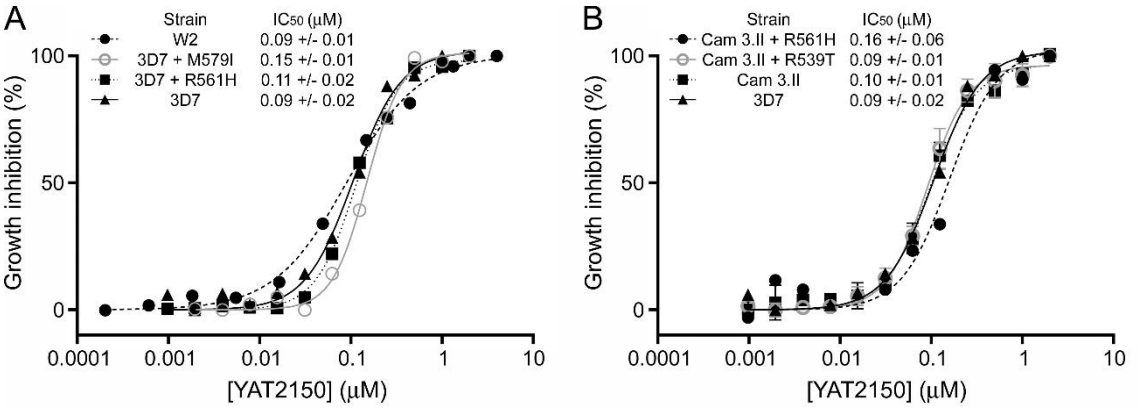

Fig. 4. YAT2150 *in vitro* growth inhibition assays in chloroquine- and artemisinin-resistant strains. (**A**) Chloroquine-resistant W2 strain and artemisinin-resistant M579I and R561H strains compared to parental 3D7 and (**B**) artemisinin-resistant R561H and R539T strains compared to parental Cam 3.II and to 3D7. In both panels means ± SD are shown.

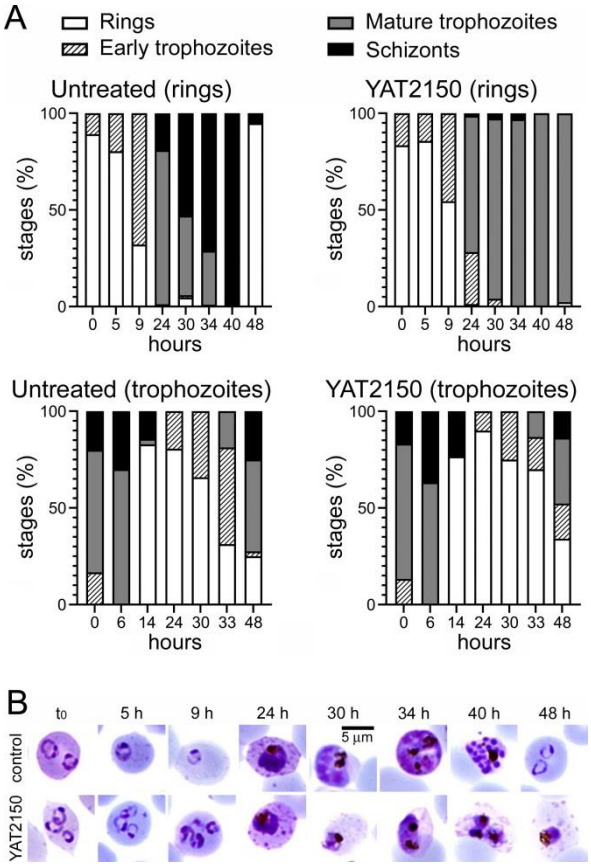

Fig. 5. Stage of growth inhibition of *P. falciparum* during 48 h of 200 nM YAT2150 treatment. The drug was added to synchronized parasite cultures at the ring or trophozoite stages. Giemsa-stained blood smears were prepared at the indicated time points between 0 and 48 h of incubation, and the numbers of ring stages, early trophozoites, late trophozoites and schizonts were counted in samples of at least 100 pRBCs for each time point. (**A**) Bars indicate the percentages of developmental stages present in the respective blood smears. (**B**) Representative images of pRBCs in the assay where YAT2150 was added at ring stage.

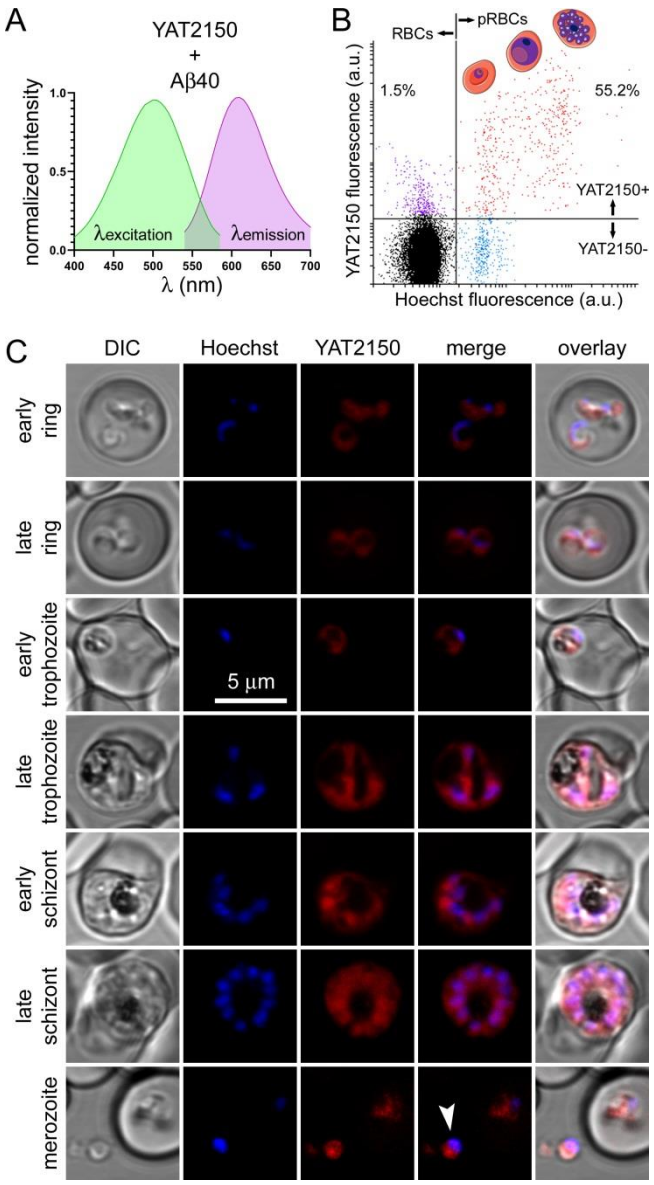

Fig. 6. Cellular and subcellular targeting of YAT2150. (**A**) Absorbance and emission spectra of YAT2150 in the presence of Aβ40. (**B**) Flow cytometry analysis of a YAT2150-stained desynchronized *P. falciparum* culture where 30,000 events were recorded. The fraction of YAT2150-positive RBCs and pRBCs is indicated (%), the latter consisting of late rings, trophozoites and schizonts, the three stages represented in the cartoons. (**C**) Confocal fluorescence microscopy examination of *P. falciparum* blood stages. The arrowhead indicates an individual merozoite. DIC: differential interference contrast image.

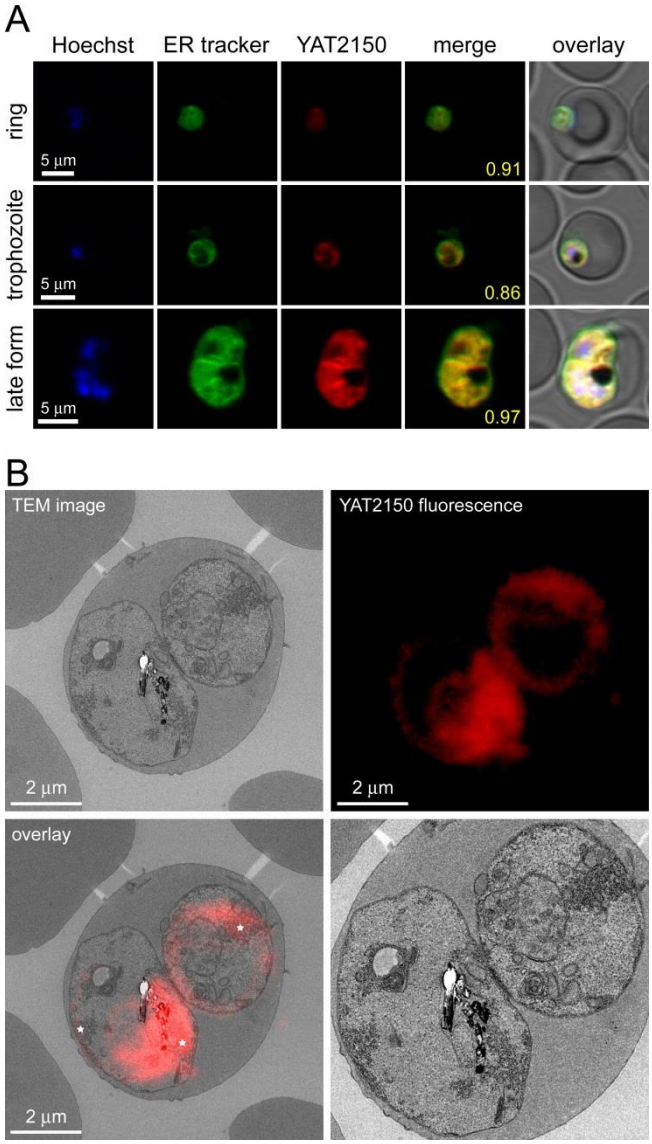

Fig. 7. Subcellular localization of YAT2150 in pRBCs. (**A**) Confocal fluorescence microscopy colocalization analysis in different *P. falciparum* blood stages of YAT2150 with the cytosolic marker ER Tracker™ Green. The merge images correspond to red (YAT2150) and green (ER Tracker) channels only. Manders' overlap correlation coefficients are indicated in yellow digits. (**B**) Correlative light and electron microscopy analysis. The stars in the overlay image indicate three ER regions. The blown up micrograph in the lower right panel is included for a better identification of subcellular structures.

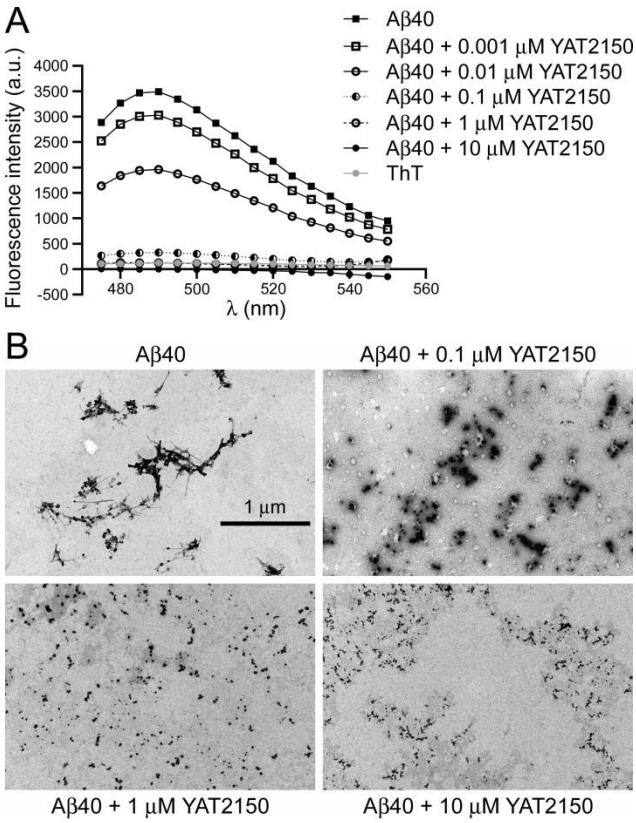

Fig. 8. Effect of YAT2150 on the *in vitro* aggregation of Aβ40. (**A**) ThT fluorescence assay. The mean fluorescence intensity value of each sample in each wavelength is represented. a.u.: arbitrary units. (**B**) TEM analysis.

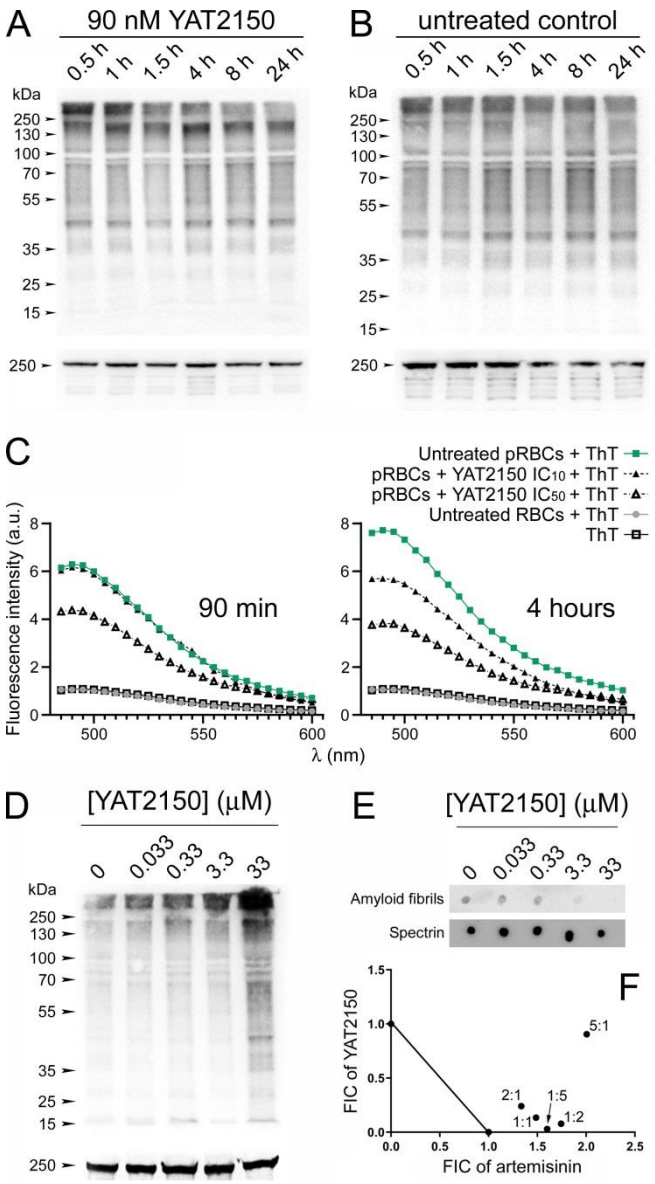

Fig. 9. Analysis of the effect of YAT2150 on markers of protein aggregation in live *P. falciparum* cultures. (**A**,**B**) Western blot assays for the detection of ubiquitinated proteins in cultures treated for 0.5 to 24 h with 90 nM YAT2150. Panel B corresponds to an untreated control. Anti-spectrin antibody is used as loading control shown at the bottom of each gel. (**C**) ThT fluorescence of *P. falciparum* culture extracts normalized to have equal protein content, either non-treated or treated with YAT2150 at its *in vitro* IC_{10} (27 nM) and IC_{50} (90 nM), for 90 min and 4 h. A non-parasitized RBC protein extract is shown as reference. The mean fluorescence intensity value of each sample in each wavelength is represented. (**D**) Western blot assays for the detection of

ubiquitinated proteins in cultures treated for 90 min with different concentrations of YAT2150. (**E**) Dot blot assay of the same samples from panel **D** using an antibody against amyloid fibrils. (**F**) Isobologram of the interaction between YAT2150 (Y) and artemisinin (A) at different Y:A ratios.

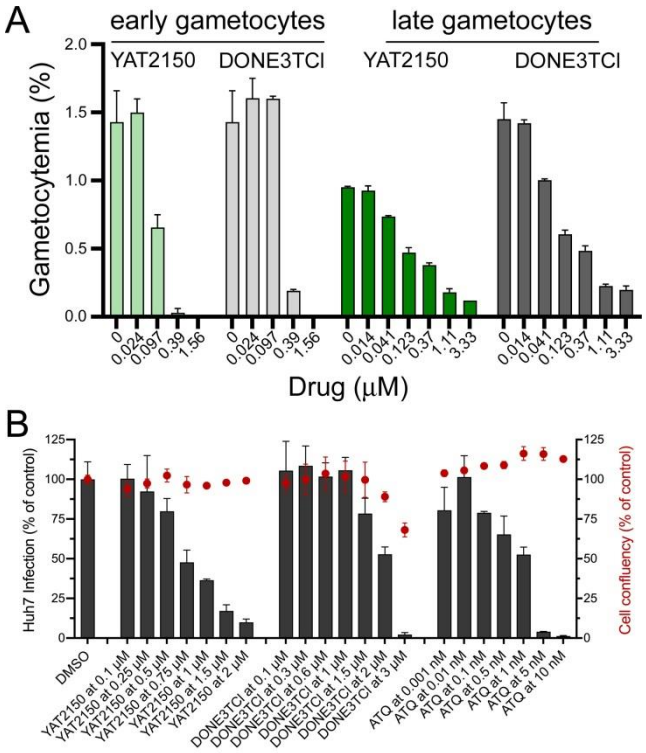

Fig. 10. *In vitro* activity of YAT2150 and DONE3TCl on *Plasmodium* gametocytes and liver stages. (**A**) Effect of the drugs on *P. falciparum* early and late gametocytes. Bars represent mean ± SD of two independent experiments. (**B**) Dose-dependent response of YAT2150, DONE3TCl and atovaquone (ATQ) against the hepatic stage of *P. berghei* infection. Total parasite load (infection scale, bars) and cell viability (cell confluency scale, red dots) are shown. Plot shows mean ± SD of three independent experiments. Results were normalized to DMSO and are represented as mean ± SD. Reference drug is atovaquone (IC_{50} = 1.63 ± 0.27 nM).

Table 1. Growth inhibition assay in the *P. falciparum* cultures done in ghost RBC preparations treated with 10 μM fluorescein-labeled aggregative peptides conjugated to CPPs from Fig. 1D.

Peptide sequence	Parasite growth relative to untreated control (%) ± SEM	*p*-value[1]
TAT	100 ± 0.9	>0.9999
TAT-LQSNIG	100.0 ± 17.5	>0.9999
TAT-NVNIYN	99.7 ± 5.2	0.9580
TAT-NFNNIYH	100.0 ± 10.8	>0.9999
TAT-NNFYYNN	100.0 ± 6.1	>0.9999
TAT-LISFIL	95.5 ± 6.4	0.5572
TAT-LYWIYY	100.0 ± 5.9	>0.9999
TP2	100 ± 9.5	>0.9999
TP2-LQSNIG	100.0 ± 4.2	>0.9999
TP2-NVNIYN	100.0 ± 12.0	>0.9999
TP2-NFNNIYH	100.0 ± 7.3	>0.9999
TP2-NNFYYNN	96.2 ± 0.3	0.7000
TP2-LISFIL	98.5 ± 0.5	0.0835
TP2-LYWIYY	84.9 ± 3.0	0.0374*
LMWP	90.9 ± 1.1	0.3430
LMWP-LQSNIG	75.2 ± 3.4	0.0188*
LMWP-NVNIYN	81.9 ± 10.1	0.2152
LMWP-NFNNIYH	66.2 ± 6.5	0.0349*
LMWP-NNFYYNN	73.6 ± 12.4	0.1665
LMWP-LISFIL	79.4 ± 9.3	0.1561
LMWP-LYWIYY	86.3 ± 6.4	0.1653

[1] *p*-value obtained applying two sided Student's *t* test in GraphPad Prism. *: $p \leq 0.05$.

Table 2. *In vitro* antiplasmodial activity in *P. falciparum* cultures of amyloid pan-inhibitors and β-sheet intercalators.

Compound	Chemical family	IC_{50} in 3D7 strain (μM) ± SEM	IC_{50} in K1 strain (μM) ± SEM	Selectivity index *in vitro*[1]
HUP5ANTRA†	aminoquinoline	0.78 ± 1.86	N/D	97.7
HUP7ANTRA†	aminoquinoline	7.53 ± 0.84	N/D	3.9
HUP10ANTRA†	aminoquinoline	8.73 ± 1.61	N/D	9.7
HUP7TH	aminoquinoline	0.13 ± 0.01	0.47 ± 0.36‡	60.0
HUP8TH	aminoquinoline	0.21 ± 0.01	0.39 ± 0.14‡	23.3
HUP9TH	aminoquinoline	0.16 ± 0.02	0.35 ± 0.06‡	30.6
HUPH10TH	aminoquinoline	0.18 ± 0.05	3.50 ± 2.29‡	18.9
HUPNTH	aminoquinoline	0.31 ± 0.02	0.43 ± 0.22‡	11.0
HUPNTCl	aminoquinoline	0.15 ± 0.01	0.52 ± 0.13‡	42.0
DP128§	aminoquinoline	0.65 ± 0.14	N/D	75.4
DONE3TCl	aminoquinoline	0.08 ± 0.03	0.36 ± 0.07§	157.5
YAT2150	bis(styrylpyridinium) salt	0.09 ± 0.02	N/D	37.8
ThT	benzothiazolium salt	1.57 ± 0.23	N/D	N/D
Congo Red	bis(naphthalenesulfonate)	>15	N/D	N/D

[1] 50% cytotoxic concentration (CC_{50})/IC_{50} in 3D7 strain. See Additional file 1: Table S9 for CC_{50} values.

† [93]

‡ [39]

§ [40]

N/D: no data.

Supporting Information for

The protein aggregation inhibitor YAT2150 has potent antimalarial activity in *Plasmodium falciparum in vitro* cultures

Inés Bouzón-Arnáiz, Yunuen Avalos-Padilla, Arnau Biosca, Omar Caño-Prades, Lucía Román-Álamo, Javier Valle, David Andreu, Diana Moita, Miguel Prudêncio, Elsa M. Arce, Diego Muñoz-Torrero, Xavier Fernàndez-Busquets*

*Corresponding author. Email: xfernandez_busquets@ub.edu

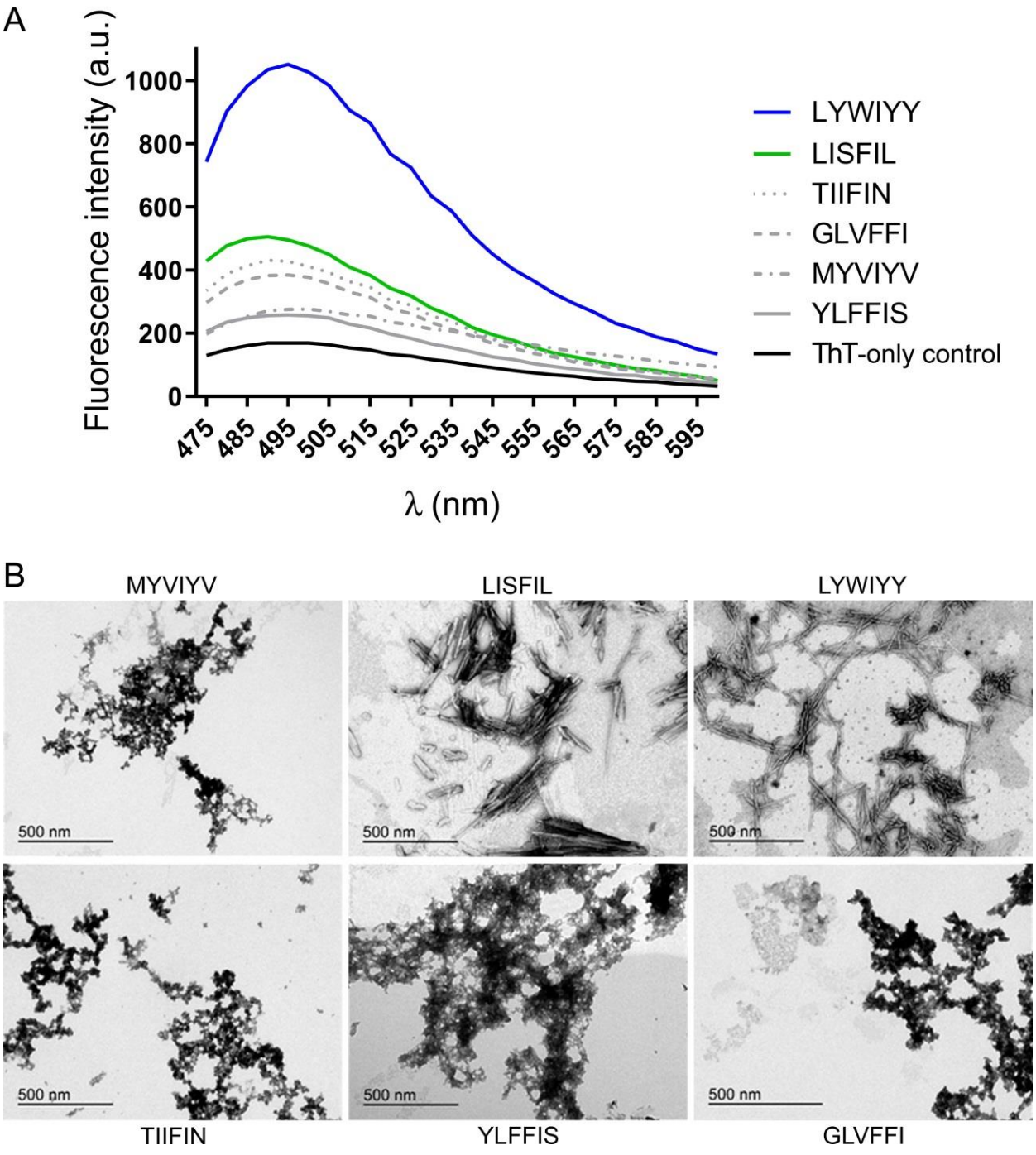

Figure S1. Analysis of the aggregation of six peptides present in *P. falciparum* proteins. (**A**) Thioflavin T fluorescence analysis. a.u.: arbitrary units. The mean fluorescence intensity value of each sample in each wavelength is represented. (**B**) Transmission electron microscopy analysis.

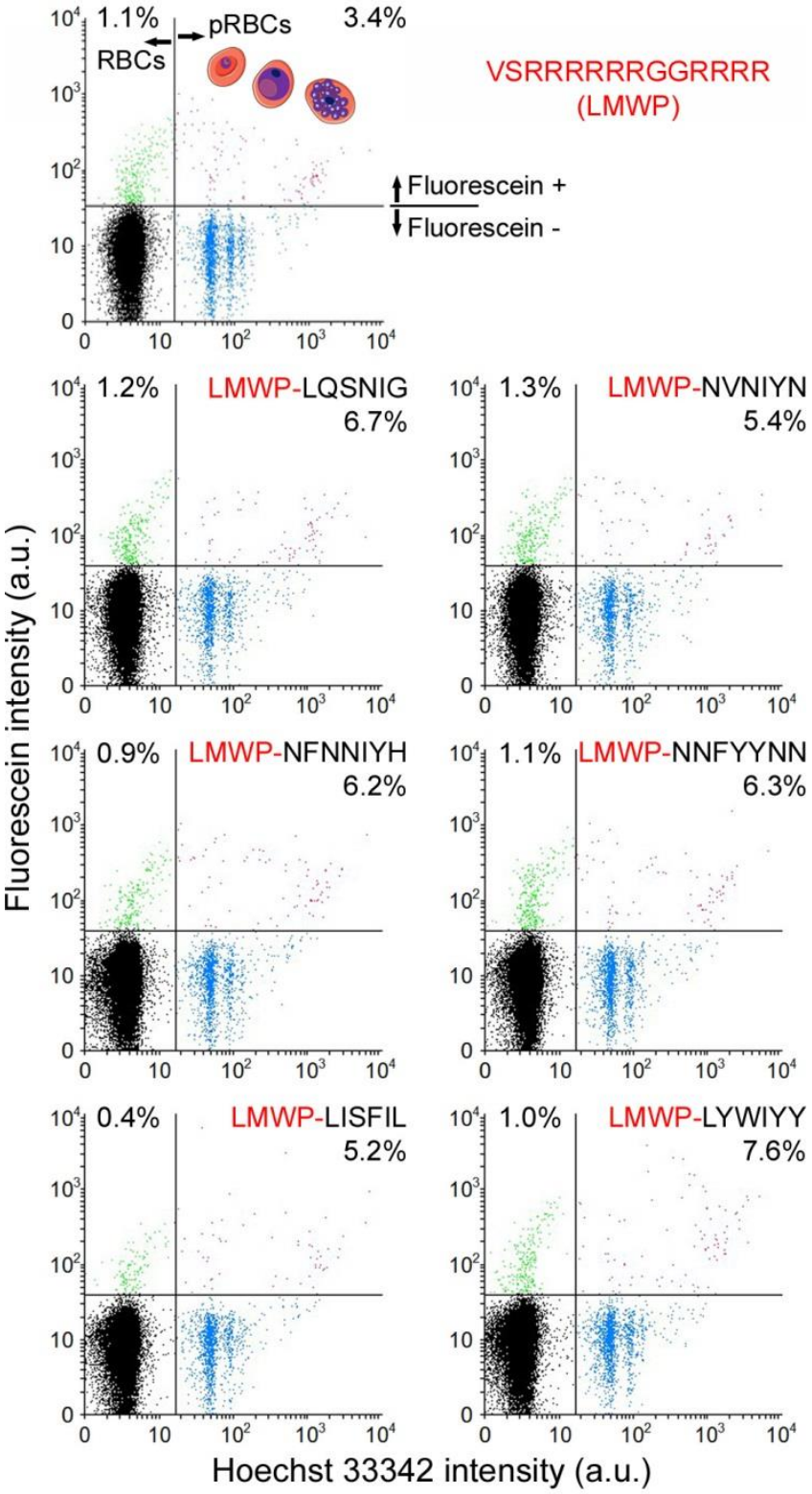

Figure S2. Flow cytometry analysis of the colocalization with RBCs and pRBCs of fluorescein-labeled LMWP-conjugated peptides. Percentages indicate the proportion of RBCs and pRBCs positive for fluorescein. a.u.: arbitrary units.

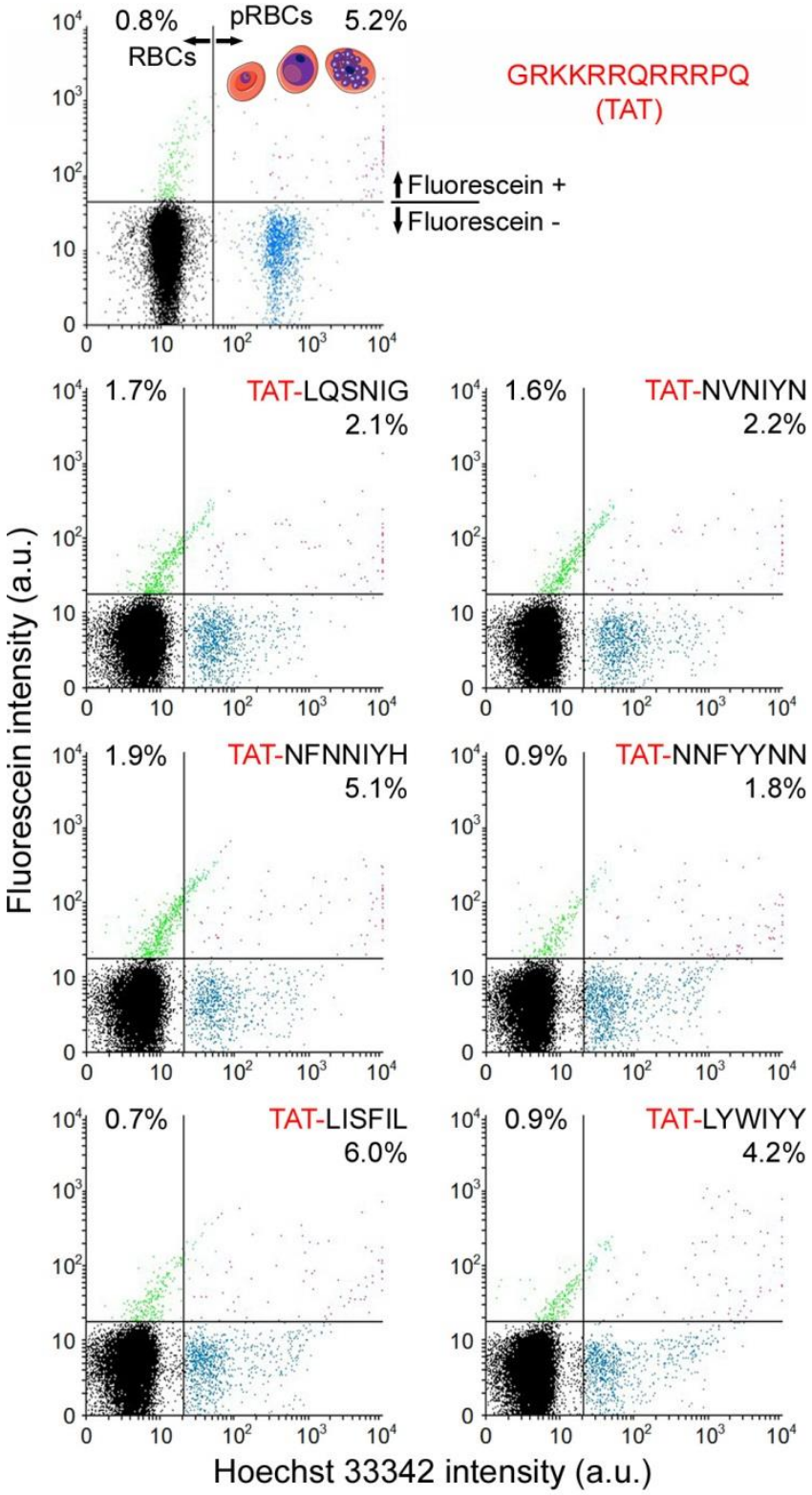

Figure S3. Flow cytometry analysis of the colocalization with RBCs and pRBCs of fluorescein-labeled TAT-conjugated peptides. Percentages indicate the proportion of RBCs and pRBCs positive for fluorescein. a.u.: arbitrary units.

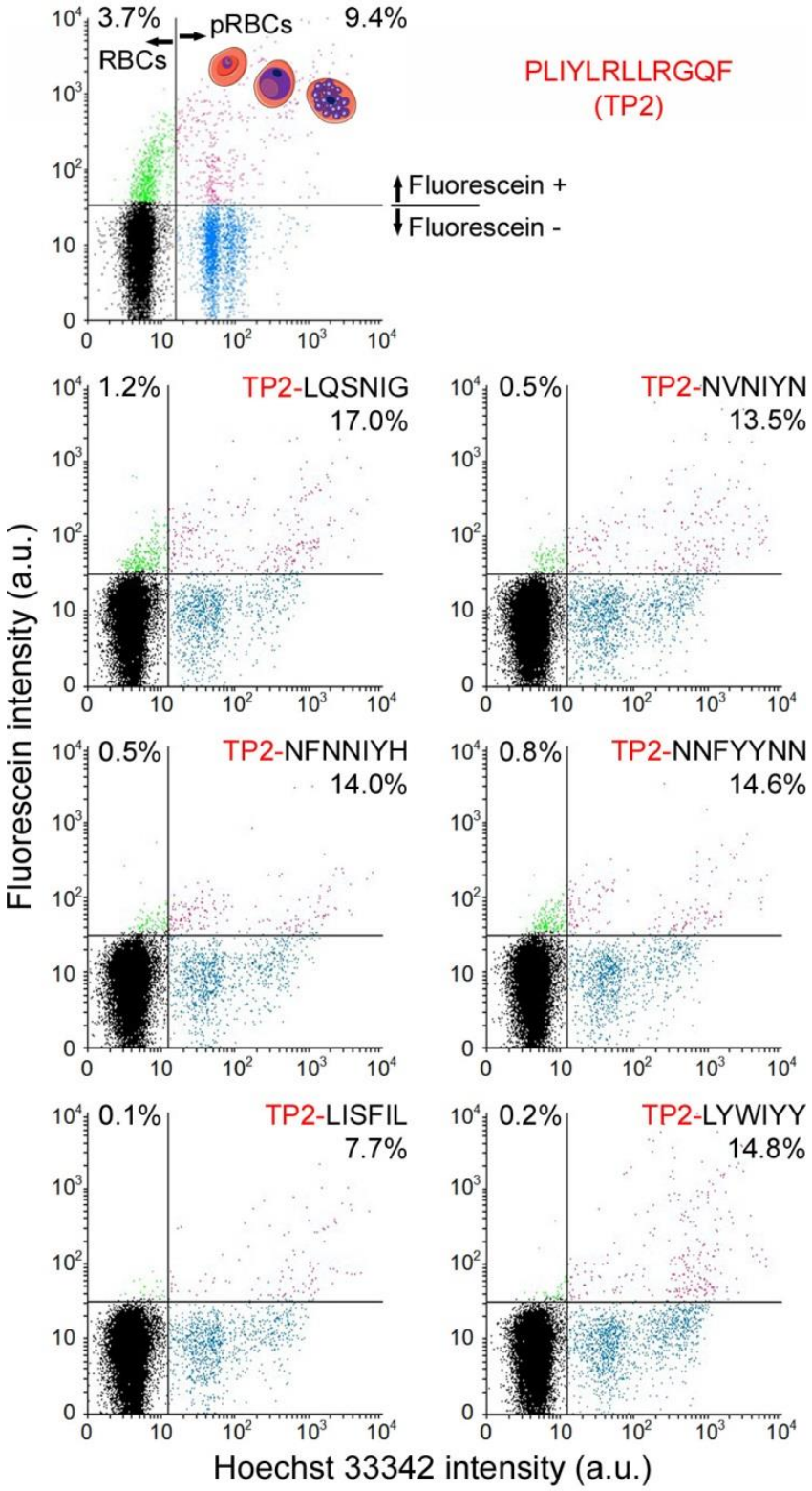

Figure S4. Flow cytometry analysis of the colocalization with RBCs and pRBCs of fluorescein-labeled TP2-conjugated peptides. Percentages indicate the proportion of RBCs and pRBCs positive for fluorescein. a.u.: arbitrary units.

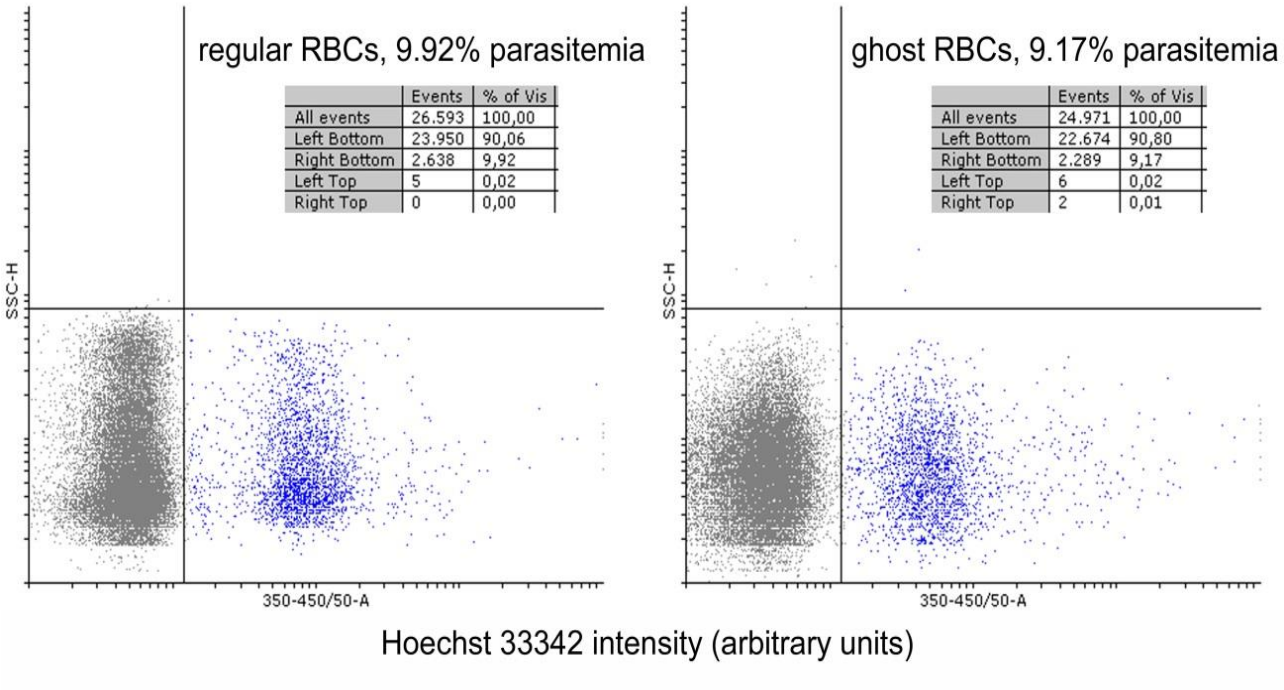

Figure S5. Flow cytometry analysis of the parasitemia, 72 h post-infection, in *P. falciparum* cultures grown in regular and ghost RBCs.

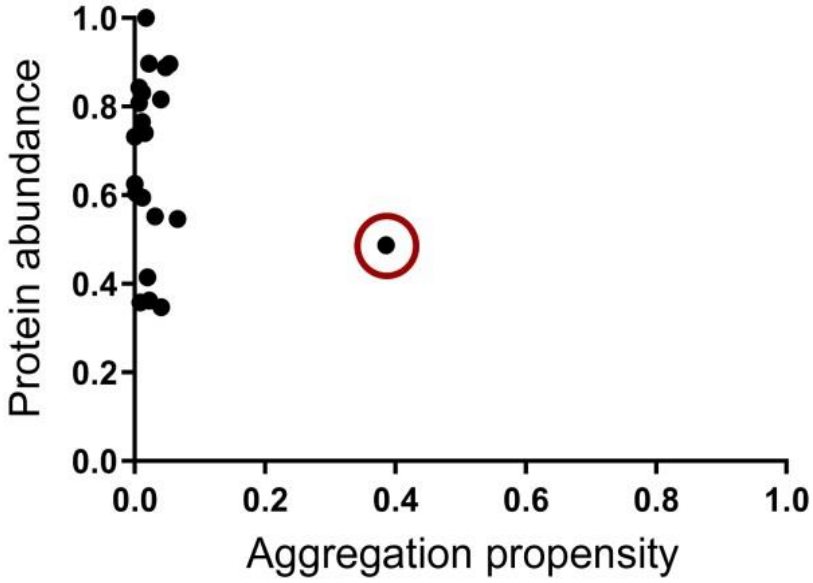

Figure S6. Aggregative proteins found in late and early *P. falciparum* blood stages represented according to their abundance and aggregation propensity normalized relative to the whole proteome. Protein aggregation propensity was calculated with the TANGO algorithm. The red circumference indicates E3 ubiquitin-protein ligase (UniProt ID: C0H4K6).

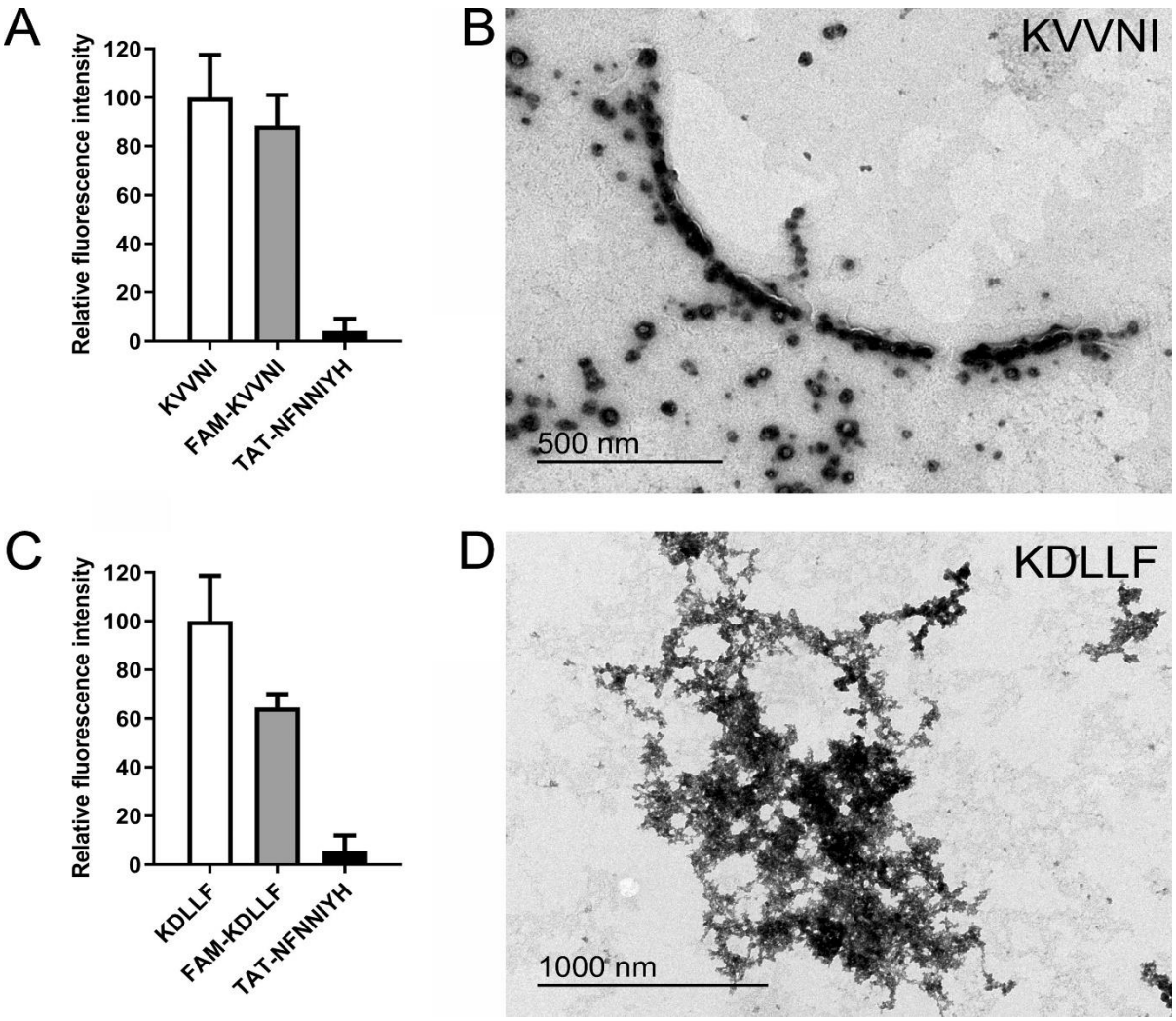

Figure S7. ***In vitro*** **analysis of the aggregation of KDLLF, KVVNI and derived peptides.** (**A**,**C**) ProteoStat® aggregation assay. TAT-NFNNIYH is included as a negative control of a low-aggregative peptide. Bars represent the mean ± SD. (**B**,**D**) Transmission electron microscopy analysis.

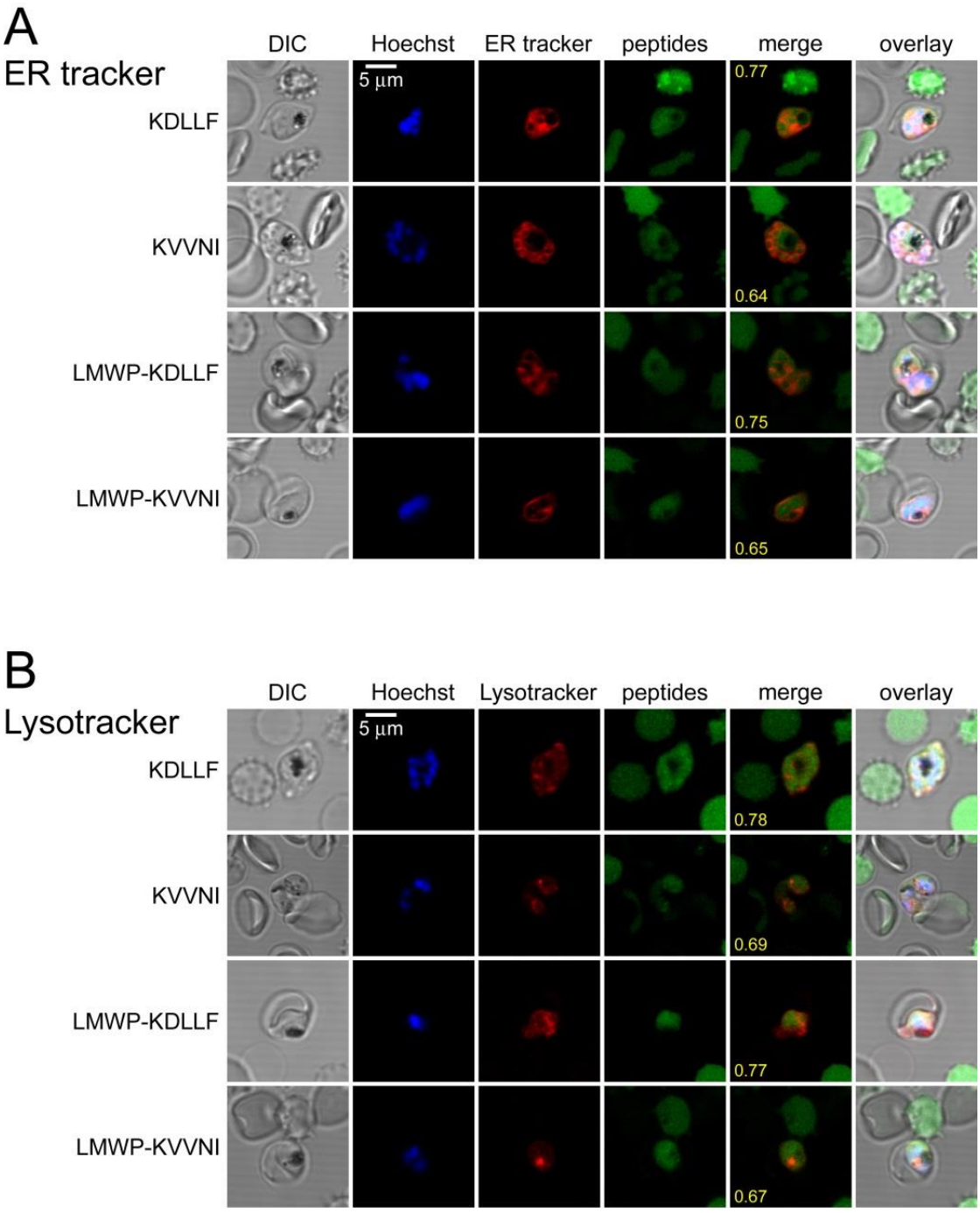

Figure S8. Confocal fluorescence microscopy analysis of the presence of the fluorescein-labeled peptides KDLLF and KVVNI, and of their LMWP elongations, in ghost pRBCs. (**A**) Colocalization analysis with the cytosolic marker ER Tracker™ Red. (**B**) Colocalization analysis with the digestive vacuole marker LysoTracker™ Red DND-99. The merge images correspond to red and green channels only. Manders' overlap correlation coefficients are indicated in yellow digits.

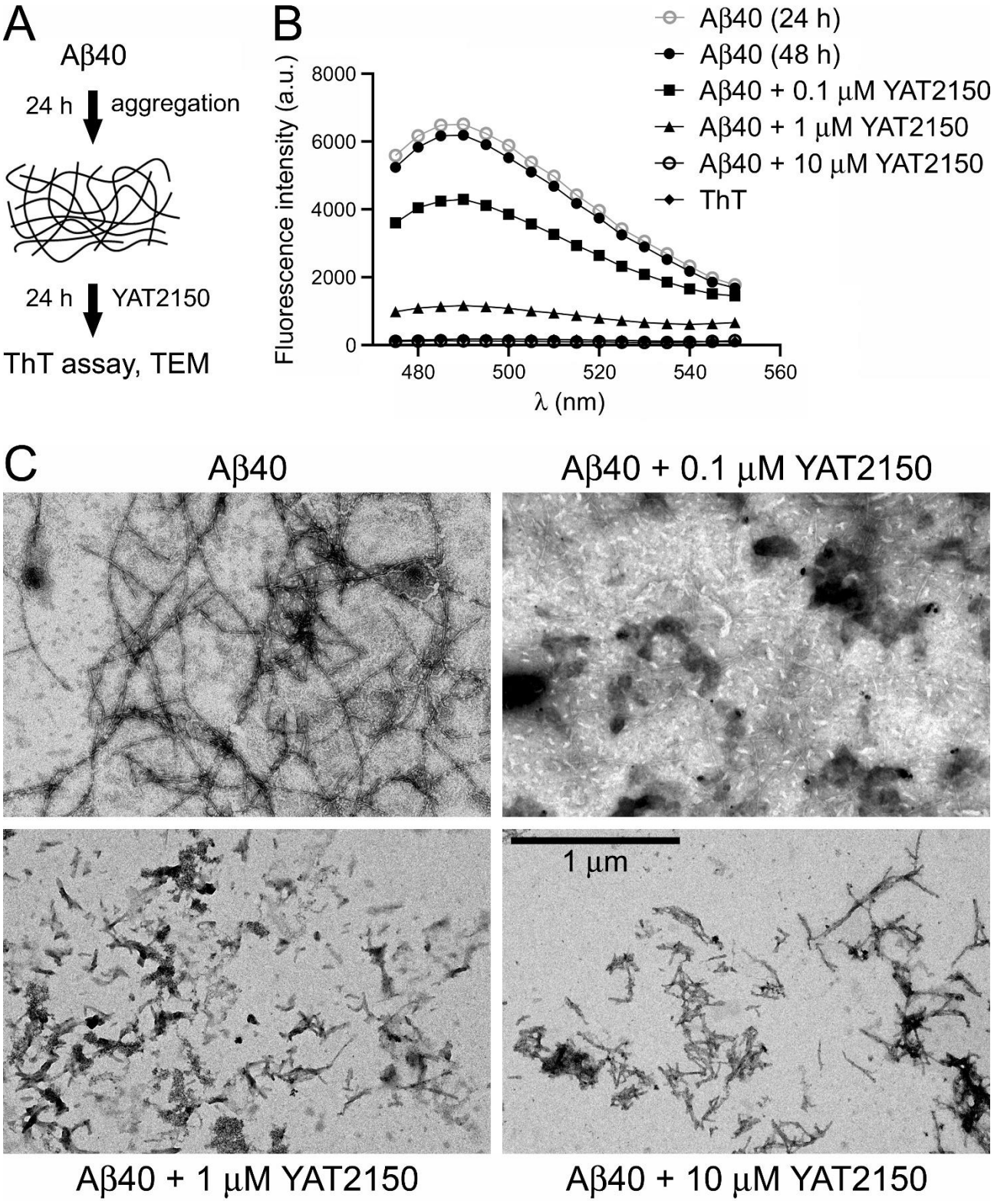

Figure S9. Effect of YAT2150 on pre-aggregated Aβ40. (**A**) Scheme of the assay. (**B**) ThT fluorescence assay. a.u.: arbitrary units. The mean fluorescence intensity value of each sample in each wavelength is represented. (**C**) TEM analysis of the samples after 48 h of incubation.

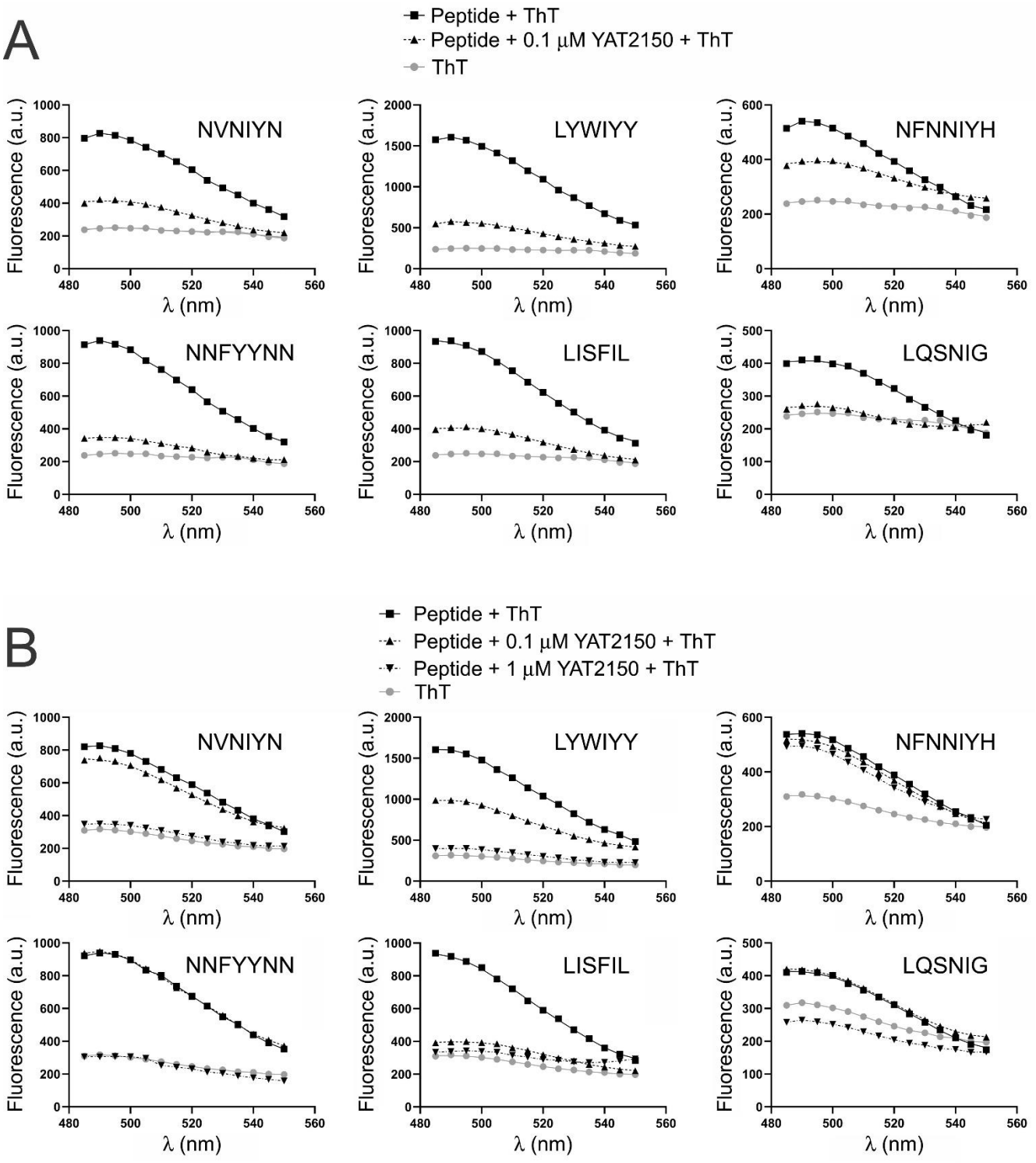

Figure S10. ThT analysis of the effect of YAT2150 on the *in vitro* aggregation of aggregative peptides present in *P. falciparum* proteins. (**A**) Inhibition of aggregation assay. (**B**) Disaggregation assay. In both panels the mean fluorescence intensity value of each sample in each wavelength is represented.

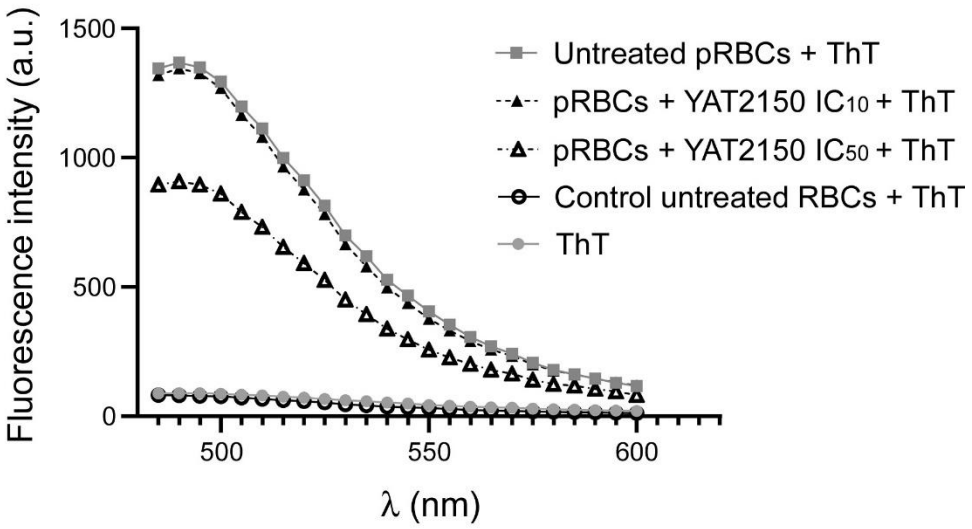

Figure S11. Determination of protein aggregation in live *P. falciparum* cultures. ThT fluorescence of *P. falciparum* culture extracts normalized to have equal protein content, either non-treated or treated with YAT2150 at its *in vitro* IC_{10} (27 nM) and IC_{50} (90 nM), for 30 h. A non-parasitized RBC protein extract is shown as reference. The mean fluorescence intensity value of each sample in each wavelength is represented**.**

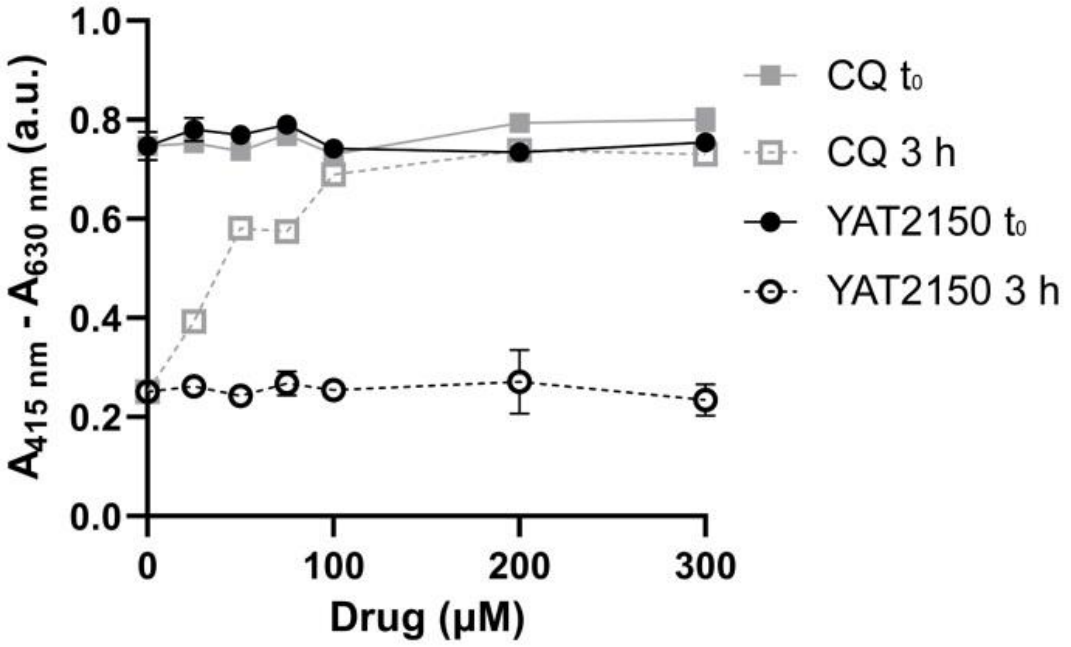

Figure S12. Hemozoin formation assay. CQ: chloroquine; a.u.: arbitrary units. Mean ± SD are plotted.

Table S1. Aggregative peptides selected from the pool of 369 proteins resisting dissolution in 0.1% SDS identified in Biosca *et al.*, 2020[1]. In **bold** are indicated the six peptides selected to be elongated by CPPs.

Peptide (aggregation score[2])	*P. falciparum* proteins containing the peptide (UniProt accession code)	C[3]
LQSNIG (96.3)	Nucleoporin NUP221, putative (Q8I398)	0.49
NVNIYN (98.7)	Uncharacterized protein (C0H4L9)	0.41
	AP2 domain transcription factor, putative (C0H5G5)	0.29
	DNA-binding chaperone, putative (Q8I5N9)	0.50
	DNA-(apurinic or apyrimidinic site) lyase (Q8I2Y2)	0.34
	Heptatricopeptide repeat-containing protein, putative (Q8IJS9)	N/D[4]
NFNNIYH (98.3)	AP2 domain transcription factor, putative (C0H5G5)	0.29
NNFYYNN (99.0)	AP2 domain transcription factor, putative (C0H5G5)	0.29
LISFIL (97.3)	ER membrane protein complex subunit 6, putative (Q8I5R2)	0.39
LYWIYY (99.7)	Eukaryotic translation initiation factor 2 subunit A, putative (Q8IJL2)	0.48
MYVIYV (99.7)	Eukaryotic translation initiation factor 3 subunit E, putative (Q8I3I5)	0.55
TIIFIN (98.3)	Exportin-7, putative (C0H530)	0.41
GLVFFI (98.3)	High molecular weight rhoptry protein 2 (C0H571)	0.70

YLFFIS (98.7)	AP3 complex subunit delta, putative (C0H4T0)	0.37
	Conserved membrane protein, unknown function (Q8I3K4)	0.43
	Conserved protein, unknown function (Q8IID6)	0.29

[1] Biosca A, Bouzón-Arnáiz I, Spanos L, Siden-Kiamos I, Iglesias V, Ventura S, Fernàndez-Busquets X (2020) Detection of protein aggregation in live *Plasmodium* parasites. Antimicrob Agents Chemother 64: e02135-19.

[2] WALTZ average aggregation score per residue.

[3] Normalized protein abundance according to PaxDb database.

[4] No abundance data available.

Table S2. Growth inhibition assay in regular *P. falciparum* cultures of fluorescein-labeled aggregative peptides conjugated to CPPs.

Peptide sequence	Highest concentration tested (μM)	Parasite growth relative to control (%) ± SEM
TAT-LQSNIG	15	99.0 ± 11.2
TAT-NVNIYN	15	97.0 ± 5.0
TAT-NFNNIYH	15	93.5 ± 1.0
TAT-NNFYYNN	7.5	100.0 ± 3.3
TAT-LISFIL	20	100.0 ± 4.5
TAT-LYWIYY	125	100.0 ± 1.2
TP2-LQSNIG	3.5	97.5 ± 3.0
TP2-NVNIYN	3.5	100.0 ± 3.8
TP2-NFNNIYH	50	100.0 ± 12.8
TP2-NNFYYNN	50	100.0 ± 4.0
TP2-LISFIL	20	96.4 ± 2.0
TP2-LYWIYY	125	99.1 ± 1.1
LMWP-LQSNIG	20	90.4 ± 6.3
LMWP-NVNIYN	20	89.5 ± 1.8
LMWP-NFNNIYH	20	84.6 ± 4.0
LMWP-NNFYYNN	200	100.0 ± 1.4
LMWP-LISFIL	20	100.0 ± 3.3
LMWP-LYWIYY	125	100.0 ± 6.9

Table S3. Growth inhibition assay in ghost RBC-enriched *P. falciparum* cultures treated with 10 µM non-modified aggregative peptides.

Peptide sequence	Parasite growth relative to control (%) ± SEM
LQSNIG	95.3 ± 7.4
NVNIYN	94.3 ± 24.6
NFNNIYH	100.0 ± 21.4
NNFYYNN	89.7 ± 12.7
LISFIL	100.0 ± 29.4
LYWIYY	100.0 ± 6.3
MYVIYV	100.0 ± 31.8
TIIFIN	100.0 ± 17.5
GLVFFI	79.4 ± 0.9
YLFFIS	77.5 ± 12.3

Table S4. Cytotoxicity assay in HUVEC cultures of the aggregative peptides which at 10 µM reduced by > 20% *P. falciparum* growth in ghost pRBC cultures. The maximum peptide concentration tested was 200 µM.

Peptide sequence	CC_{50} (µM) ± SEM
(5/6-FAM)-LMWP-LQSNIG	77.6 ± 16.0
(5/6-FAM)-LMWP-NFNNIYH	56.0 ± 1.1
(5/6-FAM)-LMWP-NNFYYNN	7.9 ± 1.3
(5/6-FAM)-LMWP-LISFIL	9.0 ± 1.1
GLVFFI	> 200*
YLFFIS	> 200**

* Growth inhibition at 200 µM was 14.9 ± 1.8%.

** Growth inhibition at 200 µM was 22.3 ± 7.9%.

Table S5. Early stage *P. falciparum* proteins resisting dissolution in 0.1% SDS. Those found also in late stages are indicated in **bold**.

UniProtKB code	Protein	Molecular weight (kDa)	Isoelectric point
A0A5K1K8J3	Glideome-associated connector	290.8	5.25
A0A5K1K967	Elongation factor 1-gamma, putative	47.7	7.39
C0H4K6	**E3 ubiquitin-protein ligase**	**460.1**	**6.58**
C0H4M6	Regulator of chromosome condensation, putative	78.8	6.89
C0H4V6	**14-3-3 protein**	**30.2**	**4.92**
C0H577	Uncharacterized protein	545.8	8.85
C6KSV0	**Histone H3**	**15.4**	**11.14**
C6KT18	**Histone H2A**	**14.1**	**10.29**
O96124	**Erythrocyte membrane protein 3**	**273.5**	**8.85**
O96258	**40S ribosomal protein S26**	**12.5**	**10.98**
Q76NM3	**L-lactate dehydrogenase**	**34.1**	**7.55**
Q7K6A4	**S-adenylmethionine synthase**	**44.8**	**6.74**
Q8I0P6	**Elongation factor 1-alpha**	**48.9**	**9.06**
Q8I2F2	PRESAN domain-containing protein	45.5	9.70
Q8I2G1	Ring-exported protein 1	83.0	5.59
Q8I3B0	**60S ribosomal protein L32**	**15.5**	**11.06**
Q8I492	**Mature parasite-infected erythrocyte surface antigen**	**168.2**	**4.78**
Q8I4R5	Rhoptry neck protein 3	263.0	9.20
Q8I4X0	**Actin-1**	**41.8**	**5.34**
Q8I5S6	**Eukaryotic translation initiation factor 3 subunit A**	**166.0**	**6.81**
Q8IAK9	PRESAN domain-containing protein	147.0	6.05
Q8IAX5	**40S ribosomal protein S16, putative**	**16.3**	**10.24**
Q8IB24	**Heat shock protein 70**	**73.9**	**5.67**

Q8IDG8	Membrane associated histidine-rich protein 2	15.8	7.37
Q8IE09	**60S ribosomal protein L23, putative**	**15.0**	**9.86**
Q8II97	Autophagy-related protein 23, putative	110.0	6.60
Q8IIV1	**Histone H2B**	**13.1**	**10.26**
Q8IIV2	**Histone H4**	**11.4**	**11.22**
Q8IJD0	**Peroxiredoxin**	**43.9**	**9.70**
Q8IKF0	**Eukaryotic initiation factor 4A**	**45.3**	**5.69**
Q8IKK7	**Glyceraldehyde-3-phosphate dehydrogenase**	**36.6**	**7.69**
Q8ILV2	**60S ribosomal protein L10, putative**	**25.2**	**9.95**
Q9TY99	**Knob-associated histidine-rich protein**	**71.3**	**9.09**

Table S6. Aggregative peptides identified in E3 ubiquitin-protein ligase (C0H4K6).

Amino acids	Sequence	WALTZ score	Number of proteins in which the peptide is present
3-18	KYLLFENSQYSYIINS	95.21	1
116-122	SFFKIIQ	94.98	1
274-281	TEIIINSE	97.99	1
314-321	KFFLSNIN	96.57	1
323-346	VDVKYITIIYTATCCIYTILDIYP	95.40	1
357-363	EAVYILN	97.99	1
377-382	VILKIF	94.31	1
409-414	YNVNIQ	96.98	2
417-429	IFFCIIQMINNIT	95.86	1
441-452	YCNIFINFFHYH	97.07	1
455-461	HILNIIC	96.46	1
678-687	IESIYNINIR	97.99	1
702-721	NLYAFMETFYIISILVHYSN	97.16	1
748-763	NNFLIIYILFTLYSFL	96.20	1
787-796	FYENIGEFIN	92.64	1
901-907	NIYYIYE	97.52	1
917-936	LCILICLSVFISLYKISLTC	94.70	1
948-953	YIFSYN	98.33	1
986-992	FTLLILK	93.98	1
1023-1031	GGLLFNITH	97.73	1
1043-1048	VLLHIV	94.31	1
1076-1090	KIYNIIFMYFYDIFN	93.87	1
1108-1112	KDLLF	96.32	10 (4 putative)
1122-1132	VFLEYSELFFN	97.08	1
1145-1151	NICSYFK	93.31	1
1182-1194	ILCYYYLIYLFSN	98.12	1

1202-1208	SCIYFYQ	95.13	1
1216-1226	YFFLYQSLLYG	99.33	1
1266-1277	RLYIFLYALLFV	97.94	1
1325-1345	LVVKIFDSYHYYLIINNLSFK	97.60	1
1387-1392	YYDYIN	92.98	2
1462-1469	QDFSYNVY	96.99	1
1647-1651	KVVNI	96.99	9 (2 putative)
1730-1747	EYNLYNYFNNNRYINYIP	96.77	1
1752-1767	YENLFNESINNNLTID	96.99	1
1775-1780	MYNNYN	98.33	3
1796-1801	NVSIFG	93.98	2
1837-1845	KQNNFNDYF	97.66	1
1935-1944	GSFNIFETFN	96.49	1
2017-2028	IFCNIENFYIYN	97.80	1
2049-2059	WNNNYNINNNN	96.32	1
2118-2125	NNNIYSLN	96.32	3
2127-2134	NNNIYSLN	96.32	3
2138-2143	NSVNYK	92.64	2
2152-2157	NNSLFM	92.64	1
2198-2209	SVSNYVDWVTYK	96.66	1

Table S7. *P. falciparum* proteins in which the peptides KDLLF and KVVNI are present.

Peptide	Proteins (UniProt accession code)	C[1]
KDLLF	E3 ubiquitin-protein ligase (C0H4K6)	0.49
	conserved protein, unknown function (Q8IJE8)	N/D[2]
	conserved membrane protein, unknown function (A0A143ZZV5)	N/D[2]
	DNA polymerase epsilon catalytic subunit A, putative (C6KTD8)	0.35
	conserved protein, unknown function (Q8IKF7)	N/D[2]
	ATP-dependent RNA helicase DHR1, putative (Q8IET8)	0.28

	Cg1 protein (Q8IBZ8)	0.39
	tetratricopeptide repeat protein, putative (Q8IM60)	0.41
	NADPH-cytochrome P450 reductase, putative (Q8IKX3)	0.58
	palmitoyltransferase DHHC12, putative (A0A146M427)	N/D[2]
KVVNI	E3 ubiquitin-protein ligase (C0H4K6)	0.49
	conserved protein, unknown function (Q8ILS9)	0.29
	conserved protein, unknown function (Q8IIT8)	0.31
	sodium/hydrogen exchanger (Q8IET0)	0.37
	S-adenosylmethionine decarboxylase/ornithine decarboxylase (Q8IJ77)	0.42
	kinesin-like protein, putative (C0H4S3)	0.20
	conserved protein, unknown function (Q8IJF2)	N/D[2]
	splicing factor 1 (Q8IE99)	0.47
	glutamate-tRNA ligase, putative (Q8IDK7)	0.70

[1] Normalized protein abundance according to PaxDb database.

[2] No abundance data available.

Table S8. Growth inhibition assay in ghost RBC-enriched *P. falciparum* cultures treated with 10 µM KDLLF and KVVNI peptides.

Peptide	Parasite growth relative to control (%) ± SEM
KDLLF	100.0 ± 1.7
FAM-KDLLF	100.0 ± 14.1
KVVNI	88.2 ± 14.2
FAM-KVVNI	94.0 ± 9.6

Table S9. *In vitro* toxicity in HUVEC cultures of amyloid pan-inhibitors.

Compound	CC_{50} (μM) ± SEM
HUP5ANTRA	76.2 ± 21.5
HUP7ANTRA	29.0 ±1.5
HUP10ANTRA	84.7 ± 13.3
HUP7TH	7.8 ± 3.4
HUP8TH	4.9 ± 1.3
HUP9TH	4.9 ± 1.0
HUPH10TH	3.4 ± 0.1
HUPNTH	3.4 ± 1.0
HUPNTCl	6.3 ± 0.5
DP128	49.0 ± 0.1
DONE3TCl	12.6 ± 2.2
YAT2150	3.4 ± 0.5

Paper 3

Paper 3 is not submitted yet for publication.

Title

YAT2150: an irresistible drug for the post-artemisinin era?

Author list

Inés Bouzón-Arnáiz[1,2,3], Mukul Rawat[4], Rachael Coyle[4], Elsa M. Arce[5], Diego Muñoz-Torrero[5], Marcus Lee[4], Xavier Fernàndez-Busquets[1,2,3*].

Affiliations

[1]Barcelona Institute for Global Health (ISGlobal, Hospital Clínic-University of Barcelona), Rosselló 149-153, 08036 Barcelona, Spain.

[2]Nanomalaria Group, Institute for Bioengineering of Catalonia (IBEC), The Barcelona Institute of Science and Technology, Baldiri Reixac 10-12, 08028 Barcelona, Spain.

[3]Nanoscience and Nanotechnology Institute (IN2UB), University of Barcelona, Martí i Franquès 1, 08028 Barcelona, Spain.

[4]Wellcome Sanger Institute, Wellcome Genome Campus, Hinxton, CB10 1SA, United Kingdom.

[5]Laboratory of Medicinal Chemistry (CSIC Associated Unit), Faculty of Pharmacy and Food Sciences, and Institute of Biomedicine (IBUB), University of Barcelona, Av. Joan XXIII, 27-31, 08028 Barcelona, Spain.

*Corresponding author. Email: xfernandez_busquets@ub.edu

Abstract

The emergence and spread of resistances to the front-line antimalarial treatments, especially to artemisinin, is one of the main current global health threats. New antimalarial drugs that tackle resistance evolution are urgently needed in order to alleviate

this situation. We have recently characterized the potent antiplasmodial activity of YAT2150, a bis(styrylpyridinium) salt (a chemical family with no other antimalarials described) whose mode of action (inhibition of protein aggregation in the parasite) is not shared with other antimalarial drugs and targets many gene products (the aggregation-prone parasite's proteome). These characteristics suggested that resistance against YAT2150 would not appear easily. We have performed assays to select *Plasmodium falciparum* parasites resistant to YAT2150 concentrations ranging from 3× to ¼ the *in vitro* IC_{50} of the compound and performed a cross-resistance assessment in *P. falciparum* lines harboring mutations that make them resistant to a variety of antimalarial drugs. Resistant parasites to YAT2150 did not emerge *in vitro*, which postulates this compound as an 'irresistible' antimalarial drug deserving attention in a likely future scenario of widespread resistance to artemisinin.

Introduction

According to the last World Malaria Report [1], in 2020 there were an estimated 241 million cases of malaria worldwide causing 627,000 deaths. With the aim of reducing the global disease burden, efforts to control it in endemic areas are numerous, including the recent recommendation by the World Health Organization (WHO) of using the RTS,S/AS01 vaccine [2] in children living in high *Plasmodium falciparum* malaria transmission areas [3]. Insecticide-based vector control methods as well as preventive treatment with sulfadoxine/pyrimethamine during pregnancy are other means used to avoid malaria infections [4]. However, prevention in high risk areas is not enough and the reliance on antimalarial drugs for treatment is strong. The reduction in the efficacy of the gold standard malaria treatment, artemisinin combination therapies (ACTs), firstly in

Asia [5] and, more recently, in Africa [6] is dangerously threatening the progress towards a malaria-free world.

Resistance to ACTs is far from being an exception, and almost all antimalarials used in the field have given rise to the emergence and spread of drug-resistant parasites shortly after their deployment [7]. A striking example of how quickly *P. falciparum* can evolve resistances to antimalarial drugs is sulfadoxine-pyrimethamine, to which resistant parasites were detected in Thailand the same year, 1967, that the drug was introduced in the country [8]. In most cases, a single gene mutation is enough to trigger the resistance mechanism. For example, point mutations in the genes *pfcrt* or *pfmdr1* confer resistance to chloroquine and other quinolines by inhibiting the entrance of the drugs into the parasite's digestive vacuole, where the target molecules of the compounds are located [9]. Artemisinin resistance is produced by point mutations in the gene *pfk13* and a number of mechanisms explaining it has been proposed [10]. Despite the emergence of resistances to ACTs, these therapies are still the most used for *P. falciparum* malaria treatment, mainly because no other drug is available yet to substitute artemisinin derivatives. Nonetheless, malaria incidence rate has reached in the last five years a plateau phase after a reductive tendency since 2000, when ACTs started to be used as front line treatments for uncomplicated malaria [1]. The implementation of triple artemisinin-containing combination therapies has been proposed with the aim of avoiding ACT resistance progress, but this would only be a way to delay the problem and gain some time before multirresistant parasites appear [11].

This scenario makes imperative the development of new antimalarial compounds. According to Medicines for Malaria Venture, new drugs should act through novel mechanisms of action in order to avoid cross-resistances with drugs already in use and they should target more than one *Plasmodium* life-cycle stage, ideally gametocytes in

order to block transmission [12]. Our group has recently characterized two new antiplasmodial compounds, DONE3TCl and YAT2150, whose mode of action is the inhibition of protein aggregation in the parasite (Bouzón-Arnáiz et al, accepted manuscript). DONE3TCl is a 4-aminoquinoline drug with an *in vitro* half maximal inhibitory concentration (IC_{50}) of 80 nM that inhibits protein aggregation *in vitro* [13]. On the other hand, YAT2150 is a bis(styrylpyridinium) salt, a chemical family where no other antimalarial drugs are known. It shows an *in vitro* IC_{50} of 90 nM both in sexual and asexual stages of *P. falciparum* and it diminishes the aggregative protein load in the parasite at concentrations similar to the *in vitro* IC_{50}. Due to its A/T-biased genome, the *P. falciparum* proteome is exceptionally enriched in proteins with asparagine repeats, which have a tendency to form insoluble aggregates [14,15]. Moreover, 90% of *P. falciparum* proteins contain at least one Low Complexity Region (LCR) where asparagine is the most represented amino acid [16]. LCRs are stretches inside proteins that have a fluctuant tertiary structure and, as a consequence, are more prone to aggregate [17]. The presence of aggregative proteins in the parasite proteome has been proven *in silico* [18] and also in live parasite cells throughout the whole life cycle, including sexual and mosquito stages [19].

YAT2150 has a number of properties that make it highly interesting as potential new antimalarial drug, namely: (i) our preliminary data suggest that it might be active against all *Plasmodium* species causing human malaria, which would make of this drug a pan-malaria treatment; (ii) it targets (binds) all stages of the parasite in the vertebrate host and in the mosquito vector; (iii) it has a low *in vitro* IC_{50} below 100 nM against all *P. falciparum* blood stages, including gametocytes; (iv) its mode of action (inhibition of protein aggregation in the parasite) targets multiple proteins, which will likely prevent a rapid resistance evolution by the pathogen, as opposed to most other current

antimalarial drugs which target products of one or a few genes; (v) YAT2150 fluoresces when interacting with its molecular targets in *Plasmodium* cells, which makes of it a theranostic agent; (vi) it belongs to an unexplored chemical family where no other antimalarial has been described up to date, which will prevent the adaptation by the parasite of preexisting resistance mechanisms to currently used drugs; (vii) its synthesis is easy and rapid (only two steps), which results in an attractive activity/cost ratio taking into account that its main clinical deployment would be in the low per capita income regions where malaria is endemic; (viii) the compound has a long shelf life (months) at room temperature;.

Thus, YAT2150 shows a promising antimalarial activity profile that is worthy of further characterization. Since, as stated above, parasite resistance evolution is one of the main challenges that future antimalarial drugs need to face, assessing if resistance to YAT2150 evolves easily *in vitro* is a first necessary step towards its potential clinical development as a new medicine in the antimalarial portfolio.

Materials and methods

In vitro culture of asexual forms of *P. falciparum*.

P. falciparum parasites were grown in human O+ red blood cells (RBCs) provided by anonymous healthy donors from the UK National Health Services Blood and Transplant (NHSBT). NHSBT obtained the informed consent from donors, and the use of RBCs was performed with approval from the NHS Cambridgeshire Research Ethics Committee and the Wellcome Sanger Institute Human Materials and Data Management Committee. Prior to use, in order to discard blood material different from RBCs, these were washed twice (10 min, 400× g) with RPMIc (Roswell Park Memorial Insititute 1640 medium with L-glutamine and sodium bicarbonate, Sigma Aldrich) supplemented with 0.5% AlbuMAX

II (Thermo Fisher Scientific) and 25 µg/L gentamycin. After washing them, RBCs were kept at 4 °C diluted in a 1:1 proportion with RPMIc. Cultures at 3% hematocrit in RPMIc were established and maintained continuously infected with *P. falciparum* at parasitemias no higher than 8%. Media was changed every other day and cultures were kept with a gas mix of 1% O_2, 3% CO_2 and 96% N_2 at 37 °C.

In vitro selection of *P. falciparum* parasites resistant to YAT2150, DONE3TCl and KAE609.

In vitro generation and selection of YAT2150-, DONE3TCl- and KAE609-resistant parasites was performed on the Dd2-derived *P. falciparum* strain Dd2-dnapol. This strain was CRISPR edited to mutate two residues (D308A and E310A) in DNA polymerase delta (Kumpornsin and Lee, unpublished results). Triplicates containing 1×10^8 or 1×10^9 parasites were initially exposed to a concentration of $3 \times IC_{50}$ of each drug. Culture medium supplemented with the drugs was changed every day until total parasite clearance was observed in Giemsa-stained blood smears. At this point, drug exposure was stopped and cultures were maintained in regular medium, which was renewed every two days and supplemented with fresh RBCs once a week. Cultures were grown in this way until parasite reemergence or for a maximum of 60 days. When parasites were seen again in blood smears, cultures were expanded and the IC_{50} values of the bulk cultures for the corresponding drug were calculated in order to determine if resistant parasites had arisen.

As a parallel strategy, 1×10^8 parasites were exposed to progressively increasing YAT2150 or DONE3TCl concentrations starting at one quarter of the IC_{50} or the IC_{50} respectively. Parasite growth was monitored by observation of Giemsa-stained blood smears every day or every other day and drug concentrations were stepwise-adjusted with the objective of not allowing total parasite clearance.

SYBR™ Green I growth determination assay.

P. falciparum cultures enriched in ring stages were diluted to 1% parasitemia and 1% hematocrit and plated in duplicates in 96-well plates. To determine the IC_{50} of the tested compounds, they were included in the cultures (100 µL culture/well) at different concentrations, and incubated in standard culturing conditions. As growth controls were used untreated infected cultures and a 1% suspension of uninfected RBCs. After 72 h of incubation, 100 µL of lysis buffer (20 mM Tris-HCl, 5 mM EDTA, 0.1% w/v saponin, and 1% v/v Triton X-100) containing SYBR™ Green I (1:1000, Invitrogen, Thermo Fisher Scientific) were added to each well and plates were incubated in the dark for 30 min. Afterwards, the fluorescence signal of each well was measured in a Synergy HTX Multi-Mode Microplate Reader (BioTek) by exciting the samples at 485 nm and collecting the emission at 535 nm. Growth inhibition data was transformed through sigmoidal fitting using GraphPad and used to determine the IC_{50} values of the drugs.

Cloning of DONE3TCl-resistant *P. falciparum* candidates by limiting dilution.

Bulk cultures possibly resistant to DONE3TCl were diluted to 0.8 parasites/200 µL and each culture was distributed in a 96-well plate. Parasites were maintained for 17 days in standard culturing conditions, and medium containing 0.4% fresh RBCs was renewed once a week. After 17 days, parasite viability was assessed using the SYBR™ Green I assay previously described, but using in this case 50 µL of both culture (taken from each well and transferred to a new plate) and lysis buffer containing SYBR™ Green I. Cultures in wells emitting the highest fluorescence values were discarded, as they could contain a mixed population with more than one initial clone; in a similar way, cultures in wells emitting the lowest fluorescence were also discarded, as possibly no parasites were

initially seeded in them. From the medium-range fluorescence emission samples, at least six clones per plate were selected and grown in standard culturing conditions for three days, when the IC_{50} of some of them was calculated.

Cross-resistance studies.

The *P. falciparum* strains Dd2 (resistant to chloroquine and mefloquine [20]) and wild type 3D7 were barcoded by CRISPR editing by inserting a short 110 bp cassette into the non-essential *pfpare* locus (Jagoe and Lee, unpublished results). These strains were mixed (Table S1) in a pool culture, which was further expanded and plated in duplicates in 24-well plates at 1% parasitemia. YAT2150 was tested at four different concentrations: IC_{50}/4 (22.5 nM), IC_{50}/2 (45 nM), IC_{50} (90 nM) and 3 × IC_{50} (270 nM), and DONE3TCl was tested at three different concentrations: IC_{50}/2 (40 nM), IC_{50} (80 nM) and 3 × IC_{50} (240 nM); an untreated control was also included in the assay. Parasites were grown for 14 days during which medium containing the query drugs was changed every other day and parasite growth was regularly monitored by flow cytometry. For flow cytometry, 2 µL of culture was mixed in 96-well plates with 198 µL of phosphate buffered saline (PBS) containing 1:1000 SYBR™ Green I and 200 nM MitoTracker™ Red FM (Thermo Fisher Scientific). After 30 min incubation, samples were read in a CytoFLEX 5 cytometer (Beckman Coulter) using excitation/emission values of 644⁄665 nm for MitoTracker™ Deep Red FM and 488/530 nm for SYBR™ Green I. If parasitemia was higher than 8%, cultures were diluted to avoid overgrowth. At day 14 (and day 0 in the case of the untreated control), cultures were transferred to 1.5-mL tubes and lysed with 0.05% saponin. Pellets were collected by centrifugation (400 × g, 5 min) and washed with PBS twice in order to remove hemoglobin. After the last washing step, pellets were resuspended in 30 µL of PBS and frozen at –20 °C.

Next generation sequencing.

For barcoding amplification, two sequential PCRs were performed. For the first one, 5 µL of each frozen pellet were mixed with CloneAmp HIFI PCR premix (1×, Takara) and 10 µM of each Illumina adapter-containing primers: p1356 (TCGGCATTCCTGCTGAACCGCTCTTCCGATCTGTAATTCGTGCGCGTCAG) and p1357 (ACACTCTTTCCCTACACGACGCTCTTCCGATCTCCTTCAATTTCGATGGGTAC) in a total volume of 25 µL/reaction. 5 µL of each PCR product were run on a gel to check that no contamination occurred and that amplification worked. Positive PCR products were purified with Ampure beads (Beckman Coulter) following the manufacturer's instructions and quantified with PicoGreen® (Invitrogen, P7589). Briefly, 1 µL of each purified sample was mixed with 100 µL of PicoGreen® reagent in black 96-well plates and incubated at room temperature for 2 min before reading fluorescence in a FLUOstar Omega plate reader (BMG Labtech) by exciting the samples at 480 nm and collecting the emission at 520 nm. DNA concentration was calculated after generating a standard curve using known concentrations of DNA standards. For the second PCR, 20 ng of DNA of the first PCR were mixed with CloneAmp HIFI PCR premix (1×, Takara) and with 10 µM of the appropriate paired-end index primers (Illumina Nextera). PCR products were purified and quantified as explained above and diluted to a final concentration of 4 nM. Samples were loaded onto an Illumina MiSeq sequencer, using a MiSeq Reagent Kit v2 (300 cycles). They were loaded at a low cluster density (< 400 k), and 50% of PhiX was spiked in, as described elsewhere for low complexity libraries [21]. Raw reads obtained after sequencing were separated according

to their unique index tags and barcodes. Reads without an intact barcode or with the barcode flanked by the incorrect genomic context were eliminated.

Statistical analysis.

Statistical differences between IC_{50} values were analysed by two-tailed Student's *t* test using GraphPad Prism 9 Software. For the barcode data statistical analysis, the DESeq2 R package [22] was used. The determination of differentially represented barcodes was carried out by comparing YAT2150 and DONE3TCl samples to either the day 0 untreated control for samples that did not grow during the assay or the day 14 untreated control if they grew. A negative binomial generalized linear model was fit for significance testing with a Wald test in which a log2 fold change >2.5 and *p* value ≤0.001 were considered significantly different.

Results

***In vitro* selection of YAT2150- and DONE3TCl-resistant parasites using a dose of 3 × IC_{50}.**

Generation of mutant resistant *P. falciparum in vitro* cultures has been used to (i) follow the development of resistance to drugs (e.g. chloroquine [23-25]), (ii) discover the molecular targets of a compound during its characterization process [26], and (iii) assess the propensity of parasites to develop resistance to new antimalarials [27]. In our case, the attempt to generate resistant parasites was performed using a concentration equal to 3 × IC_{50} of YAT2150, DONE3TCl and KAE609, a control drug that targets P-type cation-transporter ATPase4 [28] and that had already been tested in this kind of experiment with an established minimum inoculum for resistance. To increase the possibilities of

obtaining resistant parasites, a Dd2-Pol∂ *P. falciparum* strain was used. This line has point mutations in the DNA polymerase delta subunit, resulting in a mutation rate during DNA replication approximately 10- to 30-fold higher than wild type Dd2 (Kumpornsin and Lee, unpublished results).

During this assay, *P. falciparum* treated with 3 × IC_{50} of KAE609 re-emerged in all replicates after 15-17 days of parasite clearance (Table 1), independently of the initial number of cultured cells (1×10^8 or 1×10^9). These parasites were genuinely resistant to KAE609 since they exhibited an IC_{50} at least 70 times higher than the IC_{50} of this compound in Dd2-Pol∂ *P. falciparum* (Figure 1).

In DONE3TCl-treated cultures, 4 replicates re-emerged (Table 1), which did not show a clear shift in their IC_{50} values compared to the Dd2- Pol∂ parental line (Figure 2). Despite the small shift in the IC_{50} values of the bulk cultures from the 4 resistant replicates, cloning plates with the two of them showing the biggest shifts, 10^9 (1) and 10^9 (2), were prepared. The objective was to check if any particular clone was more resistant to DONE3TCl than the mixed bulk culture. However, none of the tested clones showed an IC_{50} value significantly different from the Dd2-dnapol control (Table 2).

After 60 days of parasite clearance, no resistant parasites to YAT2150 came back upon treatment of 10^8 or 10^9 parasites with 3 times the IC_{50} (Table 1). A cross-resistance assay was performed by treating with YAT2150 the re-emerged DONE3TCl bulk cultures but no shift in YAT2150 IC_{50} was observed (data not shown).

In vitro selection of YAT2150- and DONE3TCl-resistant parasites using reduced compound concentrations.

As resistant parasite appearance was not successfully observed in cultures treated with 3 × IC_{50} concentrations of DONE3TCl and YAT2150, a less aggressive resistance

generation strategy was tested. In this case, 1×10^8 parasites were treated with the IC_{50}, half the IC_{50} or one fourth the IC_{50} of YAT2150 or the IC_{50} of DONE3TCl (Table 1), and the drug concentration was stepwise increased to avoid a total parasite clearance in the cultures. In the event that a strong arrest in parasite growth was observed, drugs would be removed from the medium to allow parasites' recovery.

Despite the tight control to which cultures were submitted, it was not possible to increase YAT2150 concentrations up to values higher than its IC_{50} as parasite clearance was observed after treatment with the IC_{50} for two consecutive days, with or without previous treatment at lower concentrations. In the case of DONE3TCl, total parasite clearance was also observed when cultures were treated with the IC_{50} of the drug. Thus, no resistant parasites for any of the drugs appeared using this strategy.

Cross-resistance assessment of YAT2150 and DONE3TCl in mutant *P. falciparum* strains.

Although *de novo in vitro* resistance to YAT2150 and DONE3TCl did not appear in *P. falciparum* cultures, an alternative scenario to be considered in the wild is cross-resistance, i.e. that resistance mechanisms already developed by the parasite against certain drugs could serve for new ones [29,30]. If the only mode of action of YAT2150 and DONE3TCl was the inhibition of protein aggregation, which has not been described for other antimalarials, cross-resistances might be difficult to arise. However, other parasite processes targeted by currently used drugs might be affected by the new compounds and in this case cross-resistances could be expected. To explore this possibility, a pool of 47 parasite lines with known mutations (Table 3) that confer them resistance to a variety of antimalarial drugs was exposed to different concentrations of

YAT2150 or DONE3TCl with the objective of enriching the treated cultures in eventual resistant parasites. After 14 days, the surviving parasites were harvested and sequenced.

All tested concentrations of YAT2150 ($IC_{50}/4$, $IC_{50}/2$, IC_{50} and $IC_{50} \times 3$) drastically inhibited the growth of the culture after a couple of days of treatment (Figure 3A). In the case of DONE3TCl, the lowest concentration tested ($IC_{50}/2$) allowed parasite growth comparable to that of the untreated culture, while the other two concentrations (IC_{50} and $3 \times IC_{50}$) totally arrested parasite growth after the second day of treatment (Figure 3A).

Sequencing data showed that YAT2150-treated cultures contained roughly the same population distribution on days 0 and 14 (Figure 3B), which is in accordance with the observed lack of parasite growth. The same outcome was found in the cultures treated with the two doses of DONE3TCl that inhibited parasite growth. The parasite population of the culture treated with half the IC_{50} of DONE3TCl, which grew at a regular rate after 14 days, was compared to the untreated culture at day 14. In this case, we observed that the strains with a Dd2 background showed no differences between treated and untreated cultures, whereas the 3D7 background strains were less enriched in the treated culture than in the untreated one. However, no particular population inside the 3D7 background lines was dominant (Figure 4).

Discussion

The rampant evolution of resistances to currently used antimalarial compounds, especially artemisinin derivatives, is seriously compromising the future of malaria treatments, which calls for the urgent discovery of new drugs. These novel antimalarials need to be able to tackle resistance, i.e. they should be active against known resistant parasites as well as *in vitro* proofed towards potential resistance emergence [12]. Regarding the first characteristic, we have recently shown that YAT2150 is effective

towards *P. falciparum* strains resistant to chloroquine and artemisinin (Bouzón-Arnáiz et al, accepted manuscript). This result is here confirmed by the lack of parasite growth when a broadly-resistant parasite pool was treated with DONE3TCl or YAT2150, the latter even at low drug concentrations. This pool contained 47 different parasite lines, including some carrying mutations in four of the most widespread resistance markers: *pfmdr1*, *pfdhrfr* and *pfcrt* [31]. Intriguingly, DONE3TCl at concentrations lower than its IC_{50} seemed to be more effective against parasites with the 3D7 background than against parasites with Dd2 background. The main difference between these two strains is their sensitivity to chloroquine, which is moderately reduced in Dd2 compared to 3D7 [20]. The fact that DONE3TCl, like chloroquine, is an aminoquinoline, could explain the observed increased sensitivity to it of 3D7 parasites. However, at higher concentrations this effect disappears, and the compound is equally toxic for 3D7 and Dd2 lines, probably because DONE3TCl also inhibits protein aggregation in the parasite, a mode of action not shared with chloroquine. Protein homeostasis in *Plasmodium* has already been explored as a potential antimalarial target, and proteasome inhibitors [32] or compounds affecting the regular function of chaperones [33,34] have shown good antimalarial properties. However, in some cases, *in vitro* resistance has appeared [35]. Interestingly, one of the mutations conferring resistance to proteasome inhibitors in *Plasmodium* (*Pf*20Sβ5 A20V) was included in the pool of parasites tested against YAT2150 and DONE3TCl and was not selected by any of the drugs. This is in accordance with the protein aggregation inhibitory effect of the drugs, as an efficient proteasome does not confer an advantage towards a less aggregated proteome.

Regarding the necessity of new antimalarial drugs to be tested for *in vitro de novo* resistance, neither YAT2150 nor DONE3TCl resistant parasites arose upon treatment with the drugs. This lack of resistance evolution could be due to the mode of action of

these drugs (inhibition of protein aggregation in the parasite) and their multiple targets, i.e. the abundant aggregative proteins present in *Plasmodium* cells. A single gene mutation is not expected to confer resistance to compounds with such characteristics [36]. The re-emergence of DONE3TCl-treated parasites during *in vitro* resistance selection experiments suggests that this compound is not as lethal as YAT2150, and despite no resistant parasites appeared, this characteristic makes DONE3TCl less attractive for future development than YAT2150.

Compounds that fail in generating resistant parasites *in vitro* are called ‘irresistible’ [37] and they are considered to be less prone to stimulate the emergence of resistance if finally reaching clinical use. Because of this reason, this class of drugs is prioritized in the development of future antimalarial therapies [38]. Considering the lethality of YAT2150 and the lack of *in vitro* resistance evolution to this drug, we propose here YAT2150 as an ‘irresistible’ compound with a potential therapeutic relevance.

Figures and tables

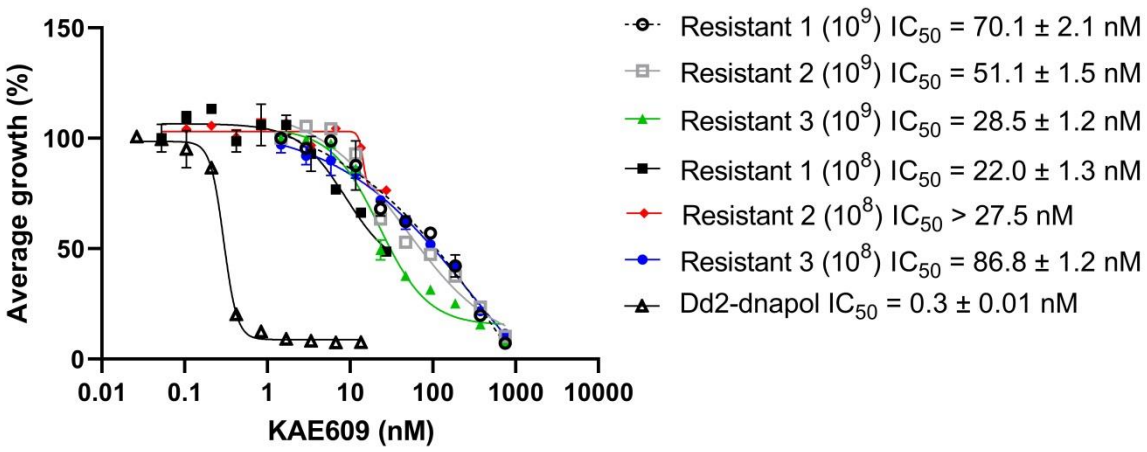

Figure 1. Growth inhibition assay in wild type *P. falciparum* Dd2-Pol∂ parasites and KAE609-resistant *in vitro* cultures treated with KAE609. IC_{50} values are expressed with their respective SE. 10^9 and 10^8 refer to the initial number of parasites used for the *in vitro* selection assay.

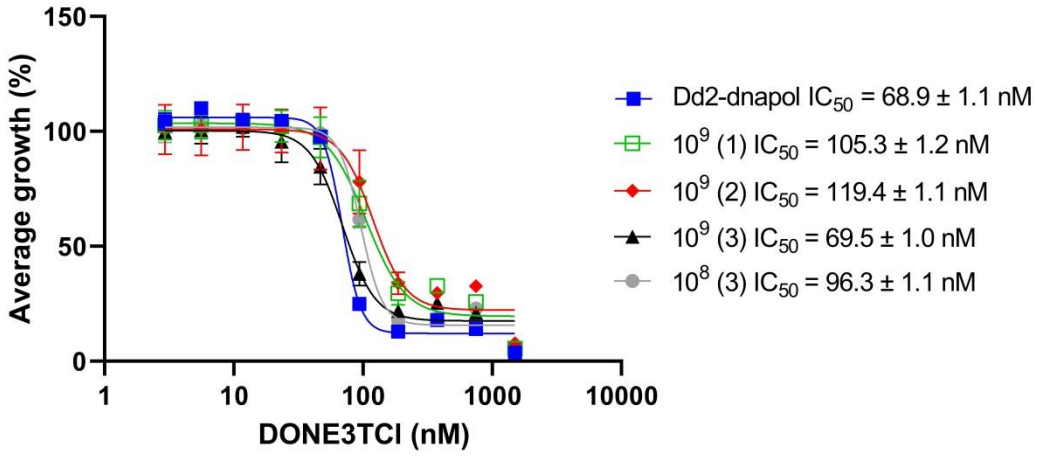

Figure 2. Growth inhibition assay in wild type *P. falciparum* Dd2-Pol∂ parasites and re-emerged DONE3TCl-treated *in vitro* cultures treated with DONE3TCl. IC_{50} values are expressed with their respective SE. 10^9 and 10^8 refer to the initial number of parasites used for the *in vitro* selection assay.

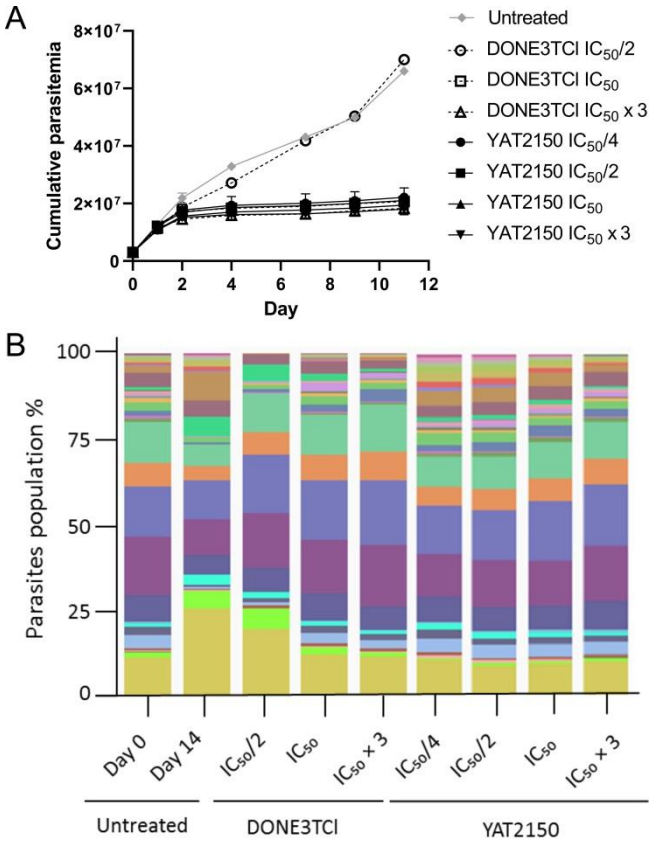

Figure 3. (A) Cumulative parasitemia of the pool culture of mutant parasites left untreated or treated with different concentrations ($IC_{50}/4$, $IC_{50}/2$, IC_{50} and $IC_{50} \times 3$) of YAT2150 or DONE3TCl. **(B)** Percentage in the pool culture of each population of parasites (represented with different colors). See Table S1 for the description of the parasite lines present in the pool. DONE3TCl and YAT2150-treated samples represent parasite population at day 14 of the experiment.

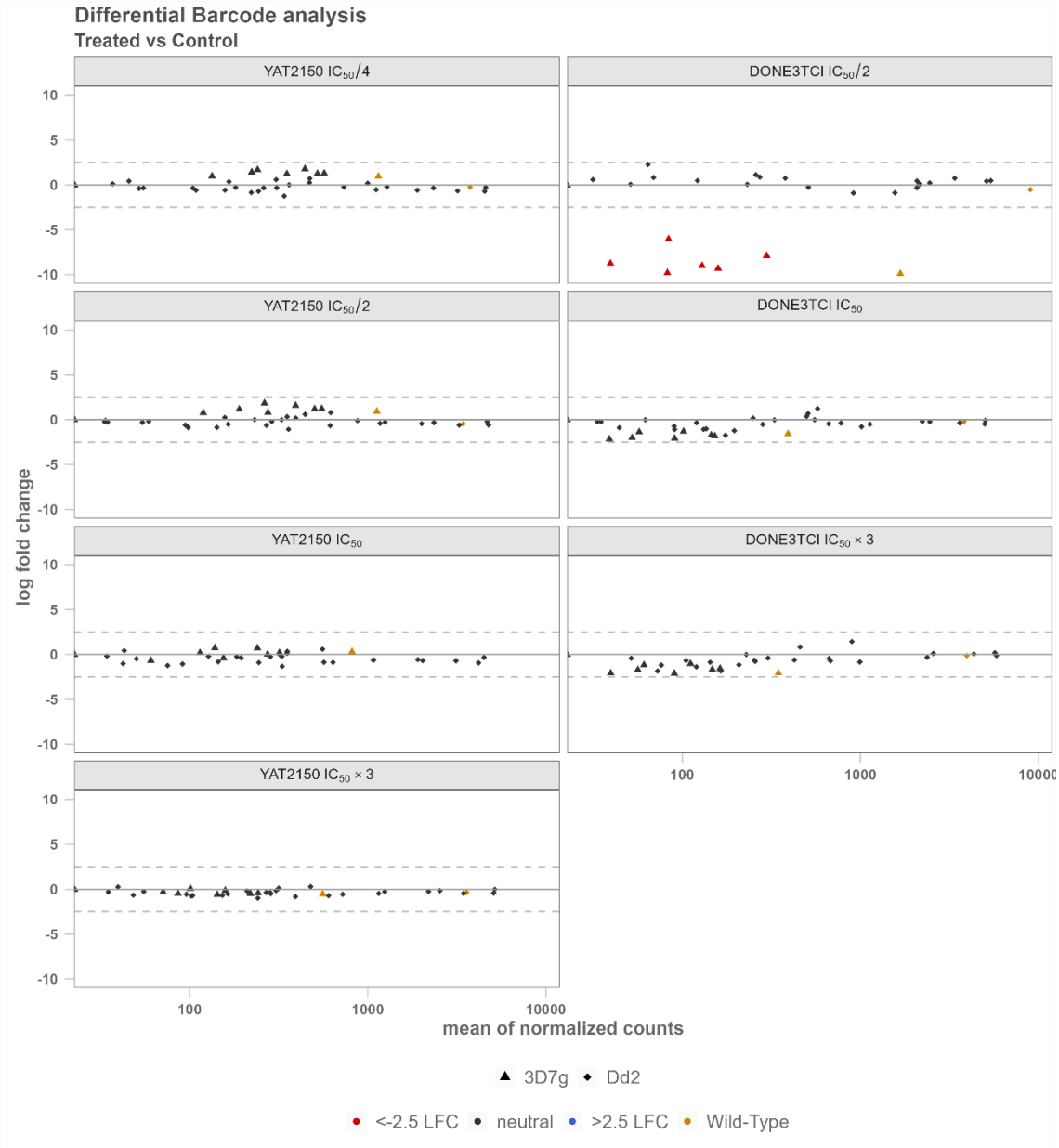

Figure 4. RNA-seq data of DONE3TCl or YAT2150-treated pool parasites compared to the appropriate untreated control. Each triangle (3D7 background) or rhombus (Dd2 background) represents one parasite line. The differential presence of each line in treated *vs.* untreated cultures is represented by the log fold change. A log fold change < –2.5 (red color) or > 2.5 (blue color) is considered to be significant.

Table 1. Result of the generation of resistant parasites to KAE609, DONE3TCl and YAT2150. *: parasites died during the experiment. **: no parasites re-emerged at day 60.

Drug	Method (drug concentration)	Day of reemergence	Number of reemerged replicates
KAE609	1×10^8 ($3 \times IC_{50}$)	17	3
KAE609	1×10^9 ($3 \times IC_{50}$)	15	3
DONE3TCl	1×10^8 ($3 \times IC_{50}$)	28	1
DONE3TCl	1×10^9 ($3 \times IC_{50}$)	30	3
DONE3TCl	1×10^8 (IC_{50})	*	N/A
YAT2150	1×10^8 ($3 \times IC_{50}$)	**	N/A
YAT2150	1×10^9 ($3 \times IC_{50}$)	**	N/A
YAT2150	1×10^8 (IC_{50})	*	N/A
YAT2150	1×10^8 (IC_{50} /2)	*	N/A
YAT2150	1×10^8 (IC_{50} /4)	*	N/A

Table 2. IC_{50} values upon treatment with DONE3TCl of Dd2-dnapol and clones of the DONE3TCl-treated and re-emerged *in vitro* cultures. N/A: not applicable. *p* value compares each strain to the parental Dd2-dnapol.

Strain	Clone	IC_{50} (nM) ± SE	*p* value
Resistant 1 (10^9)	8E	100.1 ± 1.3	0.977
	5F	108.3 ± 1.3	0.902
	11F	57.2 ± 1.1	0.789
	9H	101.4 ± 1.7	0.968
	11B	65.7 ± 1.2	0.937
Resistant 2 (10^9)	9G	63.5 ± 1.2	0.897
	2H	77.7 ± 1.4	0.695
	2A	60.6 ± 1.6	0.605
	1F	105.0 ± 2.2	0.896
	8F	73.0 ± 1.2	0.784
Dd2-Pol∂		68.9 ± 1.1	N/A

Table 3. Parasite lines present in the pool used for RNA-seq assays. The strain name, its proportion at day 0 of the experiment, the mutated gene name and the gene code in PlasmoDB are expressed in the table.

Line name	Control Day 0 (%)	Mutated gene	Code
3D7g-ABCI3-R2180P	0.0098	ATP-binding cassette (ABC) transporter	PF3D7_0319700
3D7g-ACS10-M300I	0.2955	Acyl-CoA synthetase	PF3D7_0525100
3D7g-ACS11-D648Y	0.0196	Acyl-CoA synthetase	PF3D7_1238800
3D7g-ACS11-E668K	0.0238	Acyl-CoA synthetase	PF3D7_1238801
3D7g-ATPase2-CNV2	0.5195	Phospholipid-transporting ATPase 2	PF3D7_1219600
3D7g-DHFR-TS-G378E	0.2717	Bifunctional dihydrofolate reductase-thymidylate synthase	PF3D7_0417200
3D7g-DHFR-TS-I403L	0.4733	Bifunctional dihydrofolate reductase-thymidylate synthase	PF3D7_0417201
3D7g-FTb-A515T	0.8178	Protein farnesyltransferase subunit beta	PF3D7_1147500
3D7g-MDR2-K840N	0.7618	Multidrug resistance protein 2	PF3D7_1447900
3D7g-NPC1-A1108T	0.2269	Niemann-Pick type C1-related protein	PF3D7_0107500
3D7g-WT	1.9774	NA	NA
Dd2-ACL-A597V	0.1134	Acetate-CoA ligase	PfDd2_060032500
Dd2-ATP4-A353E+CARL-I1139K	0.1092	Non-SERCA-type Ca2+ -transporting P-ATPase	PfDd2_120016700
		Cyclic amine resistance locus protein	PfDd2_030027000
Dd2-ATP4-G358S	3.9323	Non-SERCA-type Ca2+ -transporting P-ATPase	PfDd2_120016700
Dd2-AtRNAL-R487S	1.0125	Asn tRNA ligase	PfDd2_000005400
Dd2-CARL-I1139K	0.1036	Cyclic amine resistance locus protein	PfDd2_030027000
Dd2-CARL-L1073Q	0.0448	Cyclic amine resistance locus protein	PfDd2_030027000
Dd2-CARL-V1105L	0.0378	Cyclic amine resistance locus protein	PfDd2_030027000
Dd2-CPSF-Y408S-E	0.8851	CPSF (cleavage and polyadenylation specific factor), subunit A	PfDd2_030022800
Dd2-CRT-M343L	0.8444	Chloroquine resistance transporter	PfDd2_070013200
Dd2-CSC1-L800P	0.3417	CSC1-like protein	PfDd2_120055400
Dd2-cytBC1-G33V	0.0980	cytochrome b	PfDd2_000011300
Dd2-cytBC1-V284L	0.1751	cytochrome b	PfDd2_000011300
Dd2-DHFR-TS-S216R	0.9915	Bifunctional dihydrofolate reductase-thymidylate synthase	PfDd2_040022400
Dd2-DHODH-C276Y	2.5739	Dihydroorotate dehydrogenase	PfDd2_060008000
Dd2-DHODH-F227I	0.0140	Dihydroorotate dehydrogenase	PfDd2_060008001
Dd2-DHODH-L531F	0.1793	Dihydroorotate dehydrogenase	PfDd2_060008002
Dd2-DNApolD-Del	1.1693	DNApol ð-Delta	PfDd2_100022400
Dd2-eEF2-L755F	0.5700	Elongation factor 2	PfDd2_140055500
Dd2-eEF2-Y186N	0.3935	Elongation factor 2	PfDd2_140055501
Dd2-GGPPS-S228T	0.9187	Geranylgeranyl pyrophosphate synthase, putative	PfDd2_110031600
Dd2-ItRNAL-E180D	11.8348	cytoplasmic Isoleucine-tRNA synthetase	PfDd2_130038800
Dd2-ItRNAL-L810F	6.8312	cytoplasmic Isoleucine-tRNA synthetase	PfDd2_130038800
Dd2-ItRNAL-V500A	14.5558	cytoplasmic Isoleucine-tRNA synthetase	PfDd2_130038800
Dd2-kelch13-C580C	17.1381	Kelch protein K13	PfDd2_130049500
Dd2-kelch13-C580Y	7.6070	Kelch protein K13	PfDd2_130049501
Dd2-kelch13-R539T	0.5742	Kelch protein K13	PfDd2_130049502
Dd2-MCP-D195N	0.9299	mitochondrial carrier protein	PF3D7_0908800
Dd2-MDR1-F1072L	0.0056	Multidrug resistance protein 1	PfDd2_050027900
Dd2-PI4K-CNV	2.2785	Phosphatidylinositol 4-kinase	PfDd2_050014800
Dd2-PI4K-S1320L+L1418F	3.9505	Phosphatidylinositol 4-kinase	PfDd2_050014801
Dd2-PI4K-S743F+H1484Y	0.6414	Phosphatidylinositol 4-kinase	PfDd2_050014802
Dd2-PROTB5-A20V	0.3935	Proteasome subunit beta type-5	PfDd2_100016800
Dd2-PtRNAL-L482H	0.0532	Proline tRNA ligase	PfDd2_120018500
Dd2-TtRNAl-S234C	1.5460	Tyr tRNA ligase	PfDd2_000006600
Dd2-UDP-GT-F37V	0.0084	UDP-galactose transporter	PfDd2_110016400
Dd2-WT	11.7466	NA	NA

Reference List

1. World Health Organization. World Malaria Report 2021. https://www.who.int/teams/global-malaria-programme/reports/world-malaria-report-2021 . 2021.

Ref Type: Internet Communication

2. Laurens, M.B. RTS,S/AS01 vaccine (Mosquirix): an overview. *Hum. Vaccin. Immunother.* **2020**, *16* (3), 480-489.

3. World Health Organization. WHO recommends groundbreaking malaria vaccine for children at risk. 2022.

Ref Type: Internet Communication

4. Tizifa, T.A.; Kabaghe, A.N.; McCann, R.S.; van den Berg, H.; Van, V.M.; Phiri, K.S. Prevention efforts for malaria. *Curr. Trop. Med. Rep.* **2018**, *5* (1), 41-50.

5. Ménard, D.; Fidock, D.A. Accelerated evolution and spread of multidrug-resistant *Plasmodium falciparum* takes down the latest first-line antimalarial drug in southeast Asia. *Lancet Infect. Dis.* **2019**, *19* (9), 916-917.

6. Stokes, B.H.; Ward, K.E.; Fidock, D.A. Evidence of artemisinin-resistant malaria in Africa. *N. Engl. J. Med.* **2022**, *386* (14), 1385-1386.

7. Ippolito, M.M.; Moser, K.A.; Kabuya, J.B.; Cunningham, C.; Juliano, J.J. Antimalarial drug resistance and implications for the WHO Global Technical Strategy. *Curr. Epidemiol. Rep.* **2021**, *8* (2), 46-62.

8. Wongsrichanalai, C.; Pickard, A.L.; Wernsdorfer, W.H.; Meshnick, S.R. Epidemiology of drug-resistant malaria. *Lancet Infect. Dis.* **2002**, *2* (4), 209-218.

9. Wicht, K.J.; Mok, S.; Fidock, D.A. Molecular mechanisms of drug resistance in *Plasmodium falciparum* malaria. *Annu. Rev. Microbiol.* **2020**, *74*, 431-454.

10. Noreen, N.; Ullah, A.; Salman, S.M.; Mabkhot, Y.; Alsayari, A.; Badshah, S.L. New insights into the spread of resistance to artemisinin and its analogues. *J. Glob. Antimicrob. Resist.* **2021**, *27*, 142-149.

11. White, N.J. Triple artemisinin-containing combination anti-malarial treatments should be implemented now to delay the emergence of resistance. *Malar. J.* **2019**, *18* (1), 338.

12. Burrows, J.N.; Duparc, S.; Gutteridge, W.E.; Hooft van Huijsduijnen, R.; Kaszubska, W.; Macintyre, F.; Mazzuri, S.; Möhrle, J.J.; Wells, T.N.C. New developments in anti-malarial target candidate and product profiles. *Malar. J.* **2017**, *16* (1), 26.

13. Espargaró, A.; Pont, C.; Gamez, P.; Muñoz-Torrero, D.; Sabate, R. Amyloid pan-inhibitors: one family of compounds to cope with all conformational diseases. *ACS Chem. Neurosci.* **2019**, *10* (3), 1311-1317.

14. Halfmann, R.; Alberti, S.; Krishnan, R.; Lyle, N.; O'Donnell, C.W.; King, O.D.; Berger, B.; Pappu, R.V.; Lindquist, S. Opposing effects of glutamine and asparagine govern prion formation by intrinsically disordered proteins. *Mol. Cell* **2011**, *43* (1), 72-84.

15. Perutz, M.F.; Finch, J.T.; Berriman, J.; Lesk, A. Amyloid fibers are water-filled nanotubes. *Proc. Natl. Acad. Sci. U. S. A* **2002**, *99* (8), 5591-5595.

16. DePristo, M.A.; Zilversmit, M.M.; Hartl, D.L. On the abundance, amino acid composition, and evolutionary dynamics of low-complexity regions in proteins. *Gene* **2006**, *378*, 19-30.

17. Romero, P.; Obradovic, Z.; Li, X.; Garner, E.C.; Brown, C.J.; Dunker, A.K. Sequence complexity of disordered protein. *Proteins* **2001**, *42* (1), 38-48.

18. Pallarès, I.; de Groot, N.S.; Iglesias, V.; Sant'Anna, R.; Biosca, A.; Fernàndez-Busquets, X.; Ventura, S. Discovering putative prion-like proteins in *Plasmodium falciparum*: a computational and experimental analysis. *Front. Microbiol.* **2018**, *9*, 1737.

19. Biosca, A.; Bouzón-Arnáiz, I.; Spanos, L.; Siden-Kiamos, I.; Iglesias, V.; Ventura, S.; Fernàndez-Busquets, X. Detection of protein aggregation in live *Plasmodium* parasites. *Antimicrob. Agents Chemother.* **2020**, *64* (6), e02135-19.

20. Llinás, M.; Bozdech, Z.; Wong, E.D.; Adai, A.T.; DeRisi, J.L. Comparative whole genome transcriptome analysis of three *Plasmodium falciparum* strains. *Nucleic Acids Res.* **2006**, *34* (4), 1166-1173.

21. Gomes, A.R.; Bushell, E.; Schwach, F.; Girling, G.; Anar, B.; Quail, M.A.; Herd, C.; Pfander, C.; Modrzynska, K.; Rayner, J.C.; Billker, O. A genome-scale vector resource enables high-throughput reverse genetic screening in a malaria parasite. *Cell Host Microbe* **2015**, *17* (3), 404-413.

22. Love, M.I.; Huber, W.; Anders, S. Moderated estimation of fold change and dispersion for RNA-seq data with DESeq2. *Genome Biol.* **2014**, *15* (12), 550.

23. Nguyen-Dinh, P.; Trager, W. Chloroquine resistance produced *in vitro* in an African strain of human malaria. *Science* **1978**, *200* (4348), 1397-1398.

24. Barnes, D.A.; Foote, S.J.; Galatis, D.; Kemp, D.J.; Cowman, A.F. Selection for high-level chloroquine resistance results in deamplification of the pfmdr1 gene and increased sensitivity to mefloquine in *Plasmodium falciparum*. *EMBO J.* **1992**, *11* (8), 3067-3075.

25. Sidhu, A.B.; Sun, Q.; Nkrumah, L.J.; Dunne, M.W.; Sacchettini, J.C.; Fidock, D.A. In vitro efficacy, resistance selection, and structural modeling

studies implicate the malarial parasite apicoplast as the target of azithromycin. *J. Biol. Chem.* **2007**, *282* (4), 2494-2504.

26. Baragaña, B.; Hallyburton, I.; Lee, M.C.S.; Norcross, N.R.; Grimaldi, R.; Otto, T.D.; Proto, W.R.; Blagborough, A.M.; Meister, S.; Wirjanata, G.; Ruecker, A.; Upton, L.M.; Abraham, T.S.; Almeida, M.J.; Pradhan, A.; Porzelle, A.; Martínez, M.S.; Bolscher, J.M.; Woodland, A.; Luksch, T.; Norval, S.; Zuccotto, F.; Thomas, J.; Simeons, F.; Stojanovski, L.; Osuna-Cabello, M.; Brock, P.M.; Churcher, T.S.; Sala, K.A.; Zakutansky, S.E.; Jiménez-Díaz, M.B.; Sanz, L.M.; Riley, J.; Basak, R.; Campbell, M.; Avery, V.M.; Sauerwein, R.W.; Dechering, K.J.; Noviyanti, R.; Campo, B.; Frearson, J.A.; Angulo-Barturen, I.; Ferrer-Bazaga, S.; Gamo, F.J.; Wyatt, P.G.; Leroy, D.; Siegl, P.; Delves, M.J.; Kyle, D.E.; Wittlin, S.; Marfurt, J.; Price, R.N.; Sinden, R.E.; Winzeler, E.A.; Charman, S.A.; Bebrevska, L.; Gray, D.W.; Campbell, S.; Fairlamb, A.H.; Willis, P.A.; Rayner, J.C.; Fidock, D.A.; Read, K.D.; Gilbert, I.H. A novel multiple-stage antimalarial agent that inhibits protein synthesis. *Nature* **2015**, *522* (7556), 315-320.

27. Stokes, B.H.; Yoo, E.; Murithi, J.M.; Luth, M.R.; Afanasyev, P.; da Fonseca, P.C.A.; Winzeler, E.A.; Ng, C.L.; Bogyo, M.; Fidock, D.A. Covalent *Plasmodium falciparum*-selective proteasome inhibitors exhibit a low propensity for generating resistance *in vitro* and synergize with multiple antimalarial agents. *PLoS Pathog.* **2019**, *15* (6), e1007722.

28. Rottmann, M.; McNamara, C.; Yeung, B.K.; Lee, M.C.; Zou, B.; Russell, B.; Seitz, P.; Plouffe, D.M.; Dharia, N.V.; Tan, J.; Cohen, S.B.; Spencer, K.R.; Gonzalez-Paez, G.E.; Lakshminarayana, S.B.; Goh, A.; Suwanarusk, R.; Jegla, T.; Schmitt, E.K.; Beck, H.P.; Brun, R.; Nosten, F.; Renia, L.; Dartois, V.; Keller, T.H.; Fidock, D.A.; Winzeler, E.A.; Diagana, T.T. Spiroindolones, a potent compound class for the treatment of malaria. *Science* **2010**, *329* (5996), 1175-1180.

29. Siriwardana, A.; Iyengar, K.; Roepe, P.D. Endoperoxide drug cross-resistance patterns for *Plasmodium falciparum* exhibiting an artemisinin delayed-clearance phenotype. *Antimicrob. Agents Chemother.* **2016**, *60* (11), 6952-6956.

30. Cowman, A.F.; Galatis, D.; Thompson, J.K. Selection for mefloquine resistance in *Plasmodium falciparum* is linked to amplification of the *pfmdr1* gene and cross-resistance to halofantrine and quinine. *Proc. Natl. Acad. Sci. U. S. A.* **1994**, *91* (3), 1143-1147.

31. Ahouidi, A.; Ali, M.; Almagro-Garcia, J.; Amambua-Ngwa, A.; Amaratunga, C.; Amato, R.; Amenga-Etego, L.; Andagalu, B.; Anderson, T.J.C.; Andrianaranjaka, V.; Apinjoh, T.; Ariani, C.; Ashley, E.A.; Auburn, S.; Awandare, G.A.; Ba, H.; Baraka, V.; Barry, A.E.; Bejon, P.; Bertin, G.I.; Boni, M.F.; Borrmann, S.; Bousema, T.; Branch, O.; Bull, P.C.; Busby, G.B.J.; Chookajorn, T.; Chotivanich, K.; Claessens, A.; Conway, D.; Craig, A.; D'Alessandro, U.; Dama, S.; Day, N.P.; Denis, B.; Diakite, M.; Djimdé, A.; Dolecek, C.; Dondorp, A.M.; Drakeley, C.; Drury, E.;

Duffy, P.; Echeverry, D.F.; Egwang, T.G.; Erko, B.; Fairhurst, R.M.; Faiz, A.; Fanello, C.A.; Fukuda, M.M.; Gamboa, D.; Ghansah, A.; Golassa, L.; Goncalves, S.; Hamilton, W.L.; Harrison, G.L.A.; Hart, L.; Henrichs, C.; Hien, T.T.; Hill, C.A.; Hodgson, A.; Hubbart, C.; Imwong, M.; Ishengoma, D.S.; Jackson, S.A.; Jacob, C.G.; Jeffery, B.; Jeffreys, A.E.; Johnson, K.J.; Jyothi, D.; Kamaliddin, C.; Kamau, E.; Kekre, M.; Kluczynski, K.; Kochakarn, T.; Konaté, A.; Kwiatkowski, D.P.; Kyaw, M.P.; Lim, P.; Lon, C.; Loua, K.M.; Maïga-Ascofaré, O.; Malangone, C.; Manske, M.; Marfurt, J.; Marsh, K.; Mayxay, M.; Miles, A.; Miotto, O.; Mobegi, V.; Mokuolu, O.A.; Montgomery, J.; Mueller, I.; Newton, P.N.; Nguyen, T.; Nguyen, T.N.; Noedl, H.; Nosten, F.; Noviyanti, R.; Nzila, A.; Ochola-Oyier, L.I.; Ocholla, H.; Oduro, A.; Omedo, I.; Onyamboko, M.A.; Ouedraogo, J.B.; Oyebola, K.; Pearson, R.D.; Peshu, N.; Phyo, A.P.; Plowe, C.V.; Price, R.N.; Pukrittayakamee, S.; Randrianarivelojosia, M.; Rayner, J.C.; Ringwald, P.; Rockett, K.A.; Rowlands, K.; Ruiz, L.; Saunders, D.; Shayo, A.; Siba, P.; Simpson, V.J.; Stalker, J.; Su, X.Z.; Sutherland, C.; Takala-Harrison, S.; Tavul, L.; Thathy, V.; Tshefu, A.; Verra, F.; Vinetz, J.; Wellems, T.E.; Wendler, J.; White, N.J.; Wright, I.; Yavo, W.; Ye, H. An open dataset of *Plasmodium falciparum* genome variation in 7,000 worldwide samples. *Wellcome Open Res.* **2021**, *6*, 42.

32. Zhan, W.; Zhang, H.; Ginn, J.; Leung, A.; Liu, Y.J.; Michino, M.; Toita, A.; Okamoto, R.; Wong, T.T.; Imaeda, T.; Hara, R.; Yukawa, T.; Chelebieva, S.; Tumwebaze, P.K.; Lafuente-Monasterio, M.J.; Martinez-Martinez, M.S.; Vendome, J.; Beuming, T.; Sato, K.; Aso, K.; Rosenthal, P.J.; Cooper, R.A.; Meinke, P.T.; Nathan, C.F.; Kirkman, L.A.; Lin, G. Development of a highly selective *Plasmodium falciparum* proteasome inhibitor with anti-malaria activity in humanized mice. *Angew. Chem. Int. Ed. Engl.* **2021**, *60* (17), 9279-9283.

33. Banumathy, G.; Singh, V.; Pavithra, S.R.; Tatu, U. Heat shock protein 90 function is essential for *Plasmodium falciparum* growth in human erythrocytes. *J. Biol. Chem.* **2003**, *278* (20), 18336-18345.

34. Everson, N.; Bach, J.; Hammill, J.T.; Falade, M.O.; Rice, A.L.; Guy, R.K.; Eagon, S. Identification of *Plasmodium falciparum* heat shock 90 inhibitors via molecular docking. *Bioorg. Med. Chem. Lett.* **2021**, *35*, 127818.

35. Xie, S.C.; Metcalfe, R.D.; Mizutani, H.; Puhalovich, T.; Hanssen, E.; Morton, C.J.; Du, Y.; Dogovski, C.; Huang, S.C.; Ciavarri, J.; Hales, P.; Griffin, R.J.; Cohen, L.H.; Chuang, B.C.; Wittlin, S.; Deni, I.; Yeo, T.; Ward, K.E.; Barry, D.C.; Liu, B.; Gillett, D.L.; Crespo-Fernandez, B.F.; Ottilie, S.; Mittal, N.; Churchyard, A.; Ferguson, D.; Aguiar, A.C.C.; Guido, R.V.C.; Baum, J.; Hanson, K.K.; Winzeler, E.A.; Gamo, F.J.; Fidock, D.A.; Baud, D.; Parker, M.W.; Brand, S.; Dick, L.R.; Griffin, M.D.W.; Gould, A.E.; Tilley, L. Design of proteasome inhibitors with oral efficacy in vivo against *Plasmodium falciparum* and selectivity over the human proteasome. *Proc. Natl. Acad. Sci. U. S. A.* **2021**, *118* (39).

36. Cowell, A.N.; Winzeler, E.A. The genomic architecture of antimalarial drug resistance. *Brief. Funct. Genomics* **2019**, *18* (5), 314-328.

37. Carolino, K.; Winzeler, E.A. The antimalarial resistome - finding new drug targets and their modes of action. *Curr. Opin. Microbiol.* **2020**, *57*, 49-55.

38. Duffey, M.; Blasco, B.; Burrows, J.N.; Wells, T.N.C.; Fidock, D.A.; Leroy, D. Assessing risks of *Plasmodium falciparum* resistance to select next-generation antimalarials. *Trends Parasitol.* **2021**, *37* (8), 709-721.

Discussion

1. Aggregative proteins in *P. falciparum*.

The *P. falciparum* proteome contains a large proportion number of aggregation-prone proteins, which we have detected both *in silico* and *in vivo*. In this thesis, we intended to characterize the protein aggregation features of the *P. falciparum* proteome as well as to take advantage of the parasite's proteome aggregation tendency to design a radically new antimalarial strategy.

The isolation of 0.1% SDS-resistant proteins from *P. falciparum* cultures allowed us to get a first impression of how these aggregative proteins are represented in the parasite's proteome. According to Gene Ontology analysis, the most enriched biological process in which proteins detected in live parasites are involved is protein transport, especially to the nucleus. In fact, the nuclear pore and the nuclear membrane are the main cellular components where these proteins are located. This is surprising as the location in nuclear structures of protein aggregates is toxic in other cells. For instance, in neurons it is related to the development and worsening of neurodegenerative diseases, like Huntington's or spinocerebellar ataxia (Mikecz, 2009). In fact, a whole UPS system can be found in neuron nuclei and its activity is essential to prevent the toxic outcome of protein aggregation in this cellular location (Chen et al., 2008). In the *P. falciparum* nucleus, proteasomes have been found (Aminake et al., 2011), suggesting that the regulation of protein aggregation in the parasite's nucleus occurs. At the same time, an important family of *P. falciparum* transcription factors, the AP2, involved in heat-shock response (Tintó-Font et al., 2021) and sexual conversion (Yuda et al., 2021), among other crucial biological processes, has been described to be highly aggregation-prone (Pallarès et al., 2018). In fact, many other eukaryotic transcription factors contain prion-like domains (Nizhnikov et al., 2016) and in some cases, like in the *Saccharomyces cerevisiae* ISP, the aggregated conformation appears to be more efficient than the non-aggregated one (Volkov et al., 2002). Thus, the presence of aggregation-prone regions in the *P. falciparum* AP2 transcription factors points at a possible functional role of aggregative proteins in the parasite.

Despite the enrichment in nuclear locations observed *in silico* for the 0.1% SDS-resistant proteins, we observed in live parasites that the protein aggregation reagent PROTEOSTAT® (Pallarès et al., 2018) and its active principle YAT2150 gave signal throughout the parasite's cytosol. Moreover, YAT2150 staining was especially enriched in cytoplasmic regions close to the ER, where protein translation and folding take place (Schwarz & Blower, 2016). Also, protein aggregation in *P. falciparum* is maintained with different intensities throughout the whole parasite life cycle according to PROTEOSTAT® and YAT2150 staining, supporting the idea of protein aggregation playing a functional role in the parasite.

Apart from characterizing and describing protein aggregation in *P. falciparum*, the main objective of this work was taking advantage of this feature and developing a novel antimalarial strategy targeting protein aggregation. As explained in previous sections of this manuscript, protein aggregation can be deleterious for cells when it surpasses the handling capacity of the cellular proteostasis machinery (see Introduction 2.3). At the same time, aggregative proteins play important roles in essential cellular processes (see Introduction 2.3). Taking into consideration this potential dual function of aggregative proteins in the cell, we decided to impair *P. falciparum* basal protein aggregation state by two opposite strategies based on the potential toxicity for the parasite of (i) an externally induced aggregation of its own proteome, or (ii) the prevention of protein aggregation (Figure 22).

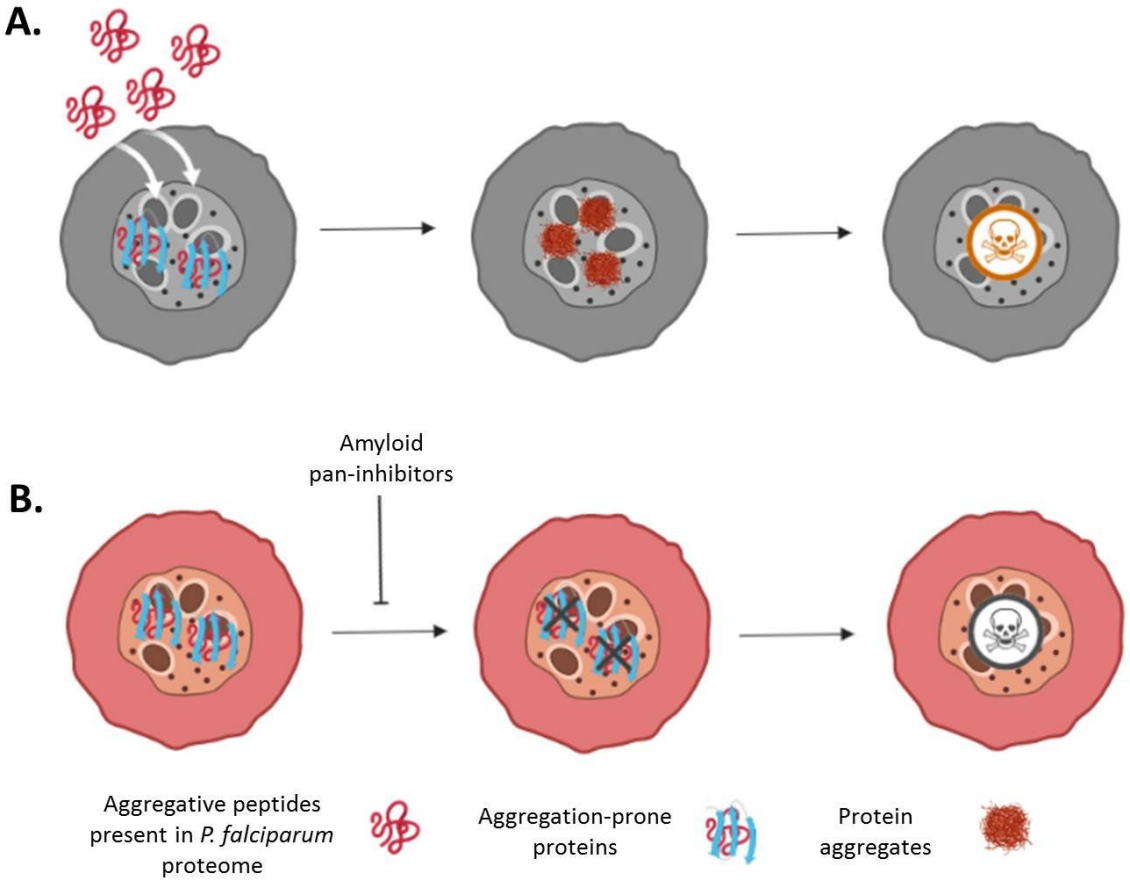

***Figure 22**. A) Scheme of the hypothesis of promoting protein aggregation as an antimalarial design strategy. B) Scheme of the hypothesis of inhibiting protein aggregation as an antimalarial design strategy. Created with BioRender.com*

2. Promoting protein aggregation as an antimalarial strategy.

We firstly explored the hypothesis of promoting protein aggregation as a potential antiplasmodial mechanism, trying to enhance protein aggregation in the parasite by treating it with aggregative peptides naturally present in its proteome (Figure 22). The attempt to use aggregative peptides with therapeutic purposes has already been successfully used in bacterial infections (Wu et al., 2021). For instance, in mice infected with *Staphylococcus aureus*, sepsis was prevented upon treatment with aggregative peptides selected from the proteome of these bacteria (Bednarska et al., 2016).

We selected a total of 13 peptides present in the *P. falciparum* proteome and that were resistant to 0.1% SDS treatment as well as predicted to be aggregative by the PLAAC (Lancaster et al., 2014) or WALTZ (Maurer-Stroh et al., 2010) algorithms, which respectively search for prion-like and amyloid-like amino acid sequences. Most of these peptides showed aggregative characteristics *in vitro*, as proven by ThT assays and TEM analysis. However, when treating parasite cultures with them they did not significantly affect *P. falciparum* viability, neither when peptide entrance to parasites was significantly improved using CPP tags and ghost RBC encapsulation. As the aggregative peptides used in this work to enhance protein aggregation in the parasite were present in its proteome, homologous seeding, i.e. the interaction of a peptide sequence with an identical one, was expected to happen. Homologous seeding is known to exacerbate protein aggregation reactions (Krebs et al., 2004); therefore the interaction of externally added aggregative peptides with their homologs in the parasite's proteome could theoretically have led to an increase on the basal protein aggregation state of the parasite. Nonetheless, we cannot discard that heterologous seeding, i. e. seeding with *Plasmodium* peptides of human proteins, is occurring to a certain degree. This would probably have reduced the amount of available peptides interacting with *Plasmodium* proteins, diminishing the potential toxic effect of peptide aggregation on parasite viability. However, if the strategy of using peptides to enhance protein aggregation in the parasite would have successfully reduced *Plasmodium* viability, heterologous seeding would have entailed an important problem for the peptides' clinical development due to the risk of triggering human protein aggregation. Moreover, we observed that the distribution of peptides inside parasites was wide, with presence in organelles like the digestive vacuole, probably diminishing the chances of the peptides to interact with their homologs in the parasite's proteome.

Nevertheless, we cannot totally discard the promotion of protein aggregation in *P. falciparum* as a valid antimalarial strategy. We overexpressed a fragment of a highly aggregation-prone *Plasmodium* protein E3-ubiquitin ligase (C0H4K6) (data not shown in

this thesis). This protein of 3893 amino acids contains 46 aggregative regions according to WALTZ and 48 LCRs according to Pfam (Mistry et al., 2021) and it is detected in the pool of 0.1% SDS-resistant proteins both in early and late *P. falciparum* stages (see paper 2). The overexpressed fragment consisted in 442 amino acids including 10 aggregative regions and 8 LCRs and the expression of the plasmid containing the query sequence was regulated by blasticidin concentration, i.e. when the blasticidin concentration in the media was increased, a higher expression of the protein fragment occurred. We observed that overexpressing parasites grew at a slower rate than wild type parasites, and that parasite viability was more compromised when blasticidin concentration in the media was increased. Even though we could not directly correlate this effect on parasite growth to an increase in *Plasmodium* protein aggregation levels, these preliminary results indicated a potential connection between these two phenomena. In this sense, it is known that DHA promotes protein misfolding and proteasome blockade in *P. falciparum* (Bridgford et al., 2018), probably leading to the increase of the protein aggregation load in the parasite.

3. YAT2150, a protein aggregation inhibitor, as a potential antimalarial compound.

Our second hypothesis was that preventing *P. falciparum* basal protein aggregation could have a toxic effect for the parasite, especially if aggregative proteins have physiological cellular activities. This hypothesis was supported by the fact of classical antimalarial compounds showing the ability to prevent the aggregation, both *in vitro* and *in vivo*, of well-known amyloid proteins (see Introduction, section 2.4).

To test this idea, we treated *P. falciparum* cultures with a set of amyloid pan-inhibitors (Figure 22), a group of molecules that were designed to prevent amyloid formation (Defaux et al., 2011; Espargaró et al., 2019; Sola et al., 2015). These compounds showed a potent antimalarial effect, and many of them can be considered highly active antimalarial drugs, since their IC_{50} values are lower than 1 µM (Egieyeh, 2021). Our attention was focused on YAT2150, because this compound belongs to a new chemical family with no other antimalarials described, it possessed a low IC_{50}, (90 nM in asexual blood stages of *P. falciparum*) and it was also active at similar concentration ranges in the sexual forms of the parasite. The ability of YAT2150 to inhibit *P. falciparum* sexual conversion together with its gametocytocidal activity makes this drug a potential inhibitor of malaria transmission. Successfully treated malaria patients with no detectable asexual parasites in their blood can carry gametocytes for weeks (Smalley & Sinden, 1977), promoting the spread of the disease. This is why WHO considers that one of the main goals of malaria treatment should be reducing the gametocyte pool in infected humans ((WHO) & (PAHO), 2017). Unfortunately, not many compounds possess antigametocyte activity (Ippolito et al., 2017), and the most potent and widely used

gametocytocide drug, primaquine, presents some problems, like its toxicity for glucose-6-phosphate dehydrogenase (G6PD)-deficient patients, which represent 3 to 30% of people living in malaria endemic areas (Ashley et al., 2014). Thus, YAT2150 could be a precious contribution to this small catalogue of transmission-blocking drugs.

With the aim of gaining some insight on the mode of action of YAT2150, we first characterized its activity as amyloid formation inhibitor *in vitro*. YAT2150 was able to potently inhibit the aggregation of the Aβ40 peptide and of a number of *P. falciparum* aggregative peptides. Furthermore, YAT2150 had the capacity of disaggregating already formed peptide aggregates. *In vivo*, the location of YAT2150 in cytosolic regions close to the ER is consistent with the activity of this molecule directly interacting with proteins and inhibiting their aggregation, as observed *in vitro.* Also, taking into consideration that YAT2150 is able to disaggregate pre-aggregated proteins, it could also act on already formed aggregates that might be functionally important for the malaria parasite. The activity of YAT2150 as a protein aggregation inhibitor *in vivo* was reinforced by the detection of a lower amyloid content in YAT2150-treated cultures, especially at high concentrations of the drug. This reduction of the amyloid content in the parasites was parallel to an increase of ubiquitinated proteins, suggesting a possible connection between these two observations. One hypothesis explaining this could be that YAT2150 prevents the formation of naturally produced amyloids by the parasite, or disentangles them, leading to the generation of amorphous protein aggregates that are ubiquitinated in order to be eliminated from the cell. On the other hand, when parasites are treated with YAT2150 concentrations near its IC_{50}, a reduction in the ubiquitinated protein content is observed, supporting the idea of the compound inhibiting regular protein aggregation in the parasite. To further confirm this, we developed an innovative, easy and quick ThT-based assay to determine the degree of protein aggregation in live parasite cultures. Using this technique we observed a reduction in the aggregated protein content of live parasites after treatment with YAT2150 IC_{50} and/or IC_{10} even at times as short as 90 minutes.

Other compounds with the abilities of inhibiting amyloid formation and disaggregating already formed amyloid structures have been proposed as treatments for neurodegenerative diseases (Berhanu & Masunov, 2010; Paul et al., 2020; Rahman et al., 2021), diabetes (Dubey et al., 2021; Paul et al., 2020) or bacterial infections (Malishev et al., 2021). Thus, the antiaggregative features of YAT2150 let the door open to the exploration of its use for a wide spectrum of diseases beyond malaria.

YAT2150 therapeutic characteristics are complemented with its fluorescent properties, making this molecule a possible theranostic agent for malaria diagnosis and treatment. The gold standard for malaria diagnosis is the microscopic observation of Giemsa-stained blood smears (Wambani & Okoth, 2022). This technique allows parasite

detection in a short time; however, skilled microscopists, as well as good quality blood smears are needed. To make the detection easier for non-specialized staff, the combination of Giemsa staining and a fluorescent probe (Guy et al., 2007) and even the substitution of Giemsa by a fluorescent marker (Sousa-Figueiredo et al., 2010) have been proposed. YAT2150 could work as this fluorescent molecule to improve microscopic diagnosis, but it could also be directly used to stain clinical samples, which could be further read in a spectrofluorimetric device. This second strategy is similar to others already in use for malaria diagnosis, like Gazelle, a device equipped with a set of magnets and a polarized light beam that passes through blood samples and is collected by a detector allowing malaria detection with a 98% of sensitivity (Kumar et al., 2020).

4. Possible functions of protein aggregation in *P. falciparum*.

As introduced previously in this manuscript (see Introduction 2.3), the function of aggregative proteins in *P. falciparum* is not fully understood yet. Whereas some evidences point at the possibility of them being functional (Filisetti et al., 2013; Frugier et al., 2010), others suggest that they do not play a physiological role in the parasite (Burdukiewicz et al., 2018; Muralidharan et al., 2011). The fact that amyloid pan-inhibitors, especially YAT2150, impair the growth of *P. falciparum* cultures as well as reduce their content of aggregative proteins is in line with the hypothesis of protein aggregation having a beneficial role for *Plasmodium*.

We have shown here that YAT2150 fluorescent signal varies its intensity during *P. falciparum* life cycle, being weaker at early ring stages and reaching its highest intensity in the merozoites. This observation matches with the amyloid properties characterized in MSP2 *in vitro* (Adda et al., 2009) and in MSP3 in live parasites (Imam et al., 2014). MSP2 and MSP3 are two of the most abundant proteins in the merozoites' surface and participate in the invasion of new RBCs. Thus, one possible role of protein aggregation in *Plasmodium* could be related to this process. Another possible function of protein aggregation in *Plasmodium* could be related to our finding of the enrichment in nuclear locations of 0.1% SDS-resistant proteins. Moreover, in this pool 8 AP2-containing transcription factors were found and the aggregation-prone nature of this family has already been described (Pallarès et al., 2018). Specifically, two of this 8 AP2 transcription factors (AP2-exp and AP2-O) regulates the expression of clonally-variant gene families (Cubillos et al., 2021; Martins et al., 2017), which are virulence factors taking part in antigenic variation (Hollin & Le Roch, 2020). Interestingly, the expression of some of these clonally-variant genes is modulated upon heat shock (Anagu et al., 2020), which is known to induce the denaturalization and aggregation of proteins.

Furthermore, another AP2 transcription factor, PfAP2-HS, is the master regulator of the heat shock response in *P. falciparum* (Tintó-Font et al., 2021). This data suggests that the disordered and aggregation-prone sequences present in AP2 transcription factors could be affected by changes in temperature, which naturally occur during the fever episodes of *P. falciparum* infection. Taking into consideration that high temperatures both promote protein aggregation and modulate AP2 transcription factors, it could be possible that upon heat stress AP2 aggregate and regulate different cellular responses. Something similar occurs in yeast with the Cdc19 kinase, which aggregates upon heat shock and recovers its non-aggregated state when the heat stress finishes regulating in this way the restart of the cell cycle after the stress condition (Saad et al., 2017). Other key elements of the heat shock response in *P. falciparum* are the heat shock proteins (see Introduction 2.2.1.2), which have been found to be exported by the parasite inside EVs (Abdi et al., 2017). In fact, it was recently observed that around 45% of the proteins exported in *P. falciparum*-derived EVs are aggregative (Avalos-Padilla et al., in preparation). EVs secreted by pRBCs are important for the communication with other parasitized cells (Mantel et al., 2013; Regev-Rudzki et al., 2013) as well as with host immune cells (Babatunde et al., 2020; Dekel et al., 2021). In both cases, EVs-mediated inter-cellular communication has the purpose of maintaining and propagating *P. falciparum* infection inside RBCs by different means, e.g. modifying the cytoskeleton of naïve RBCs (Dekel et al., 2021) or increasing the permeability of vascular endothelial cells (Babatunde et al., 2020), taking into account that almost half of the proteins inside parasite-derived EVs are aggregative they could play a role in these processes.

5. YAT2150 and resistance development.

YAT2150 appears to be a good potential antimalarial theranostic candidate, worth to be clinically developed and validated. As previously described in this manuscript, parasite's resistance development to antimalarial drugs occurs rapidly in most cases and is the main obstacle in the path of reaching malaria eradication. In recent years, the emergence of artemisinin resistance has worsened the situation, dangerously threatening the scientific efforts to reduce the disease burden (Noreen et al., 2021; Rasmussen et al., 2022; van der Pluijm et al., 2021). In this regard, WHO has set as a top priority in its agenda the development of non-artemisinin-based therapies (WHO, 2021d). In fact, the development and adoption of multiple first-line malaria therapies is considered to be an effective way to avoid resistance spread in the field (Boni et al., 2008; Rasmussen et al., 2022). In this sense, YAT2150 represents a good alternative, as its interaction with artemisinin showed an antagonistic effect and it is effective against artemisinin-resistant parasites. On the other hand, we have shown in this work that YAT2150 resistance evolution is not easy to achieve by *P. falciparum* in *in vitro* cultures. YAT2150-daily treated parasites rapidly died and never came back even when low

concentrations of the compound were used and even if the treatment was maintained and renewed for as few as a couple of consecutive days. The same lethal outcome was observed when YAT2150 treatment was interrupted and resumed after parasites' apparent recovery. Moreover, YAT2150 was proved to be effective against a pool of parasites resistant to a wide variety of antimalarial compounds. The lack of YAT2150 resistance development in *in vitro* cultures could be explained by many factors including (i) that YAT2150 belongs to a family where no other antimalarial drugs have been described, so already existing resistance mechanisms would not be effective for this compound; (ii) that YAT2150 targets protein aggregation, meaning that it acts on many gene products, so the probability of a single mutation conferring resistance to the drug is minimized; (iii) that YAT2150 possesses a fast-killing rate that quickly leads to total parasite clearance reducing the time during which parasites are exposed to the drug.

It is important to note that *in vitro* selection of resistant parasites has been successful with many antimalarial drugs, including chloroquine, sulfadoxine-pyrimethamine and artemisinin (Njokah et al., 2016; Nzila & Mwai, 2010). The fact that YAT2150 is an 'irresistible' compound reduces the probabilities of rapid resistance appearance *in vivo* (Cowell & Winzeler, 2018) and can be considered another feature that makes this compound attractive for further clinical development.

YAT2150 main characteristics
Multi-stage drug. YAT2150 targets all asexual and sexual stages of P. falciparum.
Novel mode of action. YAT2150 inhibits protein aggregation, a mode of action not shared with other antimalarials.
Targeting of many gene products. YAT2150 targets the abundant aggregative proteins of P. falciparum.
Irresistible compound. No in vitro resistances have been developed against YAT2150.
Theranostic agent. YAT2150 fluorescently stains P. falciparum.
Quick and easy synthesis. YAT2150 is synthesized in only two steps.
Long shelf storage. YAT2150 can be stored at room temperature for a long time.

Table 1. *List of YAT2150 main characteristics.*

6. Future perspectives for YAT2150.

Despite all the promising characteristics of YAT2150 that have been unravelled in this work (Table 1), this drug still shows some weaknesses, like a relatively high unspecific toxicity. YAT2150 shows a selectivity index of 37.8, whereas for antimalarials like chloroquine or dihydroartemisinin this value is higher than 1000 in similar *in vitro* assays (de Lange et al., 2018; Guetzoyan et al., 2009). Apart from unspecific toxicity,

another important challenge posed by YAT2150, which we have little explored, is its *in vivo* behaviour. After treating BALB/c mice with YAT2150 at concentrations higher than its *in vitro* IC_{50}, yet not toxic for the animals, (4.8, 9.6 and 19.2 µg/mL) we did not observe any retardation in YAT2150-treated mice survival compared to the untreated controls. The lack of efficacy *in vivo* of YAT2150 could be explained by its wide biodistribution throughout the body, which is expected for hydrophobic drugs, like YAT2150 (Oie, 1986). This predicted extensive distribution would lead to the need of increasing the dose of the drug in order to maintain its therapeutic effect; however, a high drug concentration could be toxic. To overcome these two facts, one possible solution would be modifying the chemical structure of YAT2150 by means of the synthesis of analog compounds. This strategy will provide with a family of compounds which could not only be less toxic than YAT2150 itself but also could improve some other characteristic of the drug, e.g. its antimalarial activity or its antiaggregative potency. Another way of reducing the toxicity of YAT2150 as well as of regulating its biodistribution, could be encapsulating the compound inside nanovectors, a strategy that has been proved successful for other antimalarial compounds (Urbán & Fernàndez-Busquets, 2014). In particular, immunoliposomes probed with anti-glycophorin-A antibody, which bind both infected and uninfected RBCs, showed to reduce the effective dose of chloroquine by 40 times in *P. berghei* infected mice (Moles et al., 2015).

In conclusion, we have shown in this thesis that protein aggregation is abundant in *P. falciparum* and that it can be used as a novel therapeutic target for malaria. The promotion of protein aggregation in the parasite did not significantly impair its viability; however inhibiting protein aggregation with the novel antimalarial molecule YAT2150 is toxic for *P. falciparum*. The antimalarial effect of inhibiting protein aggregation suggests that the aggregative proteins of the parasite could be essential for the correct development of *P. falciparum*.

Conclusions

1. The *P. falciparum* proteome is enriched in aggregation-prone proteins, which can be isolated *in vivo* and predicted *in silico*.

2. *P. falciparum* aggregative proteins are enriched in nuclear functions, but are distributed throughout the whole parasite, especially in the cytosolic ER adjacent regions.

3. *P. falciparum* aggregative proteins are present throughout the whole parasite cycle.

4. Aggregative peptides selected from the *P. falciparum* proteome form aggregates *in vitro*.

5. The entrance of aggregative peptides inside *P. falciparum* can be improved by the combination of two strategies: the synthesis of peptides tagged with CPPs and their encapsulation in gRBCs.

6. Treating *P. falciparum in vitro* cultures with aggregative peptides did not impair its development.

7. Treating *P. falciparum in vitro* cultures with amyloid pan-inhibitors in the <100 nM low concentrations ranges was lethal for the parasite.

8. YAT2150, which belongs to a chemical family with no other antimalarial drugs described, inhibits and reverts Aβ40 amyloid fibril formation *in vitro*.

9. YAT2150 diminishes in *in vitro P. falciparum* cultures the amount of ubiquitinated proteins, the amyloid content and the aggregated protein load according to ThT assays.

10. YAT2150 effectively stains *P. falciparum* parasites and can be considered a theranostic agent.

11. Resistance to YAT2150 is not easily acquired *in vitro* by *P. falciparum.*

12. The protein aggregation inhibitor YAT2150 is a good antiplasmodial candidate because:
    - 12.1. It has a low IC_{50} in asexual *P. falciparum* stages (90 nM).
    - 12.2. It is active against sexual *P. falciparum* stages and *P. berghei* hepatic forms.
    - 12.3. It has a novel mode of action: inhibition of protein aggregation in *P. falciparum.*

12.4. It has an easy synthesis and long shelf storage time at room temperature.

12.5. It is active against chloroquine and artemisinin-resistant *P. falciparum* strains.

13. YAT2150 is a potential alternative for malaria treatment in the post-artemisinin era.

References

Abdi, A., Yu, L., Goulding, D., Rono, M. K., Bejon, P., Choudhary, J., & Rayner, J. (2017). Proteomic analysis of extracellular vesicles from a. *Wellcome Open Res*, *2*, 50. https://doi.org/10.12688/wellcomeopenres.11910.2

Abkarian, M., Massiera, G., Berry, L., Roques, M., & Braun-Breton, C. (2011). A novel mechanism for egress of malarial parasites from red blood cells. *Blood*, *117*(15), 4118-4124. https://doi.org/10.1182/blood-2010-08-299883

Acharya, P., Kumar, R., & Tatu, U. (2007). Chaperoning a cellular upheaval in malaria: heat shock proteins in Plasmodium falciparum. *Mol Biochem Parasitol*, *153*(2), 85-94. https://doi.org/10.1016/j.molbiopara.2007.01.009

Adda, C. G., Murphy, V. J., Sunde, M., Waddington, L. J., Schloegel, J., Talbo, G. H., . . . Anders, R. F. (2009). Plasmodium falciparum merozoite surface protein 2 is unstructured and forms amyloid-like fibrils. *Molecular and Biochemical Parasitology*, *166*(2), 159-171. https://doi.org/10.1016/j.molbiopara.2009.03.012

Akide-Ndunge, O. B., Tambini, E., Giribaldi, G., Mcmillan, P. J., Müller, S., Arese, P., & Turrini, F. (2009). Co-ordinated stage-dependent enhancement of Plasmodium falciparum antioxidant enzymes and heat shock protein expression in parasites growing in oxidatively stressed or G6PD-deficient red blood cells. *Malaria Journal*, *8*(1), 113. https://doi.org/10.1186/1475-2875-8-113

Al-Bari, M. A. (2015). Chloroquine analogues in drug discovery: new directions of uses, mechanisms of actions and toxic manifestations from malaria to multifarious diseases. *J Antimicrob Chemother*, *70*(6), 1608-1621. https://doi.org/10.1093/jac/dkv018

Alam, P., Siddiqi, K., Chturvedi, S. K., & Khan, R. H. (2017). Protein aggregation: From background to inhibition strategies. *Int J Biol Macromol*, *103*, 208-219. https://doi.org/10.1016/j.ijbiomac.2017.05.048

Aminake, M. N., Arndt, H. D., & Pradel, G. (2012). The proteasome of malaria parasites: A multi-stage drug target for chemotherapeutic intervention? *Int J Parasitol Drugs Drug Resist*, *2*, 1-10. https://doi.org/10.1016/j.ijpddr.2011.12.001

Anagu, L. O., Hulse, D. R., Chakravorty, S. J., Horrocks, P. D., & Jill-Merrick, C. (2020). Heat shock modulates the expression of sirtuins and Var genes in the malaria parasite Plasmodium falciparum. *Research Square*. https://doi.org/10.21203/rs.3.rs-87990/v1

Andya, J. D., Hsu, C. C., & Shire, S. J. (2003). Mechanisms of aggregate formation and carbohydrate excipient stabilization of lyophilized humanized monoclonal antibody formulations. *AAPS PharmSci*, *5*(2), E10. https://doi.org/10.1208/ps050210

Aniweh, Y., Gao, X., Hao, P., Meng, W., Kuan Lai, S., Gunalan, K., . . . Preiser, P. R. (2017). *P. falciparum* RH5-Basigin interaction induces changes in the cytoskeleton of the host RBC. *Cellular Microbiology*, *19*(9).

Arnot, D. E., Ronander, E., & Bengtsson, D. C. (2011). The progression of the intra-erythrocytic cell cycle of Plasmodium falciparum and the role of the centriolar plaques in asynchronous mitotic division during schizogony. *Int J Parasitol*, *41*(1), 71-80. https://doi.org/10.1016/j.ijpara.2010.07.012

Arosio, P., Michaels, T. C., Linse, S., Månsson, C., Emanuelsson, C., Presto, J., . . . Knowles, T. P. (2016). Kinetic analysis reveals the diversity of microscopic mechanisms through which molecular chaperones suppress amyloid formation. *Nat Commun*, *7*, 10948. https://doi.org/10.1038/ncomms10948

Arthur, L., Pavlovic-Djuranovic, S., Smith-Koutmou, K., Green, R., Szczesny, P., & Djuranovic, S. (2015). Translational control by lysine-encoding A-rich sequences. *Sci Adv*, *1*(6). https://doi.org/10.1126/sciadv.1500154

Ashley, E. A., Recht, J., & White, N. J. (2014). Primaquine: the risks and the benefits. *Malar J*, *13*, 418. https://doi.org/10.1186/1475-2875-13-418

Atroosh, W. M., Al-Mekhlafi, H. M., Mahdy, M. A., & Surin, J. (2012). The detection of pfcrt and pfmdr1 point mutations as molecular markers of chloroquine drug resistance, Pahang, Malaysia. *Malar J*, *11*, 251. https://doi.org/10.1186/1475-2875-11-251

Auparakkitanon, S., Chapoomram, S., Kuaha, K., Chirachariyavej, T., & Wilairat, P. (2006). Targeting of hematin by the antimalarial pyronaridine. *Antimicrob Agents Chemother*, *50*(6), 2197-2200. https://doi.org/10.1128/AAC.00119-06

Babatunde, K. A., Yesodha Subramanian, B., Ahouidi, A. D., Martinez Murillo, P., Walch, M., & Mantel, P. Y. (2020). Role of Extracellular Vesicles in Cellular Cross Talk in Malaria. *Front Immunol*, *11*, 22. https://doi.org/10.3389/fimmu.2020.00022

Balaji, S. N., Deshmukh, R., & Trivedi, V. (2020). Severe malaria: Biology, clinical manifestation, pathogenesis and consequences. *J Vector Borne Dis*, *57*(1), 1-13. https://doi.org/10.4103/0972-9062.308793

Balchin, D., Hayer-Hartl, M., & Hartl, F. U. (2020). Recent advances in understanding catalysis of protein folding by molecular chaperones. *FEBS Letters*, *594*(17), 2770-2781. https://doi.org/10.1002/1873-3468.13844

Bancells, C., Llorà-Batlle, O., Poran, A., Nötzel, C., Rovira-Graells, N., Elemento, O., . . . Cortés, A. (2019). Revisiting the initial steps of sexual development in the malaria parasite Plasmodium falciparum. *Nat Microbiol*, *4*(1), 144-154. https://doi.org/10.1038/s41564-018-0291-7

Bannister, L. H., Mitchell, G. H., Butcher, G. A., & Dennis, E. D. (1986). Lamellar membranes associated with rhoptries in erythrocytic merozoites of Plasmodium knowlesi: a clue to the mechanism of invasion. *Parasitology*, *92 (Pt 2)*, 291-303. https://doi.org/10.1017/s0031182000064064

Banumathy, G., Singh, V., Pavithra, S. R., & Tatu, U. (2003). Heat Shock Protein 90 Function Is Essential for Plasmodium falciparum Growth in Human Erythrocytes. *Journal of Biological Chemistry*, *278*(20), 18336-18345. https://doi.org/10.1074/jbc.m211309200

Bard, J. A. M., Goodall, E. A., Greene, E. R., Jonsson, E., Dong, K. C., & Martin, A. (2018). Structure and Function of the 26S Proteasome. *Annual Review of Biochemistry*, *87*(1), 697-724. https://doi.org/10.1146/annurev-biochem-062917-011931

Bartoloni, A., & Zammarchi, L. (2012). Clinical aspects of uncomplicated and severe malaria. *Mediterr J Hematol Infect Dis*, *4*(1), e2012026. https://doi.org/10.4084/MJHID.2012.026

Basco, L. K., Tahar, R., Annick Keundjian, a. P. R., Annick Keundjian, a. P. R., Keundjian, A., & Ringald, P. (2000). Sequence variations in the genes encoding dihydropteroate synthase and dihydrofolate reductase and clinical response to sulfadoxine-pyrimethamine in patients with acute uncomplicated falciparum malaria. In (Vol. 182, pp. 624-628): The Journal of Infectious Diseases.

Bednarska, N. G., Van Eldere, J., Gallardo, R., Ganesan, A., Ramakers, M., Vogel, I., . . . Rousseau, F. (2016). Protein aggregation as an antibiotic design strategy. *Molecular Microbiology*, *99*(5), 849-865. https://doi.org/10.1111/mmi.13269

Berhanu, W. M., & Masunov, A. E. (2010). Natural polyphenols as inhibitors of amyloid aggregation. Molecular dynamics study of GNNQQNY heptapeptide decamer. *Biophys Chem*, *149*(1-2), 12-21. https://doi.org/10.1016/j.bpc.2010.03.003

Bharti, A. R., Letendre, S. L., Patra, K. P., Vinetz, J. M., & Smith, D. M. (2009). Malaria diagnosis by a polymerase chain reaction-based assay using a pooling strategy. *Am J Trop Med Hyg*, *81*(5), 754-757. https://doi.org/10.4269/ajtmh.2009.09-0274

Bhatt, S., Weiss, D. J., Cameron, E., Bisanzio, D., Mappin, B., Dalrymple, U., . . . Gething, P. W. (2015). The effect of malaria control on Plasmodium falciparum in Africa between 2000 and 2015. *Nature*, *526*(7572), 207-211. https://doi.org/10.1038/nature15535

Bhattacharjee, S., Coppens, I., Mbengue, A., Suresh, N., Ghorbal, M., Slouka, Z., . . . Haldar, K. (2018). Remodeling of the malaria parasite and host human red cell by vesicle amplification that induces artemisinin resistance. *Blood*, *131*(11), 1234-1247. https://doi.org/10.1182/blood-2017-11-814665

Blatch, G. L., & Shonhai, A. (2014). *Heat Shock Proteins of Malaria* (1st ed.). Springer Netherlands : Imprint: Springer,. https://doi.org/10.1007/978-94-007-7438-4

Bolognesi, B., & Tartaglia, G. G. (2013). Physicochemical principles of protein aggregation. *Prog Mol Biol Transl Sci*, *117*, 53-72. https://doi.org/10.1016/B978-0-12-386931-9.00003-9
Boni, M. F., Smith, D. L., & Laxminarayan, R. (2008). Benefits of using multiple first-line therapies against malaria. *Proc Natl Acad Sci U S A*, *105*(37), 14216-14221. https://doi.org/10.1073/pnas.0804628105
Bousema, J. T., Drakeley, C. J., & Sauerwein, R. W. (2006). Sexual-stage antibody responses to P. falciparum in endemic populations. *Curr Mol Med*, *6*(2), 223-229. https://doi.org/10.2174/156652406776055140
Boyle, M. J., Richards, J. S., Gilson, P. R., Chai, W., & Beeson, J. G. (2010). Interactions with heparin-like molecules during erythrocyte invasion by Plasmodium falciparum merozoites. *Blood*, *115*(22), 4559-4568. https://doi.org/10.1182/blood-2009-09-243725
Braak, H., & Braak, E. (1990). Cognitive impairment in Parkinson's disease: amyloid plaques, neurofibrillary tangles, and neuropil threads in the cerebral cortex. *J Neural Transm Park Dis Dement Sect*, *2*(1), 45-57. https://doi.org/10.1007/BF02251245
Brabin, B. J., Romagosa, C., Abdelgalil, S., Menéndez, C., Verhoeff, F. H., McGready, R., . . . Ordi, J. (2004). The sick placenta-the role of malaria. *Placenta*, *25*(5), 359-378. https://doi.org/10.1016/j.placenta.2003.10.019
Brancucci, N. M., Goldowitz, I., Buchholz, K., Werling, K., & Marti, M. (2015). An assay to probe Plasmodium falciparum growth, transmission stage formation and early gametocyte development. *Nat Protoc*, *10*(8), 1131-1142. https://doi.org/10.1038/nprot.2015.072
Brancucci, N. M. B., Bertschi, N. L., Zhu, L., Niederwieser, I., Chin, W. H., Wampfler, R., . . . Voss, T. S. (2014). Heterochromatin protein 1 secures survival and transmission of malaria parasites. *Cell Host Microbe*, *16*(2), 165-176. https://doi.org/10.1016/j.chom.2014.07.004
Breydo, L., & Uversky, V. N. (2011). Role of metal ions in aggregation of intrinsically disordered proteins in neurodegenerative diseases. *Metallomics*, *3*(11), 1163-1180. https://doi.org/10.1039/c1mt00106j
brgfx. *Malaria symptoms*. https://www.freepik.es/vectores/medico
Bridgford, J. L., Xie, S. C., Cobbold, S. A., Pasaje, C. F. A., Herrmann, S., Yang, T., . . . Tilley, L. (2018). Artemisinin kills malaria parasites by damaging proteins and inhibiting the proteasome. *Nat Commun*, *9*(1), 3801. https://doi.org/10.1038/s41467-018-06221-1
Bruce, M. C., Alano, P., Duthie, S., & Carter, R. (1990). Commitment of the malaria parasite Plasmodium falciparum to sexual and asexual development. *Parasitology*, *100 Pt 2*, 191-200. https://doi.org/10.1017/s0031182000061199
Bruce-Chwatt, L. J. (1965). Paleogenesis and Paleo-Epidemiology of Primate Malaria. *Bull World Health Organ*, *32*, 363-387.
Burdukiewicz, M., Sobczyk, P., Chilimoniuk, J., Gagat, P., & Mackiewicz, P. (2018). Prediction of Signal Peptides in Proteins from Malaria Parasites. *International Journal of Molecular Sciences*, *19*(12), 3709. https://doi.org/10.3390/ijms19123709
Callis, J. (2014). The Ubiquitination Machinery of the Ubiquitin System. *The Arabidopsis Book*, *12*, e0174. https://doi.org/10.1199/tab.0174
Camberg, J., Doyle, S., Johnston, D., & Wickner, S. (2013). Molecular chaperones. In S. Maloy & K. Hughes (Eds.), *Brenner's Encyclopedia of Genetics* (pp. 456-460). Academic Press.
Chaccour, C., Lines, J., & Whitty, C. J. (2010). Effect of ivermectin on Anopheles gambiae mosquitoes fed on humans: the potential of oral insecticides in malaria control. *J Infect Dis*, *202*(1), 113-116. https://doi.org/10.1086/653208
Chang, C., Lin-Hua, T., & Jantanavivat, C. (1992). Studies on a new antimalarial compound: pyronaridine. *Trans R Soc Trop Med Hyg*, *86*(1), 7-10. https://doi.org/10.1016/0035-9203(92)90414-8

Chaubey, S., Grover, M., & Tatu, U. (2014). Endoplasmic reticulum stress triggers gametocytogenesis in the malaria parasite. *J Biol Chem*, *289*(24), 16662-16674. https://doi.org/10.1074/jbc.M114.551549

Chaudhry, S. R., Lwin, N., Phelan, D., Escalante, A. A., & Battistuzzi, F. U. (2018). Comparative analysis of low complexity regions in Plasmodia. *Sci Rep*, *8*(1), 335. https://doi.org/10.1038/s41598-017-18695-y

Chen, M., Singer, L., Scharf, A., & von Mikecz, A. (2008). Nuclear polyglutamine-containing protein aggregates as active proteolytic centers. *J Cell Biol*, *180*(4), 697-704. https://doi.org/10.1083/jcb.200708131

Chen, X., & Cubillos-Ruiz, J. R. (2021). Endoplasmic reticulum stress signals in the tumour and its microenvironment. *Nature Reviews Cancer*, *21*(2), 71-88. https://doi.org/10.1038/s41568-020-00312-2

Chen, Y., Murillo-Solano, C., Kirkpatrick, M. G., Antoshchenko, T., Park, H.-W., & Pizarro, J. C. (2018). Repurposing drugs to target the malaria parasite unfolding protein response. *Scientific Reports*, *8*(1). https://doi.org/10.1038/s41598-018-28608-2

Chevli, R., & Fitch, C. D. (1982). The antimalarial drug mefloquine binds to membrane phospholipids. *Antimicrob Agents Chemother*, *21*(4), 581-586. https://doi.org/10.1128/AAC.21.4.581

Chiang, A. N., Valderramos, J. C., Balachandran, R., Chovatiya, R. J., Mead, B. P., Schneider, C., . . . Brodsky, J. L. (2009). Select pyrimidinones inhibit the propagation of the malarial parasite, Plasmodium falciparum. *Bioorg Med Chem*, *17*(4), 1527-1533. https://doi.org/10.1016/j.bmc.2009.01.024

Chiti, F., & Dobson, C. M. (2009). Amyloid formation by globular proteins under native conditions. *Nat Chem Biol*, *5*(1), 15-22. https://doi.org/10.1038/nchembio.131

Choe, Y. J., Park, S. H., Hassemer, T., Körner, R., Vincenz-Donnelly, L., Hayer-Hartl, M., & Hartl, F. U. (2016). Failure of RQC machinery causes protein aggregation and proteotoxic stress. *Nature*, *531*(7593), 191-195. https://doi.org/10.1038/nature16973

Chu, T., Tran, T., Yang, F., Beech, W., Cole, G. M., & Frautschy, S. A. (1998). Effect of chloroquine and leupeptin on intracellular accumulation of amyloid-beta (Aβ) 1-42 peptide in a murine N9 microglial cell line. *FEBS Letters*, *436*(3), 439-444. https://doi.org/10.1016/s0014-5793(98)01161-2

Clark, I. A., Alleva, L. M., Mills, A. C., & Cowden, W. B. (2004). Pathogenesis of malaria and clinically similar conditions. *Clin Microbiol Rev*, *17*(3), 509-539, table of contents. https://doi.org/10.1128/CMR.17.3.509-539.2004

Coatney, R. G. (1963). Pitfalls in a discovery:the chronicle of chloroquine. *American Journal of Tropical Medicine and Hygene*, *12*, 7.

Coleman, B. I., Skillman, K. M., Jiang, R. H. Y., Childs, L. M., Altenhofen, L. M., Ganter, M., . . . Duraisingh, M. T. (2014). A Plasmodium falciparum histone deacetylase regulates antigenic variation and gametocyte conversion. *Cell Host Microbe*, *16*(2), 177-186. https://doi.org/10.1016/j.chom.2014.06.014

Collins, L. T., Otoupal, P. B., Courtney, C. M., & Chatterjee, A. (2018). *Design of a de novo aggregating antimicrobial peptide and bacterial conjugation delivery system*. Cold Spring Harbor Laboratory.

Combrinck, J. M., Mabotha, T. E., Ncokazi, K. K., Ambele, M. A., Taylor, D., Smith, P. J., . . . Egan, T. J. (2013). Insights into the role of heme in the mechanism of action of antimalarials. *ACS Chem Biol*, *8*(1), 133-137. https://doi.org/10.1021/cb300454t

Cowell, A., & Winzeler, E. (2018). Exploration of the. *Microbiol Insights*, *11*, 1178636118808529. https://doi.org/10.1177/1178636118808529

Cowman, A. F., Healer, J., Marapana, D., & Marsh, K. (2016). Malaria: Biology and Disease. *Cell*, *167*(3), 610-624. https://doi.org/10.1016/j.cell.2016.07.055

Cowman, A. F., Tonkin, C. J., Tham, W. H., & Duraisingh, M. T. (2017). The Molecular Basis of Erythrocyte Invasion by Malaria Parasites. *Cell Host Microbe*, *22*(2), 232-245. https://doi.org/10.1016/j.chom.2017.07.003

Cox, F. E. (2010). History of the discovery of the malaria parasites and their vectors. *Parasit Vectors*, *3*(1), 5. https://doi.org/10.1186/1756-3305-3-5

Crutcher, J. M., & Hoffman, S. L. (1996). Malaria. In S. Baron (Ed.), *Medical Microbiology* (4 ed.). University of Texas Medical Branch at Galveston.

Cubillos, E. F. G., Prata, I. O., Fotoran, W. L., Ranford-Cartwright, L., & Wunderlich, G. (2021). The Transcription Factor PfAP2-O Influences Virulence Gene Transcription and Sexual Development in. *Front Cell Infect Microbiol*, *11*, 669088. https://doi.org/10.3389/fcimb.2021.669088

Cui, L., & Su, X. Z. (2009). Discovery, mechanisms of action and combination therapy of artemisinin. *Expert Rev Anti Infect Ther*, *7*(8), 999-1013. https://doi.org/10.1586/eri.09.68

Dalby, A. R. (2009). A Comparative Proteomic Analysis of the Simple Amino Acid Repeat Distributions in Plasmodia Reveals Lineage Specific Amino Acid Selection. *PLoS ONE*, *4*(7), e6231. https://doi.org/10.1371/journal.pone.0006231

Day, J., Passecker, A., Beck, H.-P., & Vakonakis, I. (2019). The Plasmodium falciparum Hsp70-x chaperone assists the heat stress response of the malaria parasite. *The FASEB Journal*, *33*(12), 14611-14624. https://doi.org/10.1096/fj.201901741r

de Lange, C., Coertzen, D., Smit, F. J., Wentzel, J. F., Wong, H. N., Birkholtz, L. M., . . . N'Da, D. D. (2018). Synthesis, in vitro antimalarial activities and cytotoxicities of amino-artemisinin-ferrocene derivatives. *Bioorg Med Chem Lett*, *28*(3), 289-292. https://doi.org/10.1016/j.bmcl.2017.12.057

Debatin, L., Streffer, J., Geissen, M., Matschke, J., Aguzzi, A., & Glatzel, M. (2008). Association between Deposition of Beta-Amyloid and Pathological Prion Protein in Sporadic Creutzfeldt-Jakob Disease. *Neurodegenerative Diseases*, *5*(6), 347-354. https://doi.org/10.1159/000121389

Defaux, J., Sala, M., Formosa, X., Galdeano, C., Taylor, M. C., Alobaid, W. A., . . . Muñoz-Torrero, D. (2011). Huprines as a new family of dual acting trypanocidal-antiplasmodial agents. *Bioorg Med Chem*, *19*(5), 1702-1707. https://doi.org/10.1016/j.bmc.2011.01.028

Dekel, E., Yaffe, D., Rosenhek-Goldian, I., Ben-Nissan, G., Ofir-Birin, Y., Morandi, M. I., . . . Regev-Rudzki, N. (2021). 20S proteasomes secreted by the malaria parasite promote its growth. *Nature Communications*, *12*(1). https://doi.org/10.1038/s41467-021-21344-8

DePristo, M. A., Zilversmit, M. M., & Hartl, D. L. (2006). On the abundance, amino acid composition, and evolutionary dynamics of low-complexity regions in proteins. *Gene*, *378*, 19-30. https://doi.org/10.1016/j.gene.2006.03.023

Derkatch, I. L., Uptain, S. M., Outeiro, T. F., Krishnan, R., Lindquist, S. L., & Liebman, S. W. (2004). Effects of Q/N-rich, polyQ, and non-polyQ amyloids on the de novo formation of the [PSI+] prion in yeast and aggregation of Sup35 in vitro. *Proc Natl Acad Sci U S A*, *101*(35), 12934-12939. https://doi.org/10.1073/pnas.0404968101

di Marco, A. (2012). *Hydrogen bonds. Basic protein structures.* http://www.chim.lu/

Dobson, C. M. (2003). Protein folding and misfolding. *Nature*, *426*(6968), 884-890. https://doi.org/10.1038/nature02261

Dogovski, C., Xie, S. C., Burgio, G., Bridgford, J., Mok, S., McCaw, J. M., . . . Tilley, L. (2015). Targeting the cell stress response of Plasmodium falciparum to overcome artemisinin resistance. *PLoS Biol*, *13*(4), e1002132. https://doi.org/10.1371/journal.pbio.1002132

Doh-Ura, K., Iwaki, T., & Caughey, B. (2000). Lysosomotropic Agents and Cysteine Protease Inhibitors Inhibit Scrapie-Associated Prion Protein Accumulation. *Journal of Virology*, *74*(10), 4894-4897. https://doi.org/10.1128/jvi.74.10.4894-4897.2000

Dondorp, A. M., Nosten, F., Yi, P., Das, D., Phyo, A. P., Tarning, J., . . . White, N. J. (2009). Artemisinin resistance in Plasmodium falciparum malaria. *N Engl J Med*, *361*(5), 455-467. https://doi.org/10.1056/NEJMoa0808859

Dubey, R., Kulkarni, S. H., Dantu, S. C., Panigrahi, R., Sardesai, D. M., Malik, N., . . . Kumar, A. (2021). Myricetin protects pancreatic β-cells from human islet amyloid polypeptide (hIAPP) induced cytotoxicity and restores islet function. *Biol Chem*, *402*(2), 179-194. https://doi.org/10.1515/hsz-2020-0176

Egan, T. J., & Ncokazi, K. K. (2005). Quinoline antimalarials decrease the rate of beta-hematin formation. *J Inorg Biochem*, *99*(7), 1532-1539. https://doi.org/10.1016/j.jinorgbio.2005.04.013

Egieyeh, S., Malan, Sarel F. and Christoffels, Alan. (2021). Cheminformatics techniques in antimalarial drug discovery and development from natural products 2: Molecular scaffold and machine learning approaches. *Physical Sciences Reviews*, *6*(3).

Eichinger, L., Pachebat, J. A., Glöckner, G., Rajandream, M. A., Sucgang, R., Berriman, M., . . . Kuspa, A. (2005). The genome of the social amoeba Dictyostelium discoideum. *Nature*, *435*(7038), 43-57. https://doi.org/10.1038/nature03481

Erath, J., Djuranovic, S., & Djuranovic, S. P. (2019). Adaptation of Translational Machinery in Malaria Parasites to Accommodate Translation of Poly-Adenosine Stretches Throughout Its Life Cycle. *Front Microbiol*, *10*, 2823. https://doi.org/10.3389/fmicb.2019.02823

Espargaró, A., Pont, C., Gamez, P., Muñoz-Torrero, D., & Sabate, R. (2019). Amyloid Pan-inhibitors: One Family of Compounds To Cope with All Conformational Diseases. *ACS Chem Neurosci*, *10*(3), 1311-1317. https://doi.org/10.1021/acschemneuro.8b00398

Everson, N., Bach, J., Hammill, J. T., Falade, M. O., Rice, A. L., Guy, R. K., & Eagon, S. (2021). Identification of Plasmodium falciparum heat shock 90 inhibitors via molecular docking. *Bioorg Med Chem Lett*, *35*, 127818. https://doi.org/10.1016/j.bmcl.2021.127818

Ezzet, F., van Vugt, M., Nosten, F., Looareesuwan, S., & White, N. J. (2000). Pharmacokinetics and pharmacodynamics of lumefantrine (benflumetol) in acute falciparum malaria. *Antimicrob Agents Chemother*, *44*(3), 697-704. https://doi.org/10.1128/AAC.44.3.697-704.2000

Faurant, C. (2011). From bark to weed: the history of artemisinin. *Parasite*, *18*(3), 215-218. https://doi.org/10.1051/parasite/2011183215

Fennell, C., Babbitt, S., Russo, I., Wilkes, J., Ranford-Cartwright, L., Goldberg, D. E., & Doerig, C. (2009). PfeIK1, a eukaryotic initiation factor 2α kinase of the human malaria parasite Plasmodium falciparum, regulates stress-response to amino-acid starvation. *Malaria Journal*, *8*(1), 99. https://doi.org/10.1186/1475-2875-8-99

Fidock, D. A., Nomura, T., Talley, A. K., Cooper, R. A., Dzekunov, S. M., Ferdig, M. T., . . . Wellems, T. E. (2000). Mutations in the P. falciparum digestive vacuole transmembrane protein PfCRT and evidence for their role in chloroquine resistance. *Mol Cell*, *6*(4), 861-871. https://doi.org/10.1016/s1097-2765(05)00077-8

Filarsky, M., Fraschka, S. A., Niederwieser, I., Brancucci, N. M. B., Carrington, E., Carrió, E., . . . Voss, T. S. (2018). GDV1 induces sexual commitment of malaria parasites by antagonizing HP1-dependent gene silencing. *Science*, *359*(6381), 1259-1263. https://doi.org/10.1126/science.aan6042

Filisetti, D., Théobald-Dietrich, A., Mahmoudi, N., Rudinger-Thirion, J., Candolfi, E., & Frugier, M. (2013). Aminoacylation of Plasmodium falciparum tRNA(Asn) and insights in the synthesis of asparagine repeats. *J Biol Chem*, *288*(51), 36361-36371. https://doi.org/10.1074/jbc.M113.522896

Fitch, C. D., Chevli, R., Kanjananggulpan, P., Dutta, P., Chevli, K., & Chou, A. C. (1983). Intracellular ferriprotoporphyrin IX is a lytic agent. *Blood*, *62*(6), 1165-1168.

Fitri, L. E., Widaningrum, T., Endharti, A. T., Prabowo, M. H., Winaris, N., & Nugraha, R. Y. B. (2022). Malaria diagnostic update: From conventional to advanced method. *J Clin Lab Anal*, *36*(4), e24314. https://doi.org/10.1002/jcla.24314

Floudas, C. A., Fung, H. K., McAllister, S. R., Mönnigmann, M., & Rajgaria, R. (2006). Advances in protein structure prediction and de novo protein design: A review. *Chemical Engineering Science*, *61*(3), 22.

Foundation, T. N. (2019). *Women who changed science. Tu YouYou.* https://www.nobelprize.org/womenwhochangedscience/stories/tu-youyou

Fowler, D. M., Koulov, A. V., Alory-Jost, C., Marks, M. S., Balch, W. E., & Kelly, J. W. (2005). Functional Amyloid Formation within Mammalian Tissue. *PLoS Biology*, *4*(1), e6. https://doi.org/10.1371/journal.pbio.0040006

Francis, S. E., Sullivan, D. J., & Goldberg, D. E. (1997). Hemoglobin metabolism in the malaria parasite Plasmodium falciparum. *Annu Rev Microbiol*, *51*, 97-123. https://doi.org/10.1146/annurev.micro.51.1.97

Fraser, C. M., Casjens, S., Huang, W. M., Sutton, G. G., Clayton, R., Lathigra, R., . . . Venter, J. C. (1997). Genomic sequence of a Lyme disease spirochaete, Borrelia burgdorferi. *Nature*, *390*(6660), 580-586. https://doi.org/10.1038/37551

Freilich, R., Arhar, T., Abrams, J. L., & Gestwicki, J. E. (2018). Protein–Protein Interactions in the Molecular Chaperone Network. *Accounts of Chemical Research*, *51*(4), 940-949. https://doi.org/10.1021/acs.accounts.8b00036

Fried, M., & Duffy, P. E. (1996). Adherence of Plasmodium falciparum to chondroitin sulfate A in the human placenta. *Science*, *272*(5267), 1502-1504. https://doi.org/10.1126/science.272.5267.1502

Frugier, M., Bour, T., Ayach, M., Santos, M. A., Rudinger-Thirion, J., Théobald-Dietrich, A., & Pizzi, E. (2010). Low Complexity Regions behave as tRNA sponges to help co-translational folding of plasmodial proteins. *FEBS Lett*, *584*(2), 448-454. https://doi.org/10.1016/j.febslet.2009.11.004

Fu, S., & Xiao, S. H. (1991). Pyronaridine: A new antimalarial drug. *Parasitol Today*, *7*(11), 310-313. https://doi.org/10.1016/0169-4758(91)90267-r

Galluzzi, L., Diotallevi, A., & Magnani, M. (2017). Endoplasmic reticulum stress and unfolded protein response in infection by intracellular parasites. *Future Science OA*, *3*(3), FSO198. https://doi.org/10.4155/fsoa-2017-0020

Gardner, B. M., Pincus, D., Gotthardt, K., Gallagher, C. M., & Walter, P. (2013). Endoplasmic reticulum stress sensing in the unfolded protein response. *Cold Spring Harb Perspect Biol*, *5*(3), a013169. https://doi.org/10.1101/cshperspect.a013169

Gardner, M. J., Hall, N., Fung, E., White, O., Berriman, M., Hyman, R. W., . . . Barrell, B. (2002). Genome sequence of the human malaria parasite Plasmodium falciparum. *Nature*, *419*(6906), 498-511. https://doi.org/10.1038/nature01097

Georgieva, D., Schwark, D., von Bergen, M., Redecke, L., Genov, N., & Betzel, C. (2006). Interactions of recombinant prions with compounds of therapeutical significance. *Biochem Biophys Res Commun*, *344*(2), 463-470. https://doi.org/10.1016/j.bbrc.2006.03.135

Gilson, P. R., Nebl, T., Vukcevic, D., Moritz, R. L., Sargeant, T., Speed, T. P., . . . Crabb, B. S. (2006). Identification and stoichiometry of glycosylphosphatidylinositol-anchored membrane proteins of the human malaria parasite Plasmodium falciparum. *Mol Cell Proteomics*, *5*(7), 1286-1299. https://doi.org/10.1074/mcp.M600035-MCP200

Gopalakrishnan, A. M., & Kumar, N. (2015). Antimalarial action of artesunate involves DNA damage mediated by reactive oxygen species. *Antimicrob Agents Chemother*, *59*(1), 317-325. https://doi.org/10.1128/AAC.03663-14

Gosline, S. J. C., Nascimento, M., Mccall, L.-I., Zilberstein, D., Thomas, D. Y., Matlashewski, G., & Hallett, M. (2011). Intracellular Eukaryotic Parasites Have a Distinct Unfolded Protein Response. *PLoS ONE*, *6*(4), e19118. https://doi.org/10.1371/journal.pone.0019118

Green, J. L., Wu, Y., Encheva, V., Lasonder, E., Prommaban, A., Kunzelmann, S., . . . Holder, A. A. (2020). Ubiquitin activation is essential for schizont maturation in Plasmodium falciparum blood-stage development. *PLOS Pathogens*, *16*(6), e1008640. https://doi.org/10.1371/journal.ppat.1008640

Guasch-Girbau, A., & Fernàndez-Busquets, X. (2021). Review of the Current Landscape of the Potential of Nanotechnology for Future Malaria Diagnosis, Treatment, and Vaccination Strategies. *Pharmaceutics*, *13*(12). https://doi.org/10.3390/pharmaceutics13122189

Guetzoyan, L., Yu, X. M., Ramiandrasoa, F., Pethe, S., Rogier, C., Pradines, B., . . . Mahy, J. P. (2009). Antimalarial acridines: synthesis, in vitro activity against P. falciparum and interaction with hematin. *Bioorg Med Chem*, *17*(23), 8032-8039. https://doi.org/10.1016/j.bmc.2009.10.005

Guy, R., Liu, P., Pennefather, P., & Crandall, I. (2007). The use of fluorescence enhancement to improve the microscopic diagnosis of falciparum malaria. *Malar J*, *6*, 89. https://doi.org/10.1186/1475-2875-6-89

Guillemin, J. (2001). Miasma, malaria, and method. *Mol Interv*, *1*(5), 246-249.

Haldar, K., Bhattacharjee, S., & Safeukui, I. (2018). Drug resistance in Plasmodium. *Nat Rev Microbiol*, *16*(3), 156-170. https://doi.org/10.1038/nrmicro.2017.161

Halfmann, R., Alberti, S., Krishnan, R., Lyle, N., O'Donnell, C. W., King, O. D., . . . Lindquist, S. (2011). Opposing effects of glutamine and asparagine govern prion formation by intrinsically disordered proteins. *Mol Cell*, *43*(1), 72-84. https://doi.org/10.1016/j.molcel.2011.05.013

Hamilton, M. J., Lee, M., & Le Roch, K. G. (2014). The ubiquitin system: an essential component to unlocking the secrets of malaria parasite biology. *Mol. BioSyst.*, *10*(4), 715-723. https://doi.org/10.1039/c3mb70506d

Han, K. T., Lin, K., Han, Z. Y., Myint, M. K., Aye, K. H., Thi, A., . . . Duparc, S. (2020). Efficacy and Safety of Pyronaridine-Artesunate for the Treatment of Uncomplicated. *Am J Trop Med Hyg*, *103*(3), 1088-1093. https://doi.org/10.4269/ajtmh.20-0185

Hawley, S. R., Bray, P. G., Mungthin, M., Atkinson, J. D., O'Neill, P. M., & Ward, S. A. (1998). Relationship between antimalarial drug activity, accumulation, and inhibition of heme polymerization in Plasmodium falciparum in vitro. *Antimicrob Agents Chemother*, *42*(3), 682-686. https://doi.org/10.1128/AAC.42.3.682

Hawley, S. R., Bray, P. G., O'Neill, P. M., Park, B. K., & Ward, S. A. (1996). The role of drug accumulation in 4-aminoquinoline antimalarial potency. The influence of structural substitution and physicochemical properties. *Biochem Pharmacol*, *52*(5), 723-733. https://doi.org/10.1016/0006-2952(96)00354-1

Hee, J. S., Mitchell, S. M., Liu, X., & Leonhardt, R. M. (2017). Melanosomal formation of PMEL core amyloid is driven by aromatic residues. *Scientific Reports*, *7*(1), 44064. https://doi.org/10.1038/srep44064

Hemingway, J., Ranson, H., Magill, A., Kolaczinski, J., Fornadel, C., Gimnig, J., . . . Hamon, N. (2016). Averting a malaria disaster: will insecticide resistance derail malaria control? *Lancet*, *387*(10029), 1785-1788. https://doi.org/10.1016/S0140-6736(15)00417-1

Hempelmann, E. (2007). Hemozoin biocrystallization in Plasmodium falciparum and the antimalarial activity of crystallization inhibitors. *Parasitol Res*, *100*(4), 671-676. https://doi.org/10.1007/s00436-006-0313-x

Hempelmann, E., & Krafts, K. (2013). Bad air, amulets and mosquitoes: 2,000 years of changing perspectives on malaria. *Malar J*, *12*, 232. https://doi.org/10.1186/1475-2875-12-232

Hollin, T., & Le Roch, K. G. (2020). From Genes to Transcripts, a Tightly Regulated Journey in. *Front Cell Infect Microbiol*, *10*, 618454. https://doi.org/10.3389/fcimb.2020.618454

How, S. C., Cheng, Y. H., Lo, C. H., Lai, J. T., Lin, T. H., Bednarikova, Z., . . . Wang, S. S. (2018). Exploring the effects of methylene blue on amyloid fibrillogenesis of lysozyme. *Int J Biol Macromol*, *119*, 1059-1067. https://doi.org/10.1016/j.ijbiomac.2018.08.038

Hughes, K. R., Philip, N., Starnes, G. L., Taylor, S., & Waters, A. P. (2010). From cradle to grave: RNA biology in malaria parasites. *Wiley Interdiscip Rev RNA*, *1*(2), 287-303. https://doi.org/10.1002/wrna.30

Humphreys, G. S., Merinopoulos, I., Ahmed, J., Whitty, C. J., Mutabingwa, T. K., Sutherland, C. J., & Hallett, R. L. (2007). Amodiaquine and artemether-lumefantrine select distinct alleles of the Plasmodium falciparum mdr1 gene in Tanzanian children treated for uncomplicated malaria. *Antimicrob Agents Chemother*, *51*(3), 991-997. https://doi.org/10.1128/AAC.00875-06

Hyde, J. E. (2005). Exploring the folate pathway in Plasmodium falciparum. *Acta Trop*, *94*(3), 191-206. https://doi.org/10.1016/j.actatropica.2005.04.002

Hébert, E. (1848-1849). *La Mal'aria*. Paris. https://commons.wikimedia.org/wiki/File:Ernest_H%C3%A9bert_-_The_Mal%27aria_-_Google_Art_Project.jpg

Iadanza, M. G., Jackson, M. P., Hewitt, E. W., Ranson, N. A., & Radford, S. E. (2018). A new era for understanding amyloid structures and disease. *Nat Rev Mol Cell Biol*, *19*(12), 755-773. https://doi.org/10.1038/s41580-018-0060-8

Imam, M., Singh, S., Kaushik, N. K., & Chauhan, V. S. (2014). Plasmodium falciparum merozoite surface protein 3: oligomerization, self-assembly, and heme complex formation. *J Biol Chem*, *289*(7), 3856-3868. https://doi.org/10.1074/jbc.M113.520239

Imbert Palafox, J. L., González Linares, L., Reyes-Cruz, V. E., Becerril Flores, M. A., Ruvalcaba Ledezma, J. C., Gonzalez Alvarez, C. M., . . . Bautista Garcia, J. E. (2020). In vitro redox activity of haemozoin and β-haemozoin interacting with the following antimalarials: artemether, lumefantrine and quinine. *Eur Rev Med Pharmacol Sci*, *24*(12), 7063-7076. https://doi.org/10.26355/eurrev_202006_21700

Ippolito, M. M., Johnson, J., Mullin, C., Mallow, C., Morgan, N., Wallender, E., . . . Rosenthal, P. J. (2017). The Relative Effects of Artemether-lumefantrine and Non-artemisinin Antimalarials on Gametocyte Carriage and Transmission of Plasmodium falciparum: A Systematic Review and Meta-analysis. *Clin Infect Dis*, *65*(3), 486-494. https://doi.org/10.1093/cid/cix336

Ismail, H. M., Barton, V., Phanchana, M., Charoensutthivarakul, S., Wong, M. H., Hemingway, J., . . . Ward, S. A. (2016). Artemisinin activity-based probes identify multiple molecular targets within the asexual stage of the malaria parasites Plasmodium falciparum 3D7. *Proc Natl Acad Sci U S A*, *113*(8), 2080-2085. https://doi.org/10.1073/pnas.1600459113

Jaikaran, E. T., & Clark, A. (2001). Islet amyloid and type 2 diabetes: from molecular misfolding to islet pathophysiology. *Biochim Biophys Acta*, *1537*(3), 179-203. https://doi.org/10.1016/s0925-4439(01)00078-3

Jain, J., Jain, S. K., Walker, L. A., & Tekwani, B. L. (2017). Inhibitors of ubiquitin E3 ligase as potential new antimalarial drug leads. *BMC Pharmacology and Toxicology*, *18*(1). https://doi.org/10.1186/s40360-017-0147-4

Jamar, N. H., Kritsiligkou, P., & Grant, C. M. (2018). Loss of mRNA surveillance pathways results in widespread protein aggregation. *Sci Rep*, *8*(1), 3894. https://doi.org/10.1038/s41598-018-22183-2

Jamar, N. H., Kritsiligkou, P., & Grant, C. M. (2021). Author Correction: Loss of mRNA surveillance pathways results in widespread protein aggregation. *Sci Rep*, *11*(1), 16722. https://doi.org/10.1038/s41598-021-95596-1

Jarrett, J. T., & Lansbury, P. T. (1993). Seeding "one-dimensional crystallization" of amyloid: a pathogenic mechanism in Alzheimer's disease and scrapie? *Cell*, *73*(6), 1055-1058. https://doi.org/10.1016/0092-8674(93)90635-4

Johnson, K. H., O'Brien, T. D., Betsholtz, C., & Westermark, P. (1989). Islet amyloid, islet-amyloid polypeptide, and diabetes mellitus. *N Engl J Med*, *321*(8), 513-518. https://doi.org/10.1056/NEJM198908243210806

Jolly, C., Morimoto, R., Robert-Nicoud, M., & Vourc'h, C. (1997). HSF1 transcription factor concentrates in nuclear foci during heat shock: relationship with transcription sites. *J Cell Sci*, *110 (Pt 23)*, 2935-2941.

Josling, G. A., & Llinas, M. (2015). Sexual development in Plasmodium parasites: knowing when it's time to commit. *Nat Rev Microbiol*, *13*(9), 573-587. https://doi.org/10.1038/nrmicro3519

Josling, G. A., Russell, T. J., Venezia, J., Orchard, L., van Biljon, R., Painter, H. J., & Llinás, M. (2020). Dissecting the role of PfAP2-G in malaria gametocytogenesis. *Nat Commun*, *11*(1), 1503. https://doi.org/10.1038/s41467-020-15026-0

Kadekoppala, M., O'Donnell, R. A., Grainger, M., Crabb, B. S., & Holder, A. A. (2008). Deletion of the Plasmodium falciparum merozoite surface protein 7 gene impairs parasite invasion of erythrocytes. *Eukaryot Cell*, *7*(12), 2123-2132. https://doi.org/10.1128/EC.00274-08

Kafsack, B. F., Rovira-Graells, N., Clark, T. G., Bancells, C., Crowley, V. M., Campino, S. G., . . . Llinás, M. (2014). A transcriptional switch underlies commitment to sexual development in malaria parasites. *Nature*, *507*(7491), 248-252. https://doi.org/10.1038/nature12920

Karshikoff, A. (2021). *Non-covalent interactions in proteins* (Second edition. ed.). World Scientific.

Keeling, P. J., & Rayner, J. C. (2015). The origins of malaria: there are more things in heaven and earth. *Parasitology*, *142 Suppl 1*, S16-25. https://doi.org/10.1017/S0031182014000766

Knowles, T. P., Waudby, C. A., Devlin, G. L., Cohen, S. I., Aguzzi, A., Vendruscolo, M., . . . Dobson, C. M. (2009). An analytical solution to the kinetics of breakable filament assembly. *Science*, *326*(5959), 1533-1537. https://doi.org/10.1126/science.1178250

Kozak, M. (1999). Initiation of translation in prokaryotes and eukaryotes. *Gene*, *234*(2), 187-208. https://doi.org/10.1016/s0378-1119(99)00210-3

Kozak, M. (2005). Regulation of translation via mRNA structure in prokaryotes and eukaryotes. *Gene*, *361*, 13-37. https://doi.org/10.1016/j.gene.2005.06.037

Krafts, K., Hempelmann, E., & Skórska-Stania, A. (2012). From methylene blue to chloroquine: a brief review of the development of an antimalarial therapy. *Parasitol Res*, *111*(1), 1-6. https://doi.org/10.1007/s00436-012-2886-x

Krebs, M. R., Morozova-Roche, L. A., Daniel, K., Robinson, C. V., & Dobson, C. M. (2004). Observation of sequence specificity in the seeding of protein amyloid fibrils. *Protein Sci*, *13*(7), 1933-1938. https://doi.org/10.1110/ps.04707004

Kreidenweiss, A., Kremsner, P. G., & Mordmüller, B. (2008). Comprehensive study of proteasome inhibitors against Plasmodium falciparum laboratory strains and field isolates from Gabon. *Malaria Journal*, *7*(1), 187. https://doi.org/10.1186/1475-2875-7-187

Kumar, H., & Tolia, N. H. (2019). Getting in: The structural biology of malaria invasion. *PLoS Pathog*, *15*(9), e1007943. https://doi.org/10.1371/journal.ppat.1007943

Kumar, R., Verma, A. K., Shrivas, S., Thota, P., Singh, M. P., Rajasubramaniam, S., . . . Bharti, P. K. (2020). First successful field evaluation of new, one-minute haemozoin-based malaria diagnostic device. *EClinicalMedicine*, *22*, 100347. https://doi.org/10.1016/j.eclinm.2020.100347

Lamonte, G. M., Almaliti, J., Bibo-Verdugo, B., Keller, L., Zou, B. Y., Yang, J., . . . Ottilie, S. (2017). Development of a Potent Inhibitor of the Plasmodium Proteasome with Reduced Mammalian Toxicity. *Journal of Medicinal Chemistry*, *60*(15), 6721-6732. https://doi.org/10.1021/acs.jmedchem.7b00671

Lancaster, A. K., Nutter-Upham, A., Lindquist, S., & King, O. D. (2014). PLAAC: a web and command-line application to identify proteins with prion-like amino acid composition. *Bioinformatics*, *30*(17), 2501-2502. https://doi.org/10.1093/bioinformatics/btu310

Laurens, M. B. (2020). RTS,S/AS01 vaccine (Mosquirix™): an overview. *Hum Vaccin Immunother*, *16*(3), 480-489. https://doi.org/10.1080/21645515.2019.1669415
Laveran, C. L. A. (1880). Note sur un nouveau parasite trouvé dans le sang de plusieurs malades atteints de fièvre palustres. *Bulletin de L'Académie Nationale de Médecine*, *9*, 1235-1236.
Leang, R., Canavati, S. E., Khim, N., Vestergaard, L. S., Borghini Fuhrer, I., Kim, S., . . . Ringwald, P. (2016). Efficacy and Safety of Pyronaridine-Artesunate for Treatment of Uncomplicated Plasmodium falciparum Malaria in Western Cambodia. *Antimicrob Agents Chemother*, *60*(7), 3884-3890. https://doi.org/10.1128/AAC.00039-16
Levkovich, S. A., Gazit, E., & Laor Bar-Yosef, D. (2021). Two Decades of Studying Functional Amyloids in Microorganisms. *Trends Microbiol*, *29*(3), 251-265. https://doi.org/10.1016/j.tim.2020.09.005
Li, G. D., Liu, S. Q., Ye, X. Y., & Qu, F. Y. (1995). Detection of 54-kDa protein overexpressed by chloroquine-resistant Plasmodium berghei ANKA strain in pyronaridine-resistant P berghei ANKA strain. *Zhongguo Yao Li Xue Bao*, *16*(1), 17-20.
Li, H., Bogyo, M., & Da Fonseca, P. C. A. (2016). The cryo-EM structure of thePlasmodium falciparum20S proteasome and its use in the fight against malaria. *The FEBS Journal*, *283*(23), 4238-4243. https://doi.org/10.1111/febs.13780
Li, H., O'Donoghue, A. J., Van Der Linden, W. A., Xie, S. C., Yoo, E., Foe, I. T., . . . Bogyo, M. (2016). Structure- and function-based design of Plasmodium-selective proteasome inhibitors. *Nature*, *530*(7589), 233-236. https://doi.org/10.1038/nature16936
Li, Y., Ogunnaike, B. A., & Roberts, C. J. (2010). Multi-variate approach to global protein aggregation behavior and kinetics: effects of pH, NaCl, and temperature for alpha-chymotrypsinogen A. *J Pharm Sci*, *99*(2), 645-662. https://doi.org/10.1002/jps.21869
Lin, C. S., Uboldi, A. D., Epp, C., Bujard, H., Tsuboi, T., Czabotar, P. E., & Cowman, A. F. (2016). Multiple Plasmodium falciparum Merozoite Surface Protein 1 Complexes Mediate Merozoite Binding to Human Erythrocytes. *J Biol Chem*, *291*(14), 7703-7715. https://doi.org/10.1074/jbc.M115.698282
Linding, R., Schymkowitz, J., Rousseau, F., Diella, F., & Serrano, L. (2004). A comparative study of the relationship between protein structure and beta-aggregation in globular and intrinsically disordered proteins. *J Mol Biol*, *342*(1), 345-353. https://doi.org/10.1016/j.jmb.2004.06.088
Liu, Y., Wei, H., Wang, J., Qu, J., Zhao, W., & Tao, H. (2007). Effects of randomizing the Sup35NM prion domain sequence on formation of amyloid fibrils in vitro. *Biochem Biophys Res Commun*, *353*(1), 139-146. https://doi.org/10.1016/j.bbrc.2006.11.143
Liu, Y. F., Oey, I., Bremer, P., Carne, A., & Silcock, P. (2017). Effects of pH, temperature and pulsed electric fields on the turbidity and protein aggregation of ovomucin-depleted egg white. *Food Res Int*, *91*, 161-170. https://doi.org/10.1016/j.foodres.2016.12.005
Lu, B. W., Baum, L., So, K. F., Chiu, K., & Xie, L. K. (2019). More than anti-malarial agents: therapeutic potential of artemisinins in neurodegeneration. *Neural Regen Res*, *14*(9), 1494-1498. https://doi.org/10.4103/1673-5374.255960
Lu, C., Zheng, X., Zhang, W., Zhao, H., Macraild, C. A., Norton, R. S., . . . Zhang, X. (2019). Interaction of merozoite surface protein 2 with lipid membranes. *FEBS Letters*, *593*(3), 288-295. https://doi.org/10.1002/1873-3468.13320
Lu, F., He, X. L., Richard, C., & Cao, J. (2019). A brief history of artemisinin: Modes of action and mechanisms of resistance. *Chin J Nat Med*, *17*(5), 331-336. https://doi.org/10.1016/S1875-5364(19)30038-X
Lu, K.-Y., Pasaje, C. F. A., Srivastava, T., Loiselle, D. R., Niles, J. C., & Derbyshire, E. (2020). Phosphatidylinositol 3-phosphate and Hsp70 protect Plasmodium falciparum from heat-induced cell death. *eLife*, *9*. https://doi.org/10.7554/elife.56773

Lu, X., & Murphy, R. M. (2015). Asparagine Repeat Peptides: Aggregation Kinetics and Comparison with Glutamine Repeats. *Biochemistry*, *54*(31), 4784-4794. https://doi.org/10.1021/acs.biochem.5b00644

Mabate, B., Zininga, T., Ramatsui, L., Makumire, S., Achilonu, I., Dirr, H. W., & Shonhai, A. (2018). Structural and biochemical characterization of Plasmodium falciparum Hsp70-x reveals functional versatility of its C-terminal EEVN motif. *Proteins: Structure, Function, and Bioinformatics*, *86*(11), 1189-1201. https://doi.org/10.1002/prot.25600

Mahler, H. C., Friess, W., Grauschopf, U., & Kiese, S. (2009). Protein aggregation: pathways, induction factors and analysis. *J Pharm Sci*, *98*(9), 2909-2934. https://doi.org/10.1002/jps.21566

Maji, S. K., Perrin, M. H., Sawaya, M. R., Jessberger, S., Vadodaria, K., Rissman, R. A., . . . Riek, R. (2009). Functional amyloids as natural storage of peptide hormones in pituitary secretory granules. *Science*, *325*(5938), 328-332. https://doi.org/10.1126/science.1173155

Malishev, R., Salinas, N., Gibson, J., Eden, A. B., Mieres-Perez, J., Ruiz-Blanco, Y. B., . . . Jelinek, R. (2021). Inhibition of Staphylococcus aureus biofilm-forming functional amyloid by molecular tweezers. *Cell Chem Biol*, *28*(9), 1310-1320.e1315. https://doi.org/10.1016/j.chembiol.2021.03.013

Mantel, P.-Y., Hoang, N., Anh, Goldowitz, I., Potashnikova, D., Hamza, B., Vorobjev, I., . . .

Marti, M. (2013). Malaria-Infected Erythrocyte-Derived Microvesicles Mediate Cellular Communication within the Parasite Population and with the Host Immune System. *Cell Host & Microbe*, *13*(5), 521-534. https://doi.org/10.1016/j.chom.2013.04.009

Marsh, K., Forster, D., Waruiru, C., Mwangi, I., Winstanley, M., Marsh, V., . . . Peshu, N. (1995). Indicators of life-threatening malaria in African children. *N Engl J Med*, *332*(21), 1399-1404. https://doi.org/10.1056/NEJM199505253322102

Martin, R. E., Marchetti, R. V., Cowan, A. I., Howitt, S. M., Bröer, S., & Kirk, K. (2009). Chloroquine transport via the malaria parasite's chloroquine resistance transporter. *Science*, *325*(5948), 1680-1682. https://doi.org/10.1126/science.1175667

Martins, R. M., Macpherson, C. R., Claes, A., Scheidig-Benatar, C., Sakamoto, H., Yam, X. Y., . . . Scherf, A. (2017). An ApiAP2 member regulates expression of clonally variant genes of the human malaria parasite Plasmodium falciparum. *Sci Rep*, *7*(1), 14042. https://doi.org/10.1038/s41598-017-12578-y

Mata-Cantero, L., Chaparro, M. J., Colmenarejo, G., Cid, C., Cortes Cabrera, A., Rodriguez, M. S., . . . Gomez-Lorenzo, M. G. (2019). Identification of Small Molecules Disrupting the Ubiquitin Proteasome System in Malaria. *ACS Infectious Diseases*, *5*(12), 2105-2117. https://doi.org/10.1021/acsinfecdis.9b00216

Maurer-Stroh, S., Debulpaep, M., Kuemmerer, N., Lopez de la Paz, M., Martins, I. C., Reumers, J., . . . Rousseau, F. (2010). Exploring the sequence determinants of amyloid structure using position-specific scoring matrices. *Nat Methods*, *7*(3), 237-242. https://doi.org/10.1038/nmeth.1432

McGowan, D. P., van Roon-Mom, W., Holloway, H., Bates, G. P., Mangiarini, L., Cooper, G. J., . . . Snell, R. G. (2000). Amyloid-like inclusions in Huntington's disease. *Neuroscience*, *100*(4), 677-680. https://doi.org/10.1016/s0306-4522(00)00391-2

Meshnick, S. R., Thomas, A., Ranz, A., Xu, C. M., & Pan, H. Z. (1991). Artemisinin (qinghaosu): the role of intracellular hemin in its mechanism of antimalarial action. *Mol Biochem Parasitol*, *49*(2), 181-189. https://doi.org/10.1016/0166-6851(91)90062-b

Meyer, P., Prodromou, C., Hu, B., Vaughan, C., Roe, S. M., Panaretou, B., . . . Pearl, L. H. (2003). Structural and functional analysis of the middle segment of hsp90: implications for ATP hydrolysis and client protein and cochaperone interactions. *Mol Cell*, *11*(3), 647-658. https://doi.org/10.1016/s1097-2765(03)00065-0

Mfuh, K. O., Achonduh-Atijegbe, O. A., Bekindaka, O. N., Esemu, L. F., Mbakop, C. D., Gandhi, K., . . . Nerurkar, V. R. (2019). A comparison of thick-film microscopy, rapid diagnostic test, and polymerase chain reaction for accurate diagnosis of Plasmodium falciparum malaria. *Malar J*, *18*(1), 73. https://doi.org/10.1186/s12936-019-2711-4

Mikecz, A. v. (2009). Protein aggregation in the cell nucleus: structure, function and topology. *The Open Biology Journal*, *2*, 6.

Mistry, J., Chuguransky, S., Williams, L., Qureshi, M., Salazar, G. A., Sonnhammer, E. L. L., . . . Bateman, A. (2021). Pfam: The protein families database in 2021. *Nucleic Acids Res*, *49*(D1), D412-D419. https://doi.org/10.1093/nar/gkaa913

Mok, S., Ashley, E. A., Ferreira, P. E., Zhu, L., Lin, Z., Yeo, T., . . . Bozdech, Z. (2015). Drug resistance. Population transcriptomics of human malaria parasites reveals the mechanism of artemisinin resistance. *Science*, *347*(6220), 431-435. https://doi.org/10.1126/science.1260403

Moles, E., Urbán, P., Jiménez-Díaz, M. B., Viera-Morilla, S., Angulo-Barturen, I., Busquets, M. A., & Fernàndez-Busquets, X. (2015). Immunoliposome-mediated drug delivery to Plasmodium-infected and non-infected red blood cells as a dual therapeutic/prophylactic antimalarial strategy. *J Control Release*, *210*, 217-229. https://doi.org/10.1016/j.jconrel.2015.05.284

Molnar, C., & Gair, J. (2015). Biological molecules. In C. Molnar & J. Gair (Eds.), *Concepts of Biology-1st Canadian Edition*. BCcampus.

Monsellier, E., & Chiti, F. (2007). Prevention of amyloid-like aggregation as a driving force of protein evolution. *EMBO reports*, *8*(8), 737-742. https://doi.org/10.1038/sj.embor.7401034

Mota, M. M., Pradel, G., Vanderberg, J. P., Hafalla, J. C., Frevert, U., Nussenzweig, R. S., . . . Rodríguez, A. (2001). Migration of Plasmodium sporozoites through cells before infection. *Science*, *291*(5501), 141-144. https://doi.org/10.1126/science.291.5501.141

Moxon, C. A., Gibbins, M. P., McGuinness, D., Milner, D. A., & Marti, M. (2020). New Insights into Malaria Pathogenesis. *Annu Rev Pathol*, *15*, 315-343. https://doi.org/10.1146/annurev-pathmechdis-012419-032640

Mullié, C., Jonet, A., Desgrouas, C., Taudon, N., & Sonnet, P. (2012). Differences in anti-malarial activity of 4-aminoalcohol quinoline enantiomers and investigation of the presumed underlying mechanism of action. *Malar J*, *11*, 65. https://doi.org/10.1186/1475-2875-11-65

Mungthin, M., Bray, P. G., Ridley, R. G., & Ward, S. A. (1998). Central role of hemoglobin degradation in mechanisms of action of 4-aminoquinolines, quinoline methanols, and phenanthrene methanols. *Antimicrob Agents Chemother*, *42*(11), 2973-2977. https://doi.org/10.1128/AAC.42.11.2973

Muralidar, S., Ambi, S. V., Sekaran, S., Thirumalai, D., & Palaniappan, B. (2020). Role of tau protein in Alzheimer's disease: The prime pathological player. *Int J Biol Macromol*, *163*, 1599-1617. https://doi.org/10.1016/j.ijbiomac.2020.07.327

Muralidharan, V., Oksman, A., Iwamoto, M., Wandless, T. J., & Goldberg, D. E. (2011). Asparagine repeat function in a Plasmodium falciparum protein assessed via a regulatable fluorescent affinity tag. *Proceedings of the National Academy of Sciences*, *108*(11), 4411-4416. https://doi.org/10.1073/pnas.1018449108

Muralidharan, V., Oksman, A., Pal, P., Lindquist, S., & Goldberg, D. E. (2012). Plasmodium falciparum heat shock protein 110 stabilizes the asparagine repeat-rich parasite proteome during malarial fevers. *Nature Communications*, *3*(1), 1310. https://doi.org/10.1038/ncomms2306

Musteikyte, G., Ziaunys, M., & Smirnovas, V. (2020). Methylene blue inhibits nucleation and elongation of SOD1 amyloid fibrils. *PeerJ*, *8*, e9719. https://doi.org/10.7717/peerj.9719

Mwai, L., Diriye, A., Masseno, V., Muriithi, S., Feltwell, T., Musyoki, J., . . . Carret, C. K. (2012). Genome wide adaptations of Plasmodium falciparum in response to lumefantrine selective drug pressure. *PLoS One*, *7*(2), e31623. https://doi.org/10.1371/journal.pone.0031623

Ménard, D., Khim, N., Beghain, J., Adegnika, A. A., Shafiul-Alam, M., Amodu, O., . . . Consortium, K. (2016). A Worldwide Map of Plasmodium falciparum K13-Propeller Polymorphisms. *N Engl J Med*, *374*(25), 2453-2464. https://doi.org/10.1056/NEJMoa1513137

Möhrle, J. J., Zhao, Y., Wernli, B., Franklin, M. R., & Kappes, B. (1997). Molecular cloning, characterization and localization of PfPK4, an eIF-2α kinase-related enzyme from the malarial parasite Plasmodium falciparum. *Biochemical Journal*, *328*(2), 677-687. https://doi.org/10.1042/bj3280677

Nair, S., Miller, B., Barends, M., Jaidee, A., Patel, J., Mayxay, M., . . . Anderson, T. J. (2008). Adaptive copy number evolution in malaria parasites. *PLoS Genet*, *4*(10), e1000243. https://doi.org/10.1371/journal.pgen.1000243

Navarro, S., Villar-Piqué, A., & Ventura, S. (2014). Selection against toxic aggregation-prone protein sequences in bacteria. *Biochim Biophys Acta*, *1843*(5), 866-874. https://doi.org/10.1016/j.bbamcr.2014.01.020

Necula, M., Breydo, L., Milton, S., Kayed, R., van der Veer, W. E., Tone, P., & Glabe, C. G. (2007). Methylene blue inhibits amyloid Abeta oligomerization by promoting fibrillization. *Biochemistry*, *46*(30), 8850-8860. https://doi.org/10.1021/bi700411k

Neva, F. A., & Brown, H. W. (1996). *Basic clinical parasitology.* Appleton & Lange.

NIH. *https://clinicaltrials.gov/*. Retrieved 01/24/2022 from

Nizhnikov, A. A., Antonets, K. S., Bondarev, S. A., Inge-Vechtomov, S. G., & Derkatch, I. L. (2016). Prions, amyloids, and RNA: Pieces of a puzzle. *Prion*, *10*(3), 182-206. https://doi.org/10.1080/19336896.2016.1181253

Njokah, M. J., Kang'ethe, J. N., Kinyua, J., Kariuki, D., & Kimani, F. T. (2016). In vitro selection of Plasmodium falciparum Pfcrt and Pfmdr1 variants by artemisinin. *Malar J*, *15*(1), 381. https://doi.org/10.1186/s12936-016-1443-y

Nnaemeka, N., Emeka, E., & Oguzie, N. C. O., Akaranta. (2015). Comparative study on the inhibitive effect of Sulfadoxine–Pyrimethamine and an industrial inhibitor on the corrosion of pipeline steel in petroleum pipeline water. *Arabian Journal of Chemistry*, *2*(7), 10.

Noreen, N., Ullah, A., Salman, S. M., Mabkhot, Y., Alsayari, A., & Badshah, S. L. (2021). New insights into the spread of resistance to artemisinin and its analogues. *J Glob Antimicrob Resist*, *27*, 142-149. https://doi.org/10.1016/j.jgar.2021.09.001

Nzila, A., & Mwai, L. (2010). In vitro selection of Plasmodium falciparum drug-resistant parasite lines. *J Antimicrob Chemother*, *65*(3), 390-398. https://doi.org/10.1093/jac/dkp449

Nzila, A., Ward, S. A., Marsh, K., Sims, P. F., & Hyde, J. E. (2005). Comparative folate metabolism in humans and malaria parasites (part II): activities as yet untargeted or specific to Plasmodium. *Trends Parasitol*, *21*(7), 334-339. https://doi.org/10.1016/j.pt.2005.05.008

Nzila, A. M., Mberu, E. K., Sulo, J., Dayo, H., Winstanley, P. A., Sibley, C. H., & Watkins, W. M. (2000). Towards an understanding of the mechanism of pyrimethamine-sulfadoxine resistance in Plasmodium falciparum: genotyping of dihydrofolate reductase and dihydropteroate synthase of Kenyan parasites. *Antimicrob Agents Chemother*, *44*(4), 991-996. https://doi.org/10.1128/AAC.44.4.991-996.2000

Oie, S. (1986). Drug distribution and binding. *J Clin Pharmacol*, *26*(8), 583-586. https://doi.org/10.1002/j.1552-4604.1986.tb02953.x

Olliaro, P. (2001). Mode of action and mechanisms of resistance for antimalarial drugs. *Pharmacol Ther*, *89*(2), 207-219. https://doi.org/10.1016/s0163-7258(00)00115-7

Omura, S., & Crump, A. (2004). The life and times of ivermectin - a success story. *Nat Rev Microbiol*, *2*(12), 984-989. https://doi.org/10.1038/nrmicro1048

Organization, W. H. (2018). *Malaria Rapid Diagnostic Tests performance. Summary results of WHO product testing of malaria RDTs: round 1-8 (2008-2018).*

Ottesen, E. A., Hooper, P. J., Bradley, M., & Biswas, G. (2008). The global programme to eliminate lymphatic filariasis: health impact after 8 years. *PLoS Negl Trop Dis*, *2*(10), e317. https://doi.org/10.1371/journal.pntd.0000317

Pallarès, I., de Groot, N. S., Iglesias, V., Sant'Anna, R., Biosca, A., Fernàndez-Busquets, X., & Ventura, S. (2018). Discovering Putative Prion-Like Proteins in. *Front Microbiol*, *9*, 1737. https://doi.org/10.3389/fmicb.2018.01737

Pallavi, R., Acharya, P., Chandran, S., Daily, J. P., & Tatu, U. (2010). Chaperone expression profiles correlate with distinct physiological states of Plasmodium falciparum in malaria patients. *Malaria Journal*, *9*(1), 236. https://doi.org/10.1186/1475-2875-9-236

Panchal, M., Rawat, K., Kumar, G., Kibria, K. M., Singh, S., Kalamuddin, M., . . . Tuteja, R. (2014). Plasmodium falciparum signal recognition particle components and anti-parasitic effect of ivermectin in blocking nucleo-cytoplasmic shuttling of SRP. *Cell Death Dis*, *5*, e994. https://doi.org/10.1038/cddis.2013.521

Pandey, N., Strider, J., Nolan, W. C., Yan, S. X., & Galvin, J. E. (2008). Curcumin inhibits aggregation of α-synuclein. *Acta Neuropathologica*, *115*(4), 479-489. https://doi.org/10.1007/s00401-007-0332-4

Parhizgar, A. R., & Tahghighi, A. (2017). Introducing New Antimalarial Analogues of Chloroquine and Amodiaquine: A Narrative Review. *Iran J Med Sci*, *42*(2), 115-128.

Paul, A., Frenkel-Pinter, M., Escobar Alvarez, D., Milordini, G., Gazit, E., Zacco, E., & Segal, D. (2020). Tryptophan-galactosylamine conjugates inhibit and disaggregate amyloid fibrils of Aβ42 and hIAPP peptides while reducing their toxicity. *Commun Biol*, *3*(1), 484. https://doi.org/10.1038/s42003-020-01216-5

Paul, G., Deshmukh, A., Kumar Chourasia, B., Kalamuddin, M., Panda, A., Kumar Singh, S., . . . Malhotra, P. (2018). Protein-protein interaction studies reveal the. *Biochem J*, *475*(6), 1197-1209. https://doi.org/10.1042/BCJ20180017

Pavlovic Djuranovic, S., Erath, J., Andrews, R. J., Bayguinov, P. O., Chung, J. J., Chalker, D. L., . . . Djuranovic, S. (2020). translational machinery condones polyadenosine repeats. *Elife*, *9*. https://doi.org/10.7554/eLife.57799

Peatey, C. L., Skinner-Adams, T. S., Dixon, M. W., McCarthy, J. S., Gardiner, D. L., & Trenholme, K. R. (2009). Effect of antimalarial drugs on Plasmodium falciparum gametocytes. *J Infect Dis*, *200*(10), 1518-1521. https://doi.org/10.1086/644645

Perutz, M. F., Pope, B. J., Owen, D., Wanker, E. E., & Scherzinger, E. (2002). Aggregation of proteins with expanded glutamine and alanine repeats of the glutamine-rich and asparagine-rich domains of Sup35 and of the amyloid beta-peptide of amyloid plaques. *Proc Natl Acad Sci U S A*, *99*(8), 5596-5600. https://doi.org/10.1073/pnas.042681599

Picken, M., Maria. (2020). The Pathology of Amyloidosis in Classification: A Review. *Acta Haematologica*, *143*(4), 322-334. https://doi.org/10.1159/000506696

Prabakaran, R., Rawat, P., Thangakani, A. M., Kumar, S., & Gromiha, M. M. (2021). Protein aggregation: in silico algorithms and applications. *Biophysical Reviews*, *13*(1), 71-89. https://doi.org/10.1007/s12551-021-00778-w

Pradines, B., Briolant, S., Henry, M., Oeuvray, C., Baret, E., Amalvict, R., . . . Rogier, C. (2010). Absence of association between pyronaridine in vitro responses and polymorphisms in genes involved in quinoline resistance in Plasmodium falciparum. *Malar J*, *9*, 339. https://doi.org/10.1186/1475-2875-9-339

Prasad, R., Atul, Kolla, V. K., Legac, J., Singhal, N., Navale, R., . . . Sijwali, P. S. (2013). Blocking Plasmodium falciparum Development via Dual Inhibition of Hemoglobin Degradation and the Ubiquitin Proteasome System by MG132. *PLoS ONE*, *8*(9), e73530. https://doi.org/10.1371/journal.pone.0073530

Premji, Z. G. (2009). Coartem: the journey to the clinic. *Malar J*, *8 Suppl 1*, S3. https://doi.org/10.1186/1475-2875-8-S1-S3

Price, R. N., Uhlemann, A. C., Brockman, A., McGready, R., Ashley, E., Phaipun, L., . . . Krishna, S. (2004). Mefloquine resistance in Plasmodium falciparum and increased pfmdr1 gene copy number. *Lancet*, *364*(9432), 438-447. https://doi.org/10.1016/S0140-6736(04)16767-6

Progress in medicinal chemistry. In (pp. v.). London. Amsterdam: Elsevier.

Quang Bui, P., Hong Huynh, Q., Thanh Tran, D., Thanh Le, D., Quang Nguyen, T., Van Truong, H., . . . Thi Ta, T. (2020). Pyronaridine-artesunate Efficacy and Safety in Uncomplicated Plasmodium falciparum Malaria in Areas of Artemisinin-resistant Falciparum in Viet Nam (2017-2018). *Clin Infect Dis*, *70*(10), 2187-2195. https://doi.org/10.1093/cid/ciz580

Quang, H. H., Chavchich, M., Trinh, N. T. M., Edgel, K. A., Edstein, M. D., & Martin, N. J. (2021). Multidrug-Resistant Plasmodium falciparum Parasites in the Central Highlands of Vietnam Jeopardize Malaria Control and Elimination Strategies. *Antimicrob Agents Chemother*, *65*(4). https://doi.org/10.1128/AAC.01639-20

Rahman, M. U., Rehman, A. U., Arshad, T., & Chen, H. F. (2021). Disaggregation mechanism of prion amyloid for tweezer inhibitor. *Int J Biol Macromol*, *176*, 510-519. https://doi.org/10.1016/j.ijbiomac.2021.02.094

Raskatov, J. A., & Teplow, D. B. (2017). Using chirality to probe the conformational dynamics and assembly of intrinsically disordered amyloid proteins. *Sci Rep*, *7*(1), 12433. https://doi.org/10.1038/s41598-017-10525-5

Rasmussen, C., Alonso, P., & Ringwald, P. (2022). Current and emerging strategies to combat antimalarial resistance. *Expert Rev Anti Infect Ther*, *20*(3), 353-372. https://doi.org/10.1080/14787210.2021.1962291

Rathore, S., Datta, G., Kaur, I., Malhotra, P., & Mohmmed, A. (2015). Disruption of cellular homeostasis induces organelle stress and triggers apoptosis like cell-death pathways in malaria parasite. *Cell Death & Disease*, *6*(7), e1803-e1803. https://doi.org/10.1038/cddis.2015.142

Rawe, S. L., & McDonnell, C. (2020a). Thecinchona alkaloids and the aminoquinolines. In Graham & L. Patrick (Eds.), *Antimalarial agents* (pp. 65-98). Elsevier.

Rawe, S. L., & McDonnell, C. (2020b). The cinchona alkaloids and the aminoquinolines. In Graham & L. Patrick (Eds.), *Antimalarial agents* (pp. 65-98). Elsevier.

Reddy, R. C., Vatsala, P. G., Keshamouni, V. G., Padmanaban, G., & Rangarajan, P. N. (2005). Curcumin for malaria therapy. *Biochem Biophys Res Commun*, *326*(2), 472-474. https://doi.org/10.1016/j.bbrc.2004.11.051

Regev-Rudzki, N., Wilson, W., Danny, Carvalho, G., Teresa, Sisquella, X., Coleman, M., Bradley, Rug, M., . . . Cowman, F., Alan. (2013). Cell-Cell Communication between Malaria-Infected Red Blood Cells via Exosome-like Vesicles. *Cell*, *153*(5), 1120-1133. https://doi.org/10.1016/j.cell.2013.04.029

Remme, J., De Sole, G., & van Oortmarssen, G. J. (1990). The predicted and observed decline in onchocerciasis infection during 14 years of successful control of Simulium spp. in west Africa. *Bull World Health Organ*, *68*(3), 331-339. https://doi.org/10.1089/ten.2005.11.1105

Roberts, L. (2016). Malaria wars. *Science*, *352*(6284), 398-402, 404-395. https://doi.org/10.1126/science.352.6284.398

Romero, P., Obradovic, Z., Li, X., Garner, E. C., Brown, C. J., & Dunker, A. K. (2001). Sequence complexity of disordered protein. *Proteins*, *42*(1), 38-48. https://doi.org/10.1002/1097-0134(20010101)42:1<38::aid-prot50>3.0.co;2-3

RTS, S. C. T. P. (2015). Efficacy and safety of RTS,S/AS01 malaria vaccine with or without a booster dose in infants and children in Africa: final results of a phase 3, individually randomised, controlled trial. *Lancet*, *386*(9988), 31-45. https://doi.org/10.1016/S0140-6736(15)60721-8

Rubel, M. S., Fedotov, S. A., Grizel, A. V., Sopova, J. V., Malikova, O. A., Chernoff, Y. O., & Rubel, A. A. (2020). Functional Mammalian Amyloids and Amyloid-Like Proteins. *Life*, *10*(9), 156. https://doi.org/10.3390/life10090156

Rudlaff, R. M., Kraemer, S., Streva, V. A., & Dvorin, J. D. (2019). An essential contractile ring protein controls cell division in Plasmodium falciparum. *Nat Commun*, *10*(1), 2181. https://doi.org/10.1038/s41467-019-10214-z

Saad, S., Cereghetti, G., Feng, Y., Picotti, P., Peter, M., & Dechant, R. (2017). Reversible protein aggregation is a protective mechanism to ensure cell cycle restart after stress. *Nature Cell Biology*, *19*(10), 1202-1213. https://doi.org/10.1038/ncb3600

Sabate, R., Rousseau, F., Schymkowitz, J., & Ventura, S. (2015). What Makes a Protein Sequence a Prion? *PLoS Computational Biology*, *11*(1), e1004013. https://doi.org/10.1371/journal.pcbi.1004013

Salvatella, X. (2013). Structural aspects of amyloid formation. *Prog Mol Biol Transl Sci*, *117*, 73-101. https://doi.org/10.1016/B978-0-12-386931-9.00004-0

Samadoulougou, S., Kirakoya-Samadoulougou, F., Sarrassat, S., Tinto, H., Bakiono, F., Nebié, I., & Robert, A. (2014). Paracheck® rapid diagnostic test for detecting malaria infection in under five children: a population-based survey in Burkina Faso. *Malar J*, *13*, 101. https://doi.org/10.1186/1475-2875-13-101

Sanchez, C. P., Rotmann, A., Stein, W. D., & Lanzer, M. (2008). Polymorphisms within PfMDR1 alter the substrate specificity for anti-malarial drugs in Plasmodium falciparum. *Mol Microbiol*, *70*(4), 786-798. https://doi.org/10.1111/j.1365-2958.2008.06413.x

Santos, J., Pujols, J., Pallarès, I., Iglesias, V., & Ventura, S. (2020). Computational prediction of protein aggregation: Advances in proteomics, conformation-specific algorithms and biotechnological applications. *Comput Struct Biotechnol J*, *18*, 1403-1413. https://doi.org/10.1016/j.csbj.2020.05.026

Saravanan, K. M., Zhang, H., Xi, W., & Wei, Y. (2020). On the Conformational Dynamics of β-Amyloid Forming Peptides: A Computational Perspective. *Front Bioeng Biotechnol*, *8*, 532. https://doi.org/10.3389/fbioe.2020.00532

Schlagenhauf, P. (2004). Malaria: from prehistory to present. *Infect Dis Clin North Am*, *18*(2), 189-205, table of contents. https://doi.org/10.1016/j.idc.2004.01.002

Schofield, L., & Grau, G. E. (2005). Immunological processes in malaria pathogenesis. *Nat Rev Immunol*, *5*(9), 722-735. https://doi.org/10.1038/nri1686

Scholtz, J. M., & Baldwin, R. L. (1992). The mechanism of alpha-helix formation by peptides. *Annu Rev Biophys Biomol Struct*, *21*, 95-118. https://doi.org/10.1146/annurev.bb.21.060192.000523

Schwarz, D. S., & Blower, M. D. (2016). The endoplasmic reticulum: structure, function and response to cellular signaling. *Cell Mol Life Sci*, *73*(1), 79-94. https://doi.org/10.1007/s00018-015-2052-6

Schwarz, N. G., Adegnika, A. A., Breitling, L. P., Gabor, J., Agnandji, S. T., Newman, R. D., . . . Grobusch, M. P. (2008). Placental malaria increases malaria risk in the first 30 months of life. *Clin Infect Dis*, *47*(8), 1017-1025. https://doi.org/10.1086/591968

Selkoe, D. J. (1991). Alzheimer's disease. In the beginning.. *Nature*, *354*(6353), 432-433. https://doi.org/10.1038/354432a0

Sessler, N., Krug, K., Nordheim, A., Mordmüller, B., & Macek, B. (2012). Analysis of the Plasmodium falciparum proteasome using Blue Native PAGE and label-free quantitative mass spectrometry. *Amino Acids*, *43*(3), 1119-1129. https://doi.org/10.1007/s00726-012-1296-9

Sibley, C. H., Hyde, J. E., Sims, P. F., Plowe, C. V., Kublin, J. G., Mberu, E. K., . . . Nzila, A. M. (2001). Pyrimethamine-sulfadoxine resistance in Plasmodium falciparum: what next? *Trends Parasitol*, *17*(12), 582-588. https://doi.org/10.1016/s1471-4922(01)02085-2

Siddiqi, M. K., Alam, P., Chaturvedi, S. K., Shahein, Y. E., & Khan, R. H. (2017). Mechanisms of protein aggregation and inhibition. *9*, 20.

Singh, G. P., Chandra, B. R., Bhattacharya, A., Akhouri, R. R., Singh, S. K., & Sharma, A. (2004). Hyper-expansion of asparagines correlates with an abundance of proteins with prion-like domains in Plasmodium falciparum. *Mol Biochem Parasitol*, *137*(2), 307-319. https://doi.org/10.1016/j.molbiopara.2004.05.016

Sinha, A., Hughes, K. R., Modrzynska, K. K., Otto, T. D., Pfander, C., Dickens, N. J., . . . Waters, A. P. (2014). A cascade of DNA-binding proteins for sexual commitment and development in Plasmodium. *Nature*, *507*(7491), 253-257. https://doi.org/10.1038/nature12970

Sisowath, C., Strömberg, J., Mårtensson, A., Msellem, M., Obondo, C., Björkman, A., & Gil, J. P. (2005). In Vivo Selection of Plasmodium falciparum pfmdr1 86N Coding Alleles by Artemether-Lumefantrine (Coartem). *The Journal of infectious diseases*, *191*(6), 1014-1017. https://doi.org/10.1086/427997

Smalley, M. E., & Sinden, R. E. (1977). Plasmodium falciparum gametocytes: their longevity and infectivity. *Parasitology*, *74*(1), 1-8. https://doi.org/10.1017/s0031182000047478

Sola, I., Castellà, S., Viayna, E., Galdeano, C., Taylor, M. C., Gbedema, S. Y., . . . Muñoz-Torrero, D. (2015). Synthesis, biological profiling and mechanistic studies of 4-aminoquinoline-based heterodimeric compounds with dual trypanocidal–antiplasmodial activity. *Bioorganic & Medicinal Chemistry*, *23*(16), 5156-5167. https://doi.org/10.1016/j.bmc.2015.01.031

Somé, A. F., Séré, Y. Y., Dokomajilar, C., Zongo, I., Rouamba, N., Greenhouse, B., . . . Rosenthal, P. J. (2010). Selection of known Plasmodium falciparum resistance-mediating polymorphisms by artemether-lumefantrine and amodiaquine-sulfadoxine-pyrimethamine but not dihydroartemisinin-piperaquine in Burkina Faso. *Antimicrob Agents Chemother*, *54*(5), 1949-1954. https://doi.org/10.1128/AAC.01413-09

Sousa-Figueiredo, J. C., Oguttu, D., Adriko, M., Besigye, F., Nankasi, A., Arinaitwe, M., . . . Stothard, J. R. (2010). Investigating portable fluorescent microscopy (CyScope) as an alternative rapid diagnostic test for malaria in children and women of child-bearing age. *Malar J*, *9*, 245. https://doi.org/10.1186/1475-2875-9-245

Sowunmi, A., Balogun, S. T., Gbotosho, G. O., & Happi, C. T. (2008). Plasmodium falciparum gametocyte sex ratios in children with acute, symptomatic, uncomplicated infections treated with amodiaquine. *Malar J*, *7*, 169. https://doi.org/10.1186/1475-2875-7-169

Stocks, P. A., Bray, P. G., Barton, V. E., Al-Helal, M., Jones, M., Araujo, N. C., . . . O'Neill, P. M. (2007). Evidence for a common non-heme chelatable-iron-dependent activation mechanism for semisynthetic and synthetic endoperoxide antimalarial drugs. *Angew Chem Int Ed Engl*, *46*(33), 6278-6283. https://doi.org/10.1002/anie.200604697

Stover, K. R., King, S. T., & Robinson, J. (2012). Artemether-lumefantrine: an option for malaria. *Ann Pharmacother*, *46*(4), 567-577. https://doi.org/10.1345/aph.1Q539

Straimer, J., Gnädig, N. F., Witkowski, B., Amaratunga, C., Duru, V., Ramadani, A. P., . . . Fidock, D. A. (2015). Drug resistance. K13-propeller mutations confer artemisinin resistance in Plasmodium falciparum clinical isolates. *Science*, *347*(6220), 428-431. https://doi.org/10.1126/science.1260867

Sullivan, D. J. (2017). Quinolines block every step of malaria heme crystal growth. *Proc Natl Acad Sci U S A*, *114*(29), 7483-7485. https://doi.org/10.1073/pnas.1708153114

Sutherland, C. J. (2009). Surface antigens of Plasmodium falciparum gametocytes--a new class of transmission-blocking vaccine targets? *Mol Biochem Parasitol*, *166*(2), 93-98. https://doi.org/10.1016/j.molbiopara.2009.03.007

Tanaka, K. (2009). The proteasome: Overview of structure and functions. *Proceedings of the Japan Academy, Series B*, *85*(1), 12-36. https://doi.org/10.2183/pjab.85.12

Tandoh, K. Z., Wilson, M. D., Quashie, N. B., & Duah-Quashie, N. O. (2021). Implicating extracellular vesicles in Plasmodium falciparum artemisinin resistance development. *Traffic*, *22*(6), 194-200. https://doi.org/10.1111/tra.12787

Tavares, J., Formaglio, P., Thiberge, S., Mordelet, E., Van Rooijen, N., Medvinsky, A., . . . Amino, R. (2013). Role of host cell traversal by the malaria sporozoite during liver infection. *J Exp Med*, *210*(5), 905-915. https://doi.org/10.1084/jem.20121130

Tesina, P., Lessen, L. N., Buschauer, R., Cheng, J., Wu, C. C., Berninghausen, O., . . . Green, R. (2020). Molecular mechanism of translational stalling by inhibitory codon combinations and poly(A) tracts. *EMBO J*, *39*(3), e103365. https://doi.org/10.15252/embj.2019103365

Tham, W. H., Healer, J., & Cowman, A. F. (2012). Erythrocyte and reticulocyte binding-like proteins of Plasmodium falciparum. *Trends Parasitol*, *28*(1), 23-30. https://doi.org/10.1016/j.pt.2011.10.002

Thomas, J. A., Tan, M. S. Y., Bisson, C., Borg, A., Umrekar, T. R., Hackett, F., . . . Blackman, M. J. (2018). A protease cascade regulates release of the human malaria parasite Plasmodium falciparum from host red blood cells. *Nat Microbiol*, *3*(4), 447-455. https://doi.org/10.1038/s41564-018-0111-0

Tintó-Font, E., Michel-Todó, L., Russell, T. J., Casas-Vila, N., Conway, D. J., Bozdech, Z., . . . Cortés, A. (2021). A heat-shock response regulated by the PfAP2-HS transcription factor protects human malaria parasites from febrile temperatures. *Nature Microbiology*, *6*(9), 1163-1174. https://doi.org/10.1038/s41564-021-00940-w

Tiwari, M. K., & Chaudhary, S. (2020). Artemisinin-derived antimalarial endoperoxides from bench-side to bed-side: Chronological advancements and future challenges. *Med Res Rev*, *40*(4), 1220-1275. https://doi.org/10.1002/med.21657

Torrentino-Madamet, M., Alméras, L., Desplans, J., Priol, Y. L., Belghazi, M., Pophillat, M., . . . Parzy, D. (2011). Global response of Plasmodium falciparum to hyperoxia: a combined transcriptomic and proteomic approach. *Malaria Journal*, *10*(1), 4. https://doi.org/10.1186/1475-2875-10-4

Touil, F., Pratt, S., Mutter, R., & Chen, B. (2006). Screening a library of potential prion therapeutics against cellular prion proteins and insights into their mode of biological activities by surface plasmon resonance. *J Pharm Biomed Anal*, *40*(4), 822-832. https://doi.org/10.1016/j.jpba.2005.08.011

Trager, W., & Gill, G. S. (1992). Enhanced gametocyte formation in young erythrocytes by Plasmodium falciparum in vitro. *J Protozool*, *39*(3), 429-432.

Urbán, P., & Fernàndez-Busquets, X. (2014). Nanomedicine against malaria. *Curr Med Chem*, *21*(5), 605-629. https://doi.org/10.2174/09298673113206660292https://doi.org/10.1111/j.1550-7408.1992.tb01476.x

van Biljon, R., van Wyk, R., Painter, H. J., Orchard, L., Reader, J., Niemand, J., . . . Birkholtz, L. M. (2019). Hierarchical transcriptional control regulates Plasmodium falciparum sexual differentiation. *BMC Genomics*, *20*(1), 920. https://doi.org/10.1186/s12864-019-6322-9

van der Pluijm, R. W., Amaratunga, C., Dhorda, M., & Dondorp, A. M. (2021). Triple Artemisinin-Based Combination Therapies for Malaria - A New Paradigm? *Trends Parasitol*, *37*(1), 15-24. https://doi.org/10.1016/j.pt.2020.09.011

Velichutina, I. V., Rogers, M. J., McCutchan, T. F., & Liebman, S. W. (1998). Chimeric rRNAs containing the GTPase centers of the developmentally regulated ribosomal rRNAs of Plasmodium falciparum are functionally distinct. *RNA*, *4*(5), 594-602. https://doi.org/10.1017/s1355838298980049

Vembar, S. S., Droll, D., & Scherf, A. (2016). Translational regulation in blood stages of the malaria parasite Plasmodium spp.: systems-wide studies pave the way. *Wiley Interdiscip Rev RNA*, *7*(6), 772-792. https://doi.org/10.1002/wrna.1365

Venture, M. f. M. *History of antimalarials*. https://www.mmv.org/malaria-medicines/history-antimalarials
Vinetz, J. M. (2005). Plasmodium ookinete invasion of the mosquito midgut. *Curr Top Microbiol Immunol*, *295*, 357-382.
Vogtherr, M., Grimme, S., Elshorst, B., Jacobs, D. M., Fiebig, K., Griesinger, C., & Zahn, R. (2003). Antimalarial drug quinacrine binds to C-terminal helix of cellular prion protein. *J Med Chem*, *46*(17), 3563-3564. https://doi.org/10.1021/jm034093h
Volkov, K. V., Aksenova, A. Y., Soom, M. J., Osipov, K. V., Svitin, A. V., Kurischko, C., . . . Mironova, L. N. (2002). Novel non-Mendelian determinant involved in the control of translation accuracy in Saccharomyces cerevisiae. *Genetics*, *160*(1), 25-36. https://doi.org/10.1093/genetics/160.1.25
Wambani, J., & Okoth, P. (2022). Impact of Malaria Diagnostic Technologies on the Disease Burden in the Sub-Saharan Africa. *J Trop Med*, *2022*, 7324281. https://doi.org/10.1155/2022/7324281
Wang, J., Zhang, C. J., Chia, W. N., Loh, C. C., Li, Z., Lee, Y. M., . . . Lin, Q. (2015). Haem-activated promiscuous targeting of artemisinin in Plasmodium falciparum. *Nat Commun*, *6*, 10111. https://doi.org/10.1038/ncomms10111
Wang, L., Delahunty, C., Fritz-Wolf, K., Rahlfs, S., Helena Prieto, J., Yates, J. R., & Becker, K. (2015). Characterization of the 26S proteasome network in Plasmodium falciparum. *Scientific Reports*, *5*(1), 17818. https://doi.org/10.1038/srep17818
Wang, P., Lee, C. S., Bayoumi, R., Djimde, A., Doumbo, O., Swedberg, G., . . . Hyde, J. E. (1997). Resistance to antifolates in Plasmodium falciparum monitored by sequence analysis of dihydropteroate synthetase and dihydrofolate reductase alleles in a large number of field samples of diverse origins. *Mol Biochem Parasitol*, *89*(2), 161-177. https://doi.org/10.1016/s0166-6851(97)00114-x
Wang, Q., Fujioka, H., & Nussenzweig, V. (2005). Exit of Plasmodium sporozoites from oocysts is an active process that involves the circumsporozoite protein. *PLoS Pathog*, *1*(1), e9. https://doi.org/10.1371/journal.ppat.0010009
Warrell, D. A. (2002). Clinical features of malaria. In D. A. Warrell & H. M. Gilles (Eds.), *Essential malariology.* (4 ed., pp. 191-206). CRC Press.
Warrell, D. A., Hemingway, J., Marsh, K., Sinden, R. E., Butcher, G. A., & Snow, R. W. (2010). Malaria. In D. A. Warrell, T. M. Cox, & J. D. Firth (Eds.), *Oxford Textbook of Medicine.* (5 ed.). Oxford University Press.
Watkins, W. M., & Mosobo, M. (1993). Treatment of Plasmodium falciparum malaria with pyrimethamine-sulfadoxine: selective pressure for resistance is a function of long elimination half-life. *Trans R Soc Trop Med Hyg*, *87*(1), 75-78. https://doi.org/10.1016/0035-9203(93)90431-o
Watt, B., van Niel, G., Raposo, G., & Marks, M. S. (2013). PMEL: a pigment cell-specific model for functional amyloid formation. *Pigment Cell Melanoma Res*, *26*(3), 300-315. https://doi.org/10.1111/pcmr.12067
White, N. J. (2019). Triple artemisinin-containing combination anti-malarial treatments should be implemented now to delay the emergence of resistance. *Malar J*, *18*(1), 338. https://doi.org/10.1186/s12936-019-2955-z
WHO (2012). Pyronaridine and artesunate: new anti-malarial approved. *WHO Drug Information*, *26*(2), 115.
WHO (2015). Guidelines for the treatment of malaria. In (3 ed.). Geneva: World Health Organization.
WHO (2016). Global technical strategy for malaria. 2016-2030. In. Geneva.
WHO (2017). *Malaria in pregnant women.* https://www.who.int/malaria/areas/high_risk_groups/pregnancy/en/
WHO (2020). World malaria report 2020: 20 years of global progress and challenges. In. Geneva.

WHO (2021a). *Countries and territories certified malaria-free by WHO.* https://www.who.int/teams/global-malaria-programme/elimination/countries-and-territories-certified-malaria-free-by-who
WHO (2021b). WHO Guidelines for malaria. In. Geneva.
WHO (2021c). World Malaria Report 2021. In. Geneva.
WHO, W. H. O. (2021d). Global technical strategy for malaria. 2016-2030. In *2021 update.* Geneva: World Health Organization.
WHO & PAHO (2017). *Diagnosis, treatment and detection strategy.*
Wicht, K. J., Mok, S., & Fidock, D. A. (2020). Molecular Mechanisms of Drug Resistance in. *Annu Rev Microbiol*, *74*, 431-454. https://doi.org/10.1146/annurev-micro-020518-115546
Williams, K. M., Qie, S., Atkison, J. H., Salazar-Arango, S., Alan Diehl, J., & Olsen, S. K. (2019). Structural insights into E1 recognition and the ubiquitin-conjugating activity of the E2 enzyme Cdc34. *Nature Communications*, *10*(1). https://doi.org/10.1038/s41467-019-11061-8
Winstanley, P., Watkins, W., Muhia, D., Szwandt, S., Amukoye, E., & Marsh, K. (1997). Chlorproguanil/dapsone for uncomplicated Plasmodium falciparum malaria in young children: pharmacokinetics and therapeutic range. *Trans R Soc Trop Med Hyg*, *91*(3), 322-327. https://doi.org/10.1016/s0035-9203(97)90093-6
Wong, W., Bai, X. C., Sleebs, B. E., Triglia, T., Brown, A., Thompson, J. K., . . . Baum, J. (2017). Mefloquine targets the Plasmodium falciparum 80S ribosome to inhibit protein synthesis. *Nat Microbiol*, *2*, 17031. https://doi.org/10.1038/nmicrobiol.2017.31
Wongsrichanalai, C., Pickard, A. L., Wernsdorfer, W. H., & Meshnick, S. R. (2002). Epidemiology of drug-resistant malaria. *Lancet Infect Dis*, *2*(4), 209-218. https://doi.org/10.1016/s1473-3099(02)00239-6
Wu, G., Khodaparast, L., De Vleeschouwer, M., Housmans, J., Houben, B., Schymkowitz, J., & Rousseau, F. (2021). Investigating the mechanism of action of aggregation-inducing antimicrobial Pept-ins. *Cell Chem Biol*, *28*(4), 524-536.e524. https://doi.org/10.1016/j.chembiol.2020.12.008
Wu, L. J. (1988). [Effects of large doses of pyronaridine and chloroquine on the ultrastructure of the erythrocytic stages of pyronaridine-resistant line of Plasmodium berghei]. *Zhongguo Yao Li Xue Bao*, *9*(1), 87-89.
Wu, L. J., Rabbege, J. R., Nagasawa, H., Jacobs, G., & Aikawa, M. (1988). Morphological effects of pyronaridine on malarial parasites. *Am J Trop Med Hyg*, *38*(1), 30-36. https://doi.org/10.4269/ajtmh.1988.38.30
Xie, S. C., Metcalfe, R. D., Hanssen, E., Yang, T., Gillett, D. L., Leis, A. P., . . . Tilley, L. (2019). The structure of the PA28–20S proteasome complex from Plasmodium falciparum and implications for proteostasis. *Nature Microbiology*, *4*(11), 1990-2000. https://doi.org/10.1038/s41564-019-0524-4
Xie, S. C., Ralph, S. A., & Tilley, L. (2020). K13, the Cytostome, and Artemisinin Resistance. *Trends Parasitol*, *36*(6), 533-544. https://doi.org/10.1016/j.pt.2020.03.006
Xu, J., Zhao, C., Huang, X., & Du, W. (2019). Regulation of Artemisinin and Its Derivatives on the Assembly Behavior and Cytotoxicity of Amyloid Polypeptides hIAPP and Aβ. *ACS Chem Neurosci*, *10*(11), 4522-4534. https://doi.org/10.1021/acschemneuro.9b00385
Yang, A. S. P., O'Neill, M. T., Jennison, C., Lopaticki, S., Allison, C. C., Armistead, J. S., . . . Boddey, J. A. (2017). Cell Traversal Activity Is Important for Plasmodium falciparum Liver Infection in Humanized Mice. *Cell Rep*, *18*(13), 3105-3116. https://doi.org/10.1016/j.celrep.2017.03.017
Yang, T., Yeoh, L. M., Tutor, M. V., Dixon, M. W., McMillan, P. J., Xie, S. C., . . . Cobbold, S. A. (2019). Decreased K13 Abundance Reduces Hemoglobin Catabolism and Proteotoxic Stress, Underpinning Artemisinin Resistance. *Cell Rep*, *29*(9), 2917-2928.e2915. https://doi.org/10.1016/j.celrep.2019.10.095

Young, J. A., Fivelman, Q. L., Blair, P. L., de la Vega, P., Le Roch, K. G., Zhou, Y., . . . Winzeler, E. A. (2005). The Plasmodium falciparum sexual development transcriptome: a microarray analysis using ontology-based pattern identification. *Mol Biochem Parasitol*, *143*(1), 67-79. https://doi.org/10.1016/j.molbiopara.2005.05.007

Yuda, M., Kaneko, I., Murata, Y., Iwanaga, S., & Nishi, T. (2021). Mechanisms of triggering malaria gametocytogenesis by AP2-G. *Parasitol Int*, *84*, 102403. https://doi.org/10.1016/j.parint.2021.102403

Zhang, B. (2017). *Advancing bioinformatics methods for in-depth proteome analysis based on high-resolution mass spectrometry* Karolinska Institutet.]. Stockholm.

Zhang, M., Fennell, C., Ranford-Cartwright, L., Sakthivel, R., Gueirard, P., Meister, S., . . . Nussenzweig, V. (2010). The Plasmodium eukaryotic initiation factor-2alpha kinase IK2 controls the latency of sporozoites in the mosquito salivary glands. *J Exp Med*, *207*(7), 1465-1474. https://doi.org/10.1084/jem.20091975

Zhang, S., Chen, H., & Gerhard, G. S. (2010). Heme synthesis increases artemisinin-induced radical formation and cytotoxicity that can be suppressed by superoxide scavengers. *Chem Biol Interact*, *186*(1), 30-35. https://doi.org/10.1016/j.cbi.2010.03.021

Zhu, L., Tripathi, J., Rocamora, F. M., Miotto, O., van der Pluijm, R., Voss, T. S., . . . I, T. R. t. A. C. (2018). The origins of malaria artemisinin resistance defined by a genetic and transcriptomic background. *Nat Commun*, *9*(1), 5158. https://doi.org/10.1038/s41467-018-07588-x